Studies on hydrophobically modified poly (vinyl alcohol)s-based materials for biomedical applications

陳　曦

February 2020

Studies on hydrophobically modified poly (vinyl alcohol)s-based materials for biomedical applications

陳　曦

Doctoral Program in Materials Science and Engineering

Submitted to the Graduate School of
Pure and Applied Science
in Partial Fulfillment of the Requirements
for the Degree of Doctor of Philosophy
in Engineering

at the
University of Tsukuba

Index i-iv

Chapter 1 General introduction 1
1.1. Poly(vinyl alcohol) 2
1.1.1. Application of PVA as biomaterial 2
1.2. Application of PVA for skin adhesives 2
1.2.1. The importance of skin adhesives 2
1.2.2. Classifications of skin adhesives 3
1.2.3. The performance of PVA as skin adhesive 3
1.3. Application of PVA for antithrombogenic coating 4
1.3.1. The importance of antithrombogenic materials 4
1.3.2. Thrombus formation 4
1.3.3. Different antithrombogenic materials 4
1.3.4. The relationship between intermediate water and antithrombogenic property 5
1.3.5. The relationship between γ chain activity and antithrombogenic property 5
1.3.6. The performance of PVA as antithrombogenic coating 6
1.4. Application of PVA for bone filler 6
1.4.1. Vertebral compression fracture 6
1.4.2. Vertebral augmentation 7
1.4.3. Classifications of bone fillers 8
1.4.4. The performance of PVA as bone filler 8
1.5. Application of PVA for cerebral aneurysm embolization material 9
1.5.1. Cerebral aneurysm 9
1.5.2. Subarachnoid hemorrhage 9
1.5.3. Treatment options for people with cerebral aneurysm 9
1.5.4. The performance of PVA as cerebral aneurysm embolization material 9
1.6. Application of PVA for submucosal injection material 10
1.6.1. Endoscopic submucosal dissection 10
1.6.2. Submucosal injection material 10
1.6.3. Commercial submucosal injection material 10
1.7. Amphiphilic polymers 11
1.8. Purpose and objective of this study 11
1.8.1. Hydrophobically modified poly(vinyl alcohol) 11
1.8.2. Enhance the skin adhesion property by hydrophobic modification 11
1.8.3. Enhance the antithrombogenic property by hydrophobic modification 12
1.8.4. Enhance the property of bone filler by hydrophobic modification 12
1.8.5. Enhance the volume embolization ratio by hydrophobic modification 13
1.8.6. Preparation of SIM with multi-function for ESD by hydrophobic modification 14
References 15

Chapter 2 Enhanced skin adhesive property of hydrophobically modified poly(vinyl alcohol) films 20
2.1. Abstract 21
2.2. Introduction 22
2.3. Materials and methods 22

2.3.1. Materials 22
2.3.2. Synthesis of hm-PVA 23
2.3.3. Characterization of hm-PVAs 23
2.3.4. Glass transition temperature of hm-PVAs 23
2.3.5. Preparation of hm-PVA films 24
2.3.6. Tensile strength of hm-PVA films 24
2.3.7. Surface wettability measurement of hm-PVA films 24
2.3.8. Cytocompatibility test of hm-PVAs 24
2.3.9. Bonding strength measurement of the hm-PVA films 25
2.3.10. Lap-shear strength measurement of hm-PVA films 25
2.3.11. T-peel strength measurement 25
2.3.12. Statistical analysis 25
2.4. Results and discussion 26
2.4.1. Synthesis and characterization of hm-PVAs 26
2.4.2. Glass transition temperature of hm-PVAs 27
2.4.3. Tensile strength of hm-PVA films 28
2.4.4. Surface wettability of hm-PVA films 28
2.4.5. Cytocompatibility of hm-PVAs 29
2.4.6. Adhesion test of hm-PVA on porcine skin 29
2.5. Conclusions 33
References 34

Chapter 3 Hydrophobically modified poly (vinyl alcohol)s as antithrombogenic coating materials 37
3.1. Abstract 38
3.2. Introduction 39
3.3. Materials and methods 40
3.3.1. Materials 40
3.3.2. Synthesis of hm-PVAs 40
3.3.3. Characterization of hm-PVA 40
3.3.4. Solubility of the hm-PVAs 41
3.3.5. Swelling degree of the hm-PVAs 41
3.3.6. Preparation of hm-PVA-coated PP films 41
3.3.7. Stability of hm-PVAs-coated PP films 41
3.3.8. In vitro platelet adhesion and platelet activation test 42
3.3.9. Quantification of protein adsorption on the hm-PVA-coated PP films 42
3.3.10. Activity of the fibrinogen γ chain 42
3.3.11. Quantification of the amount of hydration water 42
3.3.12. In vitro antithrombogenicity test 43
3.3.13. Statistical analysis 43
3.4. Results and discussion 43
3.4.1. Synthesis and characterization of hm-PVAs 43
3.4.2. Preparation of hm-PVA-coated PP films 45
3.4.3. Stability of hm-PVAs-coated PP films 48
3.4.4. In vitro platelet adhesion and activation test 49
3.4.5. Quantification of protein adsorption and activity of fibrinogen γ chain 50
3.4.6. Quantification of the amount of hydration water 52
3.4.7. In vitro antithrombogenicity test 53
3.5. Conclusions 54

References 55

Chapter 4 Injectable, non-diffusible and pre-filled bone paste composed of α-Tricalcium phosphate and hydrophobically modified poly(vinyl alcohol) 58

4.1. Abstract 59
4.2. Introduction 60
4.3. Materials and methods 61
4.3.1. Materials 61
4.3.2. Synthesis of hm-PVAs 62
4.3.3. Characterization of hm-PVAs 62
4.3.4. Evaluation of injectability 62
4.3.5. Stability of α-TCP/hm-PVA bone pastes in water or blood after injection 62
4.3.6. Measurement of compressive strength 63
4.3.7. Osteoblast adhesion test 63
4.3.8. Statistical analysis 64
4.4. Results and discussion 64
4.4.1. Synthesis and characterization of hm-PVAs 64
4.4.2. Injectability of α-TCP/hm-PVA bone pastes 65
4.4.3. Stability of α-TCP/hm-PVA bone pastes in water or blood after injection 67
4.4.4. Compressive strength 68
4.4.5. Osteoblast adhesion test 71
4.5. Conclusions 73
References 74

Chapter 5 Injectable inclusion complex composed of α-cyclodextrin and hydrophobically modified poly(vinyl alcohol) as cerebral aneurysm embolization material 76

5.1. Abstract 77
5.2. Introduction 78
5.3. Materials and methods 79
5.3.1. Materials 79
5.3.2. Synthesis of hm-PVAs 79
5.3.3. Characterization of hm-PVAs 79
5.3.4. Preparation of α-CD/hm-PVA mixtures 80
5.3.5. Shear viscosity 80
5.3.6. 2D 1H NMR study of α-CD/hm-PVA mixtures 80
5.3.7. Structural recovery evaluation 80
5.3.8. Thixotropic evaluation 80
5.3.9. Evaluation of Injectability 81
5.3.10. Stability of α-CD/hm-PVA inclusion complexes in PBS 81
5.3.11. Stability test of α-CD/5C9-PVA inclusion complexes 81
5.3.12. Statistical analysis 81
5.4. Results and discussion 81
5.4.1. Synthesis and characterization of hm-PVAs 81
5.4.2. Shear viscosity of α-CD/hm-PVA mixtures 82
5.4.3. 2D ^{1}H-NMR study of α-CD/hm-PVA inclusion complexes 84
5.4.4. Structural recovery evaluation 85
5.4.5. Evaluation of Injectability 87
5.4.6. Embolization of cerebral aneurysm model with α-CD/hm-PVA inclusion complexes 88

5.5. Conclusions 90
References 91

Chapter 6 Adhesive submucosal injection material with multi-functions for endoscopic submucosal dissection 93
6.1. Abstract 94
6.2. Introduction 95
6.3. Materials and methods 96
6.3.1. Materials 96
6.3.2. Synthesis of hm-PVAs 97
6.3.3. Characterization of hm-PVAs 97
6.3.4. Preparation of α-CD/hm-PVA inclusion complexes 97
6.3.5. Shear viscosity 98
6.3.6. Structural recovery evaluation 98
6.3.7. Evaluation of injectability 98
6.3.8. Mucosa elevation effect 98
6.3.9. Evaluation of tissue adhesion 98
6.3.10. Burst strength measurement 99
6.3.11. Blood coagulation evaluation 99
6.3.12. Underwater stability test 99
6.3.13. Statistical analysis 100
6.4. Results and discussion 100
6.4.1. Synthesis and characterization of hm-PVAs 100
6.4.2. Shear viscosity of α-CD/hm-PVA inclusion complexes 101
6.4.3. Structural recovery evaluation 102
6.4.4. Evaluation of Injectability 103
6.4.5. Mucosa elevation effect of α-CD/hm-PVA inclusion complexes 103
6.4.6. Evaluation of tissue adhesion 104
6.4.7. Measurement of the burst strength of a porcine stomach 106
6.4.8. Blood coagulation evaluation 107
6.4.9. Water stability test 108
6.5. Conclusions 110
References 111

Chapter 7 Concluding remarks 114

List of publication 117

List of presentation and awards 118

Acknowledgements 120

Chapter 1

General introduction

1.1. Poly(vinyl alcohol)

Poly(vinyl alcohol) (PVA) is recognized among the largest volume of synthetic polymers that have been produced worldwide for almost one century, and it has attracted considerable research interest [1]. This is due to its exceptional properties which decided for its widespread use, especially in medical and pharmaceutical fields [2]. However, several researches revealed that PVA-based biomaterials have some limitations that may limit their use or performance [3, 4]. To overcome these limitations, various methods have been reported [5-7].

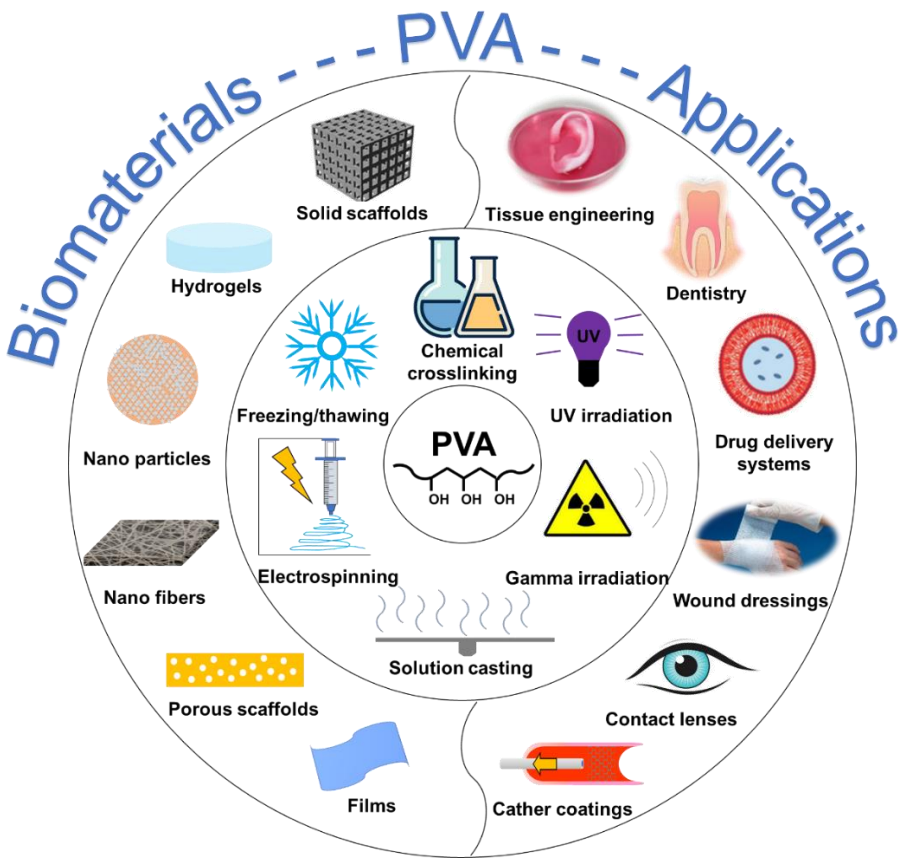

Figure 1-1. Application of PVA as biomaterials in many fields.

1.1.1. Application of PVA as biomaterial

Polyvinyl alcohol (PVA), a hydrophilic, biodegradable and biocompatible polymer, has been widely used in various areas including the biotechnological and biomedical field due to its excellent chemical and physical properties, easy processing technique and high cytocompatibility [8]. Applications of PVA in the biomedical field include contact lenses [9], wound dressing [10], coatings for sutures [11] and catheters [12] as shown in Figure 1-1. Among these, skin adhesives, antithrombogenic coatings, bone fillers and aneurysm embolism materials using PVA have attracted attention.

1.2. Application of PVA for skin adhesives

1.2.1. The importance of skin adhesives

With the aging society, the importance of wearable sensors is increasing. Wearable sensors are integrated into soft materials directly contact with the body in order to monitor health condition and provide clinically relevant data for care [13]. To date, common approach to fabricating soft sensors consisted of integrating conducting material patterns onto a stretchable substrate [14-17]. However, these materials do not possess adhesive property to skin and need to fix onto skin with commercially available adhesives.

1.2.2. Classifications of skin adhesives

Currently, acrylic-based medical bandages that are commercially available are widely used [18]. Although acrylic-based adhesives have high adhesion strength, massive exfoliation of the stratum corneum that occurs when exfoliating causes great pain to the patients [19, 20]. Chemical substances remaining on the skin surface can cause allergic and inflammatory reactions [21]. In addition, silicone pressure sensitive adhesives with low exfoliation of the stratum corneum have been developed [22, 23], however, they are prone to shifting since weak retention to skin [24]. Furthermore, silicone adhesives are relatively expensive. Recently, bioinspired skin adhesives with various multiscale architectures have been reported, including patches with gecko's feet [25, 26], mussel [27], and octopus's suckers [20] (shown in Figure 1-2). However, such adhesives are complicated in production process and not suitable for mass production.

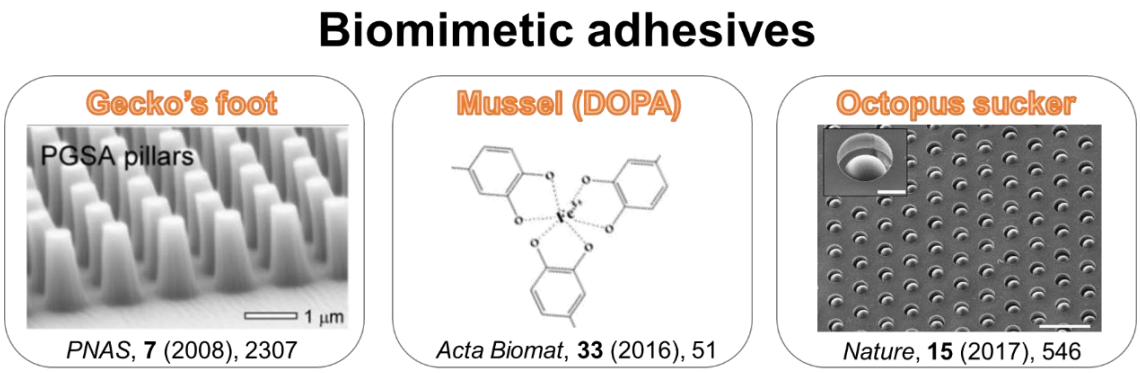

Figure 1-2. Different types of biomimetic adhesives.

1.2.3. The performance of PVA as skin adhesive

At present, there is an urgent need to develop adhesives having strong adhesion, low exfoliation and low allergic reaction. PVA has been extensively studied as a potential skin adhesive. However, as shown in Table 1-1, adhesion strength of PVA film to skin is not strong enough compared with the commercial adhesives since its high hydrophilicity and solubility.

Table 1-1. Adhesive types and their properties.

Adhesive		Adhesion	Stratum corneum exfoliation	Allergic reaction
Acrylic-based adhesive		Strong	High	High
Silicone-based adhesive		Moderate	Low	Low
Biomimetic adhesives	Gecko	Moderate	Low	Low
	Mussel	Strong	High	High
	Octopus	Moderate	Low	Low
PVA-based adhesive		Weak	Low	Low

1.3. Application of PVA for antithrombogenic coating

1.3.1. The importance of antithrombogenic materials

Along with the aging society, patients with vascular and cardiovascular diseases are increasing. These patients often require surgical treatments for implanting stents, artificial heart machines, and hemodialyzers. Since these medical devices directly contact with blood, they are easily recognized as foreign bodies by the biological defense system. Under this circumstance, hemostasis, inflammation, and thrombus formation are evoked [28-30]. When thrombus formation is formed on the surface of the device, problems occur such as a reduction in the performance of the device. In order to minimize the biological defense reactions, the surface of blood-contacting devices should be antithrombogenic to ensure normal blood flow.

1.3.2. Thrombus formation

Thrombus formation depend on the several factors. The medical devices contact with blood, an immediate local cellular response takes place [31]. Platelets migrate to the surface of medical device, where they secrete several cellular factors and mediators. These mediators promote clot formation. Figure 1-3 shows the mechanism of thrombus formation on the device surface which contacts with blood.

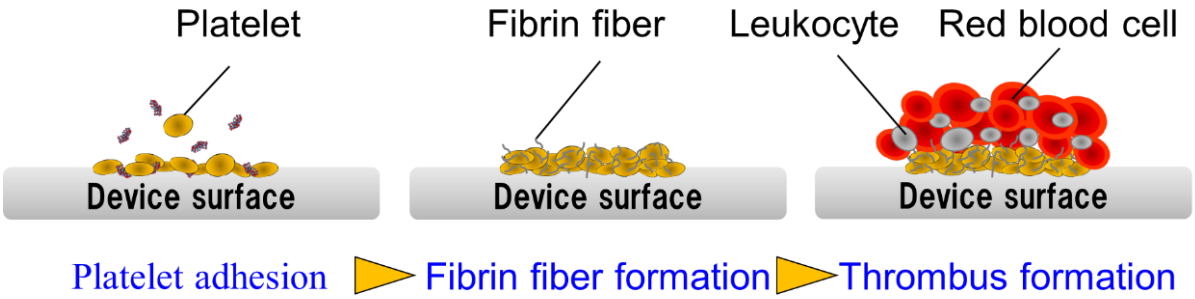

Figure 1-3. Mechanism of thrombus formation on the device surface.

1.3.3. Different antithrombogenic materials

As shown in Figure 1-4, there are three major types of antithrombogenic materials. The first type is to reduce the interaction between the blood components (fibrinogen, albumin, and platelets) and the device surface. Various antithrombogenic materials such as poly (2-methacryloyloxyethyl phosphorylcholine) (MPC) brushes [32-34], poly (2-methoxyethyl acrylate) (PMEA) coatings [35], and poly (ethylene glycol) (PEG) brushes [36, 37] have been reported. These materials are hydrophilic, which can inhibit the protein and platelet adhesion. Besides, PMEA coating with a massive amount of intermediate water (IW) on the surface can reduce the adhesion of blood components.

The second type is to immobilize the biologically active substances (heparin and urokinase (UK)) on the device surface [38, 39]. Heparin activates the anticoagulant function of antithrombin and thus suppresses blood coagulation. By taking into consideration the fibrinolytic activity of UK, which is a plasminogen activator, an antithrombogenic material has been developed by immobilizing it on a material surface. Immobilized UK can catalytically transform plasminogen into plasmin in the blood, which shows antithrombogenicity by constantly dissolving the fibrins produced on the material surface.

The third type is to cover the biomaterial surface with endothelial cells [40]. This kind of surface can resist the interaction between blood protein effectively because of mimicking the structure of blood vessel.

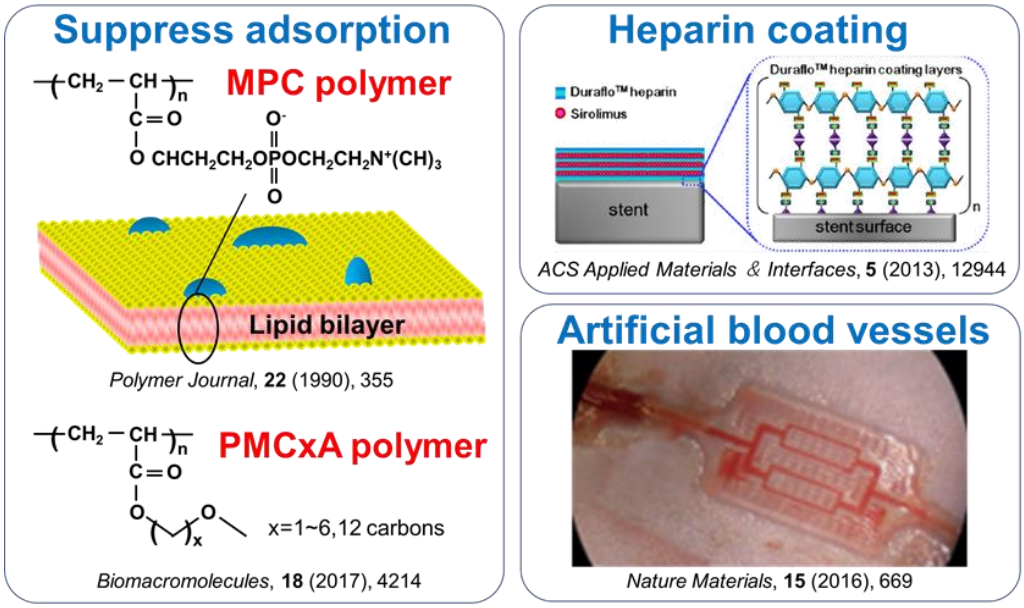

Figure 1-4. Several kinds of antithrombogenic materials.

1.3.4. The relationship between intermediate water and antithrombogenic property

According to the strength of water-polymer interaction, the hydration water can be classified into three kinds of water [41]. Figure 1-5 shows the hydration structure of PMEA coating. The water which strongly interacts with polymer is nonfreezing water (NFW), and another one weakly interacts with polymer is free water (FW). Between the NFW and FW is intermediate water (IW), and it is known as minimum requirement to cause the polymers to be antithrombogenic. IW on the surface can reduce the adhesion of blood components [42, 43].

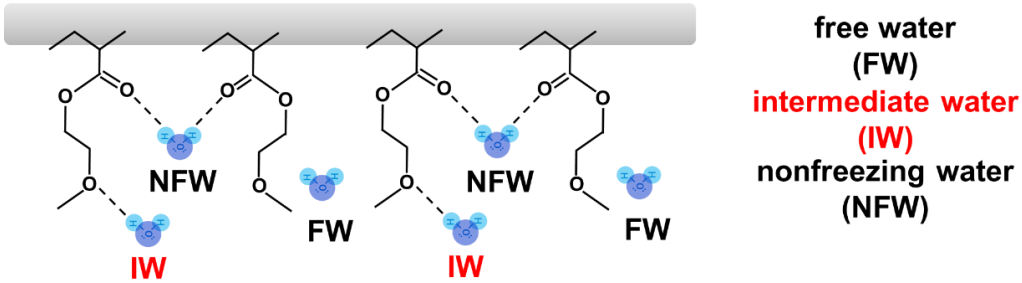

Figure 1-5. Hydration structure of PMEA surface.

1.3.5. The relationship between γ chain activity and antithrombogenic property

Platelet adhesion is the most crucial step for the thrombus formation. The platelet adhesion can be stimulated by adsorption and conformational alteration of fibrinogen which has a platelet bonding site at c terminus in the γ chain. Therefore, inhibiting the adsorption or conformational alteration of fibrinogen is a facile approach to improve antithrombogenicity on device surfaces [44, 45]. In general, fibrinogen adsorbed to a hydrophobic surface remains linear and there are few RGD units on the surface. On the other hand, fibrinogen adsorbed on a hydrophilic surface has a three-dimensional structure, and many RGD units are present on the surface (Figure 1-6). These results indicate that platelet activity is strongly related to hydrophobicity of material surface.

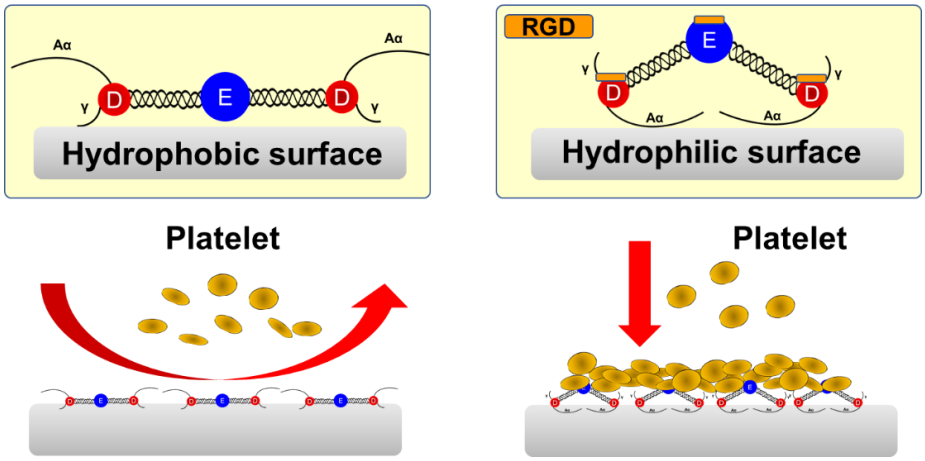

Figure 1-6. The relationship between γ chain activity and thrombus formation.

1.3.6. The performance of PVA as antithrombogenic coating

PVA is known as an antithrombogenic material. The low protein adsorption and the good blood compatibility of PVA can be attributed to the hydrophilic surface. However, PVA coating is not stable in blood due to high water solubility. As shown in Table 1-2, PVA has low antithrombotic durability compared with the other antithrombogenic materials. To overcome this drawback, some researches on modified PVA were conducted.

Table 1-2. Antithrombogenic materials and their properties.

Antithrombogenic materials		Fibrinogen adhesion	Platelet adhesion	Antithrombog-enic property	Endurance
Cover endothelial cells		Low	Low	Excellent	Long
Immobilize heparin		Moderate	Moderate	Normal	Short
Coating	PEG	Low	Low	Excellent	Long
	MPC	Low	High	Excellent	Long
	PMEA	Low	Low	Excellent	Long
	PVA	Low	Low	Normal	Short

1.4. Application of PVA for bone filler

1.4.1. Vertebral compression fracture

Along with a growing elderly population, there is an increase in cases of osteoporotic compression fractures of the vertebrae [46]. Vertebral compression fracture (VCF) occurs when the bony block or vertebral body in the spine collapses, which can lead to severe pain, deformity and loss of height [47]. These fractures more commonly occur in the thoracic spine (the middle portion of the spine), especially in the lower part

(Figure 1-7). While osteoporosis is the most common cause, these fractures may also be caused by trauma or metastatic tumors. VCF can lead to the deterioration of pulmonary function and the compression of abdominal organs, which impair the daily life of elderly patients [48].

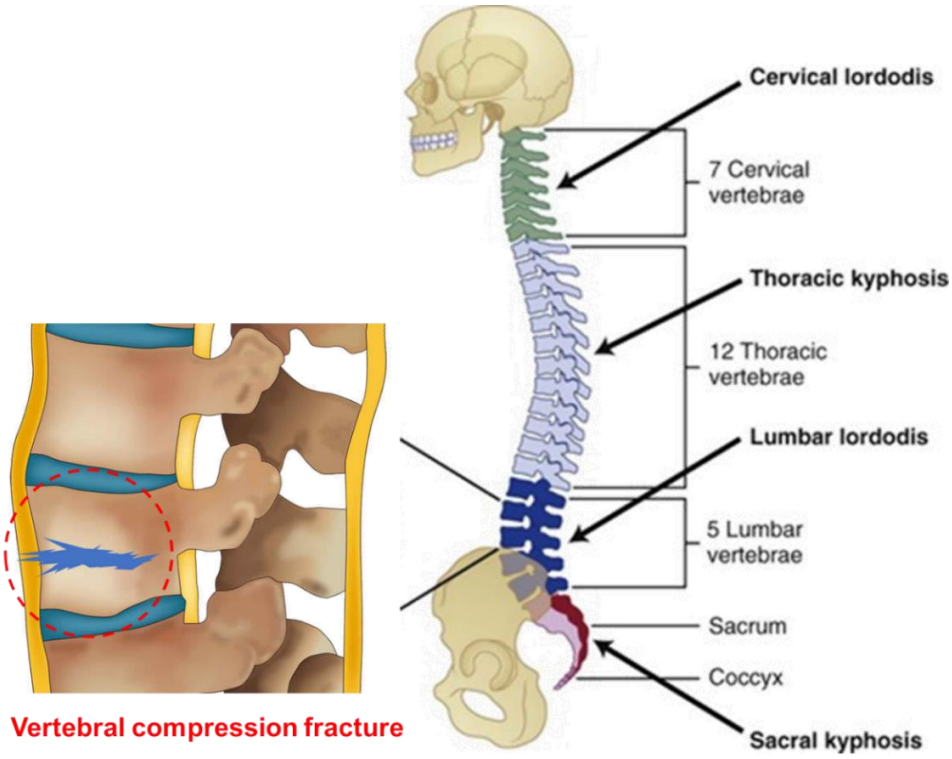

Figure 1-7. Vertebral structure and vertebral compression fracture site.

1.4.2. Vertebral augmentation

Vertebral augmentation, which includes percutaneous vertebroplasty (PVP) and Balloon Kyphoplasty (BKP) [49], are similar spinal procedures in which bone cement is injected through a small hole in the skin into a fractured vertebra to try to relieve back pain caused by a vertebral compression fracture (Figure 1-8). For elderly patients, PVP surgery, a minimally invasive treatment, is most acceptable with injection by a relatively small needle.

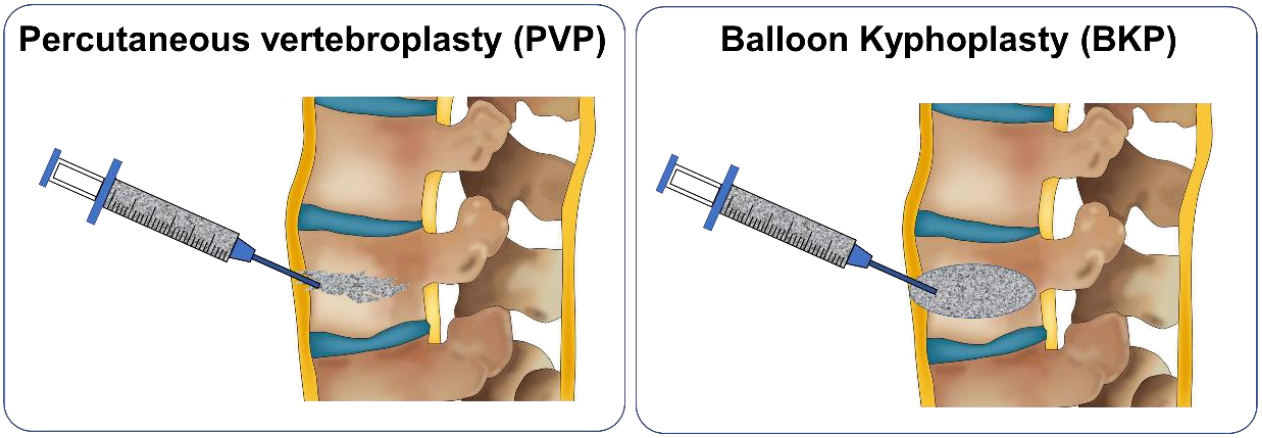

Figure 1-8. Two mainstream vertebroplasties.

1.4.3. Classifications of bone fillers

Currently, a bone cement composed of poly (methyl methacrylate) (PMMA) is widely used in clinical treatment. However, PMMA-based bone cement generates heat of at least 80 ℃ during the polymerization process of methyl methacrylate (MMA), causing severe damage to the tissue around the injection site [50]. In addition, some unreacted MMA monomer or oligomer elutes from the injection site before completely solidifying, then diffuses into the lungs inducing an adverse effect [51, 52]. Furthermore, PMMA cement shows a high compressive strength of over 80 MPa which greatly exceeds the average strength of vertebrae in the elderly (2.37 MPa), and its Young's modulus (1 GPa) is also higher than average (0.35 GPa) [53]. For these reasons, patients who undergo vertebral dilatation surgery are inclined to refracture around the injection site [54, 55].

To overcome the risks of refracture, an elastic material composed of silicone and barium sulphate has been applied in vertebral dilatation surgery [56, 57]. The greatest feature of this material is low stiffness [58]; however, it is also compromised by its polymerization reaction, and the diffusion of the monomer or oligomer still pose health hazards to patients [59].

Calcium phosphate-based bone pastes are also commercially available biomaterials for bone defects [60]. The application of calcium phosphate paste relies on the hydration reaction of calcium phosphate instead of a polymeric reaction [61, 62]. Generally, α-type tricalcium phosphate (α-TCP) is used due to its high curing rate and strength compared to that of another crystal form, β-type tricalcium phosphate (β-TCP) [63]. However, the possibility of diffusion leakage from the bone fracture site is also a problem in the practical application of calcium phosphate paste. Furthermore, components of calcium phosphate paste gradually dissolve in water, so it is difficult to cure in a bleeding site and to maintain adequate strength. Therefore, the use of calcium phosphate pastes alone in vertebroplasty is limited [64]. Also, preparation processes of bone cements as well as calcium phosphate pastes are complex and time-consuming [65].

1.4.4. The performance of PVA as bone filler

In the previous study, bone paste composed of α-TCP and PVA was prepared. Both of α-TCP and PVA dissolve in water, so this kind of bone paste it is difficult to cure in a bleeding site. Furthermore, as shown in Table 1-3, this bone filler has a hydrophilic surface, so osteoblasts are not able to adhere.

Table 1-3. Bone fillers and their properties.

Bone filler	Injectability	Compressive strength	Young's modulus	Osteoblasts adhesion
Endurance	High	Strong	Strong	Moderate
VK100	High	Weak	Weak	Moderate
Biopex-R	High	Moderate	Moderate	Excellent
α-TCP/PVA	High	Moderate	Moderate	Poor

1.5. Application of PVA for cerebral aneurysm embolization material

1.5.1. Cerebral aneurysm

A cerebral aneurysm is an abnormal focal dilation of an artery in the brain caused by weakening of the inner muscular layer (the intima) of a blood vessel wall. The vessel develops a "blister-like" dilation that can become thin and rupture without warning.

1.5.2. Subarachnoid hemorrhage

The resultant bleeding into the space around the brain is called a subarachnoid hemorrhage (SAH) [66]. In fact, the most common cause of SAHs is attributed to ruptured cerebral aneurysms [67, 68]. Further, SAHs can lead to stroke, coma, and/or death. Although urgent therapy can save the lives of patients when SAH occurs, only about 1 in 3 people can restore their cerebral function after treatment [69].

1.5.3. Treatment options for people with cerebral aneurysm

Generally, there are three treatment options for people with cerebral aneurysm, including conservative management, surgical therapy (clipping), and endovascular therapy (coiling) [70] (Figure 1-9). The mechanical sophistication of available clips, along with the advent of the operating microscope in the 1960s, have made surgical clipping a standardized treatment of both ruptured and unruptured cerebral aneurysms [71]. However, the invasive and technically challenging process makes surgical clipping not an ideal treatment for patients [72]. The development of Guglielmi detachable coils (GDCs) approved by FDA in 1995 revolutionized endovascular treatment of cerebral aneurysms [73], advancing development of endovascular therapy with a microcatheter.

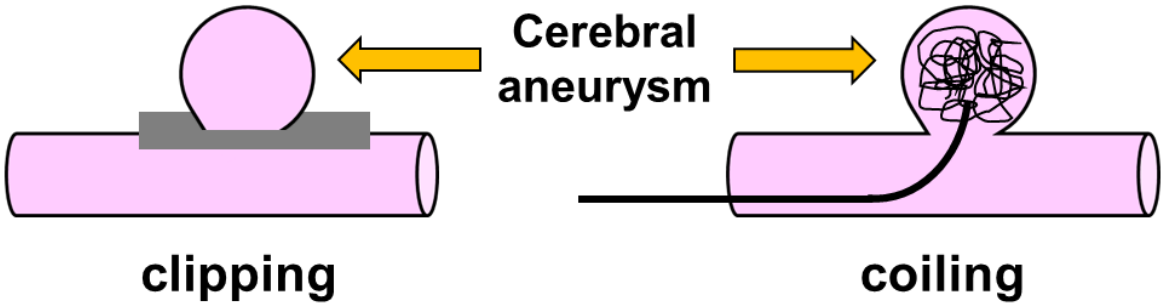

Figure 1-9. Cerebral aneurysm treatment.

1.5.4. The performance of PVA as cerebral aneurysm embolization material

Previous studies demonstrated embolization by injection of ethylene vinyl alcohol dissolved in dimethyl sulfoxide (DMSO) into aneurysm, which formed aggregates in that area [74, 75]. However, as shown in Table 1-4, injection of an organic solvent into the blood vessel limited its clinical application as it can cause side effects on cranial nerves [76]. On the other hand, PVA particle was used as cerebral aneurysm embolization material. However, the curative of cerebral aneurysm treated with PVA particle is worse than that of GDCs. The main reason is that embolization with PVA is temporary and the cerebral aneurysm may reopen.

Table 1-4. Cerebral aneurysm embolization materials and their properties.

Bone filler	Surgery operability	Volume embolization ratio	Toxicity	Curative of cerebral aneurysm
Coil	Moderate	Moderate	No toxicity	Excellent
Onyx-R	Excellent	Excellent	No toxicity	Moderate
PVA particle	Moderate	Moderate	Toxic	Moderate

1.6. Application of PVA for submucosal injection material

1.6.1. Endoscopic submucosal dissection

Endoscopic resection of various gastrointestinal (GI) lesions has changed dramatically since the emergence of endoscopic submucosal dissection (ESD) in the 1990s which is developed from endoscopic mucosal resection (EMR). This kind of therapeutic modality is less invasive and relies on flexible, tube-like imaging tools called endoscopes to remove neoplasms formed at GI mucosa and submucosa. Currently, ESD technique is widely used in Japan as the first-line treatment for early-stage GI cancer with low risk of lymph node metastasis.

1.6.2. Submucosal injection material

Since early GI tumor does not clearly protrude on the surface of mucosa, serious situations such as inadequate resection, perforation, or bleeding may occur during surgical operation. To minimize these damages, submucosal injection material (SIM) has been applied to separate the mucosa and muscularis layers which then enables safe circumferential mucosal incision and submucosal dissection by electrosurgical knife (Figure 1-10).

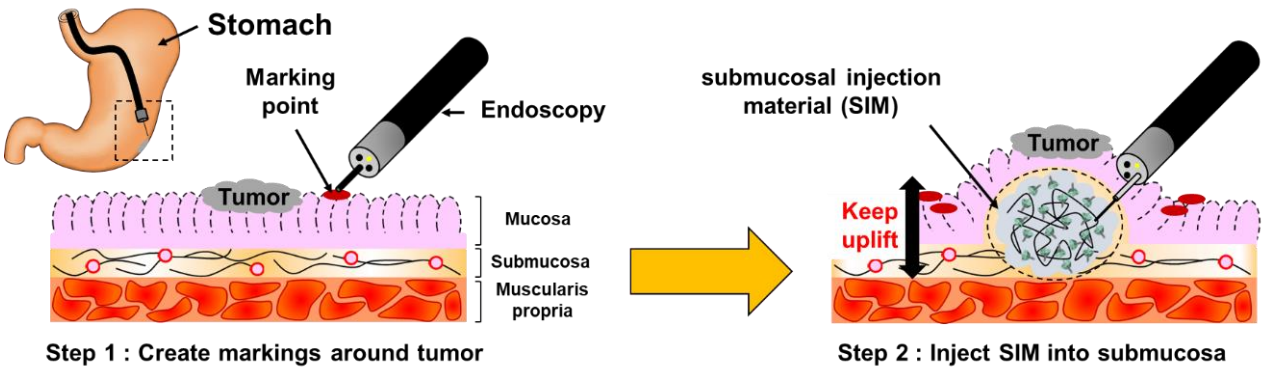

Figure 1-10. The application of submucosal injection material during ESD surgery.

1.6.3. Commercial submucosal injection material

The normal saline is the commonly used SIM as it is cheap and easy to use. However, the cushion created by normal saline is sustained for a short period due to the rapid resorption by surrounding tissue. As a result, repeated injections are needed which may compromise the efficiency of ESD. To overcome the limitation of normal saline, several SIMs have been investigated including polysaccharides (such as glucose) and charged molecules that are more viscous and less easily resorbed than normal saline (Table 1-5). Of all, only sodium hyaluronate solution and sodium alginate solution are approved as material for submucosal injection in Japan.

Table 1-5. Submucosal injection materials and their properties.

SIM	Component	Concentration	Injectability	Submucosal cushion formation
normal saline	NaCl	0.9 w/v%	Excellent	Poor
sodium hyaluronate	sodium hyaluronate	0.8 wt%	Excellent	Moderate
sodium alginate	sodium alginate	1.2 wt%	Excellent	Moderate
PVA	PVA	10 w/v%	Poor	Moderate

1.7. Amphiphilic polymers

Well-defined amphiphilic polymers consisting of hydrophilic and hydrophobic components have complex structural designs and are well controlled in the self-assembly of molecules. It is also at the forefront of smart materials research due to the multifunctionality of material engineering and medicine [77]. More importantly, these materials show high performance in various applications, including advanced delivery carriers [78], tissue engineering [79], template-directed colloidal self-assembly [80], surface modification, and many other applications throughout industry.

1.8. Purpose and objective of this study

1.8.1. Hydrophobically modified poly(vinyl alcohol)

The hydrophobically modified poly(vinyl alcohol) (hm-PVA) was prepared via the reaction between the hydroxy groups of PVA and an aldehyde according to a procedure reported previously. In this study, we report five works using hm-PVA.

1.8.2. Enhance the skin adhesion property by hydrophobic modification

In our previous study, hydrophobically modified biopolymers were used to prepare surgical sealants, films, porous membranes and nano particle to adhere biological tissue in order to accomplish soft tissue adhesion. It was demonstrated that hydrophobic modification could effectively enhance the bonding strength

to soft tissues even under wet conditions. The most important factors to enhance the interfacial strength include anchoring effect of hydrophobic groups to phospholipid membrane of cells and enhanced interaction of amphiphilic polymers with extracellular proteins. We hypothesized that hydrophobic modification of PVA would also increase the adhesion onto soft tissue such as skin (Figure 1-11).

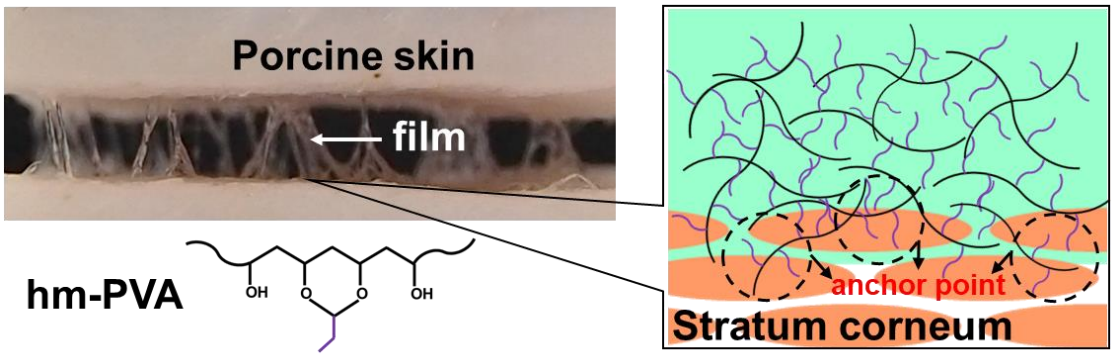

Figure 1-11. Skin adhesion property of hm-PVA.

1.8.3. Enhance the antithrombogenic property by hydrophobic modification

It was reported that alkylated surface could improve the platelet compatibility. The surface grafted with alkyl chains could adsorb albumin from blood, and at the same time inhibit adsorption of fibrinogen, which will also inhibit the adhesion of platelets. Moreover, previous research indicated that polymers such as PMEA and PEG contain methoxy group (C-O-C structure) showed good antithrombogenicity because of high amount of the IW. However, detailed research of antithrombogenic property of hm-PVAs with acetal group (C-O-C structure) has not yet been reported. In this study, we synthesized hm-PVAs with 3, 6, 9, and 12 methylene carbons to examine the prediction that PVA with alkyl group and acetal group will show good antithrombogenicity (Figure 1-12).

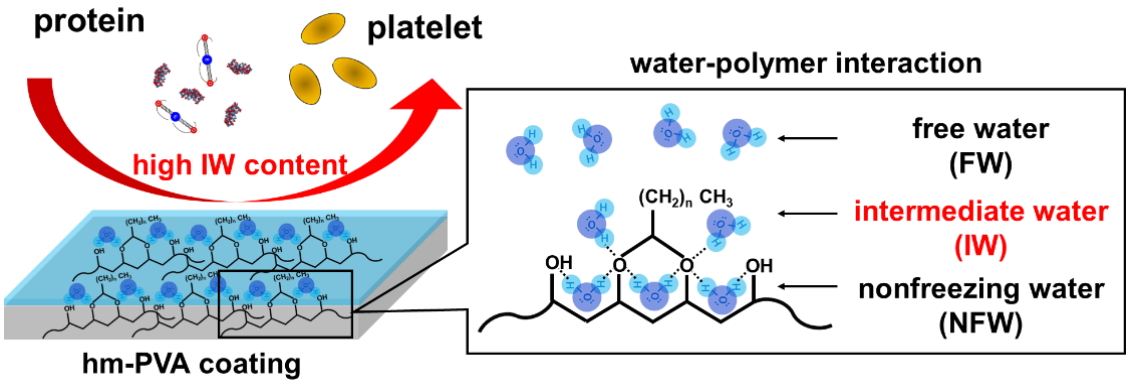

Figure 1-12. Antithrombogenic property of hm-PVA.

1.8.4. Enhance the property of bone filler by hydrophobic modification

The ideal bone filler has to meet the requirements of clinical practice such as having an injectable property, curability in a water/blood environment, non-diffusibility and biological safety. Focusing on the water-insoluble characteristic of hm-PVA, we developed an injectable, non-diffusible and pre-filled type bone paste composed of α-TCP and hm-PVA. Using dimethyl sulfoxide (DMSO), which is used as a solvent of a non-adhesive liquid embolic agent for cerebral arteriovenous malformations, we successfully prepared a pre-

filled type bone paste that did not require mixing before injection (Figure 1-13).

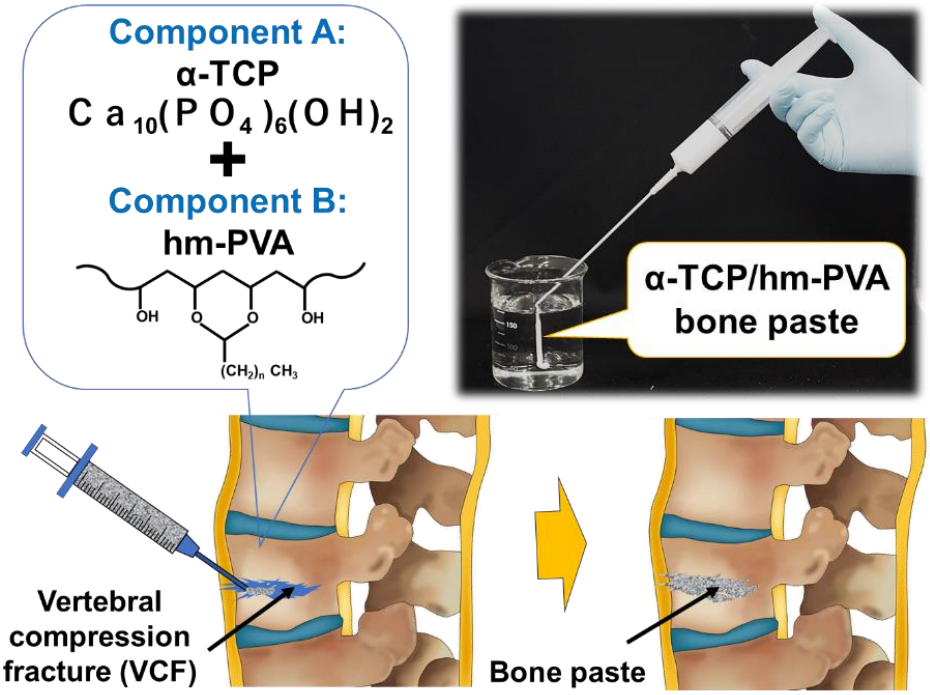

Figure 1-13. A novel bone paste composed of hm-PVA.

1.8.5. Enhance the volume embolization ratio by hydrophobic modification

Focusing on the water insolubility of hydrophobically modified poly(vinyl alcohol) (hm-PVA) [11, 81] and the inclusion ability of α-cyclodextrin (α-CD) to hydrophobic groups, we developed an inclusion complex composed of α-CD and hm-PVA without using any organic solvent as a cerebral aneurysm embolization material (Figure 1-14). In this study, fundamental properties of the α-CD/hm-PVA inclusion process as well as potential applications of the resulting complex as a material for cerebral aneurysm embolization were evaluated.

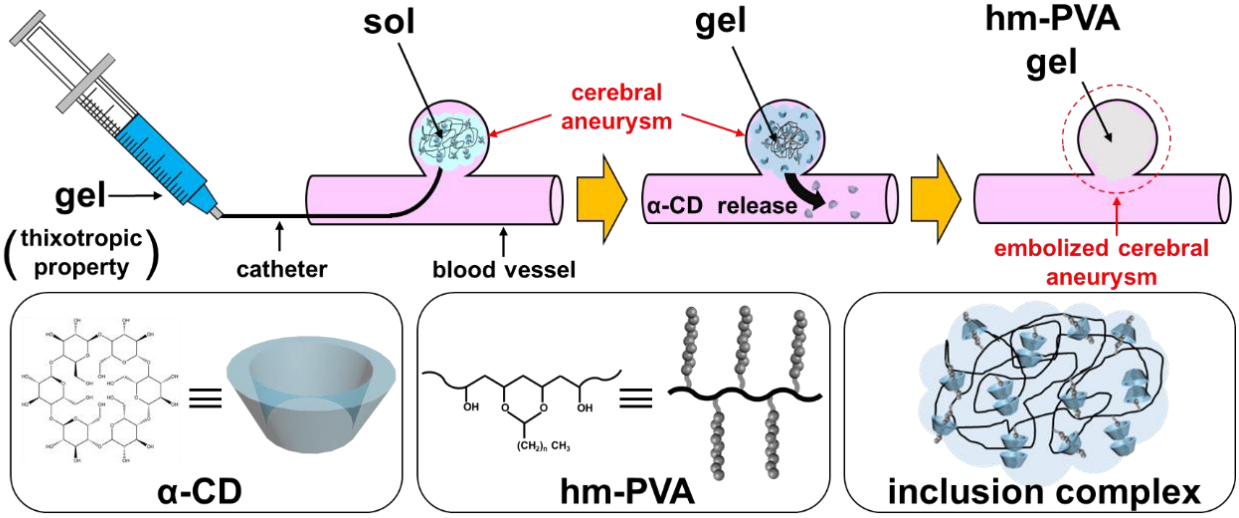

Figure 1-14. Schematic illustration of cerebral aneurysm embolization using α-CD/hm-PVA inclusion complex.

1.8.6. Preparation of SIM with multi-function for ESD by hydrophobic modification

Focusing on the water insolubility of hm-PVA, in which alkyl group (nonanal, C9) is introduced into PVA, and the hydrophobic groups inclusion ability of α-cyclodextrin (α-CD), an inclusion complex (α-CD/C9-PVA) was fabricated in aqueous solution (as potential submucosal injection and wound dressing material). After the injection of α-CD/C9-PVA inclusion complex, the submucosal cushion formation, tissue adhesion, burst strength of perforation site, blood and wound sealing effect were evaluated.

References

[1] M. Teodorescu, M. Bercea, S. Morariu, Biomaterials of PVA and PVP in medical and pharmaceutical applications: Perspectives and challenges, Biotechnology Advances, 37 (2019) 109-131.
[2] C.M. Hassan, N.A. Peppas, Structure and applications of poly(vinyl alcohol) hydrogels produced by conventional crosslinking or by freezing/thawing methods, in: A. Abe (Ed.) Biopolymers/Pva Hydrogels/Anionic Polymerisation Nanocomposites2000, pp. 37-65.
[3] S. Roy, S. Kuddannaya, T. Das, H.Y. Lee, J. Lim, X. Hu, Y.C. Yoona, J. Kim, A novel approach for fabricating highly tunable and fluffy bioinspired 3D poly(vinyl alcohol) (PVA) fiber scaffolds, Nanoscale, 9 (2017) 7081-7093.
[4] F.M. Ali, R.M. Kershi, M.A. Sayed, Y.M. AbouDeif, Evaluation of structural and optical properties of Ce3+ ions doped (PVA/PVP) composite films for new organic semiconductors, Physica B-Condensed Matter, 538 (2018) 160-166.
[5] J.K. Li, N. Wang, X.S. Wu, Poly(vinyl alcohol) nanoparticles prepared by freezing-thawing process for protein/peptide drug delivery, Journal of Controlled Release, 56 (1998) 117-126.
[6] M.L. Zhai, F. Yoshii, T. Kume, K. Hashim, Syntheses of PVA/starch grafted hydrogels by irradiation, Carbohydrate Polymers, 50 (2002) 295-303.
[7] B. Bolto, T. Tran, M. Hoang, Z.L. Xie, Crosslinked poly(vinyl alcohol) membranes, Progress in Polymer Science, 34 (2009) 969-981.
[8] T.S. Gaaz, A.B. Sulong, M.N. Akhtar, A.A.H. Kadhum, A.B. Mohamad, A.A. Al-Amiery, Properties and Applications of Polyvinyl Alcohol, Halloysite Nanotubes and Their Nanocomposites, Molecules, 20 (2015) 22833-22847.
[9] S.H. Hyon, W.I. Cha, Y. Ikada, M. Kita, Y. Ogura, Y. Honda, POLY(VINYL ALCOHOL) HYDROGELS AS SOFT CONTACT-LENS MATERIAL, Journal of Biomaterials Science-Polymer Edition, 5 (1994) 397-406.
[10] E.A. Kamoun, X. Chen, M.S.M. Eldin, E.R.S. Kenawy, Crosslinked poly(vinyl alcohol) hydrogels for wound dressing applications: A review of remarkably blended polymers, Arabian Journal of Chemistry, 8 (2015) 1-14.
[11] X. Chen, T. Taguchi, Hydrophobically modified poly(vinyl alcohol)s as antithrombogenic coating materials, Materials Science & Engineering C-Materials for Biological Applications, 102 (2019) 289-298.
[12] M. Chaouat, C. Le Visage, W.E. Baille, B. Escoubet, F. Chaubet, M.A. Mateescu, D. Letourneur, A Novel Cross-linked Poly(vinyl alcohol) (PVA) for Vascular Grafts, Advanced Functional Materials, 18 (2008) 2855-2861.
[13] V. Custodio, F.J. Herrera, G. Lopez, J.I. Moreno, A Review on Architectures and Communications Technologies for Wearable Health-Monitoring Systems, Sensors, 12 (2012) 13907-13946.
[14] C. Luo, N.S. Liu, H. Zhang, W.J. Liu, Y. Yue, S.L. Wang, J.Y. Rao, C.X. Yang, J. Su, X.L. Jiang, Y.H. Gao, A new approach for ultrahigh-performance piezoresistive sensor based on wrinkled PPy film with electrospun PVA nanowires as spacer, Nano Energy, 41 (2017) 527-534.
[15] C.X. Hu, Y.L. Zhang, X.D. Wang, L. Xing, L.Y. Shi, R. Ran, Stable, Strain-Sensitive Conductive Hydrogel with Antifreezing Capability, Remoldability, and Reusability, Acs Applied Materials & Interfaces, 10 (2018) 44000-44010.
[16] W.J. Liu, N.S. Liu, Y. Yue, J.Y. Rao, F. Cheng, J. Su, Z.T. Liu, Y.H. Gao, Piezoresistive Pressure Sensor Based on Synergistical Innerconnect Polyvinyl Alcohol Nanowires/Wrinkled Graphene Film, Small, 14 (2018).
[17] S. Park, S.W. Heo, W. Lee, D. Inoue, Z. Jiang, K. Yu, H. Jinno, D. Hashizume, M. Sekino, T. Yokota, K. Fukuda, K. Tajima, T. Someya, Self-powered ultra-flexible electronics via nano-grating-patterned organic

photovoltaics, Nature, 561 (2018) 516-+.
[18] M.K. Kwak, H.E. Jeong, K.Y. Suh, Rational Design and Enhanced Biocompatibility of a Dry Adhesive Medical Skin Patch, Advanced Materials, 23 (2011) 3949-3953.
[19] A.J. Singer, J.V. Quinn, J.E. Hollander, The cyanoacrylate topical skin adhesives, Am. J. Emerg. Med., 26 (2008) 490-496.
[20] D.W. Kim, S. Baik, H. Min, S. Chun, H.J. Lee, K.H. Kim, J.Y. Lee, C. Pang, Highly Permeable Skin Patch with Conductive Hierarchical Architectures Inspired by Amphibians and Octopi for Omnidirectionally Enhanced Wet Adhesion, Advanced Functional Materials, 29 (2019).
[21] S.J. Canipa, M.L. Chilton, R. Hemingway, D.S. Macmillan, A. Myden, J.P. Plante, R.E. Tennant, J.D. Vessey, T. Steger-Hartmann, J. Gould, J. Hillegass, S. Etter, B.P.C. Smith, A. White, P. Sterchele, A. De Smedt, D. O'Brien, R. Parakhia, A quantitative in silico model for predicting skin sensitization using a nearest neighbours approach within expert-derived structure-activity alert spaces, Journal of Applied Toxicology, 37 (2017) 985-995.
[22] M. He, Q.Y. Zhang, J.Y. Guo, Synthesis and characterization of silicone based Pressure sensitive adhesive, in: S.Q. Liu, M. Zuo (Eds.) Emerging Focus on Advanced Materials, Pts 1 and 22011, pp. 1773-1778.
[23] A.K. Antosik, P. Bednarczyk, Z. Czech, Aging of silicone pressure-sensitive adhesives, Polymer Bulletin, 75 (2018) 1141-1147.
[24] H. Matsumura, R. Imai, N. Ahmatjan, Y. Ida, M. Gondo, D. Shibata, K. Wanatabe, Removal of adhesive wound dressing and its effects on the stratum corneum of the skin: comparison of eight different adhesive wound dressings, Int. Wound J., 11 (2014) 50-54.
[25] W.G. Bae, D. Kim, M.K. Kwak, L. Ha, S.M. Kang, K.Y. Suh, Enhanced skin adhesive patch with modulus-tunable composite micropillars, Adv Healthc Mater, 2 (2013) 109-113.
[26] X. Chen, R. Mizuta, N. Fukata, T. Taguchi, Design of bio-inspired adhesive surface composed of hexanoyl group-modified gelatin and silicon nanowire, Colloids and Surfaces B-Biointerfaces, 178 (2019) 111-119.
[27] K. Yamagishi, I. Kirino, I. Takahashi, H. Amano, S. Takeoka, Y. Morimoto, T. Fujie, Tissue-adhesive wirelessly powered optoelectronic device for metronomic photodynamic cancer therapy, Nature Biomedical Engineering, 3 (2019) 27-36.
[28] M.B. Gorbet, M.V. Sefton, Biomaterial-associated thrombosis: roles of coagulation factors, complement, platelets and leukocytes, Biomaterials, 25 (2004) 5681-5703.
[29] J.M. Anderson, A. Rodriguez, D.T. Chang, Foreign body reaction to biomaterials, Seminars in Immunology, 20 (2008) 86-100.
[30] I.H. Jaffer, J.C. Fredenburgh, J. Hirsh, J.I. Weitz, Medical device-induced thrombosis: what causes it and how can we prevent it?, Journal of Thrombosis and Haemostasis, 13 (2015) S72-S81.
[31] D.C. Leslie, A. Waterhouse, J.B. Berthet, T.M. Valentin, A.L. Watters, A. Jain, P. Kim, B.D. Hatton, A. Nedder, K. Donovan, E.H. Super, C. Howell, C.P. Johnson, T.L. Vu, D.E. Bolgen, S. Rifai, A.R. Hansen, M. Aizenberg, M. Super, J. Aizenberg, D.E. Ingber, A bioinspired omniphobic surface coating on medical devices prevents thrombosis and biofouling, Nature Biotechnology, 32 (2014) 1134-1140.
[32] K. Ishihara, T. Ueda, N. Nakabayashi, Preparation of phospholipid polymers and their properties as polymer hydrogel membranes, Polymer Journal, 22 (1990) 355-360.
[33] W. Feng, S.P. Zhu, K. Ishihara, J.L. Brash, Adsorption of fibrinogen and lysozyme on silicon grafted with poly(2-methacryloyloxyethyl phosphorylcholine) via surface-initiated atom transfer radical polymerization, Langmuir, 21 (2005) 5980-5987.
[34] W. Feng, J.L. Brash, S.P. Zhu, Non-biofouling materials prepared by atom transfer radical polymerization grafting of 2-methacryloloxyethyl phosphorylcholine: Separate effects of graft density and chain length on protein repulsion, Biomaterials, 27 (2006) 847-855.

[35] M. Tanaka, A. Mochizuki, N. Ishii, T. Motomura, T. Hatakeyama, Study of blood compatibility with poly(2-methoxyethyl acrylate). Relationship between water structure and platelet compatibility in poly(2-methoxyethylacrylate-co-2-hydroxyethylmethacrylate), Biomacromolecules, 3 (2002) 36-41.
[36] R. Gref, M. Luck, P. Quellec, M. Marchand, E. Dellacherie, S. Harnisch, T. Blunk, R.H. Muller, 'Stealth' corona-core nanoparticles surface modified by polyethylene glycol (PEG): influences of the corona (PEG chain length and surface density) and of the core composition on phagocytic uptake and plasma protein adsorption, Colloids and Surfaces B-Biointerfaces, 18 (2000) 301-313.
[37] J. Ladd, Z. Zhang, S. Chen, J.C. Hower, S. Jiang, Zwitterionic polymers exhibiting high resistance to nonspecific protein adsorption from human serum and plasma, Biomacromolecules, 9 (2008) 1357-1361.
[38] H. Chen, Y. Teramura, H. Iwata, Co-immobilization of urokinase and thrombomodulin on islet surfaces by poly(ethylene glycol)-conjugated phospholipid, Journal of Controlled Release, 150 (2011) 229-234.
[39] L.C. Su, Y.H. Chen, M.C. Chen, Dual Drug-Eluting Stents Coated with Multi layers of Hydrophobic Heparin and Sirolimus, Acs Applied Materials & Interfaces, 5 (2013) 12944-12953.
[40] B.Y. Zhang, M. Montgomery, M.D. Chamberlain, S. Ogawa, A. Korolj, A. Pahnke, L.A. Wells, S. Masse, J. Kim, L. Reis, A. Momen, S.S. Nunes, A.R. Wheeler, K. Nanthakumar, G. Keller, M.V. Sefton, M. Radisic, Biodegradable scaffold with built-in vasculature for organ-on-a-chip engineering and direct surgical anastomosis, Nature Materials, 15 (2016) 669-677.
[41] M. Tanaka, K. Sato, E. Kitakami, S. Kobayashi, T. Hoshiba, K. Fukushima, Design of biocompatible and biodegradable polymers based on intermediate water concept, Polymer Journal, 47 (2015) 114-121.
[42] S. Kobayashi, M. Wakui, Y. Iwata, M. Tanaka, Poly(omega-methoxyalkyl acrylate)s: Nonthrombogenic Polymer Family with Tunable Protein Adsorption, Biomacromolecules, 18 (2017) 4214-4223.
[43] K. Sato, S. Kobayashi, A. Sekishita, M. Wakui, M. Tanaka, Synthesis and Thrombogenicity Evaluation of Poly(3-methoxypropionic acid vinyl ester): A Candidate for Blood-Compatible Polymers, Biomacromolecules, 18 (2017) 1609-1616.
[44] J.H. Seo, S. Kakinoki, Y. Inoue, T. Yamaoka, K. Ishihara, N. Yui, Designing dynamic surfaces for regulation of biological responses, Soft Matter, 8 (2012) 5477-5485.
[45] L.D. Zhang, B. Casey, D.K. Galanakis, C. Marmorat, S. Skoog, K. Vorvolakos, M. Simon, M.H. Rafailovich, The influence of surface chemistry on adsorbed fibrinogen conformation, orientation, fiber formation and platelet adhesion, Acta Biomaterialia, 54 (2017) 164-174.
[46] J.L. Old, M. Calvert, Vertebral compression fractures in the elderly, American Family Physician, 69 (2004) 111-116.
[47] N. Bogduk, J. MacVicar, J. Borowczyk, The Pain of Vertebral Compression Fractures Can Arise in the Posterior Elements, Pain Medicine, 11 (2010) 1666-1673.
[48] H.K. Svensson, E.H. Olofsson, J. Karlsson, T. Hansson, L.E. Olsson, A painful, never ending story: older women's experiences of living with an osteoporotic vertebral compression fracture, Osteoporosis International, 27 (2016) 1729-1736.
[49] D.J. Theodorou, S.J. Theodorou, T.D. Duncan, S.R. Garfin, W.H. Wong, Percutaneous balloon kyphoplasty for the correction of spinal deformity in painful vertebral body compression fractures, Clin. Imaging, 26 (2002) 1-5.
[50] K. Serbetci, F. Korkusuz, N. Hasirci, Thermal and mechanical properties of hydroxyapatite impregnated acrylic bone cements, Polym. Test, 23 (2004) 145-155.
[51] M.A. Rothermich, J.M. Buchowski, D.B. Bumpass, G.A. Patterson, Pulmonary Cement Embolization After Vertebroplasty Requiring Pulmonary Wedge Resection, Clin. Orthop. Rel. Res., 472 (2014) 1652-1657.
[52] P. Shridhar, Y.F. Chen, R. Khalil, A. Plakseychuk, S.K. Cho, B. Tillman, P.N. Kumta, Y. Chun, A Review of PMMA Bone Cement and Intra-Cardiac Embolism, Materials, 9 (2016).

[53] X. Banse, T.J. Sims, A.J. Bailey, Mechanical properties of adult vertebral cancellous bone: Correlation with collagen intermolecular cross-links, Journal of Bone and Mineral Research, 17 (2002) 1621-1628.
[54] A.L. Wagner, E. Baskurt, Refracture with cement extrusion following percutaneous vertebroplasty of a large interbody cleft, American Journal of Neuroradiology, 27 (2006) 230-231.
[55] S.M. Oliveira, C.C. Barrias, I.F. Almeida, P.C. Costa, M.R.P. Ferreira, M.F. Bahia, M.A. Barbosa, Injectability of a bone filler system based on hydroxyapatite microspheres and a vehicle with in situ gel-forming ability, Journal of Biomedical Materials Research Part B-Applied Biomaterials, 87B (2008) 49-58.
[56] R. Bornemann, Y. Rommelspacher, T.R. Jansen, K. Sander, D.C. Wirtz, R. Pflugmacher, Elastoplasty: A Silicon Polymer as a New Filling Material for Kyphoplasty in Comparison to PMMA, Pain Physician, 19 (2016) 885-892.
[57] A. Gasbarrini, R. Ghermandi, Y.E. Akman, M. Girolami, S. Boriani, Elastoplasty as a promising novel technique: Vertebral augmentation with an elastic silicone-based polymer, Acta Orthopaedica Et Traumatologica Turcica, 51 (2017) 209-214.
[58] T.L. Schulte, A. Keiler, F. Riechelmann, T. Lange, W. Schmoelz, Biomechanical comparison of vertebral augmentation with silicone and PMMA cement and two filling grades, European Spine Journal, 22 (2013) 2695-2701.
[59] T.A.J. Urlings, E. van der Linden, Elastoplasty: First Experience in 12 Patients, Cardiovascular and Interventional Radiology, 36 (2013) 479-483.
[60] R.Z. LeGeros, Properties of osteoconductive biomaterials: Calcium phosphates, Clin. Orthop. Rel. Res., (2002) 81-98.
[61] C.S. Liu, W. Gai, S.H. Pan, Z.S. Liu, The exothermal behavior in the hydration process of calcium phosphate cement, Biomaterials, 24 (2003) 2995-3003.
[62] T.J. Brunner, M. Bohner, C. Dora, C. Gerber, W.J. Stark, Comparison of amorphous TCP nanoparticles to micron-sized alpha-TCP as starting materials for calcium phosphate cements, Journal of Biomedical Materials Research Part B-Applied Biomaterials, 83B (2007) 400-407.
[63] N. Eliaz, N. Metoki, Calcium Phosphate Bioceramics: A Review of Their History, Structure, Properties, Coating Technologies and Biomedical Applications, Materials, 10 (2017).
[64] J. Hamada, Y. Kai, M. Morioka, K. Kazekawa, Y. Ishimaru, H. Iwata, Y. Ushio, A nonadhesive liquid embolic agent composed of ethylene vinyl alcohol copolymer and ethanol mixture for the treatment of cerebral arteriovenous malformations: experimental study, Journal of Neurosurgery, 97 (2002) 889-895.
[65] E.F. Burguera, H.H.K. Xu, M.D. Weir, Injectable and rapid-setting calcium phosphate bone cement with dicalcium phosphate dihydrate, Journal of Biomedical Materials Research Part B-Applied Biomaterials, 77B (2006) 126-134.
[66] I. van der Schaaf, A. Algra, M. Wermer, A. Molyneux, M. Clarke, J. van Gijn, G. Rinkel, Endovascular coiling versus neurosurgical clipping for patients with aneurysmal subarachnoid haemorrhage, The Cochrane database of systematic reviews, (2005) CD003085-CD003085.
[67] L. Zhao, L. Zhang, X. Zhang, Z. Li, L. Tian, Y.-X.J. Wang, An Analysis of 1256 Cases of Sporadic Ruptured Cerebral Aneurysm in a Single Chinese Institution, Plos One, 9 (2014).
[68] M. Korja, J. Kaprio, Controversies in epidemiology of intracranial aneurysms and SAH, Nature Reviews Neurology, 12 (2016).
[69] A.K. Petridis, M.A. Kamp, J.F. Cornelius, T. Beez, K. Beseoglu, B. Turowski, H.J. Steiger, Aneurysmal Subarachnoid Hemorrhage, Dtsch Arztebl Int, 114 (2017) 226-236.
[70] N. Ajiboye, N. Chalouhi, R.M. Starke, M. Zanaty, R. Bell, Unruptured Cerebral Aneurysms: Evaluation and Management, TheScientificWorldJournal, 2015 (2015) 954954-954954.
[71] N.A. Martin, The combination of endovascular and surgical techniques for the treatment of intracranial

aneurysms, Neurosurgery Clinics of North America, 9 (1998) 897-+.
[72] L.B. Ross, A. Weill, M. Piotin, J. Moret, Endovascular treatment of distally located giant aneurysms, Neurosurgery, 47 (2000) 1147-1152.
[73] G. Guglielmi, History of the genesis of detachable coils A review, Journal of Neurosurgery, 111 (2009) 1-8.
[74] A.J. Molyneux, S. Cekirge, I. Saatci, G. Gal, Cerebral Aneurysm Multicenter European Onyx (CAMEO) trial: Results of a prospective observational study in 20 European centers, American Journal of Neuroradiology, 25 (2004) 39-51.
[75] M. Kurdi, S. Baeesa, M. Bin-Mahfoodh, K. Kurdi, Onyx Embolization of Ruptured Intracranial Aneurysm Associated with Behcet's Disease, Case reports in vascular medicine, 2013 (2013) 797045-797045.
[76] J.I. Hamada, Y. Kai, T. Mizuno, M. Morioka, K. Kazekawa, H. Iwata, Y. Ushio, A nonadhesive liquid embolic agent of ethylene vinyl alcohol copolymer and ethanol mixture for cerebral arteriovenous malformations - Clinical experience, Interventional Neuroradiology, 10 (2004) 135-142.
[77] A.B. Kutikov, J. Song, Biodegradable PEG-Based Amphiphilic Block Copolymers for Tissue Engineering Applications, Acs Biomaterials Science & Engineering, 1 (2015) 463-480.
[78] V.P. Torchilin, Structure and design of polymeric surfactant-based drug delivery systems, Journal of Controlled Release, 73 (2001) 137-172.
[79] H.Y. Tian, Z.H. Tang, X.L. Zhuang, X.S. Chen, X.B. Jing, Biodegradable synthetic polymers: Preparation, functionalization and biomedical application, Progress in Polymer Science, 37 (2012) 237-280.
[80] Y. Meng, D. Gu, F.Q. Zhang, Y.F. Shi, H.F. Yang, Z. Li, C.Z. Yu, B. Tu, D.Y. Zhao, Ordered mesoporous polymers and homologous carbon frameworks: Amphiphilic surfactant templating and direct transformation, Angewandte Chemie-International Edition, 44 (2005) 7053-7059.
[81] X. Chen, T. Taguchi, Injectable, Non-Diffusible, and Pre-Filled Bone Paste Composed of α-Tricalcium Phosphate and Hydrophobically Modified Poly(Vinyl Alcohol), Advanced Engineering Materials, 21 (2019) 1900660.

Chapter 2

Enhanced skin adhesive property of Hydrophobically modified poly(vinyl alcohol) films

2.1. Abstract

Hydrophobically modified poly(vinyl alcohol) (hm-PVA) films with various alkyl chain lengths were prepared. Their surface/mechanical properties, cytocompatibility, and porcine skin adhesion strength were evaluated. Hm-PVAs had 10 °C higher glass transition temperature than poly(vinyl alcohol) (PVA) (33.4 ± 2.5 °C). The water contact angle (WCA) of the hm-PVA films increased with alkyl chain length and/or hydrophobic group modification ratio. The tensile strength of the hm-PVA films decreased with increasing alkyl chain length and/or hydrophobic group modification ratio. Hm-PVA with short chain lengths (4 mol% propanal-modified PVA; 4C3-PVA) had low cytotoxicity compared with long alkyl chain length hm-PVAs (4 mol% hexanal and nonanal-modified PVA; 4C6-PVA and 4C9-PVA). The 4C3-PVA film had the highest porcine skin adhesion strength. Thus, 4C3-PVA film is promising as an adhesive for wearable medical devices.

2.2. Introduction

Wearable sensors are integrated into soft materials. They directly contact the body to monitor the health condition and provide clinically relevant data [1]. Most research in this field has involved testing rigid electronic devices developed by the semiconductor industry [2]. Recently, the research focus has shifted towards wearable sensing platforms with stretchable and flexible electronics and excellent mechanical properties. A typical method of fabricating soft sensors consisted of integrating conducting material patterns into a stretchable substrate [3-6]. However, these materials do not adhere to skin and must be affixed with commercially available adhesives.

Commercially available acrylic-based medical bandages are currently used to affix wearable sensors [7]. Acrylic-based adhesives have high adhesion strength. Nevertheless, they may cause massive exfoliation of the stratum corneum and severe pain [8, 9]. Moreover, the chemical residues they leave on the skin surface may induce allergic and inflammatory reactions [10]. Pressure-sensitive silicone-based adhesives were developed that have a low propensity for inducing exfoliation of the stratum corneum [11, 12]. On the other hand, their skin retention is weak and they shift easily [13]. Furthermore, they are relatively expensive. Bioinspired skin adhesives with various multiscale architectures were recently reported. They include patches simulating gecko feet [14, 15], microneedles [16], octopus suckers [17], and mussel [18]. However, their fabrication processes are complex and impractical for mass production.

Polyvinyl alcohol (PVA) is a hydrophilic, biodegradable, and biocompatible polymer. It has been widely used in in biotechnology and biomedicine as it has excellent physicochemical properties, is easy to process, and is highly cytocompatible [19-21]. PVA has been used to fabricate contact lenses, wound dressings, and suture and catheter coatings [22]. It has excellent film-forming and adhesive properties on soft tissues [23]. It is, therefore, biocompatible and non-irritating to skin [24]. However, the skin adhesion strength of PVA film is low relative to commercial adhesives as it is highly hydrophilic and water soluble. Various techniques for insolubilizing PVA have been reported. One method applying a crosslinking agent to the hydroxyl groups in PVA [25, 26]. Another involves serially freeze-thawing the PVA to form hydrogels with strong hydrogen bonds [27-29]. Insoluble PVA film was also produced by modifying a hydrophobic functional group [30].

In our previous studies, we used hydrophobically modified biopolymers to prepare surgical sealants [31-33], films [34, 35], porous membranes [36], and nanoparticles [37] for adhesion to soft biological tissue. Hydrophobic modification enhances bonding strength even to wet soft tissues. The most important factors increasing the interfacial strength are the anchoring effect of the hydrophobic groups to phospholipid membranes [38] and enhancement of the interactions between amphiphilic polymers and extracellular proteins [31]. We hypothesized that the hydrophobic modification of PVA should strengthen its adhesion to soft tissue such as skin. The hydrophobic group could anchor phospholipid membranes of corneocytes on stratum corneum and enhance the interactions with keratinocyte lipids (ceramide, fatty acid, cholesterol).

Here, we synthesized hydrophobically modified poly(vinyl alcohol) (hm-PVA) with various alkyl chain lengths (3, 6, and 9 methylene carbons). We tested the theory that PVA with alkyl groups will be adhesive. Bonding, shearing and peeling of hm-PVA and cell adhesion to hm-PVA films were also evaluated.

2.3. Materials and methods

2.3.1. Materials

Ethanol (EtOH, 99.5%), dimethyl sulfoxide (DMSO), 6N hydrochloric acid (HCl), 10% (v/v) formalin in neutral buffer solution, Dulbecco's phosphate buffered saline (D-PBS), and 99.9% dimethyl

sulfoxide-d_6 (DMSO-d_6) with 0.05% (w/v) tetramethylsilane (TMS) were purchased from Wako Pure Chemical Industries Ltd. (Osaka, Japan). Otsuka normal saline 2-port was acquired from Otsuka Pharmaceutical Co., Ltd. (Tokyo, Japan). PVA (M_W = 88,000; saponification degree > 98.5%) was procured from Nacalai Tesque, Inc. (Kyoto, Japan). Propanal (C3), hexanal (C6), and nonanal (C9) were obtained from Tokyo Chemical Industry Co. Ltd. (Tokyo, Japan). Normal human dermal fibroblasts (NHDF) were purchased from Lonza Biologics (Invitrogen, Portland, OR, USA). Triton X-100 stock solution was acquired from Cayman Chemical Co. Ltd. (Biomol GmbH, Hamburg, Germany). The nuclear stain 4',6-diamidino-2-phenylindole dihydrochloride (DAPI) solution was procured from Dojindo Laboratories (Tokyo, Japan). Medium 106 and TrypLE™ Express were obtained from Thermo Fisher Scientific (Tokyo, Japan). Low-serum growth supplement (LSGS), penicillin/streptomycin solution, and phalloidin-tetramethyl rhodamine B isothiocyanate peptide from *Amanita phalloides* were purchased from Sigma-Aldrich Corp. (St. Louis, MO, USA). Porcine skin was acquired from Tokyo Shibaura Organ Co. Ltd. (Tokyo, Japan). The porcine skin was washed and shaved with a clipper (Thrive MODEL 515R, Daito Electric Industry, Osaka, Japan).

2.3.2. Synthesis of hm-PVA

The hm-PVAs were prepared by nucleophilic substitution reaction between aldehydes and the PVA hydroxyl groups following a previously reported procedure [25, 39]. PVA (10 g) was dissolved in 98 mL H_2O at 80 °C for 60 min. Then 100 mL DMSO and 2 mL of 1 N HCl were added to the solution to form a 200-mL solution comprising 5% (w/v) PVA and 1% (v/v) 1 N HCl. Various amounts of aldehyde groups (C3, C6, and C9) were added to the solution and the mixtures were stirred at 50 °C for 1 h. A reflux condenser was used in all processes. The hm-PVA (H_2O/DMSO = 50/50 (v/v)) product was added to 600 mL cold ethanol and the mixture was stirred for 1 h. The precipitated hm-PVAs were washed at least thrice with 300 mL EtOH to remove any unreacted aldehyde and DMSO. The solvent was evaporated under vacuum to obtain purified white hm-PVAs crystals which were then finely ground in a mill (Wonder Crusher WC-3; Osaka Chemical, Osaka, Japan).

2.3.3. Characterization of hm-PVAs

The chemical structures of the hm-PVAs were analyzed by nuclear magnetic resonance (^{1}H-NMR) spectroscopy (AL300; JEOL Ltd., Tokyo, Japan) using a 0.5% (w/v) hm-PVA/DMSO-d_6 solution at 25 °C. Each sample was scanned 8 times. Fourier transform-infrared spectroscopy (FT-IR; 8400S, Shimadzu Corp., Kyoto, Japan) was conducted to confirm the presence of acetal groups in the hm-PVAs. The scan range was 700–4,000 cm^{-1} and each sample was scanned 64 times. The hydrophobic group modification ratios of the hm-PVAs were determined by ^{1}H-NMR spectroscopy. The modification ratios were calculated as follows:

$$\text{Modification ratio (mol\%)} = [\{\text{Integral area } (CH_3 \text{ proton})/3\}\ c\ /\text{Area } (\alpha\text{CH proton})] \times 100 \qquad (1)$$

where the integral area (αCH proton) is the area of the peak at 3.87 ppm corresponding to the αCH proton in the PVA and hm-PVA backbones and the integral area (CH_3 proton) is the area of the peak at 0.85 ppm assigned to the CH_3 proton in the hydrophobic groups of the hm-PVAs.

2.3.4. Glass transition temperature of hm-PVAs

In this study, PVA and hm-PVAs powders were dried at 40 °C under vacuum for 24 h before DSC measurement. The glass transition temperatures (Tg) of the hm-PVAs were determined by differential scanning calorimetry (DSC) based on the technical standards established by the American Society for Testing and Materials (ASTM) E1356-03 [40]. Briefly, approximately 15 mg of each hm-PVA was placed in an aluminum pan and sealed with an autosealer. Thermograms were recorded in the range of -50 °C to 100 °C by DSC (Thermo Plus EVO 8230; Rigaku Corporation, Tokyo, Japan) at a heating rate of 10 °C min^{-1} under a N_2 atmosphere.

2.3.5. Preparation of hm-PVA films

Hm-PVAs were dissolved in 40% (v/v) aqueous EtOH to obtain a 1% (w/v) solution. The hm-PVA solutions were then poured into silicone moulds 1 mm thick. These were dried on a clean bench (As One, Osaka, Japan) at 25 °C overnight. The dry hm-PVA films were peeled off from the silicone sheets. Surface morphology was observed by scanning electron microscopy (SEM, S4800, Hitachi Co., Tokyo, Japan). And the thickness of hm-PVA films was measured with a coolant proof micrometer (MDC-MX, Mitutoyo Corporation, Kanagawa, Japan).

2.3.6. Tensile strength of hm-PVA films

The tensile strengths of the hm-PVA films were determined according to the Japanese Industrial Standard (JIS) K 7161. Briefly, hm-PVA films were cut into standard rectangles 150 mm long and 15 mm wide. The tensile strengths of the hm-PVA films were measures with a texture analyzer (TA-XT2i; Stable Micro Systems, Godalming, UK) at a tracking speed of 5 mm min^{-1}.

2.3.7. Surface wettability measurement of hm-PVA films

The water contact angles (WCA) of the hm-PVA films were measured with a contact angle meter (sessile drop method) (CAM; DM700; Kyowa Interface Science, Saitama, Japan). The hm-PVA films were placed on a glass sheet and deionized (DI) water was added to them dropwise to evaluate their water wettability.

2.3.8. Cytocompatibility test of hm-PVAs

Normal human dermal fibroblasts (NHDF) were cultured in Medium 106 (Thermo Fisher Scientific, Waltham, MA, USA) supplemented with 10% (w/v) low-serum growth supplement (LSGS) (Sigma-Aldrich Corp., St. Louis, MO, USA) under standard cell culture conditions (sterility; 37 °C; humidified 5% CO_2 atmosphere). One hundred microliters culture medium containing 5×10^3 NHDF cells was placed in each well of 96-well plates and incubated for 24 h to ensure cell adhesion to the polystyrene surface. The culture medium in each well was then removed. Then 100-μL culture medium aliquots containing various hm-PVA concentrations were added to each well. After incubation for an additional 24 h, 10 μL cell count reagent (WST-8) was added to each well followed by incubation for 2 h. The absorbances of the well contents were measured at 450 nm in a microplate reader (Spark10M; Tecan, Osaka, Japan). All operations were conducted on a clean bench (As One, Osaka, Japan). The actin cytoskeletons of the NHDF cells were stained with phalloidin-tetramethyl rhodamine B isothiocyanate peptide and their nuclei were stained with DAPI. Briefly, the media was removed and the wells were washed with phosphate-buffered saline (PBS) solution. Then 100 μL fresh fixative solution (4% (v/v) paraformaldehyde (PFA) in PBS) was added to each well and the cells

were fixed at room temperature for 15 min. The fixative solution was then removed and the wells were washed with PBS. Then 0.2% (v/v) Triton X-100 solution was added to each well and left for 10 min at room temperature. The Triton X-100 was then removed by washing thrice with PBS. Blocking solution (1% (v/v) BSA in PBS) was added to each well and left for 1 h. After removing the blocking solution, 400 μL phalloidin-tetramethyl rhodamine B isothiocyanate peptide in 1% (v/v) BSA (1:100 dilution) was added to each well and left for 1 h. Each well was then washed at least thrice with PBS. DAPI in PBS (1:100 dilution) was added to each well, left for 10 min, and washed thrice with PBS. The stained cells were then observed under an inverted fluorescence phase contrast microscope (BZ-X700; Keyence Co., Tokyo, Japan).

2.3.9. Bonding strength measurement of the hm-PVA films

Bonding strengths of the hm-PVA films on porcine skin were determined according to ASTM F2258-05. Briefly, porcine skin was cut into 25 mm × 25 mm squares and placed on the surface of a heater set to 37 °C. A sterile cotton surgical gauze was used to remove excess moisture from the skin surfaces. The hm-PVA films (25 mm × 25 mm) were applied to the skin and 50 μL of 40% (v/v) EtOH was dropped on the film surfaces to induce them to swell. The bonding energy of hm-PVA films was measured by texture analyzer (TA-XT2i; Stable Micro Systems, Godalming, UK) at 2 N applied force, 3 min waiting time, and 10 mm min^{-1} tracking speed.

To elucidate the adhesion mechanism, a cross-section of the porcine skin was observed after the bonding test. It was fixed in 10% (v/v) formalin neutral buffer solution, stained with hematoxylin and eosin (H&E), and examined under an inverted fluorescence phase contrast microscope (BZ-X700; Keyence Co., Tokyo, Japan).

2.3.10. Lap-shear strength measurement of hm-PVA films

The lap-shear strengths of the hm-PVA films were evaluated according to ASTM F2255-05. Briefly, porcine skin was cut into 50 mm × 25 mm rectangles and placed on the surface of the heater set to 37 °C. A sterile cotton surgical gauze was used to remove excess moisture from the skin surfaces. The hm-PVA films (length 25 mm, width 10 mm) were applied to skin rectangles. Then, 20 μL of 40% (v/v) EtOH was dropped on the film surface and other pieces of skin were superimposed on them. A 200 g weight was placed on each composition and left there at 37 °C for 3 min. The lap-shear strengths of the hm-PVA films were measured by texture analyzer at 5 mm min^{-1} tracking speed.

2.3.11. T-peel strength measurement

The T-peel strengths of the hm-PVA films on porcine skin were determined according to ASTM F2256-05. Briefly, porcine skin was cut into a 150 mm × 15 mm rectangles and excess moisture was removed from them with a mesh. The hm-PVA films were applied to the skin rectangles and 40% (v/v) EtOH was sprayed onto them. After drying at 25 °C for 1 h, the peeling strengths of the hm-PVA films (150 mm × 15 mm) were established by texture analyzer at 200 mm min^{-1} tracking speed. The average values of the peeling force were calculated over a 40–100 mm displacement range.

2.3.12. Statistical analysis

Statistical analysis was carried out using Tukey-Kramer test with KyPlot software. Statistically significant differences were accepted when $p < 0.05$. Data were presented as means ± standard deviations (SD).

2.4. Results and discussion

2.4.1. Synthesis and characterization of hm-PVAs

The chemical structures of hm-PVAs with various alkyl chain lengths (C3, C6, and C9) are shown in Figure 2-1a. From the SEM images, it was indicated that the light transmissive hm-PVA films were flat. The hm-PVAs were prepared via the reaction between the hydroxy groups of PVA and aldehydes (Figure 2-1b) according to a previously reported procedure [25, 39]. Under acidic conditions, aldehydes react with hydroxyl groups by nucleophilic substitution and rapidly form stable hexagonal ring structures [39]. Figure 2-1c shows the ^{1}H-NMR spectra for hm-PVAs with different numbers of methylene carbons. The chemical shifts at 0.85 ppm and 1.26 ppm were assigned to the CH_3 and αCH_2 protons, respectively, in the hydrophobic groups of the hm-PVAs. Thus, the aldehyde groups were successfully introduced into the PVA molecules. The hm-PVA structure was also analyzed by FT-IR spectra (Figure 2-1d). The peak at 2,930 cm^{-1} was attributed to the C-H stretching vibration of αCH_2 in the acetal groups of the hm-PVAs. Therefore, hm-PVAs with different numbers of methylene carbons were successfully synthesized. The modification ratios of the hydrophobic groups (Table 2-1) were calculated from the ^{1}H-NMR data.

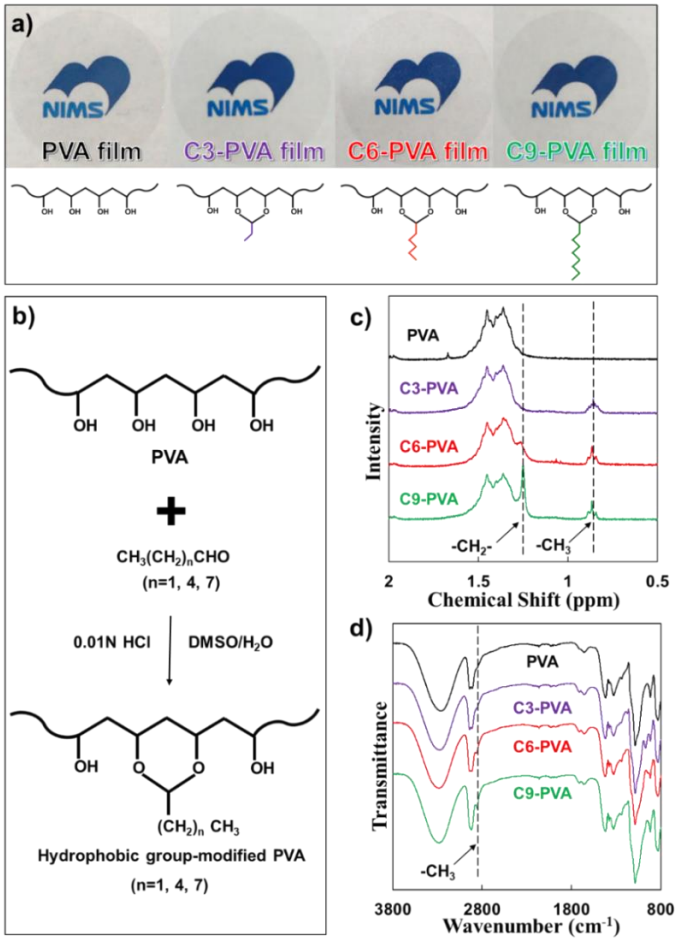

Figure 2-1. a) Photographs and chemical structures of various hm-PVA films. b) Synthesis of hm-PVAs. c) ^{1}H-NMR and d) FT-IR spectra for the hm-PVAs.

Table 2-1. Modification ratios of the hm-PVAs.

Abbreviation	Hydrophobic group reagent	Hydrophobic group reagent addition (mol%)	Hydrophobic group modification (mol%)
4C3-PVA	Propanal	10	4
12C3-PVA	Propanal	25	12
23C3-PVA	Propanal	50	23
4C6-PVA	Hexanal	10	4
4C9-PVA	Nonanal	10	4

2.4.2. Glass transition temperature of hm-PVAs

The glass transition temperatures (Tg) of the hm-PVAs were determined by DSC as previously reported [40]. The results shown in Figure 2-2b and 2-2d were obtained from the thermal analysis curve (Figure 2-2a and 2-2c). In Figure 2-2a, Tg is represented by the intersection of the two dotted lines. In general, Tg of polymer increases with an increasing of molecular weight [41]. The Tg of PVA (Mw = 89,000-98,000; saponification degree = 99%) is 28.9 °C [40]. This result is close to the Tg (33.4 ± 2.5 °C) of unmodified PVA (Mw = 88,000; saponification degree > 98.5%) measured in this study. However, the Tg of PVA (Mw = 115,000; saponification degree = 100%) increases to 80 °C due to higher molecular weight [42]. Interestingly, the unmodified PVA had the lowest Tg whereas the Tg for 4C3-PVA, 4C6-PVA, and 4C9-PVA rose to 47.1 ± 0.3 °C, 45.7 ± 2.2 °C, and 44.5 ± 3 °C, respectively (Figure 2-2b). However, there were no significant differences among the hm-PVAs of varying alkyl chain length in terms of Tg. In contrast, the Tg of 12C3-PVA and 23C3-PVA were 43.8 ± 0.6 °C and 51.3 ± 0.7 °C (Figure 2-2d). The Tg of the hm-PVAs was 10 °C higher than that of PVA as a consequence of hydrophobic modification resulting from alkyl chain (C3, C6, and C9) aggregation. These findings also confirmed the successful integration of the alkyl groups into the PVA molecules.

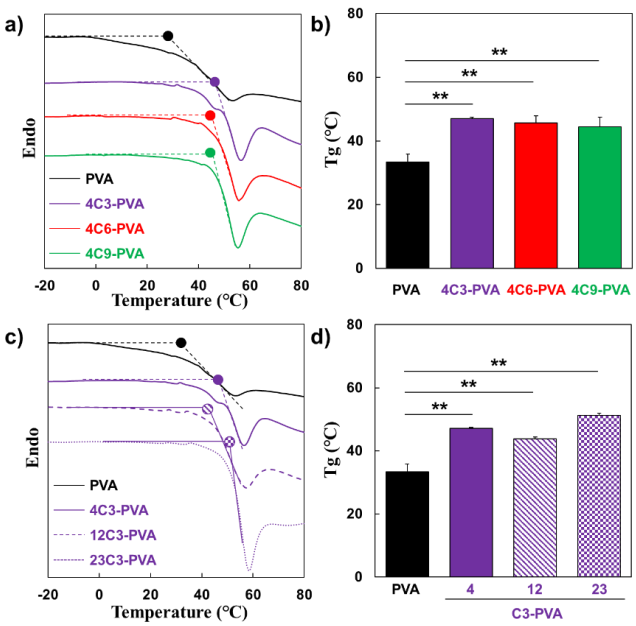

Figure 2-2. Thermal analysis of hm-PVAs. a), b) Glass transition temperatures of hm-PVAs with different alkyl chain lengths. c), d) Glass transition temperatures of C3-PVAs with various hydrophobic modification ratios. Data are means ± S.D. (**P < 0.01, n = 3).

2.4.3. Tensile strength of hm-PVA films

Figure 2-3a shows the tensile strengths of hm-PVA films with various alkyl chain lengths. The tensile strengths decreased with increasing alkyl chain length. The stretching strength of the original PVA film was 105.5 ± 6.7 MPa. The tensile strength of pure PVA film is reported to be 40-90 MPa [43, 44]. These values are lower than PVA film used in this study. The reason for this phenomenon is that PVA (saponification degree > 98.5%) used in this study has higher saponification degree compared with previous reports (88%-98%). For the 4C3-PVA film it was 96.9 ± 4.3 MPa and the values for the 4C6-PVA and 4C9-PVA films were 66.0 ± 7.7 MPa and 51.5 ± 9.8 MPa, respectively. A similar trend was observed for the Young's moduli of the various films. For the PVA and 4C3-PVA films, the Young's moduli were 4.5 ± 0.22 GPa and 4.6 ± 0.56 GPa, respectively. In contrast, they were 3.7 ± 0.08 GPa and 2.0±0.24 GPa for the 4C6-PVA and 4C9-PVA films, respectively. Long alkyl chains in the PVA molecule inhibit intermolecular hydrogen bonding. Figure 2-3b shows the ratios of hydrophobic modification to tensile strength. Here, C3-PVA with various modification ratios were used as typical hm-PVA films. The tensile strengths of the C3-PVA films decreased with increasing hydrophobic modification ratio. Relative to 4C3-PVA film, the tensile strengths of the 12C3-PVA and 23C3-PVA films were much lower (47.4 ± 1.6 MPa and 24.3 ± 2.1 MPa, respectively). A similar trend was observed for the Young's moduli of the C3-PVA films with various hydrophobic modification ratios. The Young's moduli for 4C3-PVA, 12C3-PVA, and 23C3-PVA were 4.6 ± 0.56 GPa, 2.5 ± 0.09 GPa, and 1.8 ± 0.04 GPa, respectively. Higher hydrophobic modification ratios inhibit intermolecular hydrogen bonding in C3-PVA.

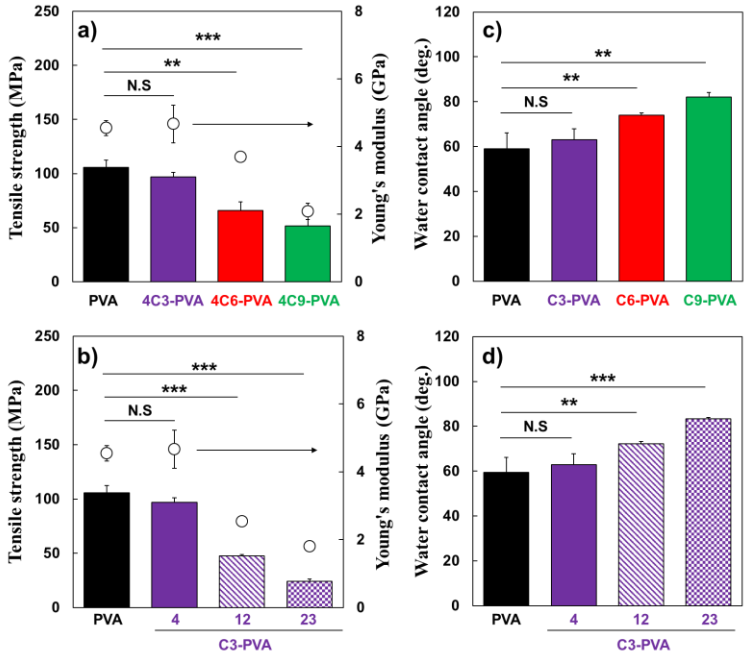

Figure 2-3. a) Tensile strengths of hm-PVA films with different alkyl chain lengths. b) Tensile strengths of C3-PVAs films with various hydrophobic modification ratios. c) Water contact angles of hm-PVA films with different alkyl chain lengths. d) Water contact angles of C3-PVAs films with various hydrophobic modification ratios. Data are means ± S.D. (**P < 0.01, ***P < 0.001, n = 3).

2.4.4. Surface wettability of hm-PVA films

The surface wettability of the films differs between the side exposed to air and that in contact with the substrate [45]. Here, we measured the WCA of hm-PVA films exposed to the air. Figure 2-3c shows the

WCA of hm-PVA films with various alkyl chain lengths and modification ratios. The WCA for the original PVA film was lower (59.4 ± 6.8 °) than those of the hm-PVA films with different alkyl chain lengths (62.8 ± 4.9–83.3 ± 0.6 °). The WCA of the hm-PVA films increased with alkyl chain length. The longer alkyl chains incorporated in the PVA molecule integrated on the surfaces of the hm-PVA films. Figure 2-3d shows that the WCA of the hm-PVA films increased with hydrophobic modification ratio. Film surface hydrophobicity increases with the number of alkyl groups introduced into the PVA molecule.

2.4.5. Cytocompatibility of hm-PVAs

To evaluate hm-PVA cytocompatibility, NHDF cells were cultured under various concentrations of hm-PVAs. Figure 2-4 shows cell viability and conditions after 24 h incubation. Figure 2-4a indicates that the NHDF cells spread over the tissue culture polystyrene (TCPS) surfaces. Cell density decreased with increasing hm-PVA concentration. However, the morphology of the surviving cells did not change. Figure 2-4b shows cell viability at various hm-PVA concentrations. NHDF cell viability was over 80% in medium with low (0.1 mg mL^{-1}) concentrations of all hm-PVAs except 4C3-PVA. Cell viability decreased with increasing hm-PVA concentration. In contrast, NHDF viability was highest at all 4C3-PVA concentrations (0.1–10 mg mL^{-1}). The hm-PVAs with comparatively longer side chains (4C6-PVA and 4C9-PVA) were more toxic than that those with no or shorter side chains (PVA and 4C3-PVA). Thus, 4C3-PVA is relatively nontoxic to skin cells.

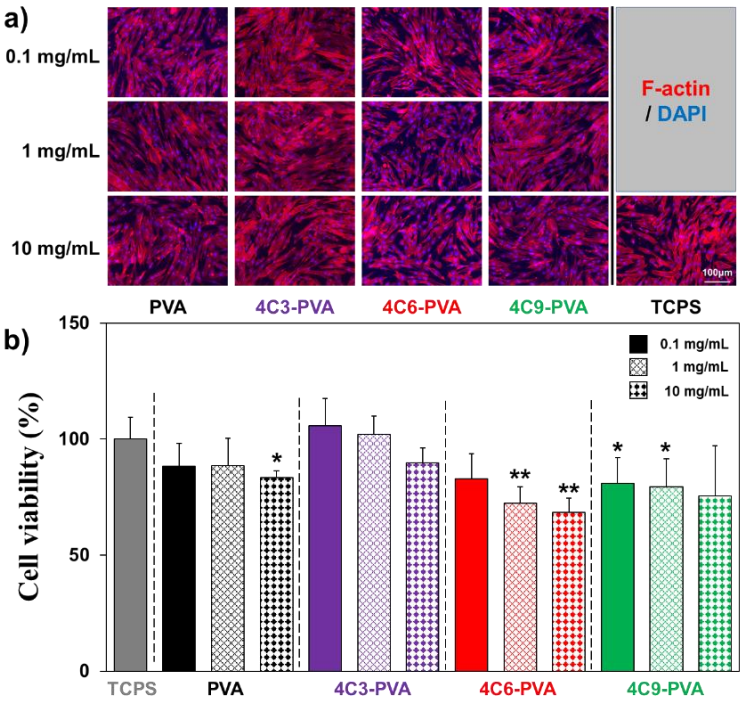

Figure 2-4. Cytocompatibility test of hm-PVAs. a) Staining of NHDF cells with phalloidin-tetramethyl rhodamine B isothiocyanate peptide (red) and DAPI (blue). b) Viability of NHDF cells at various hm-PVA concentrations after 24 h incubation (**$P < 0.01$, n = 4)

2.4.6. Adhesion test of hm-PVA on porcine skin

We determined the adhesive properties of hm-PVA films by measuring bonding, lap-shear, and T-peel strength. Bonding strength was evaluated according to ASTM F2258-05 (Figure 2-5a). Figure 2-5b shows the force-distance curve used to calculate bonding strength. The bonding energy of 4C3-PVA film (5.50 ± 1.45

J m^{-2}) was nearly 5 times higher than that of the original PVA film (1.10 ± 0.23 J m^{-2}) (Figure 2-5c). The 4C6-PVA and 4C9-PVA have longer side chains than those of 4C3-PVA. Nevertheless, the bonding energies of the 4C6-PVA and 4C9-PVA films were 1.94 ± 0.46 J m^{-2} and 1.09±0.15 J m^{-2}, respectively, which were close to that for PVA. The 4C3-PVA film had high wettability and penetrated the gap on the skin surface. Moreover, the tensile strength of 4C3-PVA film was as strong as that of the original PVA film. Thus, the 4C3-PVA film also had high bulk strength. This property substantially enhances the adhesion of the film to the surface. The modified alkyl groups (C3) readily anchored to the skin cell membranes and had strong interfacial adhesion. However, interfacial peeling occurred between the porcine skin surface and the PVA film as the latter has no alkyl side chains. The 4C6-PVA and 4C9-PVA films were anchored by their alkyl groups to the surfaces. Nevertheless, they had low adhesion strength as their wettability was weak and their skin surface gap penetration was poor.

Figures 2-5d-f show the effects of alkyl chain length on hm-PVAs lap-shear strength. This parameter was measured according to ASTM F2255-05 (Figure 2-5d). Figure 2-5e shows the force-distance curve for the lap-shear strength measurement. Figure 2-5f shows the lap-shear strengths of the hm-PVA films on porcine skin. These values were calculated from the force-distance curve (Figure 2-5e). The results indicated that hydrophobic modification enhanced lap-shear strength. The lap-shear strength of the 4C3-PVA film was 2.53 ± 0.71 kPa which was over two times higher than that of the original PVA film (1.12 ± 0.10 kPa). However, the lap-shear strengths of the 4C6- and 4C9-PVA films were comparatively lower than that of 4C3-PVA (2.24 ± 0.17 kPa and 1.72 ± 0.21 kPa, respectively). The anchor effect of the alkyl groups (C3, C6, and C9) drew the hm-PVA films into close contact with the porcine skin surface. Thus, the hm-PVA films had significantly greater resistance to transverse stress than the original PVA film.

Figure 2-5g-i shows the T-peel strength of hm-PVAs after adhesion to porcine skin according to ASTM F2256-05. Figure 2-5h shows the force-displacement curve for the T-peel strength measurement. The T-peel strengths of the hm-PVA films on porcine skin were calculated from this curve (Figure 2-5h). The T-peel strength of 4C3-PVA film was 10.4 ± 1.4 N m^{-1} which was nearly twice that of the original PVA (5.6 ± 1.5 N m^{-1}). However, the peeling force decreased with increasing alkyl chain length. The values for the C6-PVA and the C9-PVA were 9.1±0.7 N m^{-1} and 8.4±1.9 N m^{-1}, respectively. Figure 2-3c indicates that film surface wettability increases with decreasing alkyl chain length. Enhancement of the peeling strength is determined by the balance between surface wettability and alkyl chain anchoring.

Figure 2-5j-l shows the influences of the hydrophobic modification ratio on the bonding and lap-shear strength. Bonding strength decreased with increasing hydrophobic modification ratio because of low wettability (Figure 2-5k). Moreover, shearing strength decreased with increasing hydrophobic modification ratio because of weak hydrogen interactions among hm-PVA molecules (Figure 2-5*l*).

Debonding occurred after the hm-PVA films were applied to porcine skin. Figure 2-6a shows that the PVA film peeled off the entire porcine skin surface. Therefore, interfacial adhesion between original the PVA film and the skin tissue is weak. In contrast, the 4C3-PVA film strongly adhered to the upper and lower skin surfaces. Thus, the alkyl groups (C3) of 4C3-PVA were well anchored to the stratum corneum of the porcine skin. Peeling of the 4C6-PVA and 4C9-PVA films from the film-skin interfaces increased with hydrophobic modification ratio. The 4C6-PVA and 4C9-PVA films had low wettability and, by extension, poor affinity for the porcine skin. Figure 2-6b shows the histology of the hm-PVA film-porcine skin interface after bonding strength measurement. No stratum corneum exfoliation was observed on either tissue surface when the original PVA film was applied. Thus, interfacial adhesion between the PVA film and the skin was quite weak. High stratum corneum exfoliation rates were confirmed for both skin surfaces when 4C3-PVA film was applied to them. Therefore, this type of film adhered strongly to porcine skin. For the 4C6-PVA and 4C9-PVA films, there was partial stratum corneum exfoliation. For this reason, adhesion and penetration of

these materials on porcine skin were lower than those for 4C3-PVA. These findings are consistent with those shown in Figure 2-6a.

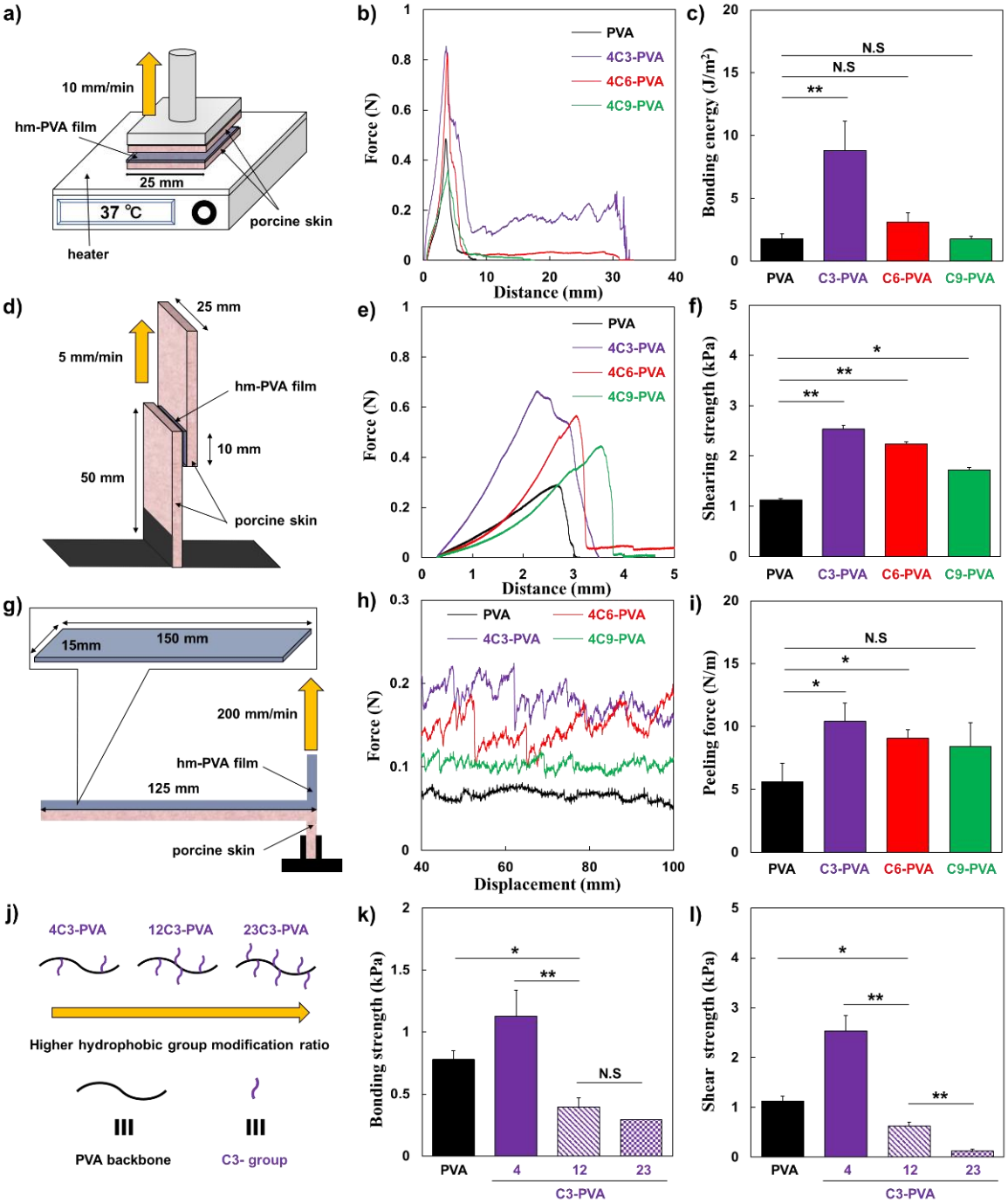

Figure 2-5. Adhesive strength evaluation test. a) Schematic of bonding energy measurement apparatus. b) Force-distance curve for bonding strength measurement. c) Bonding energies of hm-PVA films adhering to porcine skin. d) Schematic of lap-shear strength measurement apparatus . e) Force-distance curve for lap-shear strength measurement. f) Lap-shear strengths of hm-PVA films adhering to porcine skin. g) Schematic of T-peel strength measurement apparatus. h) Force-displacement curve for T-peel strength measurement. i) T-peel strengths of hm-PVA films adhering to porcine skin. j) Structure of C3-PVA with relatively higher hydrophobic group modification ratio. k) Bonding strengths of C3-PVAs films with various hydrophobic modification ratios. l) Lap-shear strengths of C3-PVAs films with different hydrophobic modification ratios. Data are means ± S.D. (*P < 0.05, **P < 0.01, ***P < 0.001, n = 3).

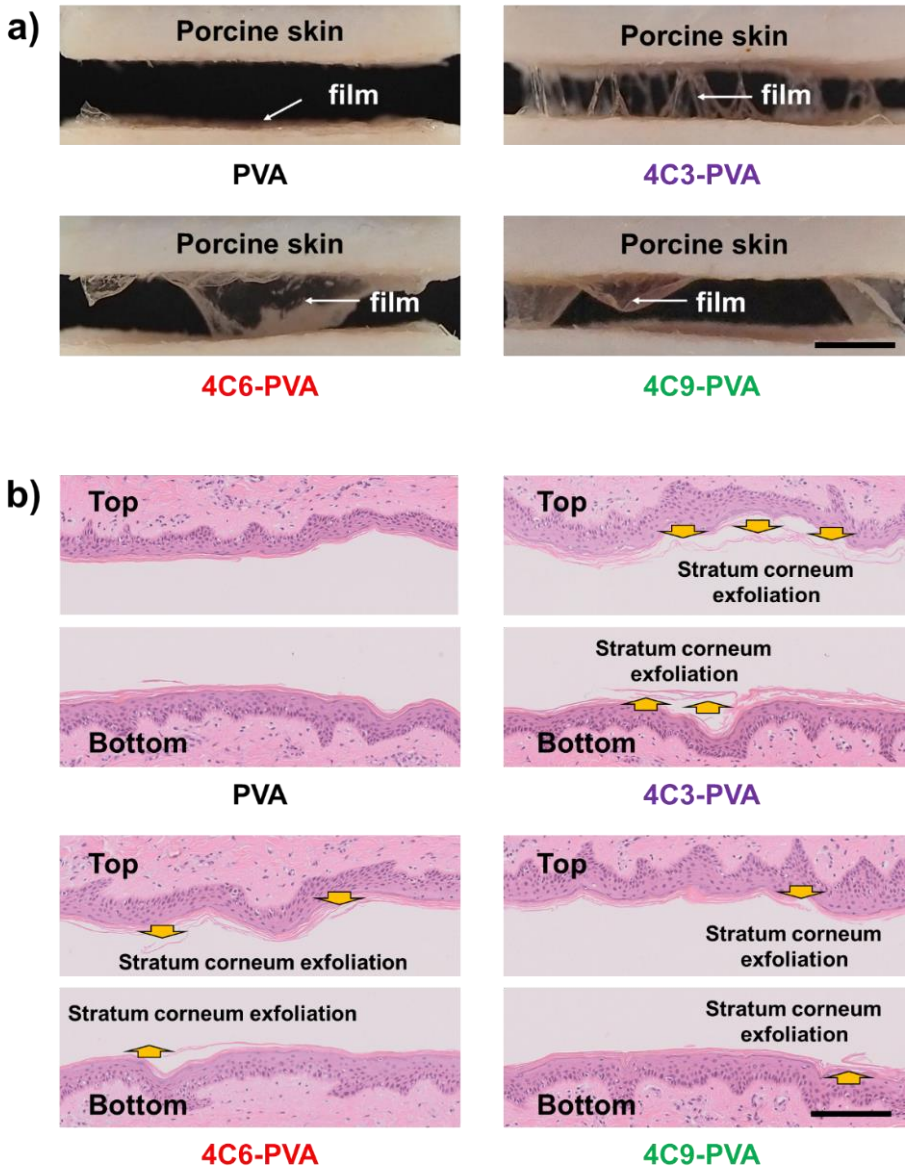

Figure 2-6. a) Bonding strength measurements for hm-PVA films (Scale bar = 5 mm). b) Histology of hm-PVA film-porcine skin interface after bonding strength measurement. Yellow arrow indicates stratum corneum exfoliation site (Scale bar = 100 μm).

Based on the foregoing results, we proposed a bonding mechanism for hm-PVA films on porcine skin and illustrated it in Figure 2-7. During bonding, the PVA and 4C3-PVA films readily penetrate the gap on the skin surface. However, the 4C6-PVA and 4C9-PVA films have low wettability and their penetration in the skin surface is weak. The alkyl groups (C3, C6, and C9) easily anchor to the stratum corneum. The 4C3-PVA film has a large contact surface and numerous alkyl group anchor points. After measuring the bonding strengths, we determined that the PVA film readily peels off the skin surface and causes no stratum corneum exfoliation as it lacks an anchor effect. In contrast, 4C3-PVA film tightly adheres to the skin surface and induces stratum corneum exfoliation as it has a strong alkyl group anchor effect. However, the 4C6-PVA and 4C9-PVA films partially peel off the skin surface and promote relatively little stratum corneum exfoliation as they have low wettability.

Film	Adhesion mechanism	Hydrophobic groups anchor to porcine skin	Bonding/shearing /peeling strength to porcine skin
PVA	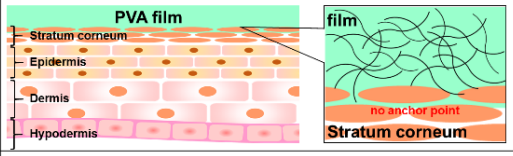	None	Low
4C3-PVA	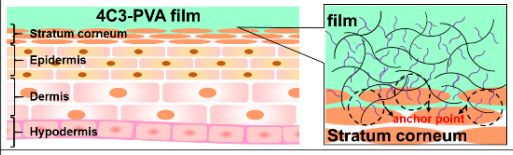	High	High
4C6-, 4C9-PVA	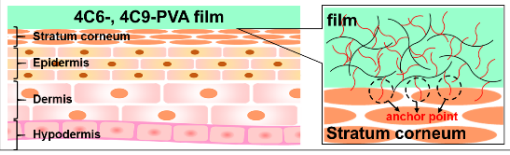	Moderate	Moderate

Figure 2-7. Bonding strength mechanism of hm-PVA films adhering to porcine skin.

2.5. Conclusions

We prepared hm-PVA films and evaluated their surface properties, mechanical strength, and adhesion to porcine skin by measuring their bonding, lap-shear, and T-peel strengths according to ASTM methods. We assessed the cytocompatibility of hm-PVAs in physical contact with skin cells. The water contact angles of the hm-PVA films increased with alkyl chain length and/or alkyl group modification ratio. The tensile strengths of the hm-PVA films decreased with increasing alkyl chain length and/or alkyl group modification ratio. The 4C3-PVA film showed excellent cytocompatibility compared to other hm-PVAs with long alkyl chain lengths (4C6-PVA and 4C9-PVA). When it was applied to porcine skin, it presented with the highest bonding/lap-shear/T-peel strengths. Therefore, 4C3-PVA film may be an effective adhesive or bonding material for wearable medical devices.

References

[1] V. Custodio, F.J. Herrera, G. Lopez, J.I. Moreno, A Review on Architectures and Communications Technologies for Wearable Health-Monitoring Systems, Sensors, 12 (2012) 13907-13946.
[2] B.W. An, J.H. Shin, S.Y. Kim, J. Kim, S. Ji, J. Park, Y. Lee, J. Jang, Y.G. Park, E. Cho, S. Jo, J.U. Park, Smart Sensor Systems for Wearable Electronic Devices, Polymers, 9 (2017).
[3] C. Luo, N.S. Liu, H. Zhang, W.J. Liu, Y. Yue, S.L. Wang, J.Y. Rao, C.X. Yang, J. Su, X.L. Jiang, Y.H. Gao, A new approach for ultrahigh-performance piezoresistive sensor based on wrinkled PPy film with electrospun PVA nanowires as spacer, Nano Energy, 41 (2017) 527-534.
[4] C.X. Hu, Y.L. Zhang, X.D. Wang, L. Xing, L.Y. Shi, R. Ran, Stable, Strain-Sensitive Conductive Hydrogel with Antifreezing Capability, Remoldability, and Reusability, Acs Applied Materials & Interfaces, 10 (2018) 44000-44010.
[5] W.J. Liu, N.S. Liu, Y. Yue, J.Y. Rao, F. Cheng, J. Su, Z.T. Liu, Y.H. Gao, Piezoresistive Pressure Sensor Based on Synergistical Innerconnect Polyvinyl Alcohol Nanowires/Wrinkled Graphene Film, Small, 14 (2018).
[6] S. Park, S.W. Heo, W. Lee, D. Inoue, Z. Jiang, K. Yu, H. Jinno, D. Hashizume, M. Sekino, T. Yokota, K. Fukuda, K. Tajima, T. Someya, Self-powered ultra-flexible electronics via nano-grating-patterned organic photovoltaics, Nature, 561 (2018) 516-+.
[7] M.K. Kwak, H.E. Jeong, K.Y. Suh, Rational Design and Enhanced Biocompatibility of a Dry Adhesive Medical Skin Patch, Advanced Materials, 23 (2011) 3949-3953.
[8] A.J. Singer, J.V. Quinn, J.E. Hollander, The cyanoacrylate topical skin adhesives, Am. J. Emerg. Med., 26 (2008) 490-496.
[9] D.W. Kim, S. Baik, H. Min, S. Chun, H.J. Lee, K.H. Kim, J.Y. Lee, C. Pang, Highly Permeable Skin Patch with Conductive Hierarchical Architectures Inspired by Amphibians and Octopi for Omnidirectionally Enhanced Wet Adhesion, Advanced Functional Materials, 29 (2019).
[10] S.J. Canipa, M.L. Chilton, R. Hemingway, D.S. Macmillan, A. Myden, J.P. Plante, R.E. Tennant, J.D. Vessey, T. Steger-Hartmann, J. Gould, J. Hillegass, S. Etter, B.P.C. Smith, A. White, P. Sterchele, A. De Smedt, D. O'Brien, R. Parakhia, A quantitative in silico model for predicting skin sensitization using a nearest neighbours approach within expert-derived structure-activity alert spaces, Journal of Applied Toxicology, 37 (2017) 985-995.
[11] M. He, Q.Y. Zhang, J.Y. Guo, Synthesis and characterization of silicone based Pressure sensitive adhesive, in: S.Q. Liu, M. Zuo (Eds.) Emerging Focus on Advanced Materials, Pts 1 and 22011, pp. 1773-1778.
[12] A.K. Antosik, P. Bednarczyk, Z. Czech, Aging of silicone pressure-sensitive adhesives, Polymer Bulletin, 75 (2018) 1141-1147.
[13] H. Matsumura, R. Imai, N. Ahmatjan, Y. Ida, M. Gondo, D. Shibata, K. Wanatabe, Removal of adhesive wound dressing and its effects on the stratum corneum of the skin: comparison of eight different adhesive wound dressings, Int. Wound J., 11 (2014) 50-54.
[14] W.G. Bae, D. Kim, M.K. Kwak, L. Ha, S.M. Kang, K.Y. Suh, Enhanced skin adhesive patch with modulus-tunable composite micropillars, Adv Healthc Mater, 2 (2013) 109-113.
[15] X. Chen, R. Mizuta, N. Fukata, T. Taguchi, Design of bio-inspired adhesive surface composed of hexanoyl group-modified gelatin and silicon nanowire, Colloids and Surfaces B-Biointerfaces, 178 (2019) 111-119.
[16] S.Y. Yang, E.D. O'Cearbhaill, G.C. Sisk, K.M. Park, W.K. Cho, M. Villiger, B.E. Bouma, B. Pomahac, J.M. Karp, A bio-inspired swellable microneedle adhesive for mechanical interlocking with tissue, Nat Commun, 4 (2013) 1702.
[17] S. Baik, D.W. Kim, Y. Park, T.J. Lee, S. Ho Bhang, C. Pang, A wet-tolerant adhesive patch inspired by protuberances in suction cups of octopi, Nature, 546 (2017) 396-400.

[18] K. Yamagishi, I. Kirino, I. Takahashi, H. Amano, S. Takeoka, Y. Morimoto, T. Fujie, Tissue-adhesive wirelessly powered optoelectronic device for metronomic photodynamic cancer therapy, Nature Biomedical Engineering, 3 (2019) 27-36.
[19] N. Georgieva, R. Bryaskova, R. Tzoneva, New Polyvinyl alcohol-based hybrid materials for biomedical application, Mater. Lett., 88 (2012) 19-22.
[20] N.H. Sulaiman, M.J. Ghazali, B.Y. Majlis, J. Yunas, M. Razali, Influence of Polyvinylalcohol on the Size of Calcium Ferrite Nanoparticles Synthesized Using a Sol-gel Technique, in: F. Ibrahim, J. Usman, M.S. Mohktar, M.Y. Ahmad (Eds.) International Conference for Innovation in Biomedical Engineering and Life Sciences, Icibel2015, Springer, New York, 2016, pp. 198-202.
[21] X. Chen, T. Taguchi, Hydrophobically modified poly(vinyl alcohol)s as antithrombogenic coating materials, Materials Science & Engineering C-Materials for Biological Applications, 102 (2019) 289-298.
[22] T.S. Gaaz, A.B. Sulong, M.N. Akhtar, A.A.H. Kadhum, A.B. Mohamad, A.A. Al-Amiery, Properties and Applications of Polyvinyl Alcohol, Halloysite Nanotubes and Their Nanocomposites, Molecules, 20 (2015) 22833-22847.
[23] M. Chaouat, C. Le Visage, W.E. Baille, B. Escoubet, F. Chaubet, M.A. Mateescu, D. Letourneur, A Novel Cross-linked Poly(vinyl alcohol) (PVA) for Vascular Grafts, Advanced Functional Materials, 18 (2008) 2855-2861.
[24] A. Miyamoto, S. Lee, N.F. Cooray, S. Lee, M. Mori, N. Matsuhisa, H. Jin, L. Yoda, T. Yokota, A. Itoh, M. Sekino, H. Kawasaki, T. Ebihara, M. Amagai, T. Someya, Inflammation-free, gas-permeable, lightweight, stretchable on-skin electronics with nanomeshes, Nature Nanotechnology, 12 (2017) 907-+.
[25] H.S. Mansur, C.M. Sadahira, A.N. Souza, A.A.P. Mansur, FTIR spectroscopy characterization of poly (vinyl alcohol) hydrogel with different hydrolysis degree and chemically crosslinked with glutaraldehyde, Mater. Sci. Eng. C-Biomimetic Supramol. Syst., 28 (2008) 539-548.
[26] Y. Zhang, P.C. Zhu, D. Edgren, Crosslinking reaction of poly(vinyl alcohol) with glyoxal, Journal of Polymer Research, 17 (2010) 725-730.
[27] C.M. Hassan, N.A. Peppas, Structure and applications of poly(vinyl alcohol) hydrogels produced by conventional crosslinking or by freezing/thawing methods, in: A. Abe (Ed.) Biopolymers/Pva Hydrogels/Anionic Polymerisation Nanocomposites2000, pp. 37-65.
[28] C.M. Hassan, N.A. Peppas, Structure and morphology of freeze/thawed PVA hydrogels, Macromolecules, 33 (2000) 2472-2479.
[29] R. Ricciardi, F. Auriemma, C. De Rosa, F. Laupretre, X-ray diffraction analysis of poly(vinyl alcohol) hydrogels, obtained by freezing and thawing techniques, Macromolecules, 37 (2004) 1921-1927.
[30] H.F. Gao, H. Yang, Characteristics of poly(vinyl alcohol) films crosslinked by cinnamaldehyde with improved transparency and water resistance, J. Appl. Polym. Sci., 134 (2017) 8.
[31] R. Mizuta, T. Ito, T. Taguchi, Effect of alkyl chain length on the interfacial strength of surgical sealants composed of hydrophobically-modified Alaska-pollock-derived gelatins and poly(ethylene)glycol-based four-armed crosslinker, Colloids Surf B Biointerfaces, 146 (2016) 212-220.
[32] Y. Mizuno, R. Mizuta, M. Hashizume, T. Taguchi, Enhanced sealing strength of a hydrophobically-modified Alaska pollock gelatin-based sealant, Biomaterials Science, 5 (2017) 982-989.
[33] R. Mizuta, T. Taguchi, Enhanced Sealing by Hydrophobic Modification of Alaska Pollock-Derived Gelatin-Based Surgical Sealants for the Treatment of Pulmonary Air Leaks, Macromolecular Bioscience, 17 (2017).
[34] K. Yoshizawa, T. Taguchi, Enhanced bonding strength of hydrophobically modified gelatin films on wet blood vessels, Int J Mol Sci, 15 (2014) 2142-2156.
[35] K. Yoshizawa, T. Taguchi, Bonding behavior of hydrophobically modified gelatin films on the intestinal

surface, Journal of Bioactive and Compatible Polymers, 29 (2014) 560-571.
[36] K. Yoshizawa, R. Mizuta, T. Taguchi, Enhanced angiogenesis of growth factor-free porous biodegradable adhesive made with hexanoyl group-modified gelatin, Biomaterials, 63 (2015) 14-23.
[37] A. Nishiguchi, F. Sasaki, H. Maeda, M. Kabayama, A. Ido, T. Taguchi, Multifunctional Hydrophobized Microparticles for Accelerated Wound Healing after Endoscopic Submucosal Dissection, Small (Weinheim an der Bergstrasse, Germany), (2019) e1901566-e1901566.
[38] M. Ito, T. Taguchi, Enhanced insulin secretion of physically crosslinked pancreatic beta-cells by using a poly(ethylene glycol) derivative with oleyl groups, Acta Biomaterialia, 5 (2009) 2945-2952.
[39] K. Tomihata, Y. Ikada, Crosslinking of hyaluronic acid with glutaraldehyde, J. Polym. Sci. Pol. Chem., 35 (1997) 3553-3559.
[40] L.V. Thomas, U. Arun, S. Remya, P.D. Nair, A biodegradable and biocompatible PVA-citric acid polyester with potential applications as matrix for vascular tissue engineering, Journal of Materials Science-Materials in Medicine, 20 (2009) 259-269.
[41] I. Restrepo, C. Medina, V. Meruane, A. Akbari-Fakhrabadi, P. Flores, S. Rodriguez-Llamazares, The effect of molecular weight and hydrolysis degree of poly(vinyl alcohol)(PVA) on the thermal and mechanical properties of poly(lactic acid)/PVA blends, Polimeros-Ciencia E Tecnologia, 28 (2018) 169-177.
[42] J. Rault, R. Gref, Z.H. Ping, Q.T. Nguyen, J. Neel, GLASS-TRANSITION TEMPERATURE REGULATION EFFECT IN A POLY(VINYL ALCOHOL)-WATER SYSTEM, Polymer, 36 (1995) 1655-1661.
[43] S. Peng, M. Zhou, F. Liu, C. Zhang, X. Liu, J. Liu, L. Zou, J. Chen, Flame-retardant polyvinyl alcohol membrane with high transparency based on a reactive phosphorus-containing compound, Royal Society Open Science, 4 (2017).
[44] C. Peng, G. Chen, Preparation and Assessment of Heat-Treated alpha-Chitin Nanowhiskers Reinforced Poly(viny alcohol) Film for Packaging Application, Materials, 11 (2018).
[45] Y. Liang, J.W. Shi, P. Xiao, J. He, F. Ni, J.W. Zhang, Y.J. Huang, C.F. Huang, T. Chen, A lotus-inspired Janus hybrid film enabled by interfacial self-assembly and in situ asymmetric modification, Chemical Communications, 54 (2018) 12804-12807.

Chapter 3

Hydrophobically modified poly (vinyl alcohol)s as antithrombogenic coating materials

3.1. Abstract

Hydrophobically modified poly (vinyl alcohol)s (hm-PVAs) with various alkyl chain lengths (3–12) were synthesized and were coated on poly (propylene) (PP) films. The blood compatibilities of the hm-PVAs-coated films were evaluated. The C6-PVA-coated PP film showed suppressed platelet adhesion as compared to the other hm-PVA-coated PP films, especially the 15C6-PVA-coated PP film, in which 30 mol% of OH groups were substituted by C6 groups. The fibrinogen adsorption was also inhibited on this film. The hydration water structure of the films was analyzed using differential scanning calorimetry (DSC). 15C6-PVA showed the highest (4.8 wt%) intermediate water (IW), and hence exhibited good blood compatibility. The fibrinogen γ chain activity of the 15C6-PVA-coated PP film was 18 % lower than that of the PP film, indicating that hm-PVAs can inhibit fibrinogen γ chain activation. These results showed that by simple hydrophobic modification, PVA could be used as a blood contacting material.

3.2. Introduction

Along with the aging society, patients with vascular and cardiovascular diseases are increasing. These patients often require surgical treatments for implanting stents, artificial heart machines, and hemodialyzers. Since these medical devices directly contact with blood, they are easily recognized as foreign bodies by the biological defense system. Under this circumstance, hemostasis, inflammation, and thrombus formation are evoked [1-3]. In order to minimize the biological defense reactions, biocompatible medical devices should be used. Moreover, the surface of blood-contacting devices should be antithrombogenic to ensure normal blood flow.

In general, there are three major approaches to design devices with antithrombogenic surfaces. The first approach is to reduce the interaction between the blood components (fibrinogen, albumin, and platelets) and the device surface. Various antithrombogenic materials such as poly (2-methacryloyloxyethyl phosphorylcholine) (MPC) brushes [4-6], poly (2-methoxyethyl acrylate) (PMEA) coatings [7], and poly (ethylene glycol) (PEG) brushes [8, 9] have been reported. The surface of MPC/PEG brushes is super hydrophilic, which can inhibit the protein adhesion. PMEA coating with a massive amount of intermediate water (IW) on the surface can reduce the adhesion of blood components. According to the strength of water-polymer interaction, the hydration water can be classified into three kinds of water. The water which strongly interacts with polymer is nonfreezing water (NFW), and another one weakly interacts with polymer is free water (FW). Between the NFW and FW is intermediate water (IW), and it is known as minimum requirement to cause the polymers to be antithrombogenic [10]. So, the materials mentioned above exhibit remarkable antithrombogenicity. The second approach is to immobilize the biologically active substances (heparin and urokinase (UK)) on the device surface [11, 12]. Heparin activates the anticoagulant function of antithrombin and thus suppresses blood coagulation. By taking into consideration the fibrinolytic activity of UK, which is a plasminogen activator, an antithrombogenic material has been developed by immobilizing it on a material surface. Immobilized UK can catalytically transform plasminogen into plasmin in the blood, which shows antithrombogenicity by constantly dissolving the fibrins produced on the material surface. The third approach is to cover the biomaterial surface with endothelial cells [13]. This kind of surface can resist the interaction between blood protein effectively because of mimicking the structure of blood vessel. Among these approaches for the development of antithrombogenic polymeric materials, the first one is the most widely adopted.

Platelet adhesion is the most crucial step for the thrombus formation. The platelet adhesion can be stimulated by adsorption and conformational alteration of fibrinogen which has a platelet bonding site at c terminus in the γ chain [14, 15]. Therefore, inhibiting the adsorption or conformational alteration of fibrinogen is a facile approach to improve antithrombogenicity on device surfaces.

PVA is known as an antithrombogenic material [16]. The low protein adsorption and the good blood compatibility of PVA can be attributed to the hydrophilic surface. However, PVA coating is not stable in blood due to high water solubility. To overcome this drawback, some researches on modified PVA were conducted [17-19]. In the previous study, it was reported that alkylated surface could improve the platelet compatibility. The surface grafted with alkyl chains could adsorb albumin from blood, and at the same time inhibit adsorption of fibrinogen, which will also inhibit the adhesion of platelets [17, 20, 21]. Moreover, previous research indicated that polymers such as PMEA and PEG contain methoxy group (C-O-C structure) showed good antithrombogenicity because of high amount of the IW [22]. However, detailed research of antithrombogenic property of hm-PVAs with acetal group (C-O-C structure) has not yet been reported. In this study, we synthesized hm-PVAs with 3, 6, 9, and 12 methylene carbons to examine the prediction that PVA with alkyl group and acetal group will show good antithrombogenicity. The antithrombogenicity of the hm-PVAs was evaluated after coating them on a polypropylene (PP) film by carrying out platelet adhesion tests. The

adsorption behavior of fibrinogen on the hm-PVA-coated PP films was also examined. Furthermore, the hydration water structure of the hydrated hm-PVAs was analyzed by differential scanning calorimetry (DSC) to elucidate the generation of antithrombogenicity of the hm-PVA-coated PP films.

3.3. Materials and methods

3.3.1. Materials

Ethanol (EtOH, 99.5 %), super dehydrated dimethyl sulfoxide (DMSO), 6N hydrochloric acid (HCl), 10 % formalin neutral buffer solution, Dulbecco's phosphate buffered saline (D-PBS) without Ca and Mg, fibrinogen from human plasma, and 99.9 % dimethyl sulfoxide-d6 (DMSO-d6) containing 0.05 w/v% tetramethylsilane (TMS) were purchased from Wako Pure Chemical Industries, Ltd. (Osaka, Japan). Otsuka normal saline 2-port was purchased from Otsuka Pharmaceutical Co., Ltd. (Tokyo, Japan). The Micro BCA™ protein assay kit was purchased from Thermo Fisher Scientific Ltd. (Waltham, USA). PVA (Mw = 88,000, saponification degree was over 98.5 %), human serum albumin (HSA) from human plasma, and Blocking One (5 wt% bovine serum albumin in PBS) were purchased from Nacalai Tesque, Inc. (Kyoto, Japan). Sodium dodecyl sulfate (SDS), propanal (C3), hexanal (C6), nonanal (C9), and dodecanal (C12) were purchased from Tokyo Chemical Industry Co., Ltd (Tokyo, Japan). Mouse monoclonal anti-human fibrinogen γ antibody and hydrogen peroxidase (HRP) conjugated goat anti-mouse IgG antibody were purchased from Abcam Co., Ltd (Cambridge, England). ELISA TMB (hydrogen peroxide and tetramethylbenzidine) and stop solutions (1 N H_2SO_4) were purchased from R & D Systems Co., Ltd. (Minneapolis, America). The polypropylene (PP) film (thickness = 200 μm) was purchased from Acricaundy Co., Ltd. (Tokyo, Japan).

3.3.2. Synthesis of hm-PVAs

The hm-PVAs were prepared through the nucleophilic substitution reaction between an aldehyde and the hydroxy groups of PVA by following a previously reported procedure [23-27]. First, PVA (10 g) was dissolved in 98 mL of H_2O at 80 ℃ for 1 h. To this solution, 100 mL of DMSO and 2 mL of 1N HCl were added to form a 200 mL solution of 5 w/v% PVA and 1 v/v% 1N HCl. DMSO was added to sufficiently disperse the aldehyde group into the solution and to prevent product precipitation. Different amounts of aldehyde groups (C3, C6, C9, C12) were added into the solution, and the resulting mixtures were stirred at 50 ℃ for 1 h. A reflux condenser was used in all the processes. After the reaction, the resulting hm-PVA (H_2O/DMSO = 50/50 (v/v)) solution was added to 600 mL (around 3 times) cold EtOH under stirring for 1 h. The hm-PVAs precipitated from the solution. The precipitate obtained was washed with 300 mL of EtOH at least three times to remove the unreacted aldehyde and DMSO. Afterwards, the solvent was evaporated under vacuum to obtain purified hm-PVAs as white crystals. Finally, the crystals were crushed finely using a crusher (Wonder crusher WC-3, Osaka Chemical, Osaka, Japan).

3.3.3. Characterization of hm-PVA

The chemical structures of the hm-PVAs were analyzed by proton nuclear magnetic resonance (^{1}H NMR) spectroscopy (AL300, JEOL, Tokyo, Japan) using a 0.5 w/v% hm-PVA/DMSO-d6 solution at 25 ℃. The number of scans was 8 times for each sample. Fourier transform infrared spectroscopy (FT-IR, 8400S, Shimadzu, Kyoto, Japan) analysis was carried out to confirm the presence of acetal groups in the hm-PVAs. The scan range was 700 cm^{-1} to 4000 cm^{-1} and the number of scans was 64 times for each sample. Hydrophobic

group modification ratios of the hm-PVAs were determined by ^{1}H NMR spectroscopy. The modification ratios were calculated by following equation:

$$\text{Modification ratio (mol\%)} = [\{\text{Integral area } (CH_3 \text{ proton})/3\} / \text{Integral area } (\alpha CH \text{ proton})] \times 100$$

where integral area (CH_3 proton) is the area of peak at 0.85 ppm assigned to the CH_3 proton in the hydrophobic groups in the hm-PVAs, integral area (αCH proton) is the area of peak at 3.87 ppm corresponded to the αCH proton in the backbone of PVA or hm-PVAs.

3.3.4. Solubility of the hm-PVAs

The hm-PVAs were dissolved in H_2O/EtOH solvent at 80 °C to form a 1w/v% solution. Dissolution was qualitatively confirmed (○Soluble; △Slightly Dissoluble; ×Insoluble).

3.3.5. Swelling degree of the hm-PVAs

The hm-PVAs were dissolved in H_2O/EtOH solvent to form a 5w/v% solution. The solution was poured into a mold (4mm×4mm×0.4mm) followed by drying in a clean bench for over 24 h to obtain a hm-PVA film. The hm-PVA film was cut into small size (ϕ = 10 mm) by punch. The hm-PVA films were then accurately weighted and placed in 25 mL centrifuge tubes. 20 mL of MQ water / normal saline / PBS was poured into each tube, and the tubes were incubated at 37 °C. The samples were removed after 1, 3, and 5 min, blotted with a soft paper to remove the surface water, and weighted. The degree of swelling was calculated according to the following equation:

$$Ds = (Ws - Wd)/Wd \times 100\%$$

where W_d is the weight of the dry film, and W_s is the weight of the swollen film.

3.3.6. Preparation of hm-PVA-coated PP films

The hm-PVA-coated PP films were prepared using the dip coating method. First, the PP film surface (ϕ = 10 mm) was exposed to an ultraviolet (UV) light (185 and 284 nm) (MIYATA ELEVAM, Kanagawa, Japan) for 30 min to remove the organic pollutants on it and to oxidize it. The film was then dipped into a 1 w/v% hm-PVA (H_2O/EtOH) solution for 5 s, followed by drying in a clean bench for over 24 h. The surface of the hm-PVA-coated PP films was characterized using a contact angle meter (sessile drop method) (CAM, DM700, Kyowa Interface Science, Saitama, Japan), FT-IR (8400S, Shimadzu, Kyoto, Japan), atomic force microscope (AFM, MFP-3D-BIO, Asylum Research, Santa Barbara, USA), and X-ray photoelectron spectroscopy (XPS, Quantera SXM, Nippon Steel & Sumikin Technology, Tokyo, Japan).

3.3.7. Stability of hm-PVAs-coated PP films

The PP film surface (ϕ = 10 mm) was exposed to an UV light for 30 min to remove the organic pollutants on it and to oxidize it. The film was then dipped into a 1 w/v% hm-PVA (H_2O/EtOH) solution for 5 s, followed by drying in a clean bench for over 24 h. After that, the hm-PVAs-coated PP films were incubated in PBS solution at 37 °C for 1h and 24 h. The remained membranes were confirmed by FT-IR measurement.

3.3.8. In vitro platelet adhesion and platelet activation test

Platelet adhesion tests were performed according to a previously reported method [28-32]. First, platelet-rich plasma (PRP) was obtained from the whole blood of Wistar rats by centrifugation. Then, the plasma solution (200 μL) was seeded on each hm-PVA-coated film. These films were subsequently incubated at 37 °C for 1 h. Each hm-PVA-coated PP film was then rinsed with D-PBS and fixed by immersing in 10 % neutral buffered formalin for 2 h. Finally, each film was rinsed with Milli-Q water and subjected to critical point drying using tert-butyl alcohol. The adhered platelets were observed using scanning electron microscopy (SEM, S4800, Hitachi, Tokyo, Japan). Platelet attachment was quantified by acquiring 9 random SEM images from three parallel experiments and evaluated by ImageJ software. The shape of platelet is usually used to represent the grade of platelet activation [33]. The morphology of the adhered platelets was also investigated by SEM observation.

3.3.9. Quantification of protein adsorption on the hm-PVA-coated PP films

The amount of proteins adsorbed on the surface of the hm-PVA-coated PP films was determined by conducting a Micro BCA™ assay according to a previously reported method [22, 28, 29]. Each hm-PVA-coated PP film was immersed in a 1 mg/mL human fibrinogen/D-PBS solution or 5 mg/mL HSA/D-PBS solution and was then incubated at 37 °C for 1 h. After the incubation, each hm-PVA-coated PP film was rinsed thrice with D-PBS. The adsorbed proteins were extracted by incubating the films in a solution of 5 % sodium dodecyl sulfate (SDS) and 0.1N NaOH at 37 °C for 1 h in a shaking incubator [34, 35]. The extracted proteins were assessed by conducting a Micro BCA assay. In this study, 0.5, 1, 2, 5, 10, and 20 μg/mL protein (fibrinogen and albumin) solutions were used as the standard.

3.3.10. Activity of the fibrinogen γ chain

The activities of the fibrinogen γ chains adsorbed onto the hm-PVA-coated PP films were evaluated by immunochemistry [33]. In brief, the hm-PVA-coated PP films were immersed in a 1 mL fibrinogen (1 mg/mL) solution in a tube and were then incubated at 37 °C for 1 h. Subsequently, the hm-PVA-coated PP films were rinsed thoroughly with D-PBS to remove any loosely adhered fibrinogen. The surface of the hm-PVA-coated PP films was then blocked with Blocking One (5 wt% bovine serum albumin in PBS) for 1 h at 37 °C followed by washed with D-PBS. Then, the hm-PVA-coated PP films were incubated in a 1 mL solution of mouse monoclonal anti-human fibrinogen γ antibody (100 μL of antibody was diluted 200 times using D-PBS) at 37 °C for 1 h. The hm-PVA-coated PP films were then rinsed thoroughly with D-PBS followed by the addition of 500 μL of HRP-conjugated goat anti-mouse IgG antibody (diluted 1000 times using D-PBS) and incubation at 37 °C for 1 h. The hm-PVA-coated PP film was then washed thoroughly with wash buffer (0.1 wt% Tween 20/PBS). Finally, 450 μL of a TMB solution was added to the hm-PVA-coated PP films, and the reaction was carried out in the dark for 20 min. The reaction was terminated by the addition of 150 μL of 1 N H_2SO_4. The reaction mixture (150 μL) was transferred to a 96-well plate, and its absorbance at 450 nm was measured using a microplate reader (Spark10M, Tecan, Osaka, Japan).

3.3.11. Quantification of the amount of hydration water

The amount of hydration water was determined by DSC (Thermo plus EVO 8230, Rigaku Corporation). Briefly, approximately 5 mg of the hydrated hm-PVAs was placed in an aluminum pan and sealed by an auto sealer. The hydrated hm-PVAs were then cooled to -60 °C at a cooling rate of 5.0 °C/min. The hm-PVAs were held at -60 °C for 5 min and were then heated to 50 °C at the same rate under a nitrogen purge flow. The equilibrium water content (EWC) of polymers was determined using equation:

$$EWC\ (wt\%) = (Ws - Wd)/Ws \times 100\ \%$$

where Wd and Ws are the weights of the dry and hydrated samples, respectively.
The amounts of different types of water in polymers were determined using equation:

$$EWC\ (wt\%) = Wnf + Wi + Wf$$
$$Wf = (\Delta Hc/333.5\ (J/g))$$
$$Wi = (\Delta Hm/333.5\ (J/g)) - Wf$$
$$Wnf = EWC\ (wt\%) - (\Delta Hm/333.5\ (J/g))$$

where Wnf, Wi, and Wf are the amounts of nonfreezing, intermediate, and free waters, respectively; ΔHc and ΔHm are the enthalpy changes during crystallization (around -25 °C) and ice melting (around 0 °C), respectively.

3.3.12. In vitro antithrombogenicity test

The antithrombogenic test was performed according to a previously reported method [36]. Briefly, each hm-PVA-coated PP film was placed in a tube and immersed in 1.0 mL of whole rat blood (Wistar rats, 7–11 weeks old, Charles River, Japan) at 37 °C for 30 min. After incubation, the hm-PVA-coated PP films were removed and rinsed gently three times with normal saline. The films were then fixed with 10 % neutral buffered formalin and were subjected to critical point drying using tert-butyl alcohol. Finally, the formation of thrombus was observed by SEM (S4800, Hitachi, Tokyo, Japan). All the animal experiments were approved by the Institutional Animal Experiment Committee of the National Institute for Material Science of Japan.

3.3.13. Statistical analysis

Statistical analysis was carried out using Tukey-Kramer test with KyPlot software. Statistically significant differences were accepted when $p < 0.05$. Data were presented as means ± standard deviations (SD).

3.4. Results and discussion

3.4.1. Synthesis and characterization of hm-PVAs

The hm-PVAs were prepared via the reaction between the hydroxy groups of PVA and an aldehyde (Figure 3-1a) according to a procedure reported previously [23-27]. Under acidic conditions, aldehydes reacted with hydroxyl groups via a nucleophilic substitution reaction to a stable hexagonal ring structure was obtained eventually [23-27]. Figure 3-1b shows ^{1}H NMR spectra of the hm-PVAs with different number of methylene carbons. The chemical shift at 2.54 ppm and 3.33 ppm were assigned to H_2O and DMSO-d6 respectively. The chemical shifts ranged from 1.26 ppm to 1.56 ppm corresponded to the βCH_2 proton in the backbone of PVA and hm-PVA. And the chemical shift at 3.87 ppm corresponded to the αCH proton in the backbone of PVA

and hm-PVA [23]. The chemical shift at 0.85 ppm was assigned to the CH_3 proton of the hydrophobic groups in the hm-PVAs. The chemical shift at 1.26 ppm corresponded to the CH_2 proton of the hydrophobic groups in the hm-PVAs [25, 37]. Besides, the peak increased in the following order: C3-PVA< C6-PVA < C9-PVA < C12-PVA. The longer alkyl group, the higher amount of CH_2 proton of the hydrophobic groups in the hm-PVA. These results indicated that the reaction between the hydroxy groups of PVA and the aldehyde was successful. Figure 3-1c shows the FT-IR spectra of the hm-PVAs with different number of methylene carbons. The wavenumber at 3180-3550 cm^{-1} corresponds to the unreacted hydroxy groups of the hm-PVAs. The peak observed at 1,080 cm^{-1} corresponds to the antisymmetric stretch of the C-O-C bonds in the acetal groups of the hm-PVAs [24]. The peak at 2,930 cm^{-1} corresponded to the C-H stretch of αCH_2 in the hydrophobic groups of the hm-PVA. These results confirmed that the hm-PVAs with different number of methylene carbons were successfully synthesized.

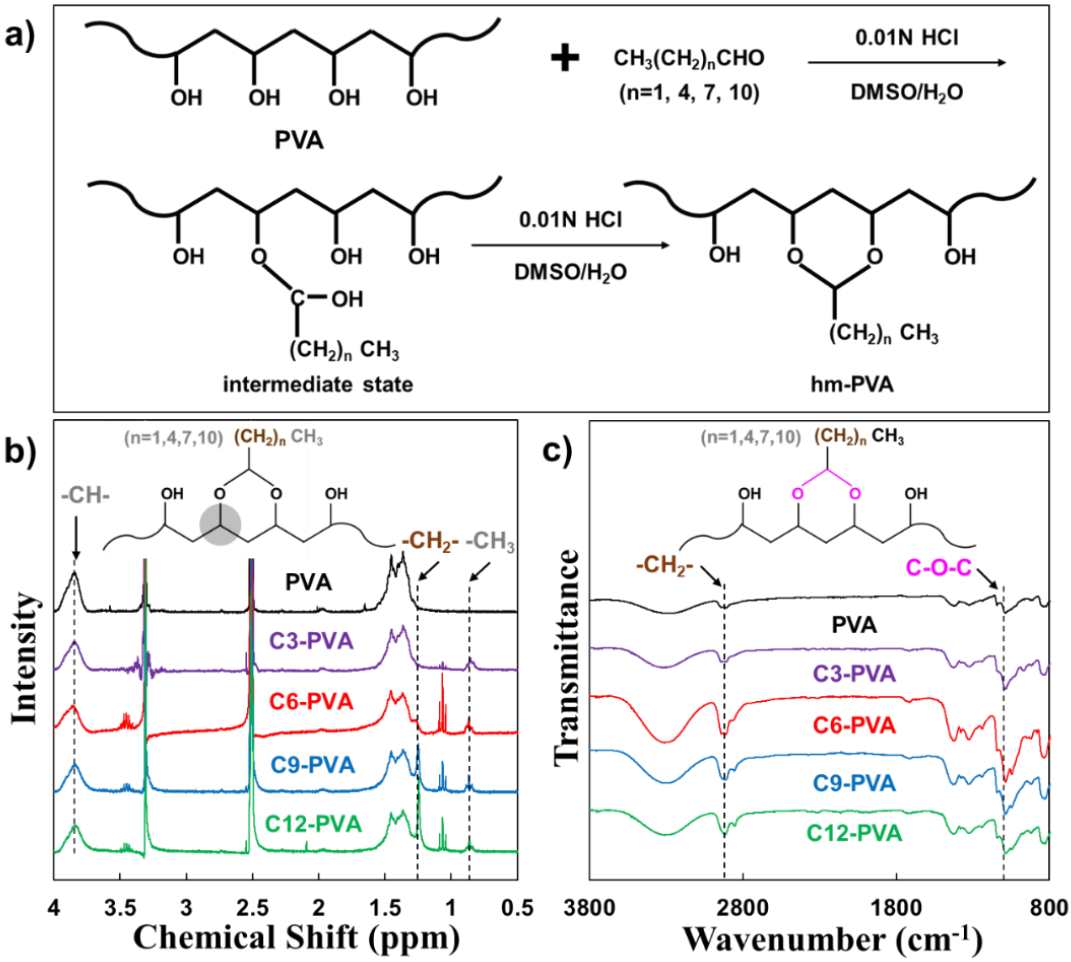

Figure 3-1. a) Synthesis of the hm-PVAs. 1H NMR b) and FT-IR c) spectra of the hm-PVAs.

The number of hydroxy groups of PVA was same to the αCH proton in backbone of PVA molecule. So, it was easy to calculate the hydrophobic modification ratio from equation 1. The modification ratio of the hydrophobic groups (shown in Table 3-1) was calculated using the ^1H NMR results. As can be seen from Table 1, the modification ratio increased with an increase in the addition of aldehyde (C3, C6, C9, and C12). About 50 mol% aldehyde was introduced into PVA molecules.

Table 3-1. Modification ratio of the hm-PVAs.

Abbreviation	Hydrophobic group reagent	Hydrophobic group reagent added (mol%)	Hydrophobic group modification (mol%)
4C3-PVA	Propanal	10	4
12C3-PVA	Propanal	25	12
23C3-PVA	Propanal	50	23
4C6-PVA	Hexanal	10	4
15C6-PVA	Hexanal	25	15
19C6-PVA	Hexanal	50	19
4C9-PVA	Nonanal	10	4
17C9-PVA	Nonanal	25	17
3C12-PVA	Dodecanal	10	3

3.4.2. Preparation of hm-PVA-coated PP films

The hm-PVA-coated PP films were prepared using the dip coating method. As shown in Figure 3-2, 20C9-PVA, 19C12-PVA, and 23C12-PVA were not soluble in the H_2O/EtOH solution. Therefore, these three hm-PVAs were not used in this study. Bare PP films (UV(-)-PP) were irradiated with UV light (at 185 and 284 nm) for 30 min to remove the organic pollutants on their surfaces for obtaining UV-treated PP films (UV(+)-PP). The hm-PVAs were dip-coated on the UV(+)-PP films to obtain the hm-PVA-coated PP films. The formation of these films was confirmed by carrying out sessile drop contact angle measurements.

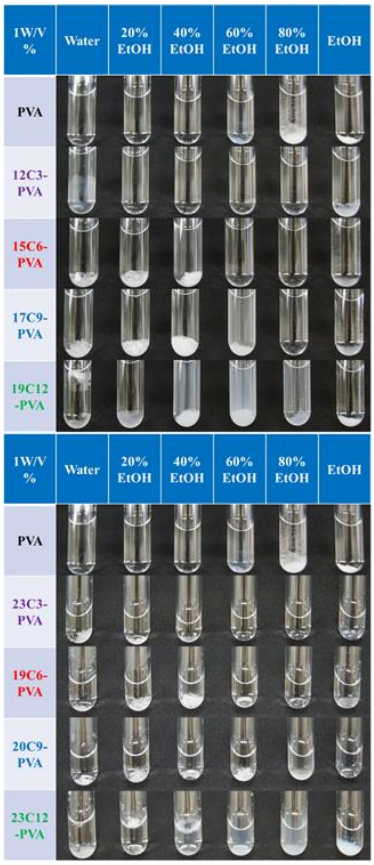

1W/V %	Water	20% EtOH	40% EtOH	60% EtOH	80% EtOH	EtOH
PVA	○	○	○	△	×	×
12C3-PVA	×	○	○	○	○	×
15C6-PVA	×	×	×	○	○	×
17C9-PVA	×	×	×	×	○	×
19C12-PVA	×	×	×	×	×	×

1W/V %	Water	20% EtOH	40% EtOH	60% EtOH	80% EtOH	EtOH
PVA	○	○	○	△	×	×
23C3-PVA	×	×	×	△	○	×
19C6-PVA	×	×	×	×	○	×
20C9-PVA	×	×	×	×	×	△
23C12-PVA	×	×	×	×	×	×

Figure 3-2. Solubility of the hm-PVAs in an H2O/EtOH solution.

Figure 3-3a shows the water contact angles of the hm-PVA-coated PP films. The water contact angle of UV(+)-PP in air was smaller (65.3°) than that of UV(-)-PP (102.6°). The PVA-coated PP film showed the lowest water contact angle of 48.2°. The water contact angle of the PVA-coated PP films increased with an increase in the alkyl chain length. In addition, the water contact angles of the 4C3-PVA-, 12C3-PVA-, and 23C3-PVA-coated PP films increased with an increase in the modification ratio of the hydrophobic groups. Similar trend was observed for the C6-PVA- and C9-PVA-coated PP films. Figure 3-3b Shows the FT-IR spectra of the hm-PVA-coated PP films. Due to the structure of the UV(-)-PP film, it was easy to find that the peak of stretch of C-H at 2,930 cm^{-1} assigned to αCH_2 in PP. The hm-PVA-coated PP films showed peaks at 3,430 and 1,080 cm^{-1} corresponding to the stretching of the hydroxyl groups and antisymmetric stretching of the C-O-C bonds in the hm-PVAs, respectively. These results were consistent with those shown in Figure 3-1c. This confirms that the hm-PVAs were successfully coated on the surface of the UV(+)-PP films.

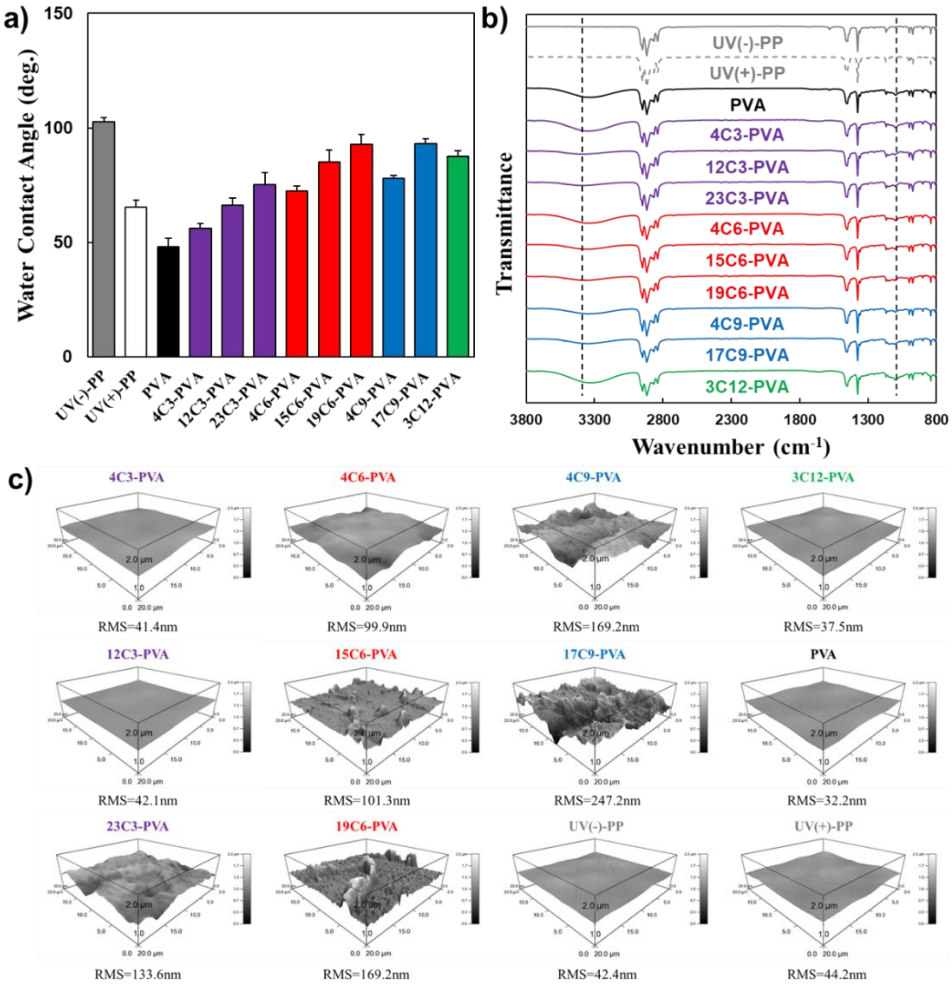

Figure 3-3. a) Water contact angles of the hm-PVA-coated PP films. b) FT-IR spectra of the hm-PVA-coated PP films c) AFM images of the hm-PVA-coated PP films, scale bar: 20 μm.

Figure 3-3c shows the AFM images of the hm-PVA-coated PP films and their root mean square (RMS) surface roughness. The UV(-)-PP and UV(+)-PP films showed flat surfaces and similar RMS surface roughness values (42.4 and 44.2 nm, respectively). However, the surface features of the hm-PVA-coated PP and UV(-)-PP films were significantly different. This indicated that the hydrophobic groups on the hm-PVA-coated PP films affected their surface roughness. The longer the alkyl length and the higher modification ratio, the higher roughness of hm-PVA-coated PP film. The RMS roughness value of the 4C6-PVA-coated PP film

was 99.9 nm, while those of the 15C6-PVA- and 19C6-PVA-coated PP films were 101.3 and 169.2 nm, respectively. Because of hydrophobic interaction, the hm-PVA with longer alkyl chain was easier to aggregate together at hydrophobic unit. The RMS roughness of the films increased with an increase in the modification ratio. And the hm-PVA with higher modification ratio also increased hydrophobic interaction to PP film and hm-PVA. The hm-PVA-coated PP film with more hydrophobic groups showed rougher surface. This result was consistent with those shown in Figure 3-1b.

Figure 3-4 shows the XPS spectra of the hm-PVA-coated PP films. Figures 3-4a, 3-4c, and 3-4e show the C1s spectra of the hm-PVA-coated PP films, while Figures 3-4b, 3-4d, and 3-4f show their O1s spectra. The peak at 283.8 eV corresponds to the C-C and C-H bonds on the surface of the hm-PVA-coated PP films. In the case of the 15C6-PVA-coated PP film, the peak at 285.3 eV can be attributed to its lesser number of C-OH bonds than that of the PVA-coated PP film. This indicates that hydrophobic group (C6) was successfully introduced in PVA molecule. Similar to the C1s peaks, the O1s peaks of the hm-PVA-coated PP films attributing to C-OH bonds showed lower intensities than that of the PVA-coated PP film. The intensity of the O1s peak for 15C6-PVA-coated PP film was significantly lower than that of the O1s peak obtained for the PVA-coated PP film (at 531.8 eV). This could be attributed to the acetalization of the hydroxy groups in the case of the 15C6-PVA-coated PP film (Figure 3-4b). The C/O ratio of the PVA-coated PP film was 1.97, which was the same as that of PVA. This confirmed that PVA was successfully adsorbed on the surface of the PP film. However, the C/O ratio of the 15C6-PVA-coated PP film was 2.71, confirming the presence of hydrophobic C6 groups on the surface (Table 3-2). Interestingly, UV(-)-PP showed a peak at 532 eV attributing to the presence of CHO or COOH groups in it. This indicated that the UV irradiation oxidized the surface of the PP film (Figure 3-4b). As shown in Figures 3-4c and 3-4d, the intensity of the peak at 285.3eV attributing to C-OH bonds decreased with an increase in the hydrophobic group modification ratio. The peaks attributing to C-C and C-H bonds were observed at 283.8 eV. It can be clearly observed that the C/O ratio increased with an increase in the hydrophobic group (C6) modification ratio. The C/O ratios of the PVA-, 4C6-PVA-, 15C6-PVA-, and 19C6-PVA-coated PP films were found to be 1.97, 2.43, 2.71, and 3.14, respectively (Table 3-2). As the number of hydrophobic groups adsorbed on the film surface increased, the hydrophobicity of the surface increased. Therefore, the intensity of the peak at 285.3eV attributing to C-OH bonds decreased with an increase the hydrophobic group length (C3 to C9). On the other hand, the intensity of the peak corresponding to C-C and C-H groups at 283.8 eV increased with an increase in the alkyl chain length (Figure 3-4e, 3-4f). The C/O ratio increased in the following order: PVA- <12C3-PVA- < 15C6-PVA- < 17C9-PVA-coated PP films (1.97, 2.34, 2.71, and 3.35, respectively.), confirming the presence of hydrophobic groups on the surface of the hm-PVA-coated PP films.

Table 3-2. Surface atomic composition of the hm-PVA-coated PP films.

Sample	C 1s (Atomic%)	O 1s (Atomic%)	C/O ratio
UV(-)-PP	99.70	0.30	332.30
UV(+)-PP	93.60	6.40	14.62
PVA	66.36	33.64	1.97
12C3-PVA	70.10	29.90	2.34
4C6-PVA	70.80	29.20	2.43
15C6-PVA	73.02	26.98	2.71
19C6-PVA	75.83	24.17	3.14
17C9-PVA	77.02	22.98	3.35

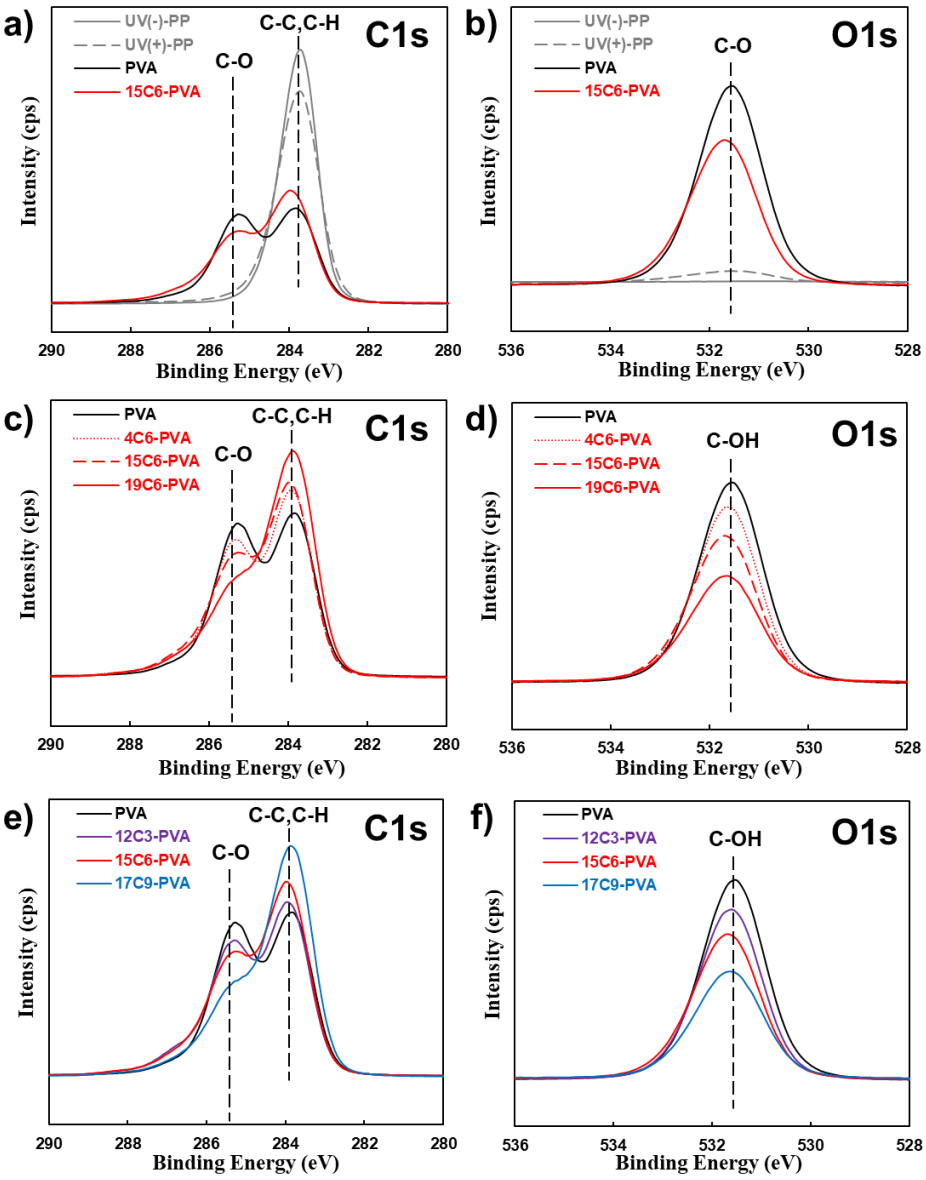

Figure 3-4. XPS spectra of the hm-PVA-coated PP films. a), c), e) C1s spectra of the hm-PVA-coated PP films; b), d), f) O1s spectra of the hm-PVA-coated PP films.

3.4.3. Stability of hm-PVAs-coated PP films

Stability is important parameter for antithrombogenic coating materials. The hm-PVAs-coated PP films were incubated in PBS solution at 37°C for 1h and 24 h. The remained membrane was confirmed by FT-IR measurement. Figure 3-5 shows the FT-IR spectra of hm-PVAs coatings on PP films after incubation in PBS for 1 h and 24 h. The PVA-, 4C3-PVA-, and 12C3-PVA-coated PP films were unstable since they were dissolved in PBS during a short time (1 h). After further incubation for 24 h, 4C6-PVA coated PP film was also dissolved. However, 23C3-PVA-, 15C6-PVA-, 19C6-PVA-, 4C9-PVA-, 17C9-PVA-, and 3C12-PVA-coated PP films were stable in PBS solution in a long period. It was found that the stability of hm-PVA-coating was increased with an increase in the length of hydrophobic group and the hydrophobic modification ratio. The reason why this phenomenon occurred was that longer hydrophobic group and higher modification ratio of hydrophobic group will enhance the hydrophobic interaction between the hm-PVA-coating and PP film.

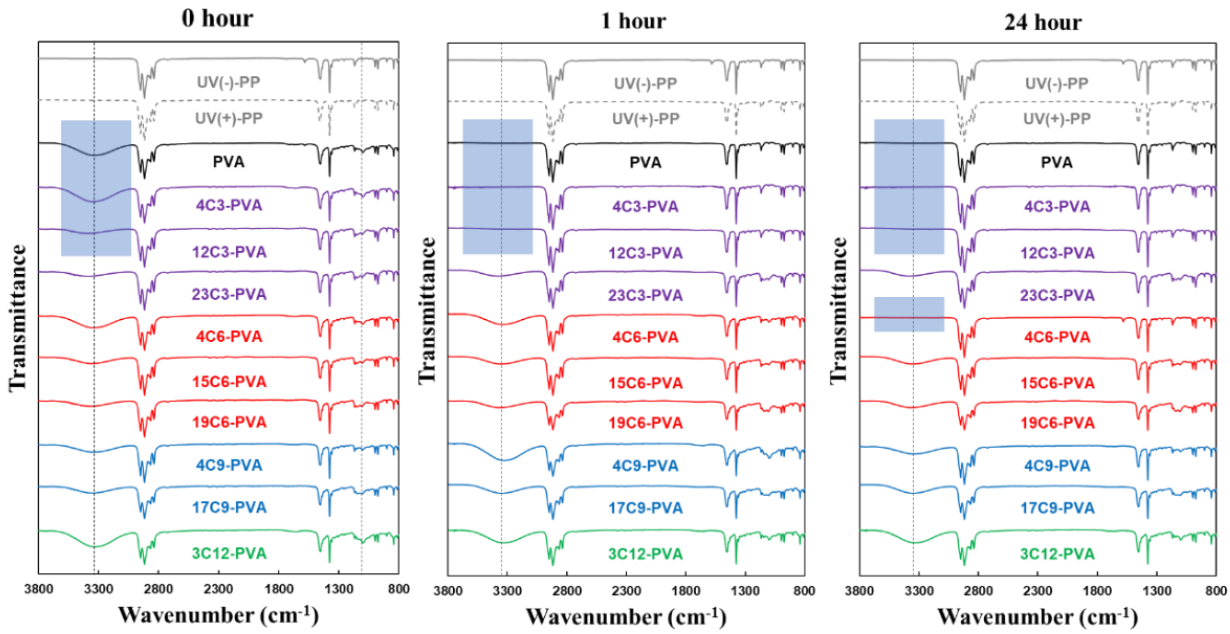

Figure 3-5. Stability of hm-PVAs coating on PP films in PBS at 37℃ for 1 h and 24 h.

3.4.4. In vitro platelet adhesion and activation test

The platelet adhesion/activation of hm-PVA-coated PP films is crucial for the evaluation of thrombus formation. They also affect the biological response when such materials contact with blood. Therefore, platelet adhesion tests were performed on the hm-PVA-coated PP films to evaluate their thrombogenicity. As shown in Figure 3-6a, the number of platelets adhered on UV(+)-PP was 9.95×10^5 cells/cm^2, which is much higher than that of UV(-)-PP (3.3×10^5 cells/cm^2). Platelet adhesion was inhibited on the surfaces of the PVA-, 4C6-PVA-, 15C6-PVA-, 19C6-PVA-, and 4C9-PVA-coated PP films (less than 1.6×10^5 cells/cm^2). On the contrary, the surfaces of the 4C3-PVA-, 12C3-PVA-, 23C3-PVA-, and 17C9-PVA-coated PP films showed increased platelet adhesion (more than 4.6×10^5 cells/cm^2). The UV(-)-PP and 3C12-PVA-coated PP films showed similar platelet adhesion.

We also evaluated the platelet activation on the surface of the hm-PVA-coated films, as shown in Figure 3-6b. The state of activation could be categorized into four main stages: (1) round shaped-adherent, (2) dendritic-partially activated, (3) spread-highly activated, and (4) fully spread-fully activated. Therefore, platelet activation could be qualitatively assessed by examining the extent of pseudopodia formation. The morphology of the platelets adhered on the samples was investigated by SEM (Figure 3-6c). On the surfaces of the PVA-, 4C6-PVA-, and 15C6-PVA-coated PP films, round platelets were predominant (72–92 %) and no spread platelets were observed. On UV(-)-PP, 4C3-PVA-PP, 12C3-PVA-PP, 23C3-PVA-PP, 17C9-PVA-PP, and 3C12-PVA-PP, four stages of platelet adhesion were observed. About 45 % of the platelets adhere on UV(+)-PP were spread or fully spread, indicating that the adhered platelets were highly activated. Interestingly, it was found that the surface roughness affected the platelet adhesion and platelet activation. Compared with 4C9-PVA-coated PP film (roughness = 169.2 nm), the rougher surface 17C9-PVA-coated PP film (roughness = 247.2 nm) adhered 5 times more platelets on the surface. And the spread-highly activated and fully spread-fully activated platelets were found on the surface of 17C9-PVA-coated PP film, while they were not found on the surface of 4C9-PVA-coated PP film. The similar phenomenon was observed on the C3-PVA-coated PP films. The platelet adsorption increased in the following order: 4C3-PVA < 12C3-PVA < 23C3-PVA.

Interestingly, platelet activation was highly inhibited on the surface of the C6-PVA-coated PP film, indicating that C6-PVA exhibited excellent antithrombogenicity.

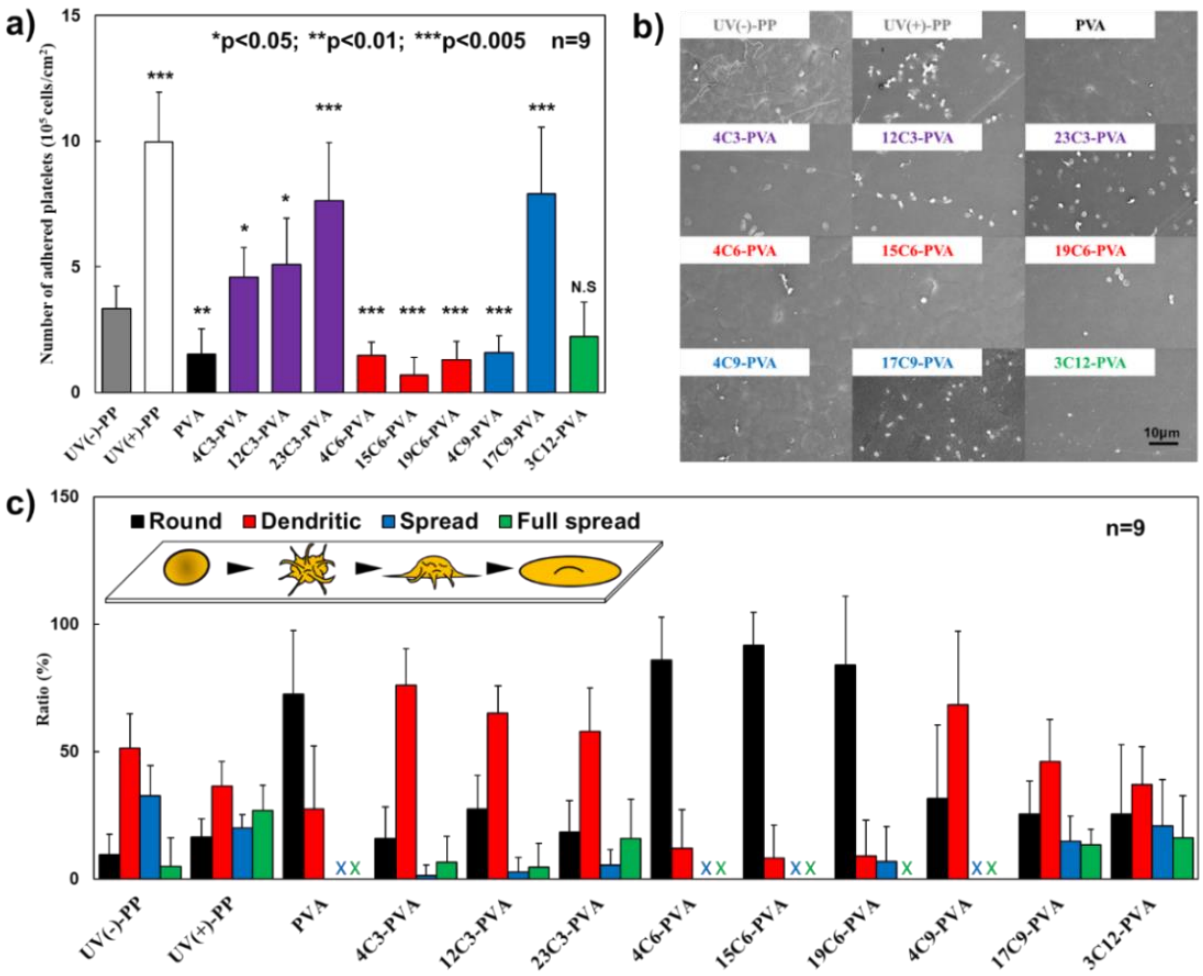

Figure 3-6. a) Number platelets adhered on the hm-PVA-coated PP films. The data represents the mean ± SD (n=9). *p<0.05 versus UV(-)-PP, **p<0.01 versus UV(-)-PP and ***p<0.005 versus UV(-)-PP. b) SEM images of the surfaces of the hm-PVA-coated PP films after incubation in platelet-rich plasma, scale bar: 10 μm. c) Quantitative analysis of morphology of the platelets adhered on the surfaces of the hm-PVA-coated PP films. The Label "x" indicates no platelet found.

3.4.5. Quantification of protein adsorption and activity of fibrinogen γ chain

Platelet adhesion is significantly affected by the amount of proteins adsorbed on the surface. Therefore, we evaluated the adhesion behavior of proteins on the hm-PVA-coated PP films using albumin and fibrinogen. Albumin is the major protein in plasma, and the total concentration of albumin in human plasma is 35–50 mg/mL [38]. On the other hand, fibrinogen is important for evaluating the adhesion behavior of platelets. Figure 3-8a shows the amount of fibrinogen adsorbed on the hm-PVA-coated PP films. The amount of fibrinogen adsorbed on UV(-)-PP was 1.07 μg/cm^2, which is similar to that of UV(+)-PP (1.24 μg cm^{-2}). The amount of fibrinogen adsorbed on the PVA-coated PP film was 0.82 μg/cm^2, which is 23% lower than that adsorbed on UV(-)-PP. In addition, the amounts of fibrinogen adsorbed on the hm-PVA-coated PP films were (27–62%) much lower than that adsorbed on UV(-)-PP film. However, there was no significant difference between the amount of fibrinogen adsorbed on the 4C3-PVA-coated PP film compared with that of UV(-)-PP film, since the stability of 4C3-PVA coating is low. The swelling speed of 4C3-PVA coating was fast (shown in Figure 3-7), and the coating was dissolved at early stage (shown in Figure 3-5). The adsorption increased

further when the alkyl chain length was increased beyond C6. In addition, all the hm-PVA-coated PP films except the C3-PVA-coated PP film showed similar albumin adsorption. It was reported that platelet adhesion could be stimulated by conformational alteration of fibrinogen which has a platelet bonding site at c terminus in the γ chain [14, 15]. And fibrinogen-γ chain activity showed the amount of γ chains on the fibrinogen absorbed surface. The more γ chains on the surface, the more platelet adhesion. The UV(-)-PP and UV(+)-PP films showed similar fibrinogen γ chain activities (Figure 3-8b). The structures of the fibrinogen adsorbed on UV(-)-PP and UV(+)-PP were similar. While, the fibrinogen γ chain activities of the 15C6-PVA- and 17C9-PVA-coated PP films were much lower than that of UV(-)-PP (82 and 80%, respectively), indicating that these hm-PVA films could inhibit the fibrinogen γ chain activation.

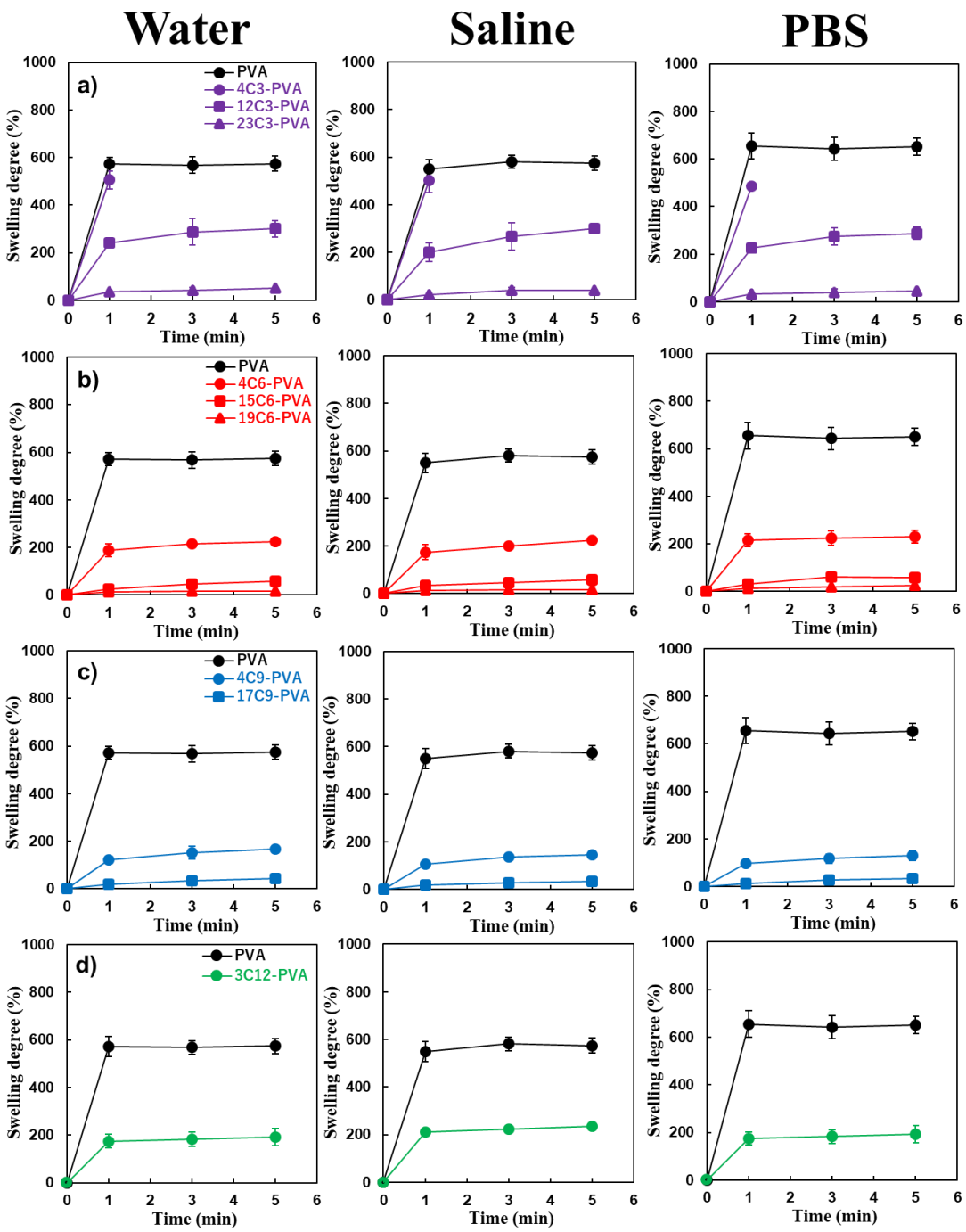

Figure 3-7. Swelling degree of the hm-PVA films with different modification ratios.

3.4.6. Quantification of the amount of hydration water

It has been reported that physicochemical properties of a material, such as hydrophilicity [15] and surface roughness [39], have influence on interface platelet adhesion behavior. In this study, it was found that the surface roughness and modification ratio of hm-PVA-coated PVA affected the platelet adhesion and platelet activation. The platelet adsorption increased in the following order: 4C3-PVA < 12C3-PVA < 23C3-PVA and 4C9-PVA < 17C9-PVA (Table 3-3). However, all C6-PVA-coated PP films showed low platelet adhesion. The platelet adsorption on 15C6-PVA-coated PP film was much lower than that of 12C3-PVA- and 17C9-PVA-coated PP film. In addition, Kobayashi et al. proved that existence of IW was an important factor for platelet adhesion inhibition [22, 28, 29]. Poly(ω-methoxyalkyl acrylate) (PMCxA) coated surface they prepared showed that number of platelets adhered on its surface decreased with an increase in the amount of IW in the hydrated polymer [28]. The generation of IW at interface could be attributed to the introduction of a methoxy group into the side chain terminus of PMCxA. In our study, two C-O-C groups in hexagonal ring structure in the main chain of hm-PVAs, showed similar structure to methoxy group. Hence, we hypothesized that IW may be present in the hm-PVAs as well. We calculated the amount of NFW, IW, and FW in the hydrated hm-PVAs.

Table 3-3. The relationship between the physical property (roughness) and hydration structure (intermediate water content) to the antithrombogenic property.

Abbreviation	Roughness (nm)	Intermediate water (wt%)	Platelet adhesion (10^5 cells/cm^2)	Anti-thrombogenic property
PVA	32.2±0.3	2.9±0.3	1.5±1.0	normal
4C3-PVA	41.4±0.6	3.2±0.1	4.6±1.2	poor
12C3-PVA	42.1±0.2	3±0.2	5.4±1.8	poor
23C3-PVA	133.6±3.9	2.6±0.1	7.6±2.3	poor
4C6-PVA	99.9±1.7	3.1±0.3	1.5±0.5	normal
15C6-PVA	101.3±5.6	4.8±0.2	0.7±0.6	excellent
19C6-PVA	169.2±7.6	4.7±0.1	1.3±0.7	normal
4C9-PVA	169.2±9.5	3.1±0.3	1.6±0.7	normal
17C9-PVA	247.2±9.3	0	7.9±2.6	poor
3C12-PVA	37.5±1.2	3±0.1	2.2±1.4	normal

Figure 3-8c shows the hydration water structure analysis of the hm-PVAs. The NFW content of the hydrated hm-PVAs was approximately 35 wt%. In the case of C3-PVA, the FW content decreased with an increase in the modification ratio. Similar phenomena were observed in C6-PVA, C9-PVA, and C12-PVA. Hydrophobic group modification increased the interaction area (acetal group) which provided the weak hydrogen bonding sites for water molecules. The water molecule moderately interacted with the acetal group was IW. It was found that the hm-PVAs with low modification ratios (4C3-PVA, 4C6-PVA, 4C9-PVA, and 3C12-PVA) showed an IW amount of 3 wt% similar to that of hydrated PVA (2.9 wt%). This phenomenon indicated that low modification ratio could not change the IW content. The length of alkyl chain also affected

the water-polymer interaction. The hydrated C3-PVA showed low IW content (2.6 wt%-3.2 wt%) due to short alkyl chain. The water molecules were easier to bond to two acetal groups as NFW instead of IW. It illustrated that short alkyl chain could not change IW content. Besides, no IW was observed in 17C9-PVA (shown in Figure 3-8c) because of long alkyl chain. Long alkyl chain enhanced the hydrophobicity and reduced the swelling property (shown in Figure 3-2a and Figure 3-7), which affected the hydration water structure on the polymer surface. Interestingly, the hydrated hm-PVA with intermediate alkyl chain (C6) and intermediate modification ratio (15mol%) showed the highest IW content (4.8 wt%) due to adequate acetal groups and moderate hydrophobicity. Therefore, it can be stated that the highest IW content of 15C6-PVA contributed to its low platelet adhesion. Figure 3-8d shows exponential approximation between the number of adhered platelets and IW content. This indicated that the IW content was an important parameter for determining the platelet adhesion of coating materials [22, 28, 29].

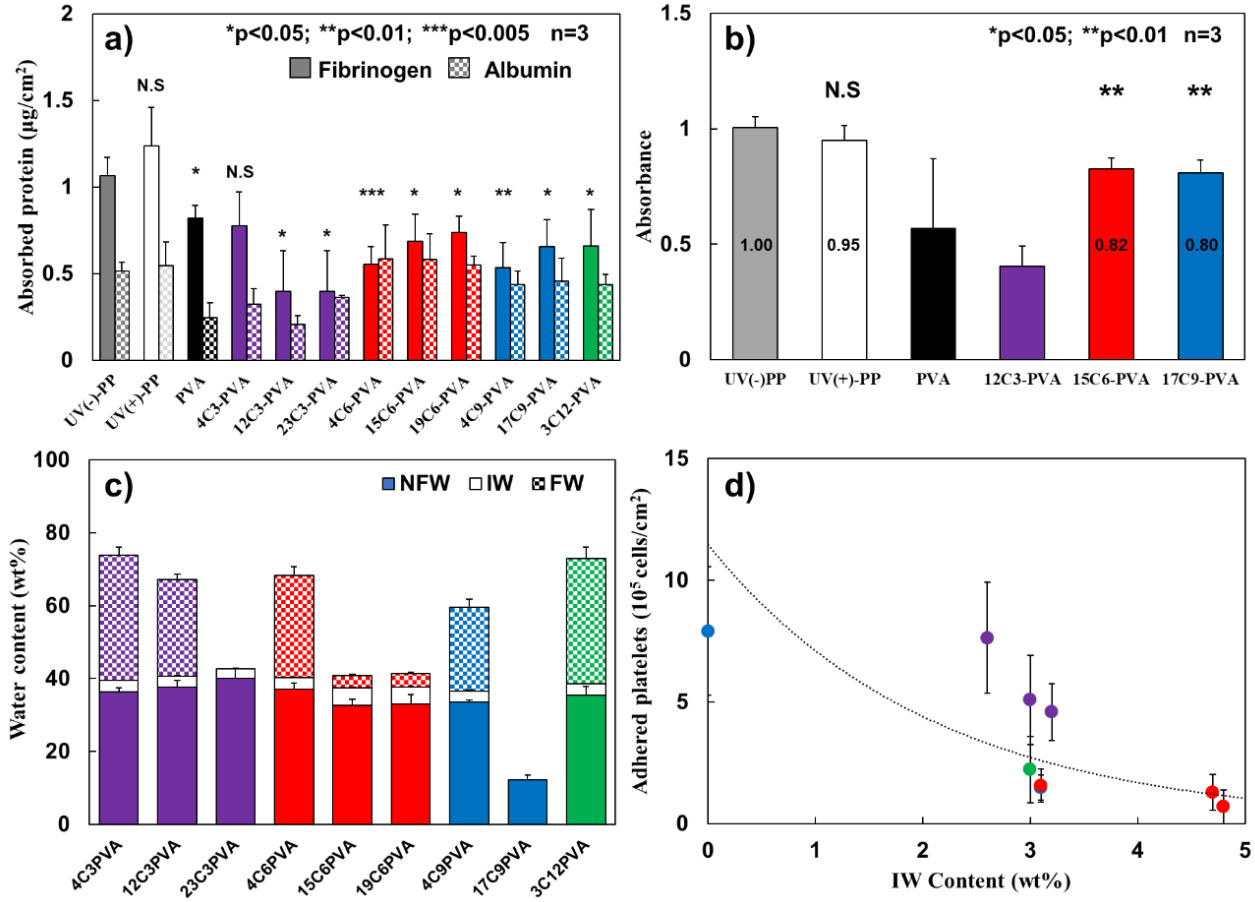

Figure 3-8. a) Analysis of the adsorbed proteins: human fibrinogen and serum albumin on the surfaces of the hm-PVA-coated PP films after incubation for 1 h. b) Fibrinogen γ chain activity on the surface of the hm-PVA-coated PP films. The data represent the mean ± SD (n=3). *p<0.05 versus UV(-)-PP, **p<0.01 versus UV(-)-PP and ***p<0.005 versus UV(-)-PP. c) Thermal and hydration water structure analyses of the hm-PVAs. d) Platelet adhesion on the hm-PVA-coated PP films in PRP as a function of IW content.

3.4.7. In vitro antithrombogenicity test

Figure 3-9 shows the results of the antithrombogenic test on the surface of the hm-PVA-coated PP films. We used eight samples of the hm-PVAs with different alkyl chain lengths for the antithrombogenic test. Macroscopic observation revealed severe thrombus formation on UV(+)-PP and UV(-)-PP. Thrombus formation was not observed on the hm-PVA-coated PP films except for the PVA-coated PP film. SEM

observations revealed that the surface of UV(+)-PP showed platelet adhesion, while UV(-)-PP showed a fibrin network. On the other hand, the PVA coating layer detached from the surface of the PP film. The 17C9-PVA coated-PP film showed some fibrin network formation. Only a small amount of deposition was observed on the surface of the 12C3-PVA- and 3C12-PVA-coated PP films. 4C6-PVA and 15C6-PVA showed smooth surfaces even after immersion in fresh rat blood. No significant differences between C6-PVA-coated PP films were observed. These results were consistent with the platelet adhesion and IW content results. Therefore, the C6-PVA-coated PP films exhibited excellent antithrombogenicity owing to their high IW content.

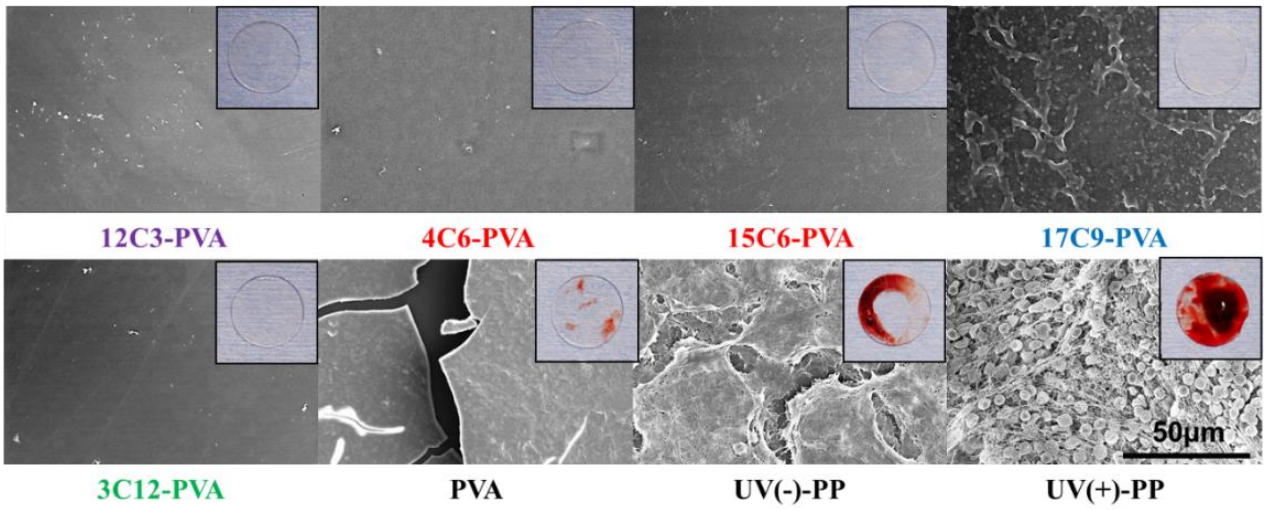

Figure 3-9. SEM images of the hm-PVA-coated PP films after immersion in whole rat blood. The inset shows the macroscopic view of the hm-PVA-coated PP films

3.5. Conclusions

In this study, we successfully synthesized hm-PVAs with acetal group. Among the hm-PVAs-coated PP films, the 15C6-PVA-coated PP film showed the lowest number of adhered platelets. The fibrinogen adsorption was also inhibited on this film. Besides, the fibrinogen γ chain activity of the 15C6-PVA-coated PP film was 18% lower than that of the PP film, indicating that 15C6-PVAs can inhibit fibrinogen γ chain activation. The DSC analysis results revealed that 15C6-PVA exhibited the highest IW content (4.8 wt%), and thus exhibited good blood compatibility. The 15C6-PVA coating exhibited good stability over 24 h. Hence, C6-PVA is expected to be a promising coating material for blood contacting medical devices.

References

[1] J.M. Anderson, A. Rodriguez, D.T. Chang, Foreign body reaction to biomaterials, Seminars in Immunology, 20 (2008) 86-100.
[2] M.B. Gorbet, M.V. Sefton, Biomaterial-associated thrombosis: roles of coagulation factors, complement, platelets and leukocytes, Biomaterials, 25 (2004) 5681-5703.
[3] I.H. Jaffer, J.C. Fredenburgh, J. Hirsh, J.I. Weitz, Medical device-induced thrombosis: what causes it and how can we prevent it?, Journal of Thrombosis and Haemostasis, 13 (2015) S72-S81.
[4] W. Feng, J.L. Brash, S.P. Zhu, Non-biofouling materials prepared by atom transfer radical polymerization grafting of 2-methacryloloxyethyl phosphorylcholine: Separate effects of graft density and chain length on protein repulsion, Biomaterials, 27 (2006) 847-855.
[5] W. Feng, S.P. Zhu, K. Ishihara, J.L. Brash, Adsorption of fibrinogen and lysozyme on silicon grafted with poly(2-methacryloyloxyethyl phosphorylcholine) via surface-initiated atom transfer radical polymerization, Langmuir, 21 (2005) 5980-5987.
[6] K. Ishihara, T. Ueda, N. Nakabayashi, Preparation of phospholipid polymers and their properties as polymer hydrogel membranes, Polymer Journal, 22 (1990) 355-360.
[7] M. Tanaka, A. Mochizuki, N. Ishii, T. Motomura, T. Hatakeyama, Study of blood compatibility with poly(2-methoxyethyl acrylate). Relationship between water structure and platelet compatibility in poly(2-methoxyethylacrylate-co-2-hydroxyethylmethacrylate), Biomacromolecules, 3 (2002) 36-41.
[8] R. Gref, M. Luck, P. Quellec, M. Marchand, E. Dellacherie, S. Harnisch, T. Blunk, R.H. Muller, 'Stealth' corona-core nanoparticles surface modified by polyethylene glycol (PEG): influences of the corona (PEG chain length and surface density) and of the core composition on phagocytic uptake and plasma protein adsorption, Colloids and Surfaces B-Biointerfaces, 18 (2000) 301-313.
[9] J. Ladd, Z. Zhang, S. Chen, J.C. Hower, S. Jiang, Zwitterionic polymers exhibiting high resistance to nonspecific protein adsorption from human serum and plasma, Biomacromolecules, 9 (2008) 1357-1361.
[10] M. Tanaka, K. Sato, E. Kitakami, S. Kobayashi, T. Hoshiba, K. Fukushima, Design of biocompatible and biodegradable polymers based on intermediate water concept, Polymer Journal, 47 (2015) 114-121.
[11] H. Chen, Y. Teramura, H. Iwata, Co-immobilization of urokinase and thrombomodulin on islet surfaces by poly(ethylene glycol)-conjugated phospholipid, Journal of Controlled Release, 150 (2011) 229-234.
[12] L.C. Su, Y.H. Chen, M.C. Chen, Dual Drug-Eluting Stents Coated with Multi layers of Hydrophobic Heparin and Sirolimus, Acs Applied Materials & Interfaces, 5 (2013) 12944-12953.
[13] B.Y. Zhang, M. Montgomery, M.D. Chamberlain, S. Ogawa, A. Korolj, A. Pahnke, L.A. Wells, S. Masse, J. Kim, L. Reis, A. Momen, S.S. Nunes, A.R. Wheeler, K. Nanthakumar, G. Keller, M.V. Sefton, M. Radisic, Biodegradable scaffold with built-in vasculature for organ-on-a-chip engineering and direct surgical anastomosis, Nature Materials, 15 (2016) 669-677.
[14] J.H. Seo, S. Kakinoki, Y. Inoue, T. Yamaoka, K. Ishihara, N. Yui, Designing dynamic surfaces for regulation of biological responses, Soft Matter, 8 (2012) 5477-5485.
[15] L.D. Zhang, B. Casey, D.K. Galanakis, C. Marmorat, S. Skoog, K. Vorvolakos, M. Simon, M.H. Rafailovich, The influence of surface chemistry on adsorbed fibrinogen conformation, orientation, fiber formation and platelet adhesion, Acta Biomaterialia, 54 (2017) 164-174.
[16] Y. Ikada, H. Iwata, F. Horii, T. Matsunaga, M. Taniguchi, M. Suzuki, W. Taki, S. Yamagata, Y. Yonekawa, H. Handa, BLOOD COMPATIBILITY OF HYDROPHILIC POLYMERS, Journal of Biomedical Materials Research, 15 (1981) 697-718.
[17] A.C. Duncan, M.V. Sefton, J.L. Brash, Effect of C-4-, C-8- and C-18-alkylation of poly(vinyl alcohol) hydrogels on the adsorption of albumin and fibrinogen from buffer and plasma: limited correlation with platelet

interactions, Biomaterials, 18 (1997) 1585-1592.
[18] W.F. Ip, M.V. Sefton, PLATELET CONSUMPTION BY POLYVINYL-ALCOHOL COATED TUBING IN CANINES, Journal of Biomedical Materials Research, 25 (1991) 875-887.
[19] J.D. Weaver, D.N. Ku, Biomaterial testing for covered stent membranes: Evaluating thrombosis and restenosis potential, Journal of Biomedical Materials Research Part B-Applied Biomaterials, 100B (2012) 103-110.
[20] M.S. Munro, A.J. Quattrone, S.R. Ellsworth, P. Kulkarni, R.C. Eberhart, ALKYL SUBSTITUTED POLYMERS WITH ENHANCED ALBUMIN AFFINITY, Transactions American Society for Artificial Internal Organs, 27 (1981) 499-503.
[21] W.G. Pitt, T.G. Grasel, S.L. Cooper, ALBUMIN ADSORPTION ON ALKYL CHAIN DERIVATIZED POLYURETHANES .2. THE EFFECT OF ALKYL CHAIN-LENGTH, Biomaterials, 9 (1988) 36-46.
[22] K. Sato, S. Kobayashi, M. Kusakari, S. Watahiki, M. Oikawa, T. Hoshiba, M. Tanaka, The Relationship Between Water Structure and Blood Compatibility in Poly(2-methoxyethyl Acrylate) (PMEA) Analogues, Macromolecular Bioscience, 15 (2015) 1296-1303.
[23] D. Christova, S. Ivanova, G. Ivanova, Water-soluble temperature-responsive poly(vinyl alcohol-co-vinyl acetal)s, Polymer Bulletin, 50 (2003) 367-372.
[24] H.S. Mansur, C.M. Sadahira, A.N. Souza, A.A.P. Mansur, FTIR spectroscopy characterization of poly (vinyl alcohol) hydrogel with different hydrolysis degree and chemically crosslinked with glutaraldehyde, Mater. Sci. Eng. C-Biomimetic Supramol. Syst., 28 (2008) 539-548.
[25] P. Piluso, F.D. Boisson, V. Bounor-Legare, E. Espuche, Acetalization of poly(vinyl alcohol) by a fatty aldehyde in water medium: Model study, kinetics, and structure analysis, J. Polym. Sci. Pol. Chem., 56 (2018) 661-671.
[26] K. Tomihata, Y. Ikada, Crosslinking of hyaluronic acid with glutaraldehyde, J. Polym. Sci. Pol. Chem., 35 (1997) 3553-3559.
[27] Y. Zhang, P.C. Zhu, D. Edgren, Crosslinking reaction of poly(vinyl alcohol) with glyoxal, Journal of Polymer Research, 17 (2010) 725-730.
[28] S. Kobayashi, M. Wakui, Y. Iwata, M. Tanaka, Poly(omega-methoxyalkyl acrylate)s: Nonthrombogenic Polymer Family with Tunable Protein Adsorption, Biomacromolecules, 18 (2017) 4214-4223.
[29] K. Sato, S. Kobayashi, A. Sekishita, M. Wakui, M. Tanaka, Synthesis and Thrombogenicity Evaluation of Poly(3-methoxypropionic acid vinyl ester): A Candidate for Blood-Compatible Polymers, Biomacromolecules, 18 (2017) 1609-1616.
[30] J. Deng, X.Y. Liu, L. Ma, C. Cheng, S.D. Sun, C.S. Zhao, Switching biological functionalities of biointerfaces via dynamic covalent bonds, Journal of Materials Chemistry B, 4 (2016) 694-703.
[31] J. Yang, M. Khan, L. Zhang, X.K. Ren, J.T. Guo, Y.K. Feng, S.P. Wei, W.C. Zhang, Antimicrobial surfaces grafted random copolymers with REDV peptide beneficial for endothelialization, Journal of Materials Chemistry B, 3 (2015) 7682-7697.
[32] J. Deng, X.Y. Liu, S.Q. Zhang, C. Cheng, C.X. Nie, C.S. Zhao, Versatile and Rapid Postfunctionalization from Cyclodextrin Modified Host Polymeric Membrane Substrate, Langmuir, 31 (2015) 9665-9674.
[33] L.W. Yang, L.L. Han, Q. Liu, Y.G. Xu, L.Y. Jia, Galloyl groups-regulated fibrinogen conformation: Understanding antiplatelet adhesion on tannic acid coating, Acta Biomaterialia, 64 (2017) 187-199.
[34] A. Hasan, S.K. Pattanayek, L.M. Pandey, Effect of Functional Groups of Self-Assembled Monolayers on Protein Adsorption and Initial Cell Adhesion, Acs Biomaterials Science & Engineering, 4 (2018) 3224-3233.
[35] A. Hasan, V. Saxena, L.M. Pandey, Surface Functionalization of Ti6Al4V via Self-assembled Monolayers for Improved Protein Adsorption and Fibroblast Adhesion, Langmuir, 34 (2018) 3494-3506.
[36] M. Inoue, M. Sasaki, A. Nakasu, M. Takayanagi, T. Taguchi, An Antithrombogenic Citric Acid-

Crosslinked Gelatin with Endothelialization Activity, Adv. Healthc. Mater., 1 (2012) 573-581.
[37] T.F. Kong, G.Q. Guo, H.T. Zhang, L. Gao, Post-synthetic modification of polyvinyl alcohol with a series of N-alkyl-substituted carbamates towards thermo and CO2-responsive polymers, Polymer Chemistry, 8 (2017) 5769-5779.
[38] R.S.E. Wang, L. Tian, Y.H. Chang, A homogeneous fluorescent sensor for human serum albumin, Journal of Pharmaceutical and Biomedical Analysis, 63 (2012) 165-169.
[39] W. Zingg, A.W. Neumann, A.B. Strong, O.S. Hum, D.R. Absolom, Effect of surface-roughness on platelet-adhesion under static and under flow conditions, Canadian Journal of Surgery, 25 (1982) 16-19.

Chapter 4

Injectable, non-diffusible and pre-filled bone paste composed of α-Tricalcium phosphate and hydrophobically modified poly(vinyl alcohol)

4.1. Abstract

In this study, injectable, non-diffusible, and pre-filled bone pastes were developed using α-tricalcium phosphate (α-TCP) and hydrophobically modified poly(vinyl alcohol)s (hm-PVAs) with various alkyl chain lengths (3–12). The resulting bone pastes showed high injectability (over 90%) when the solid-liquid ratio was lower than 3.5. The non-diffusion property of α-TCP/hm-PVAs bone pastes in water and fresh porcine blood was observed compared with α-TCP alone, α-TCP/original PVA (Org-PVA), and commercial calcium phosphate paste. Compressive strength of α-TCP/nonanal modified PVA (C9-PVA) bone pastes was 5.4±1.4 MPa within 24 h, and reached to 27.5±2.7 MPa after 7 days in water. Young's modulus of α-TCP/C9-PVA bone pastes was 0.84±0.02 GPa, which was lower than that of commercial calcium phosphate paste (1.5±0.02 GPa) and poly(methyl methacrylate)-based bone cement (1.06±0.03 GPa). Furthermore, the surface of α-TCP/C9-PVA bone pastes showed excellent cell adhesion of cultured osteoblastic cells. These results demonstrated that α-TCP/C9-PVA bone paste is a promising bone filler for percutaneous vertebroplasty (PVP) surgery.

4.2. Introduction

Along with a growing elderly population, there is an increase in cases of osteoporotic compression fractures of the vertebrae [1]. Vertebral compression fracture (VCF) can lead to the deterioration of pulmonary function and the compression of abdominal organs, which impair the daily life of elderly patients. The common surgical treatment for VCF is the use of bone filler.

Currently, a bone cement composed of poly (methyl methacrylate) (PMMA) is widely used in clinical treatment. However, PMMA-based bone cement generates heat of at least 80 ℃ during the polymerization process of methyl methacrylate (MMA), causing severe damage to the tissue around the injection site [2]. In addition, some unreacted MMA monomer or oligomer elutes from the injection site before completely solidifying, then diffuses into the lungs inducing an adverse effect [3, 4]. Furthermore, PMMA cement shows a high compressive strength of over 80 MPa which greatly exceeds the average strength of vertebrae in the elderly (2.37 MPa), and its Young's modulus (1 GPa) is also higher than average (0.35 GPa) [5]. For these reasons, patients who undergo vertebral dilatation surgery are inclined to refracture around the injection site [6, 7].

To overcome the risks of refracture, an elastic material composed of silicone and barium sulphate has been applied in vertebral dilatation surgery [8, 9]. The greatest feature of this material is low stiffness [10]; however, it is also compromised by its polymerization reaction, and the diffusion of the monomer or oligomer still pose health hazards to patients [11].

In addition to the fillers, calcium phosphate-based bone pastes are commercially available biomaterials for bone defects [12]. The application of calcium phosphate paste relies on the hydration reaction of calcium phosphate instead of a polymeric reaction [13, 14]. Generally, α-type tricalcium phosphate (α-TCP) is used due to its high curing rate and strength compared to that of another crystal form, β-type tricalcium phosphate (β-TCP) [15]. However, the possibility of diffusion leakage from the bone fracture site is also a problem in the practical application of calcium phosphate paste. Furthermore, components of calcium phosphate paste gradually dissolve in water, so it is difficult to cure in a bleeding site and to maintain adequate strength. Therefore, the use of calcium phosphate pastes alone in vertebroplasty is limited [16]. Also, preparation processes of bone cements as well as calcium phosphate pastes are complex and time-consuming [17]; therefore, pre-filled and injectable bone pastes are required.

For elderly patients, percutaneous vertebroplasty (PVP) surgery, a minimally invasive treatment, is most acceptable with injection by a relatively small needle [18]. Thus, taking these factors into consideration, the ideal bone filler has to meet the requirements of clinical practice such as having an injectable property, curability in a water/blood environment, non-diffusibility and biological safety.

In this study, focusing on the water-insoluble characteristic of hydrophobically modified poly(vinyl alcohol) (hm-PVA), we developed an injectable, non-diffusible and pre-filled type bone paste composed of α-TCP and hm-PVA (Figure 4-1). Using dimethyl sulfoxide (DMSO), which is used as a solvent of a non-adhesive liquid embolic agent for cerebral arteriovenous malformations [19-21], we successfully prepared a pre-filled type bone paste that did not require mixing before injection. Detailed bone mechanical properties and cell adhesion properties resulting from the use of α-TCP/hm-PVA bone pastes were evaluated.

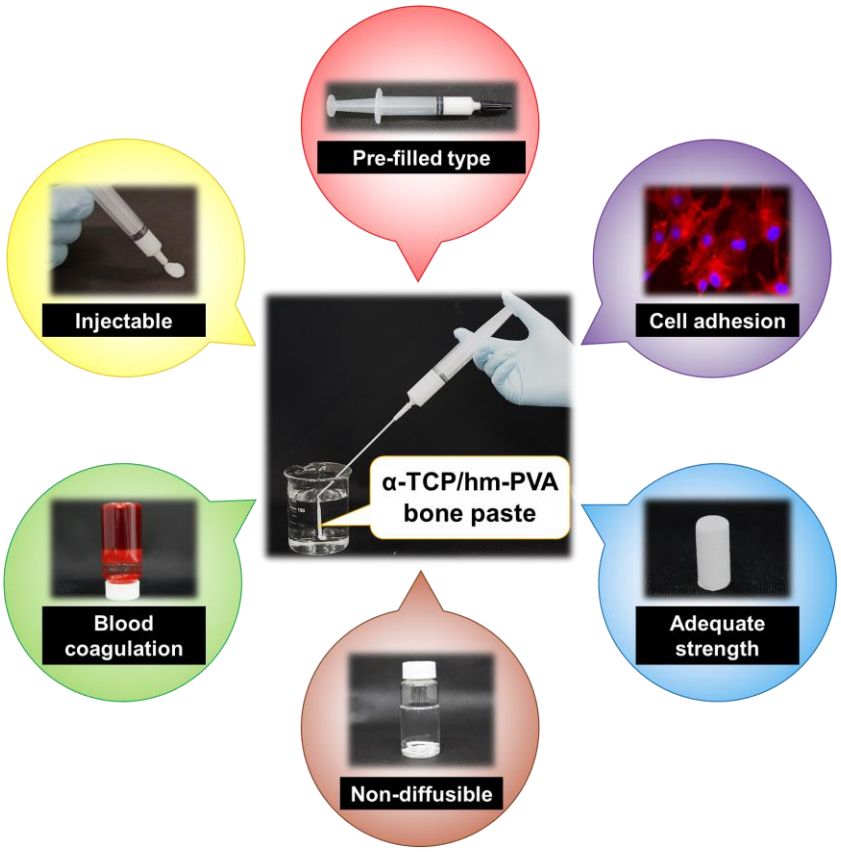

Figure 4-1. The properties of α-TCP/hm-PVA bone paste developed in this study

4.3. Materials and methods

4.3.1. Materials

Ethanol (EtOH, 99.5%), super-dehydrated DMSO, 6 N hydrochloric acid (HCl), 10% formalin neutral buffer solution, Dulbecco's phosphate buffered saline (D-PBS) without Ca and Mg, 99.9% DMSO-d_6 containing 0.05 w/v% tetramethylsilane, 4% paraformaldehyde (PFA) phosphate buffer solution and albumin from bovine serum (BSA) were purchased from Wako Pure Chemical Industries, Ltd. (Osaka, Japan). Otsuka normal saline 2-port was purchased from Otsuka Pharmaceutical Co., Ltd. (Tokyo, Japan). PVA (Mw= 88,000, saponification degree was over 98.5%) and cell count reagent SF were purchased from Nacalai Tesque, Inc. (Kyoto, Japan). Propionaldehyde (C3), hexanal (C6), nonanal (C9), and dodecyl aldehyde (C12) were purchased from Tokyo Chemical Industry Co., Ltd (Tokyo, Japan). Porcine whole blood was purchased from Tokyo Shibaura Organ Co., Ltd (Tokyo, Japan). Minimum essential medium (MEM Alpha) and TrypLE™ Express were purchased from Thermo Fisher Scientific Co., Ltd (Tokyo, Japan). Foetal bovine serum (FBS), penicillin/streptomycin solution and phalloidin-tetramethyl rhodamine B isothiocyanate peptide from Amanita phalloides were purchased from Sigma-Aldrich Co., Ltd (Missouri, USA). Biopex-R calcium phosphate cement was purchased from HOYA Technosurgical Co., Ltd (Tokyo, Japan). Endurance PMMA bone cement was purchased from Johnson & Johnson Co., Ltd (Brunswick, USA). α-Tricalcium phosphate was purchased from Taihei Chemical Industry Co., Ltd (Toki, Japan). α-Tricalcium phosphate was precisely smashed (particle size: 3.2 μm) by Nissei Engineering Co., Ltd (Tokyo, Japan). Triton X-100 stock solution was purchased from Cayman Chemical Co., Ltd (Estonia Biomol GmbH, Germany). Cell stain 4',6-Diamidino-2-phenylindole, dihydrochloride (DAPI) solution was purchased from Dojindo Laboratories (Tokyo, Japan).

4.3.2. Synthesis of hm-PVAs

The hm-PVAs were prepared through the nucleophilic substitution reaction between an aldehyde and the hydroxy groups of PVA as previously reported [22, 23]. First, PVA (10 g) was dissolved in 98 mL of H_2O at 80 ℃ for 60 min. Then, 100 mL of DMSO and 2 mL of 1 N HCl were added to form a 200 mL solution of 5 w/v% PVA and 1 v/v% 1 N HCl. Different amounts of aldehyde groups (C3, C6, C9, C12) were added into the solution, and the resulting mixtures were stirred at 50 ℃ for 1 h. A reflux condenser was used in all processes. After the reaction, the obtained hm-PVA (H_2O/DMSO = 50/50 (v/v)) solution was added to 600 mL (around 3 times) cold EtOH under stirring for 1 h. The hm-PVAs precipitated from the solution, and then the precipitation was washed with 300 mL of EtOH at least three times to remove the unreacted aldehyde and DMSO. The solvent was evaporated under vacuum to obtain purified hm-PVAs as white crystals. Finally, the crystals were crushed finely using a crusher (Wonder crusher WC-3, Osaka Chemical, Osaka, Japan).

4.3.3. Characterization of hm-PVAs

The chemical structures of the hm-PVAs were analysed by nuclear magnetic resonance (^{1}H-NMR) spectroscopy (AL300, JEOL, Tokyo, Japan) using a 0.5 w/v% hm-PVA/DMSO-d_6 solution at 25 ℃. The number of scans was 8 times for each sample. Fourier transform-infrared spectroscopy (FT-IR, 8400S, Shimadzu, Kyoto, Japan) analysis was carried out to confirm the presence of acetal groups in the hm-PVAs. The scan range was 700 cm^{-1} to 4, 000 cm^{-1} and there were 64 scans for each sample. Hydrophobic group modification ratios of the hm-PVAs were determined by ^{1}H-NMR spectroscopy. The modification ratios were calculated by following equation:

$$\text{Modification ratio (mol\%)} = [\{\text{Integral area } (CH_3 \text{ proton})/3\} / \text{Integral area } (\alpha\text{CH proton})]\times 100$$

where integral area (αCH proton) is the area of peak at 3.87 ppm corresponding to the αCH proton in the backbone of PVA and hm-PVAs; integral area (CH_3 proton) is the area of peak at 0.85 ppm assigned to the CH_3 proton in the hydrophobic groups in the hm-PVAs.

4.3.4. Evaluation of injectability

The injectability of α-TCP/hm-PVA bone pastes was evaluated according to the method previously reported [24]. α-TCP (from 1 g to 4 g) was kneaded with 1 mL of hm-PVA/DMSO solution. Then, the mixture was filled in a 2.5 mL syringe (Terumo Co., Tokyo, Japan). The syringe was set into a metal mould with a hole as shown in Figure 3a. The injectability was measured with a testing machine (EZ-LX, Shimadzu Co., Kyoto, Japan). The paste was extruded under pressure, and this process was stopped when the extrusion strength reached 100 MPa. Three specimens were tested for each group. Injectability was calculated by the following equation:

$$\text{Injectability (\%)} = 100 \times (Wt-Wr) / Wt$$

where Wt and Wr are weight of the total paste and weight of the remaining paste in syringe, respectively.

4.3.5. Stability of α-TCP/hm-PVA bone pastes in water or blood after injection

α-TCP (3.5 g) was kneaded with 1 mL of hm-PVA/DMSO solution (10 w/v%). The resulting pastes were filled in 2.5 mL syringes and injected into glass beakers containing 20 mL PBS or porcine whole blood and stirred vigorously with vortex for 5 seconds. Then, the transmittance of 3 mL supernatant of the PBS solution after injection and mixing of α-TCP/hm-PVA bone pastes was used to determine turbidity by using ultraviolet-visible near-infrared spectrophotometer (UV-vis, V660, Jasco Co., Tokyo, Japan).

4.3.6. Measurement of compressive strength

Bone pastes for measuring compressive strength were prepared following the procedures shown in Figure 5a according to the Japanese industrial standard (JIS) T 0330-4. Initially, the hm-PVA was dissolved in DMSO solvent to obtain a 10 w/v% solution. Then, α-TCP (from 1 g to 4 g) was kneaded with 1 mL of hm-PVA/DMSO solution. Samples were set into a Teflon mould (diameter of 6 mm and thickness of 12 mm) that had one side closed with a glass plate. Finally, the mould was immersed into the PBS solution at 37 ℃. DMSO present in the bone paste gradually diffused, while α-TCP/hm-PVA composites were consolidated by a hydration hardening reaction. The composite formed hydroxyapatite crystals [25] when contacted with water or blood. After 48 h when the paste was completely cured, the sample was peeled off from the mould. The surface structure of the paste was observed using a scanning electron microscopy (SEM, S4800, Hitachi Co., Tokyo, Japan). Elemental analysis of the paste surface was conducted by energy dispersive X-ray spectrometry (EDX, S4800, Hitachi Co., Tokyo, Japan). As a control, commercial products Endurance and Biopex-R were filled in the same mould and consolidated in an incubator at 37 ℃ for 2 days. The compressive strength was measured using a universal testing machine (EZ-LX, Shimadzu Co., Kyoto, Japan) according to JIS T 0330-4 with a compression speed of 0.5 mm/min.

4.3.7. Osteoblast adhesion test

Mouse osteoblastic cells (MC3T3) were cultured in MEM Alpha (Gibco) supplemented with 10% FBS (Sigma-Aldrich) and 1% penicillin/streptomycin (Sigma-Aldrich) under standard cell culture conditions: a sterile, 37 ℃, humidified, and 5% CO_2 environment. Cells at passage numbers 3–5 were used in the experiments. Before sample preparation, the α-TCP was sterilized by UV irradiation for 60 min and hm-PVA/DMSO solution was autoclaved. All operations were done in a clean bench (As One, Osaka, Japan). The pastes were set into the silicone mould (diameter of 10 mm and thickness of 1 mm) followed by immersion in PBS at 37 ℃ for 48 h. The consolidated bone disks were peeled off from the silicone sheet, and then put into a 48-well plate (Falcon, Corning, New York, USA). An amount of 30 μL of culture medium containing 2×10^4 MC3T3 cells was dropped on the surface of the bone disks. The well plate was incubated for 1 h to ensure that the MC3T3 cells had adhered to the sample. After preliminary incubation, 470 μL of culture medium was added to each well. After incubating for an additional 23 h, the bone pastes were moved into a new 48-well plate. An amount of 500 μL of culture medium and 50 μL of cell count reagent were added into each well followed by incubation for 2 h. The mixture (150 μL) was then transferred to a 96-well plate, and its absorbance at 450 nm was measured using a microplate reader (Spark10M, Tecan, Osaka, Japan). In this test, culture medium with 8×10^5, 4×10^5, 2×10^5, 1×10^5, 5×10^4, 2.5×10^4, and 1.25×10^4 MC3T3 cells were used as standard. The adsorbed osteoblasts were stained with phalloidin-tetramethyl rhodamine B isothiocyanate peptide (cytoskeleton actin) and DAPI solution (cell nucleus), respectively. Briefly, media was removed firstly, and each well was washed with PBS solution. In each well, 200 μL of fresh fixative solution (4% PFA in PBS) was dispensed and cells were fixed for 15 min at room temperature. The fixative solution was removed and washed with PBS. Then, 0.2% triton X-100 solution was added in each well for 10 min at room temperature.

The remaining triton X-100 was removed by washing gently three times with PBS, and then blocking solution (1% BSA in PBS) was dispensed into each well for 1 h incubation. The blocking solution was removed, then 400 µL phalloidin-tetramethyl rhodamine B isothiocyanate peptide in 1% BSA solution (1:100 dilution) was added into each well and incubated for 1 h. Next, each well was washed with PBS at least three times. Finally, DAPI solution in PBS (1:100 dilution) was added for 10 min, followed by washing three times with PBS. Fluorescence of stained cells was observed using inverted fluorescence phase contrast microscope (BZ-X700, Keyence Co., Tokyo, Japan).

4.3.8. Statistical analysis

Statistical analysis was carried out using Tukey-Kramer test with KyPlot software. Statistically significant differences were accepted when $p < 0.05$. Data were presented as means ± standard deviations (SD).

4.4. Results and discussion

4.4.1. Synthesis and characterization of hm-PVAs

The hm-PVAs were prepared via the reaction between the hydroxy groups of PVA and an aldehyde (Figure 4-2a) as previously reported[22, 23]. Under acidic conditions, aldehydes react with hydroxyl groups via a nucleophilic substitution reaction to form intermediates; in our experiment, the stable hexagonal ring structure was obtained in a short time[23]. Figure 4-2b shows the ^{1}H-NMR spectra of the hm-PVAs with different numbers of methylene carbons. The chemical shift at 0.85 ppm was assigned to the CH_3 proton in the hydrophobic groups of the hm-PVAs. The chemical shift at 1.26 ppm belonged to the αCH_2 proton of the hydrophobic groups in the hm-PVAs. This indicates the successful introduction of alkyl groups into the PVA molecule. The structure of the hm-PVAs was also analysed by FT-IR spectra (Figure 4-2c). The peak observed at 1,080 cm^{-1} was attributed to the antisymmetric stretch of C-O-C bonds in the acetal groups of the hm-PVAs. The C-H stretching vibration at 2,930 cm^{-1} of αCH_2 appeared in the spectra of the hm-PVA. These results revealed that hm-PVAs with different numbers of methylene carbons were successfully synthesized. The modification ratios of the hydrophobic groups (Table 4-1) were calculated using the ^{1}H-NMR results. As can be seen in Table 4-1, the modification ratio increased with the addition of aldehydes (C3, C6, C9, and C12), and about 50% of aldehydes were introduced into PVA molecules. We found that only the hm-PVA with a high modification ratio of the hydrophobic group could precipitate in water (Figure 4-3). Therefore, 23C3-PVA, 20C6-PVA, 20C9-PVA, and 23C12-PVA were used for further study.

Table 4-1. Modification ratios of the hm-PVAs

Type of hm-PVAs	Hydrophobic group reagent	Hydrophobic group reagent added (mol%)	Hydrophobic group modification (mol%)
C3-PVA	Propanal	50	23
C6-PVA	Hexanal	50	19
C9-PVA	Nonanal	50	20
C12-PVA	Dodecanal	50	23

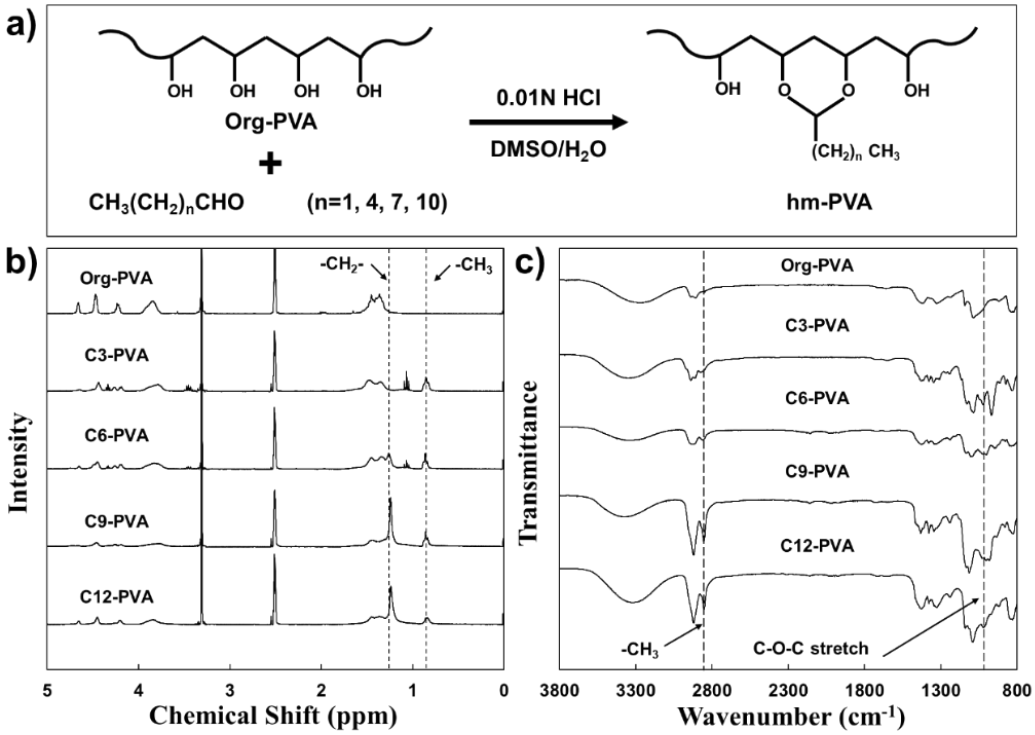

Figure 4-2. a) Synthesis of hm-PVAs. b) 1H-NMR spectra and c) FT-IR spectra of the hm-PVAs

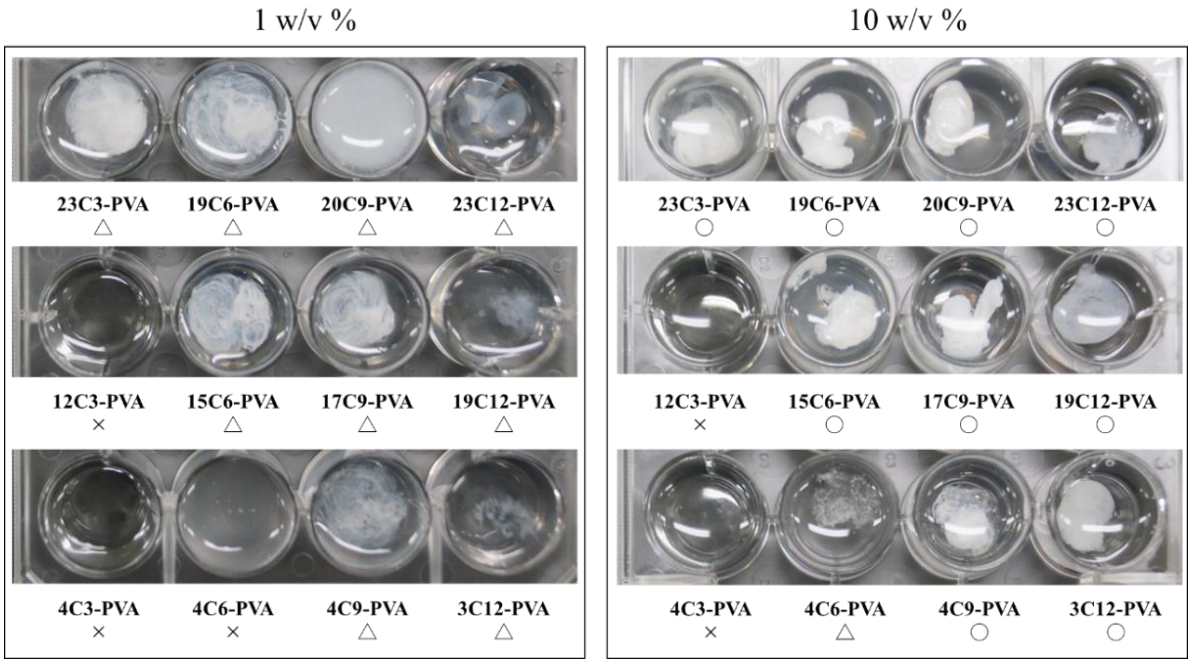

Figure 4-3. Evaluation of aggregation ability (○Dissoluble; △Slightly; ×Soluble).

4.4.2. Injectability of α-TCP/hm-PVA bone pastes

For the surgical treatment of PVP, the bone pastes used must be injectable. We therefore evaluated the injectability of the bone pastes with various solid-liquid ratios of α-TCP and C9-PVA according to the method previously reported [24] (Figure 4-4a). Injectability of α-TCP/C9-PVA bone pastes was over 90% when the solid-liquid ratio was from 2 to 3.5; while it greatly decreased when solid-liquid ratio was 3.75 (44.5±3.5%). It could be that the α-TCP/C9-PVA bone pastes with high solid density lost fluidity. We found

that there were many particles on the surface of the consolidated α-TCP/C9-PVA bone pastes with a high solid-liquid ratio (Figure 4-5) and that the average particle size was the same as that of the α-TCP used in this work (3.2 μm). This may have been because α-TCP could not be sufficiently kneaded at a solid-liquid ratio over 3.75.

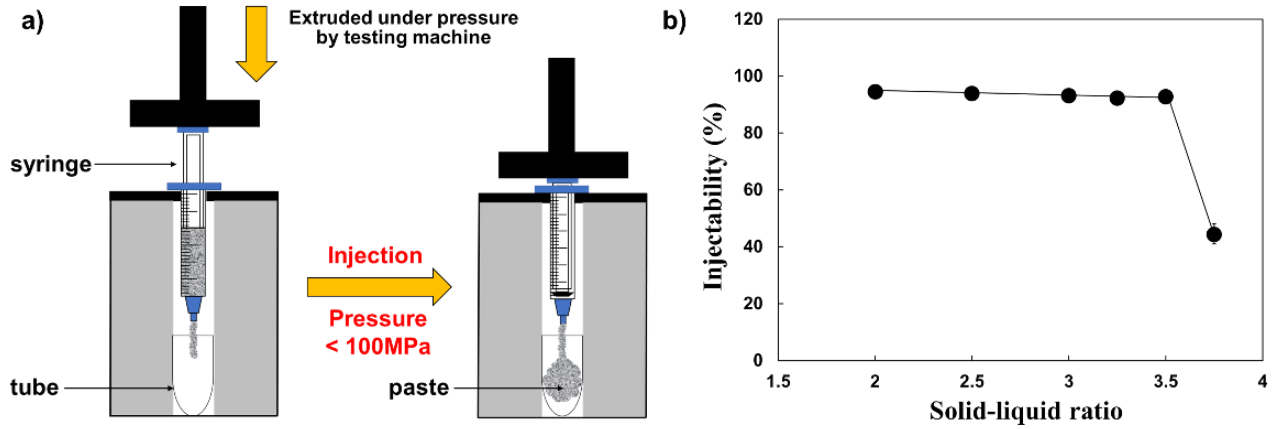

Figure 4-4. a) The process of the injectability test. b) Injectability of α-TCP/C9-PVA bone pastes. The concentration of C9-PVA/DMSO solution was 10 w/v%.

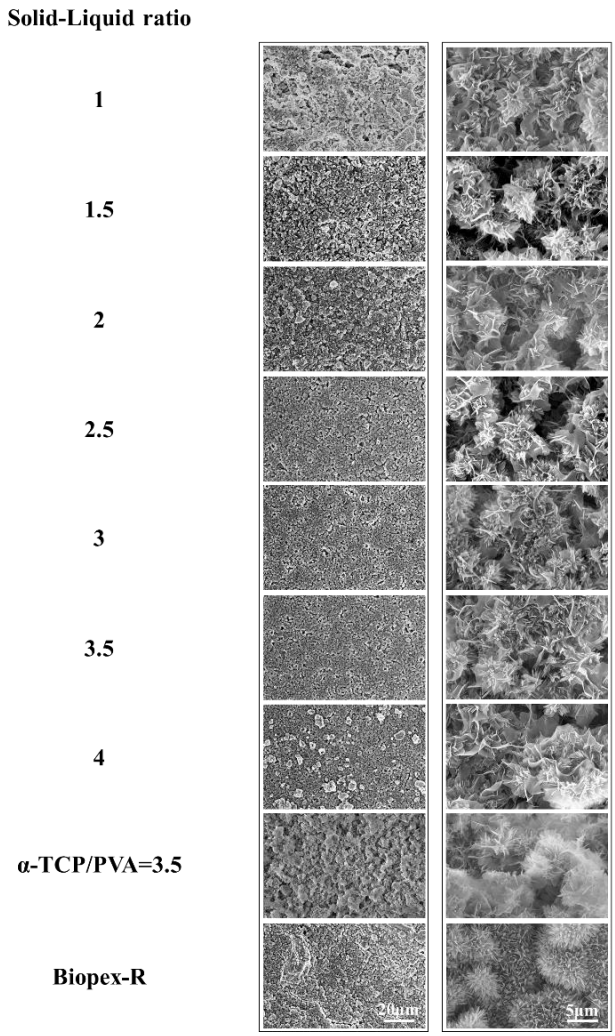

Figure 4-5. SEM images of α-TCP/C9-PVA bone pastes with different solid-liquid ratios. The concentration of PVA or hm-PVA/DMSO solution was 10 w/v%.

4.4.3. Stability of α-TCP/hm-PVA bone pastes in water or blood after injection

For the injection of bone pastes into the fractured vertebral body, the bone pastes must be stable in a water or blood environment to avoid fragmentation [26]. Therefore, we evaluated the stability of α-TCP/hm-PVA bone pastes with different alkyl chain lengths in PBS. Figures 4-6a-c show the stability of bone pastes after injection or stirring. As can be seen in Figure 4-6a, the stability of α-TCP/hm-PVA bone pastes in PBS was highly dependent on the alkyl chain length; that is, α-TCP/hm-PVA bone pastes with no or short alkyl chain, α-TCP/original PVA (Org-PVA) and α-TCP/C3-PVA, could be injected into PBS; however, they dissolved in the PBS after stirring. By contrast, stability was observed when α-TCP/hm-PVA bone pastes with long alkyl chains, α-TCP/C6-PVA, α-TCP/C9-PVA and α-TCP/C12-PVA, were injected into PBS. The injected shapes of these α-TCP/hm-PVA bone pastes were maintained even after stirring. Figure 4-6b shows the transmittance of PBS supernatant after injection of bone pastes and stirring. Supernatant of commercial calcium phosphate bone paste (Biopex-R), α-TCP/Org-PVA and α-TCP/C3-PVA bone pastes became turbid, meaning that these pastes cannot be injected in water. Meanwhile, the transmittance of α-TCP/C6-PVA, α-TCP/C9-PVA and α-TCP/C12-PVA bone pastes were much higher, which may due to the good interaction between the hydroxy groups of hm-PVAs and Ca^{2+} ions from α-TCP particles [27]. In addition, the hydrophobic interaction between the alkyl chains of hm-PVAs increased with increasing alkyl chain length. As a result, α-TCP/hm-PVA composites with long alkyl chain lengths, C6-PVA, C9-PVA and C12-PVA, were stable in water even after stirring. Compared with the hydrophobic interaction of C6-, C9- and C12-PVA, the hydrophobic interaction of C3-PVA was the weakest. Therefore, the transmittance of supernatant after injection of α-TCP/C3-PVA bone paste was 79.4±0.3%, which was much lower than that of α-TCP/C6-PVA (99.5±0.1%), α-TCP/C9-PVA (98.1±0.1%), and α-TCP/C12-PVA (96±0.1%) pastes. Figure 4-6c shows the transmittance amounts of supernatant after injection with α-TCP/C9-PVA bone pastes with different concentrations of C9-PVA from 5 to 20 w/v%. Surprisingly, there was no significant difference amongst the four samples. These results revealed that α-TCP/hm-PVA bone paste, especially α-TCP/C9-PVA bone paste, was able to consolidate in blood. Figure 4-6d shows the stability of α-TCP/hm-PVAs pastes in citric acid-containing porcine whole blood after injection and stirring. The commercial calcium phosphate paste Biopex-R did not remain after removing porcine whole blood, meaning that the paste dissolved in the blood. Meanwhile, α-TCP/Org-PVA bone paste left white particles on the sides of the glass beaker, but no uniform solid was found on the bottom of the beaker. The main reason for this was that the components of the α-TCP/Org-PVA bone paste were easily dissolved in water and blood. α-TCP/C3-PVA bone paste could be partially cured in blood; however, white particles were also found on the sides of the glass beaker due to the high solubility of α-TCP/C3-PVA bone paste. The α-TCP/hm-PVA bone pastes with long alkyl chain lengths, C6-, C9- and C12-PVA, could be injected in whole blood, and keep their shape even after stirring. Also, the dispersed white components (α-TCP particles) were not found on the sides of the glass beakers. We believe that these phenomena were due to the hydrophobicity as well as the good interaction between the hydroxy groups of hm-PVAs and Ca^{2+} ions from α-TCP. These results were consistent with Figures 4-6a-c. We also found an acceleration of blood coagulation after injection of α-TCP/C9-PVA bone paste, as shown in Figure 4-6e. This may be because Ca^{2+} ions released from the cured α-TCP/C9-PVA bone paste accelerated fibrinogen clotting in the presence of thrombin [28], as shown in Figure 4f. These results suggested that α-TCP/C9-PVA bone paste could exert a haemostatic effect even in a bloody environment.

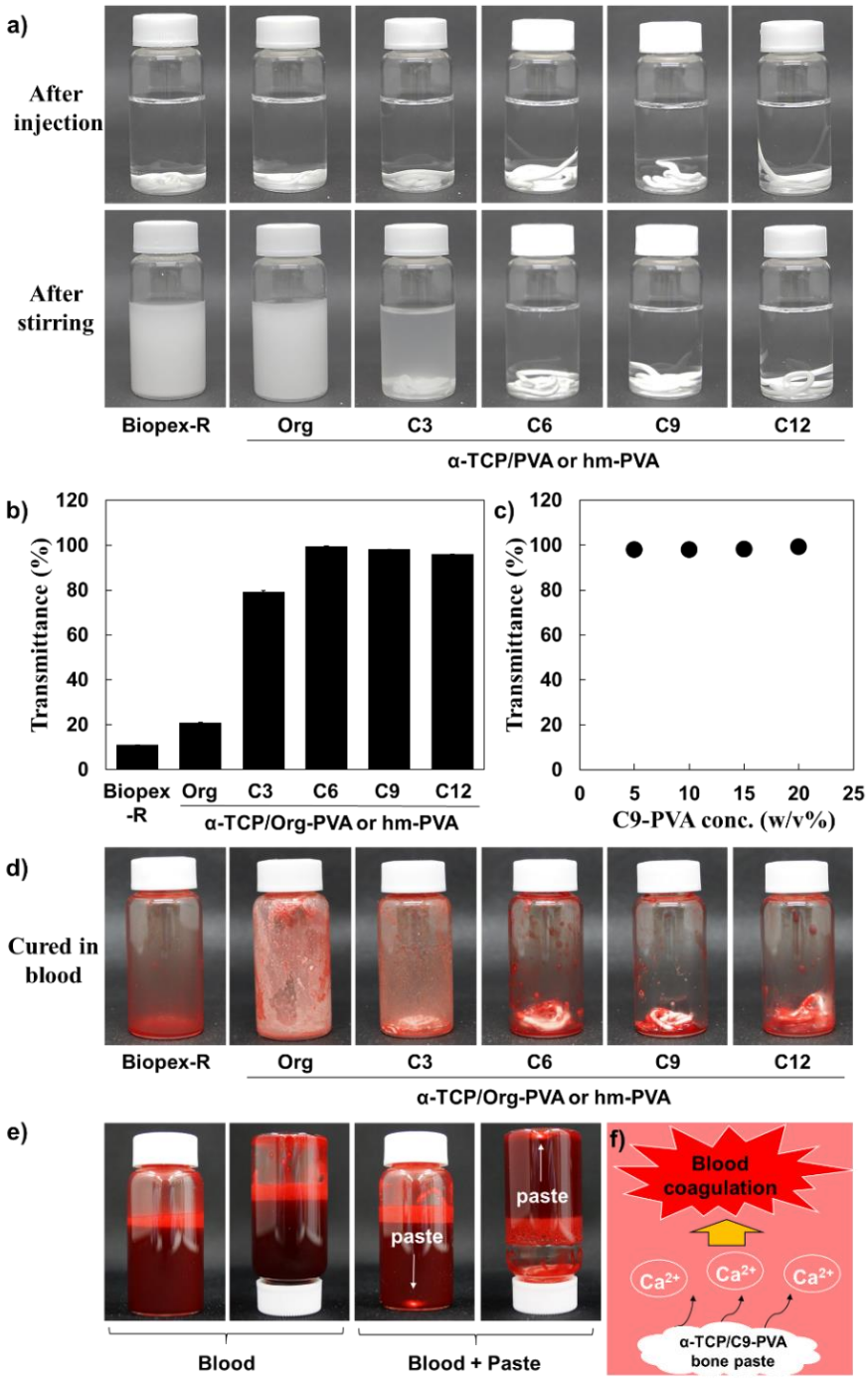

Figure 4-6. The stability of α-TCP/hm-PVA bone pastes in PBS solution or porcine whole blood. a) The images of the α-TCP/hm-PVA bone pastes after injection (upper) and after stirring (bottom) in PBS solution. b) The transmittance of PBS supernatant solution contained α-TCP/hm-PVA bone pastes after stirring. The concentration of hm-PVA/DMSO and PVA/DMSO solutions was 10 w/v%. c) The transmittance of PBS supernatant solution contained α-TCP/C9-PVA bone pastes after stirring. The concentration of C9-PVA/DMSO solution was from 5 to 20 w/v%. d) The curability test of α-TCP/hm-PVA bone pastes in porcine whole blood. e) Blood clotting occurred in fresh porcine whole blood with injection of α-TCP/C9-PVA bone paste. f) Blood coagulation mechanism of fresh porcine whole blood contained α-TCP/C9-PVA bone paste.

4.4.4. Compressive strength

The compressive strengths of α-TCP/hm-PVA bone pastes were evaluated according to JIS T 0330-4. The measurement procedure is shown in Figure 4-7a. Teflon mould was employed to prepare samples for the measurement of compressive strength. Figure 4-7b shows the effect of the solid-liquid ratio on the α-TCP/C9-PVA bone pastes. Compressive strength increased with an increase of the solid-liquid ratio. The compressive strength of the α-TCP/C9-PVA bone pastes was 7.9±0.9 MPa when the solid-liquid ratio was 2, and the strength increased to 18±1 MPa when the solid-liquid ratio was 3.5. The main reason was that the density of the inorganic component increased. Through the SEM observation of the surface of α-TCP/C9-PVA bone pastes, we observed that the pore size decreased with an increase in the solid-liquid ratio (Figure 4-5). The EDX results of α-TCP/C9-PVA bone pastes in Table 4-2 show that the concentration of element C assigned to C9-PVA decreased with an increase in the solid-liquid ratio. This was due to the decrease in the proportion of organic components in α-TCP/C9-PVA bone paste.

Table 4-2. Elemental analysis of α-TCP/C9-PVA bone pastes by EDX

Solid-Liquid ratio	C (atomic%)	O (atomic%)	Ca (atomic%)	P (atomic%)
1	25	50.7	10	14.3
1.5	12.1	55.2	13.8	18.9
2	9.6	58.6	13.3	18.5
2.5	9.8	60	12.7	17.5
3	8.7	59.3	13.6	18.4
3.5	8.3	63.7	11.8	16.2
4	8.3	61.7	12.4	17.6

On the other hand, the Young's modulus was also increased by increasing the solid-liquid ratio from 0.43±0.12 GPa to 0.77±0.03 GPa. Considering the results of the injection property (Figure 4-4), the solid-liquid ratio of α-TCP/hm-PVA bone pastes was fixed at 3.5 for further experiments. Figure 4-7c shows the effect of alkyl chain length on α-TCP/hm-PVA bone pastes. There was no significant difference on compressive strength between α-TCP paste and α-TCP/Org-PVA paste; however, Young's modulus of α-TCP/Org-PVA bone paste was lower than that of α-TCP paste due to the organic component Org-PVA. We found that the compressive strength of α-TCP/hm-PVA bone pastes were around 15 MPa. Meanwhile, the Young's modulus of the α-TCP/C3-PVA and α-TCP/C6-PVA bone pastes was higher than that of α-TCP/C9-PVA and α-TCP/C12-PVA bone pastes, as a result of the lower hydrophobic interaction of hm-PVA with short alkyl chains. Based on water stability (Figures 4-6a-c) and a moderate Young's modulus, α-TCP/C9-PVA bone pastes were used for further evaluation. Figure 4-7d shows the effect of C9-PVA concentration on α-TCP/C9-PVA bone pastes. The Young's modulus of α-TCP/C9-PVA bone pastes clearly decreased while the compressive strength was maintained (around 18 MPa) with increasing the amount of organic component. We confirmed that the compressive strength was related to the density of the inorganic component (α-TCP), while the Young's modulus was affected by the concentration of the organic component (C9-PVA). It was revealed that α-TCP/C9-PVA bone paste with low C9-PVA concentration (10 w/v%) had good injectability and curing ability in blood (Figures 4-6b and 4-7d). According to these results, α-TCP/C9-PVA bone paste with moderate C9-PVA concentration (10 w/v%) at a solid-liquid ratio of 3.5 had the appropriate conditions for use as an injectable bone paste. Figure 4-7e shows the increased compressive strength of α-TCP/C9-PVA bone pastes after immersion in PBS. The mechanical properties of α-TCP/C9-PVA bone pastes were close to cancellous bone (< 10 MPa) [29] after incubation for 24 h. The compressive strength of α-TCP/C9-PVA bone paste after

one day was 5.4±1.4 MPa, and its Young's modulus (0.35±0.09 GPa) is close to that of average vertebrae (0.35±0.14 GPa). The compressive strength of α-TCP/C9-PVA bone paste increased to 18.1±1 and 27.5±2.7 MPa after 2 days and 7 days, respectively, while the Young's modulus increased to 0.77±0.03 and 0.84±0.02 MPa after 2 days and 7 days, respectively. It was confirmed that the compressive strength and Young's modulus of α-TCP/C9-PVA bone paste reached a peak after 3 days.

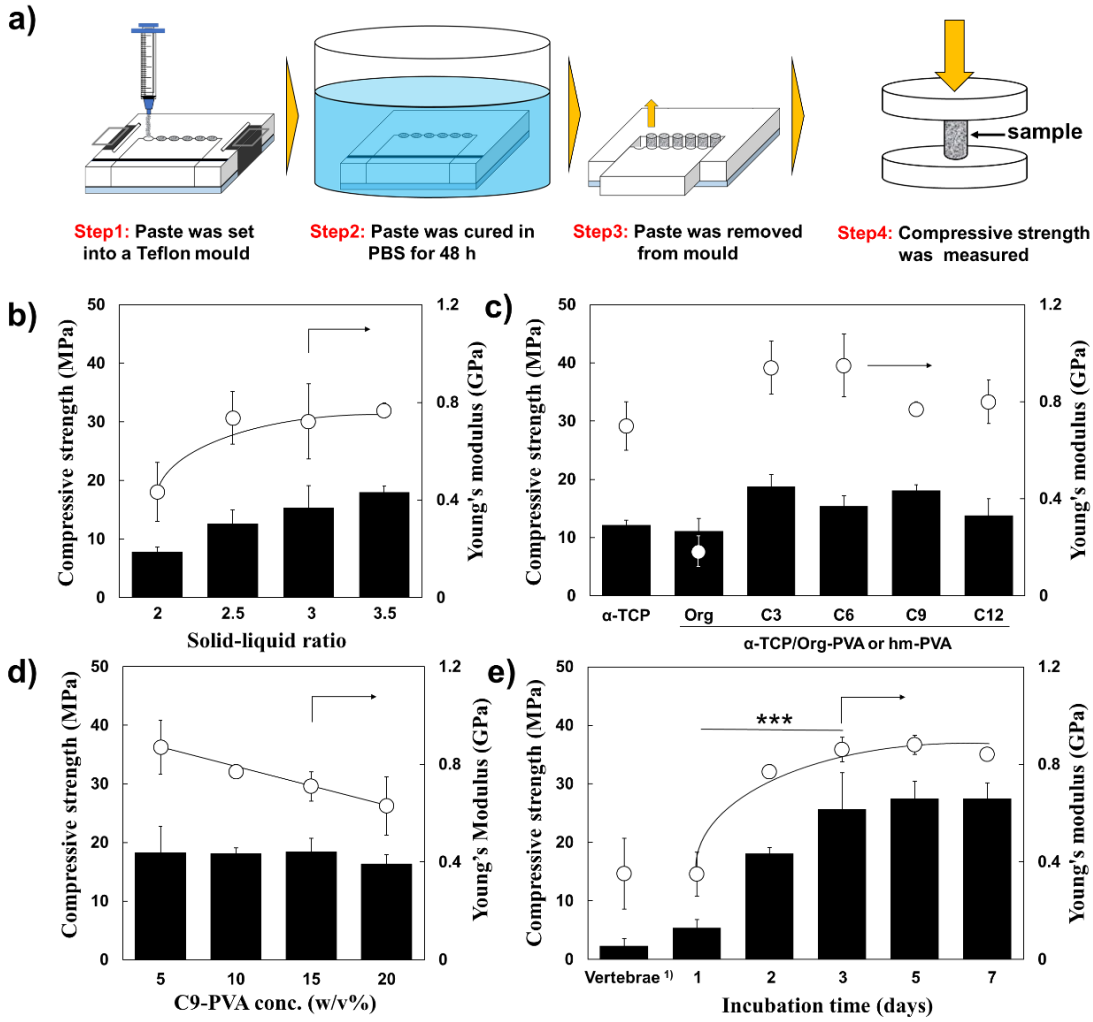

Figure 4-7. Mechanical properties of consolidated α-TCP/hm-PVA bone pastes. a) The preparation and mechanical property measurement of consolidated α-TCP/hm-PVA bone pastes. b) Compressive strength and Young's modulus of consolidated α-TCP/C9-PVA bone pastes with different solid-liquid ratios after incubation for 2 days. The concentration of C9-PVA/DMSO was 10 w/v%. c) Compressive strength and Young's modulus of consolidated α-TCP/PVA or hm-PVA bone pastes with solid-liquid ratio of 3.5 after incubation for 2 days. The concentration of hm-PVA/DMSO was 10 w/v%. d) Compressive strength and Young's modulus of consolidated α-TCP/C9-PVA bone pastes with different C9-PVA concentrations after incubation for 2 days. The solid-liquid ratio of α-TCP/C9-PVA bone pastes was 3.5. e) Compressive strength and Young's modulus of consolidated α-TCP/C9-PVA bone pastes with solid-liquid ratio of 3.5 after incubation for 1-7 days. Compressive strength is shown as a bar graph and Young's modulus is shown as a point graph. The compressive strength and Young's modulus of vertebrae 1) referred the results of Banse, X et al.; Journal of Bone and Mineral Research, 17, 2002, 1621-1628. (P***<0.001, n=5).

Figure 4-8 shows the comparison of α-TCP/C9-PVA bone paste and commercial cements (Biopex-R and Endurance). The compressive strength and Young's modulus of α-TCP/C9-PVA bone pastes were lower

compared to those of the commercial cements. The compressive strength and Young's modulus of Biopex-R reached 23.8±2.1 MPa and 1.32±0.06 GPa, respectively, on the first day, while these values increased to 57.6±2 MPa and 1.5±0.02 GPa, respectively, after 7 days. The compressive strength and Young's modulus of Endurance reached 48.9±3.5 MPa and 0.83±0.05 GPa, respectively on the first day, while these values increased to 81.5±1.7 MPa and 1.06±0.03 GPa, respectively after 7 days. The ideal bone filler, marked with a star in Figure 6, is necessary to reduce the risk of refracture. In conclusion, the values of α-TCP/C9-PVA bone paste show that it is better for use in clinical application than Biopex-R and Endurance.

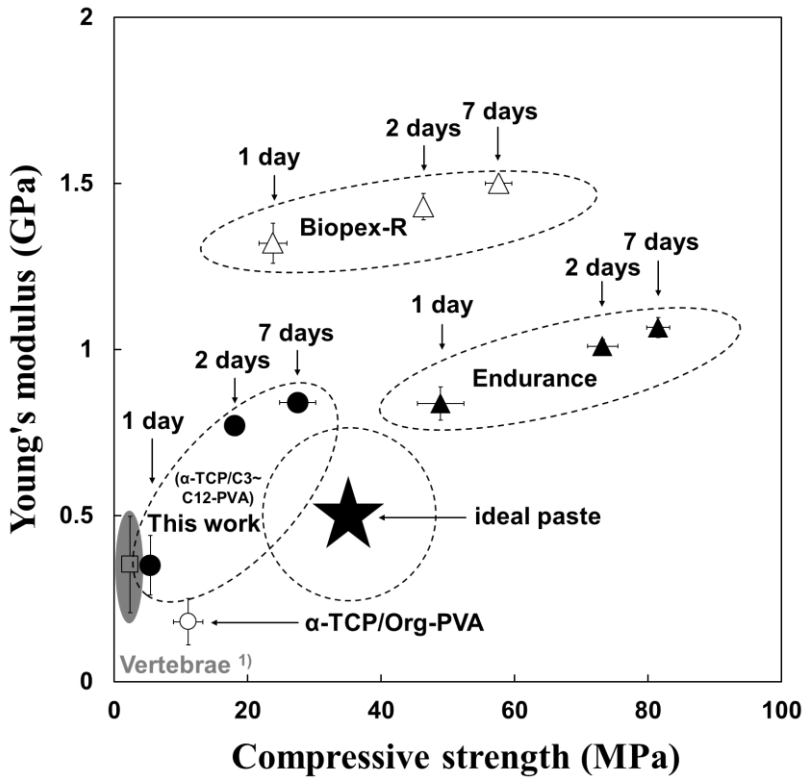

Figure 4-8. Comparison of commercial products with α-TCP/C9-PVA bone paste developed.

4.4.5. Osteoblast adhesion test

To evaluate the cell adhesion property of α-TCP/hm-PVA bone pastes after injection into a vertebral fracture site, osteoblasts were cultured on cured disk-shaped α-TCP/hm-PVA bone pastes. Figure 4-9 shows MC3T3 osteoblastic cell adhesion onto different types of α-TCP/hm-PVA bone pastes.

As shown in Figure 4-9a, cells were adhered to and spread on the surface of α-TCP/C6-PVA, α-TCP/C9-PVA and α-TCP/C12-PVA bone pastes. In contrast, cell adhesion was not observed on the surface of α-TCP, α-TCP/Org-PVA and α-TCP/C3-PVA bone pastes. There were two main reasons for this phenomenon: the dissolution of bone paste components into culture medium and the high hydrophilicity of these bone paste surfaces. First, α-TCP, Org-PVA and C3-PVA were easy to dissolve in water; therefore, the surfaces of these three types of pastes were unstable, which led to cells detaching from the surface. Second, in general, high hydrophilic surfaces show an anti-resistant property of protein adsorption as well as cell adhesion [30]. The hydrophilicity of PVA and C3-PVA was much higher compared to that of C6-, C9 and C12-PVA. On the other hand, good cell adhesion was observed on the Biopex-R surface. This may be because Biopex-R contains sodium chondroitin sulphate, a component of an extracellular matrix which controls cell traits such as cell adhesion [31], migration, differentiation and proliferation [32]; therefore, the surface of Biopex-R can work as

a cell scaffold. The PMMA-based bone cement, Endurance, also has a positive effect on cell adhesion and spreadability.

Figure 4-9b shows the quantitative data of cell adhesion on different kinds of bone pastes. We found that the osteoblast cells adhered on the surface of α-TCP/C9-PVA bone paste, whereas Biopex-R and Endurance bone cement showed no significant difference in cell adhesion after 24 h incubation. On the other hand, the number of cells adhered to the α-TCP/Org-PVA could not be determined due to its high hydrophilic surface. The number of osteoblast cells adhered to the surface of α-TCP and α-TCP/C3-PVA bone paste were 4.1×10^3 and 5.6×10^3, respectively, which was much less than that of α-TCP/C9-PVA bone paste (3.2×10^4). It was clear that the growth of osteoblast cells was much better on α-TCP/hm-PVA bone pastes with long alkyl chains than that of α-TCP/hm-PVA bone paste with short alkyl chains. These results were consistent with Figure 4-9a). We employed DMSO as an organic solvent for α-TCP/hm-PVA bone paste. DMSO is used in a commercial product as a solvent of a non-adhesive liquid embolic agent (Onyx™ liquid embolic system) for cerebral arteriovenous malformations. Therefore, we think that the use of DMSO as a solvent is safe for clinical application. The results shown in Figure 4-9 also support our materials design. The main urinary metabolite of DMSO is dimethyl sulfone ($DMSO_2$) produced by oxidation, but in breath, dimethyl sulphide (DMS) is produced by reduction and excreted [33]. Using DMSO, we successfully prepared an injectable, non-diffusible, pre-filled type of bone paste. The resulting α-TCP/hm-PVA bone pastes can be injected into marrow defect sites. We will conduct in vivo studies of this α-TCP/hm-PVA bone paste in the near future.

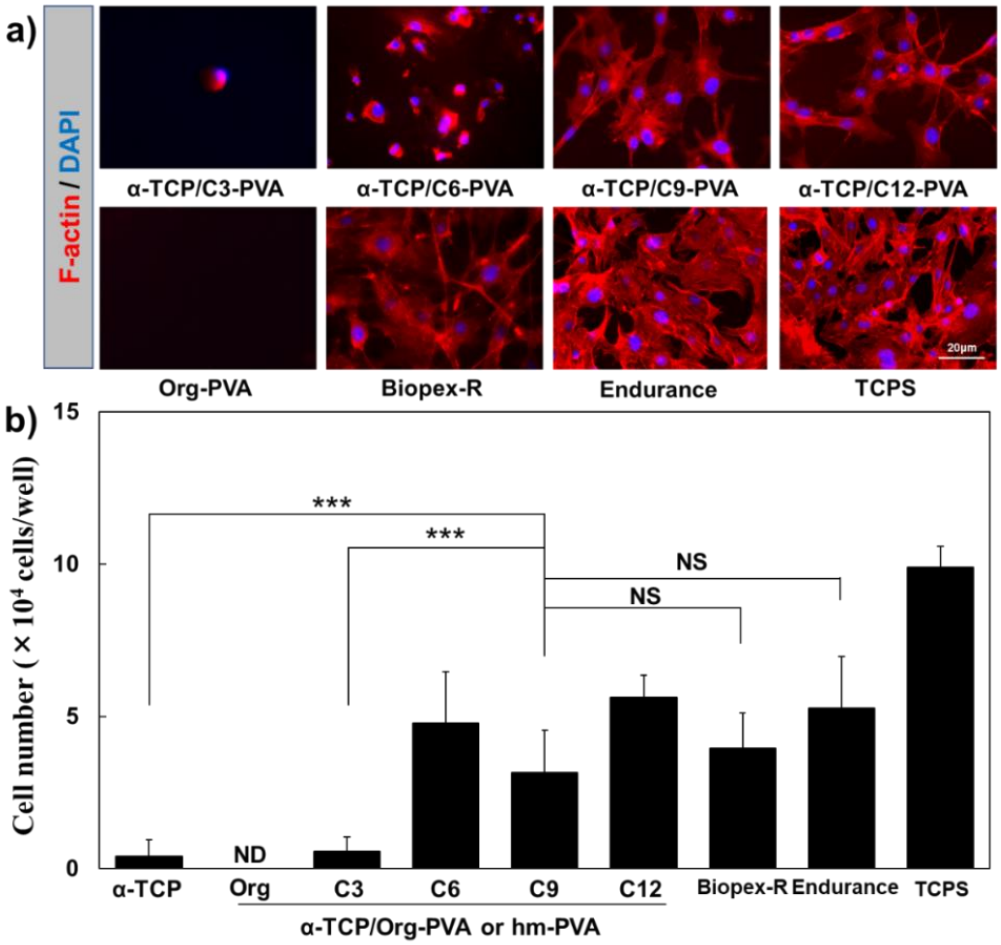

Figure 4-9. The MC3T3 adhesion on consolidated α-TCP/hm-PVA bone pastes. a) Cell staining of MC3T3 cells for phalloidin–tetramethyl rhodamine B isothiocyanate peptide and DAPI (Phalloidin–tetramethyl rhodamine B isothiocyanate peptide in red and DAPI in blue, respectively). b) Number of cells on the consolidated α-TCP/hm-PVA bone paste after 24h incubation (P***<0.001, n=3).

4.5. Conclusions

Injectable, non-diffusible and pre-filled type bone pastes composed of α-TCP and hm-PVAs with various alkyl chain lengths were developed. α-TCP/hm-PVAs bone pastes showed high injectability (over 90%) when the solid-liquid ratio was lower than 3.5. α-TCP/hm-P pastes with alkyl chains higher than C6 showed a non-diffusion property even in water and fresh porcine whole blood. The compressive strength of α-TCP/C9-PVA bone pastes increased in water and reached 27.5±2.7 MPa after 7 days. The Young's modulus of α-TCP/C9-PVA bone paste was lower than that of commercial calcium phosphate paste and PMMA-based bone cement and similar to that of ideal bone filler. Furthermore, α-TCP/C9-PVA bone paste showed excellent cell adhesion property on which osteoblastic cells were cultured. Therefore, α-TCP/C9-PVA bone paste is a promising bone filler for PVP surgery.

References

[1] J.L. Old, M. Calvert, Vertebral compression fractures in the elderly, American Family Physician, 69 (2004) 111-116.
[2] K. Serbetci, F. Korkusuz, N. Hasirci, Thermal and mechanical properties of hydroxyapatite impregnated acrylic bone cements, Polym. Test, 23 (2004) 145-155.
[3] M.A. Rothermich, J.M. Buchowski, D.B. Bumpass, G.A. Patterson, Pulmonary Cement Embolization After Vertebroplasty Requiring Pulmonary Wedge Resection, Clin. Orthop. Rel. Res., 472 (2014) 1652-1657.
[4] P. Shridhar, Y.F. Chen, R. Khalil, A. Plakseychuk, S.K. Cho, B. Tillman, P.N. Kumta, Y. Chun, A Review of PMMA Bone Cement and Intra-Cardiac Embolism, Materials, 9 (2016).
[5] X. Banse, T.J. Sims, A.J. Bailey, Mechanical properties of adult vertebral cancellous bone: Correlation with collagen intermolecular cross-links, Journal of Bone and Mineral Research, 17 (2002) 1621-1628.
[6] A.L. Wagner, E. Baskurt, Refracture with cement extrusion following percutaneous vertebroplasty of a large interbody cleft, American Journal of Neuroradiology, 27 (2006) 230-231.
[7] V. Braunstein, C.M. Sprecher, A. Gisep, L. Benneker, K. Yen, E. Schneider, P. Heini, S. Milz, Long-term reaction to bone cement in osteoporotic bone: new bone formation in vertebral bodies after vertebroplasty, Journal of Anatomy, 212 (2008) 697-701.
[8] R. Bornemann, Y. Rommelspacher, T.R. Jansen, K. Sander, D.C. Wirtz, R. Pflugmacher, Elastoplasty: A Silicon Polymer as a New Filling Material for Kyphoplasty in Comparison to PMMA, Pain Physician, 19 (2016) 885-892.
[9] A. Gasbarrini, R. Ghermandi, Y.E. Akman, M. Girolami, S. Boriani, Elastoplasty as a promising novel technique: Vertebral augmentation with an elastic silicone-based polymer, Acta Orthopaedica Et Traumatologica Turcica, 51 (2017) 209-214.
[10] T.L. Schulte, A. Keiler, F. Riechelmann, T. Lange, W. Schmoelz, Biomechanical comparison of vertebral augmentation with silicone and PMMA cement and two filling grades, European Spine Journal, 22 (2013) 2695-2701.
[11] T.A.J. Urlings, E. van der Linden, Elastoplasty: First Experience in 12 Patients, Cardiovascular and Interventional Radiology, 36 (2013) 479-483.
[12] R.Z. LeGeros, Properties of osteoconductive biomaterials: Calcium phosphates, Clin. Orthop. Rel. Res., (2002) 81-98.
[13] C.S. Liu, W. Gai, S.H. Pan, Z.S. Liu, The exothermal behavior in the hydration process of calcium phosphate cement, Biomaterials, 24 (2003) 2995-3003.
[14] T.J. Brunner, M. Bohner, C. Dora, C. Gerber, W.J. Stark, Comparison of amorphous TCP nanoparticles to micron-sized alpha-TCP as starting materials for calcium phosphate cements, Journal of Biomedical Materials Research Part B-Applied Biomaterials, 83B (2007) 400-407.
[15] N. Eliaz, N. Metoki, Calcium Phosphate Bioceramics: A Review of Their History, Structure, Properties, Coating Technologies and Biomedical Applications, Materials, 10 (2017).
[16] M. Nakano, N. Hirano, K. Matsuura, H. Watanabe, H. Kitagawa, H. Ishihara, Y. Kawaguchi, Percutaneous transpedicular vertebroplasty with calcium phosphate cement in the treatment of osteoporotic vertebral compression and burst fractures, Journal of Neurosurgery, 97 (2002) 287-293.
[17] E.F. Burguera, H.H.K. Xu, M.D. Weir, Injectable and rapid-setting calcium phosphate bone cement with dicalcium phosphate dihydrate, Journal of Biomedical Materials Research Part B-Applied Biomaterials, 77B (2006) 126-134.
[18] G.C. Anselmetti, D. Regge, E. Sardo, A. Manca, S. Cirillo, T. Meloni, F. Debernardi, Minimally invasive treatment of C2 odontoid traumatic fracture with transoral percutaneous vertebroplasty, European Radiology,

17 (2007) 850-851.
[19] G. Debrun, Nonadhesive liquid embolic agent for cerebral arteriovenous malformations: Preliminary histopathological studies in swine rete mirabile - Comment, Neurosurgery, 43 (1998) 1174-1174.
[20] J. Hamada, Y. Kai, M. Morioka, K. Kazekawa, Y. Ishimaru, H. Iwata, Y. Ushio, A nonadhesive liquid embolic agent composed of ethylene vinyl alcohol copolymer and ethanol mixture for the treatment of cerebral arteriovenous malformations: experimental study, Journal of Neurosurgery, 97 (2002) 889-895.
[21] J.I. Hamada, Y. Kai, T. Mizuno, M. Morioka, K. Kazekawa, H. Iwata, Y. Ushio, A nonadhesive liquid embolic agent of ethylene vinyl alcohol copolymer and ethanol mixture for cerebral arteriovenous malformations - Clinical experience, Interventional Neuroradiology, 10 (2004) 135-142.
[22] H.S. Mansur, C.M. Sadahira, A.N. Souza, A.A.P. Mansur, FTIR spectroscopy characterization of poly (vinyl alcohol) hydrogel with different hydrolysis degree and chemically crosslinked with glutaraldehyde, Mater. Sci. Eng. C-Biomimetic Supramol. Syst., 28 (2008) 539-548.
[23] K. Tomihata, Y. Ikada, Crosslinking of hyaluronic acid with glutaraldehyde, J. Polym. Sci. Pol. Chem., 35 (1997) 3553-3559.
[24] S.M. Oliveira, C.C. Barrias, I.F. Almeida, P.C. Costa, M.R.P. Ferreira, M.F. Bahia, M.A. Barbosa, Injectability of a bone filler system based on hydroxyapatite microspheres and a vehicle with in situ gel-forming ability, Journal of Biomedical Materials Research Part B-Applied Biomaterials, 87B (2008) 49-58.
[25] V. Sanginario, L. Ambrosio, M.P. Ginebra, J.A. Planell, Injectable composite hydrogels for orthopaedic applications. Mechanical and morphological analysis, in: M.A. Barbosa, F.J. Monteiro, R. Correia, B. Leon (Eds.) Bioceramics 16 2004, pp. 485-488.
[26] M. Bohner, N. Doebelin, G. Baroud, Theoretical and experimental approach to test the cohesion of calcium phosphate pastes, European Cells & Materials, 12 (2006) 26-35.
[27] H. Wang, N. Chen, Q. Wang, Interaction Between beta-Tricalcium Phosphate and Poly(vinyl alcohol) and Its Effect on the Thermal and Mechanical Properties of Poly(vinyl alcohol), Chemical Journal of Chinese Universities-Chinese, 35 (2014) 1810-1815.
[28] E.P. Brass, W.B. Forman, R.V. Edwards, O. Lindan, FIBRIN FORMATION - EFFECT OF CALCIUM-IONS, Blood, 52 (1978) 654-658.
[29] C. Koski, B. Onuike, A. Bandyopadhyay, S. Bose, Starch-hydroxyapatite composite bone scaffold fabrication utilizing a slurry extrusion-based solid freeform fabricator, Addit. Manuf., 24 (2018) 47-59.
[30] S.F. Chen, L.Y. Li, C. Zhao, J. Zheng, Surface hydration: Principles and applications toward low-fouling/nonfouling biomaterials, Polymer, 51 (2010) 5283-5293.
[31] U. Hempel, C. Preissler, S. Vogel, S. Moller, V. Hintze, J. Becher, M. Schnabelrauch, M. Rauner, L.C. Hofbauer, P. Dieter, Artificial Extracellular Matrices with Oversulfated Glycosaminoglycan Derivatives Promote the Differentiation of Osteoblast-Precursor Cells and Premature Osteoblasts, Biomed Research International, (2014).
[32] C.J. Handley, T. Samiric, M.Z. Ilic, Structure, Metabolism, and Tissue Roles of Chondroitin Sulfate Proteoglycans, in: N. Volpi (Ed.) Chondroitin Sulfate: Structure, Role and Pharmacological Activity 2006, pp. 219-232.
[33] K.K. Wong, G.M. Wang, J. Dreyfuss, E.C. Schreiber, ABSORPTION, EXCRETION, AND BIOTRANSFORMATION OF DIMETHYL SULFOXIDE IN MAN AND MINIATURE PIGS AFTER TOPICAL APPLICATION AS AN 80 PERCENT GEL, Journal of Investigative Dermatology, 56 (1971) 44.

Chapter 5

Injectable inclusion complex composed of α-cyclodextrin and hydrophobically modified poly(vinyl alcohol) as cerebral aneurysm embolization material

5.1. Abstract

Surgical therapy (clipping) and endovascular therapy (coiling) are the main treatment options for people with cerebral aneurysm. In recent years, minimally invasive coil embolization has been recommended. However, the surgical method presents challenges in filling rate and operability, thus highlighting the need for a novel embolization material. In this study, injectable inclusion complexes for cerebral aneurysm treatment were prepared by α-cyclodextrin (α-CD) and hydrophobically modified poly(vinyl alcohol) (hm-PVA) with various alkyl chain lengths (3, 9, and 18). As the α-CD concentration increased, the viscosity of the α-CD/hm-PVA mixtures drastically decreased. Further, 2D-NMR NOESY spectra indicated that a threaded inclusion complex was formed between α-CD and hm-PVA. By mixing hm-PVAs with different concentrations of α-CD, only hm-PVA (5 mol% nonanal-modified PVA (5C9-PVA)) with 15 mM α-CD showed a good thixotropic property. Additionally, this inclusion complex showed a gel-sol switchable property under different strain amplitudes (1% and 1000%). The α-CD/5C9-PVA inclusion complex showed good injectability, even upon using a 25 G needle. After injecting the α-CD/5C9-PVA inclusion complex into an *in vitro* cerebral aneurysm model, it formed aggregates in phosphate buffer solution at 37 ℃ and filled in the whole area. These results demonstrate that the α-CD/5C9-PVA inclusion complex could be an ideal material for cerebral aneurysm treatment.

5.2. Introduction

A cerebral aneurysm is an abnormal focal dilation of an artery in the brain that results from a weakening of the inner muscular layer (the intima) of a blood vessel wall. The vessel develops a "blister-like" dilation that can become thin and rupture without warning. The resultant bleeding into the space around the brain is called a subarachnoid hemorrhage (SAH) [1]. In fact, the most common cause of SAHs is attributed to ruptured cerebral aneurysms [2, 3]. Further, SAHs can lead to stroke, coma, and/or death. Although urgent therapy can save the lives of patients when SAH occurs, only about 1 in 3 people can restore their cerebral function after treatment [4].

People with unruptured cerebral aneurysms account for approximately 2% of adults without risk factors [5]. However, giant aneurysms, size greater than 25 mm, pose a particularly high risk and are difficult to treat [6]. Generally, there are three treatment options for people with cerebral aneurysm, including conservative management, surgical therapy (clipping), and endovascular therapy (coiling) [7]. The mechanical sophistication of available clips, along with the advent of the operating microscope in the 1960s, have made surgical clipping a standardized treatment of both ruptured and unruptured cerebral aneurysms [8]. However, the invasive and technically challenging process makes surgical clipping not an ideal treatment for patients [9]. The development of Guglielmi detachable coils (GDCs) approved by FDA in 1995 revolutionized endovascular treatment of cerebral aneurysms [10], advancing development of endovascular therapy with a microcatheter.

It is well known that the occlusion effect of the coil on the aneurysm depends on the ratio of the indwelling coil volume to the aneurysm volume (VER; volume embolization ratio). Recently, a water absorbent polymer was coated on the coil surface to increase VER [11]. In addition, coils covered with biodegradable polymer (PGLA: polyglycolic acid-co-lactide acid) threads that promote thrombosis have been developed [12]. However, the VER of these materials is limited, resulting in recanalization of the aneurysm. Therefore, development of a simple embolic material with high VER is needed.

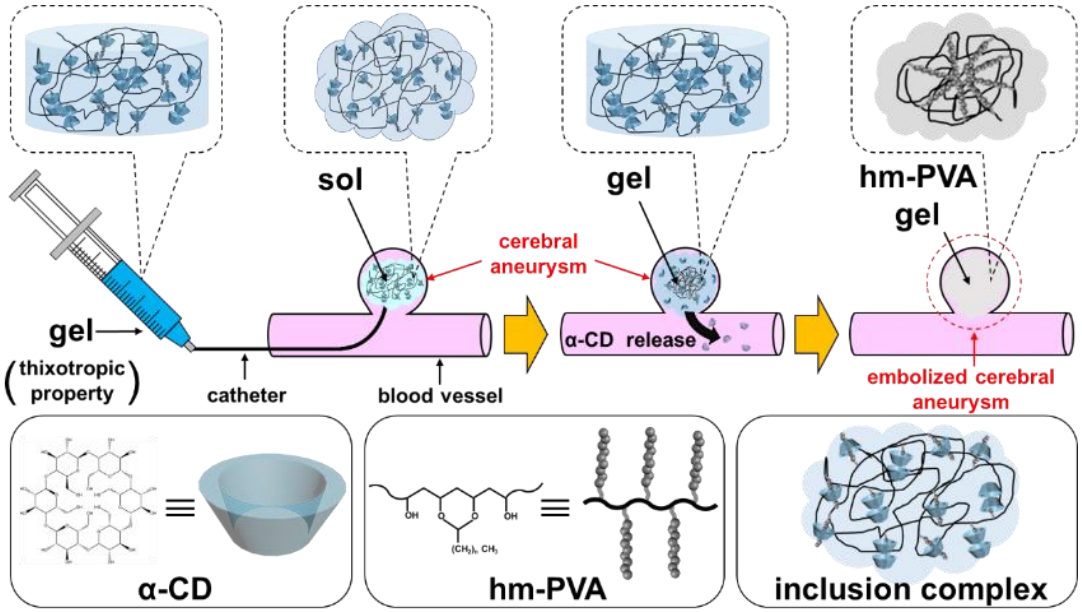

Scheme 5-1. Schematic illustration of cerebral aneurysm embolization using α-CD/hm-PVA inclusion complex. The α-CD/hm-PVA inclusion complex with thixotropic property can easily be injected into the cerebral aneurysm site using a catheter. Due to recovery of physical crosslinks (hydrophobic interaction and hydrogen bond), the α-CD/hm-PVA inclusion complex can stably fill in the cerebral aneurysm. Finally, stable hm-PVA gel formation enabled embolization of the cerebral aneurysm after α-CD release.

Previous studies demonstrated embolization by injection of ethylene vinyl alcohol dissolved in dimethyl sulfoxide (DMSO) into aneurysm, which formed aggregates in that area [13, 14]. However, injection of an organic solvent into the blood vessel limited its clinical application as it can cause side effects on cranial nerves [15]. Focusing on the water insolubility of hydrophobically modified poly(vinyl alcohol) (hm-PVA) [16, 17] and the inclusion ability of α-cyclodextrin (α-CD) to hydrophobic groups, we developed an inclusion complex composed of α-CD and hm-PVA without using any organic solvent as a cerebral artery embolization material (Scheme 5-1). In this study, fundamental properties of the α-CD/hm-PVA inclusion process as well as potential applications of the resulting complex as a material for cerebral aneurysm embolization were evaluated.

5.3. Materials and methods

5.3.1. Materials

Ethanol (EtOH, 99.5%), dimethyl sulfoxide (DMSO), 6 N hydrochloric acid (HCl), 10% formalin neutral buffer solution, Dulbecco's phosphate buffered saline (D-PBS), α-cyclodextrin, and 99.9% dimethyl sulfoxide-d_6 (DMSO-d_6) containing 0.05 w/v% tetramethylsilane (TMS) were purchased from Wako Pure Chemical Industries, Ltd. (Osaka, Japan). Otsuka normal saline 2-port was purchased from Otsuka Pharmaceutical Co., Ltd. (Tokyo, Japan). PVA (Mw = 88,000, with over 98.5% saponification degree) was purchased from Nacalai Tesque, Inc. (Kyoto, Japan). Propanal (C3), nonanal (C9), and octadecanal (C18) were purchased from Tokyo Chemical Industry Co., Ltd (Tokyo, Japan). Deuterium oxide (D_2O) containing 0.05 wt % 3-(trimethylsilyl) propionic-2,2,3,3-d_4 acid was purchased from Sigma Chemical Co. (St. Louis, MO, USA).

5.3.2. Synthesis of hm-PVAs

The hm-PVAs were prepared through the nucleophilic substitution reaction between an aldehyde and the hydroxyl groups of PVA, following a previously reported procedure [18, 19]. First, PVA (10 g) was dissolved in 48 mL of H_2O at 80°C for 60 min. Subsequently, 150 mL of DMSO and 2 mL of 1 N HCl were added to form a 200 mL solution of 5 w/v% PVA and 1 v/v% 1 N HCl. Different amounts of aldehyde groups (C3, C9, and C18) were added into the solution, and the resulting mixtures were stirred at 50°C for 1 h. A reflux condenser was used in all processes. After the reaction, the obtained hm-PVA (H_2O/DMSO = 25/75 (v/v)) solution was added to 600 mL (around 3 times) cold EtOH under stirring for 1 h. The hm-PVAs precipitated from the solution and was washed with 200 mL EtOH at least three times to remove the unreacted aldehyde and DMSO. Finally, the solvent was evaporated under vacuum to obtain purified hm-PVAs as white crystals. All crystals were crushed finely using a crusher for subsequent analysis (Wonder crusher WC-3, Osaka Chemical, Osaka, Japan).

5.3.3. Characterization of hm-PVAs

The chemical structures of the hm-PVAs were analyzed by proton nuclear magnetic resonance (^{1}H-NMR) spectroscopy (AL300, JEOL, Tokyo, Japan) using a 0.5 w/v% hm-PVA/DMSO-d_6 solution at 25 °C [16]. Eight scans for each sample were conducted. Fourier transform-infrared spectroscopy (FT-IR, 8400S, Shimadzu, Kyoto, Japan) analysis was carried out to confirm the presence of acetal groups in the hm-PVAs. The scan range was from 700 cm^{-1} to 4000 cm^{-1}, and 64 scans were conducted for each sample. Hydrophobic

group modification ratios of the hm-PVAs were determined by ^{1}H-NMR spectroscopy, and calculated using the following equation:

$$\text{Modification ratio (mol\%)} = [\{\text{Integral area } (CH_3 \text{ proton})/3\} / \text{Integral area } (\alpha CH \text{ proton})]\times 100$$

where integral area (αCH proton) is the area of the peak at 3.87 ppm corresponding to the αCH proton in the backbone of PVA and hm-PVAs, and integral area (CH_3 proton) is the area of the peak at 0.85 ppm assigned to the CH_3 proton in the hydrophobic groups of hm-PVAs.

5.3.4. Preparation of α-CD/hm-PVA mixtures

The α-CD/hm-PVA mixtures were prepared as described below. First, hm-PVA powder (200 mg) was added into a mayonnaise bottle with 2 mL of H_2O to form a 10 w/v% hm-PVA suspension. Subsequently, different amounts of α-CDs were added into this suspension, and the α-CD/hm-PVA suspension was heated in an autoclave (LSX-500, TOMY, Tokyo, Japan) at 95 ℃ for 10 min. Finally, α-CD/hm-PVA solution was stirred (200 rpm) at 25 ℃ overnight to form α-CD/hm-PVA mixtures with different concentrations of α-CD (0–30 mM).

5.3.5. Shear viscosity

The shear viscosity of α-CD/hm-PVA mixtures was evaluated using a rheometer (MCR301, Anton paar, Graz, Austria) according to the previously reported method [20]. α-CD/hm-PVA mixtures (hm-PVA concentration was 10 w/v%) containing 0-30 mM α-CD were prepared as mentioned above. The shear viscosity was measured by jig PP25 (diameter = 25 mm), with a shear rate of 0.1 S^{-1} at 298 K. Each sample was measured five times.

5.3.6. 2D 1H NMR study of α-CD/hm-PVA mixtures

To indicate the formation of a threaded inclusion complex between α-CD and the hydrophobic moiety of hm-PVAs, 2D NOESY spectra of the α-CD/hm-PVA mixtures in D_2O at 298 K were analyzed by NMR (JNM-ECS-400, JEOL, Tokyo, Japan). In total, four scans were performed for each sample.

5.3.7. Structural recovery evaluation

Three-stage structural recovery tests were conducted using a rheometer (MCR301, Anton paar, Graz, Austria) equipped with a plate of PP 25, according to the previously reported method [21, 22]. The required volume of α-CD/hm-PVA inclusion complex was 0.5 mL. Subsequently, three-stage oscillation tests with different oscillation amplitudes at constant frequency (ω = 10 rad/s) were carried out. Specifically, in Stage I, small oscillation amplitude was applied for a period of 180 s to obtain the shear moduli of the initial state (γ = 1%). For Stage II, the large strain amplitude (γ = 1000%) was applied for a period of 180 s. Finally, in Stage III, the same small oscillation amplitude as stage I was applied for 180 s, followed by recovery within a short time.

5.3.8. Thixotropic evaluation

Rheological measurements were performed with a rheometer (MCR301, Anton paar, Graz, Austria), using parallel plate PP 25 geometry (25 mm diameter; 1 mm gap). Temperature was maintained at 25°C. For thixotropy measurements, the shear rates applied were varied from 0.001 to 1000 s^{-1} in an upward sweep and immediately followed by a downward sweep.

5.3.9. Evaluation of Injectability

The injectability of prepared α-CD/hm-PVA inclusion complexes was evaluated with a testing machine (EZ-LX, Shimadzu Co., Kyoto, Japan) [23]. The inclusion complex was filled in a 2.5 mL syringe with a 20 G or 25 G needle (Terumo Co., Tokyo, Japan), which was then set into a mold with a hole. Under pressure, the α-CD/hm-PVA inclusion complex was extruded, and this process was stopped when the extrusion strength reached 250 N [24, 25]. Five specimens were tested for each group. Injectability was calculated using the following equation:

$$\text{Injectability (\%)} = 100 \times (Wt-Wr) / Wt$$

where Wt and Wr are the weight of the total and remaining paste in the syringe, respectively.

5.3.10. Stability of α-CD/hm-PVA inclusion complexes in PBS

A cerebral aneurysm model was created with silicone rubber and a glass plate. The diameter of the circle component was 10 mm. In brief, α-CD/hm-PVA inclusion complexes were injected into the circle part with a catheter. Subsequently, the cerebral aneurysm model was incubated in PBS solution at 37°C for 24 h. Finally, the remaining volume was evaluated.

5.3.11. Stability test of α-CD/5C9-PVA inclusion complexes

Rheological measurements were performed with a rheometer (MCR301, Anton paar, Graz, Austria), using parallel plate PP 25 geometry (25 mm diameter; 1 mm gap). The required volume of α-CD/5C9-PVA inclusion complex was 0.5 mL. The constant frequency ω was 10 rad/s and strain γ was 1%. Temperature was increased from 15 °C to 45 °C.

5.3.12. Statistical analysis

Statistical analysis was conducted using Tukey-Kramer test with KyPlot software. Statistically significant differences were accepted at $p < 0.05$. Data are presented as mean ± standard deviation (SD).

5.4. Results and discussion

5.4.1. Synthesis and characterization of hm-PVAs

Hm-PVAs were prepared via a reaction between the hydroxyl groups of PVA and an aldehyde with different numbers of methylene carbons (n = 1, 7, 16, Figure 5-1a). Under acidic conditions, aldehydes react with hydroxyl groups via a nucleophilic substitution reaction to form a stable hexagonal ring structure in a short time [19]. Figure 5-1b shows ^{1}H-NMR spectra of hm-PVAs with different alkyl chain lengths (C3, C9,

C18). The typical chemical shifts at 0.85 ppm and 1.26 ppm were assigned to CH_3 and αCH_2 protons in the hydrophobic moiety of hm-PVAs, respectively, which indicated the successful introduction of aldehyde groups to PVA. Hm-PVAs were also analyzed by FT-IR spectra (Figure 5-1c). The peak observed at 2,930 cm^{-1} was attributed to C-H stretching vibration of αCH_2 in the acetal groups of hm-PVAs, demonstrating that hm-PVAs were successfully synthesized. The modification ratio of hydrophobic groups was calculated from ^{1}H-NMR results, as shown in Table 5-1.

Table 5-1. Modification ratios of hm-PVAs

Abbreviation	Hydrophobic group reagent	Hydrophobic group reagent added (mol%)	Hydrophobic group modification (mol%)
5C3-PVA	Propanal	10	5
5C9-PVA	Nonanal	10	5
1C18-PVA	Octadecanal	2.5	1

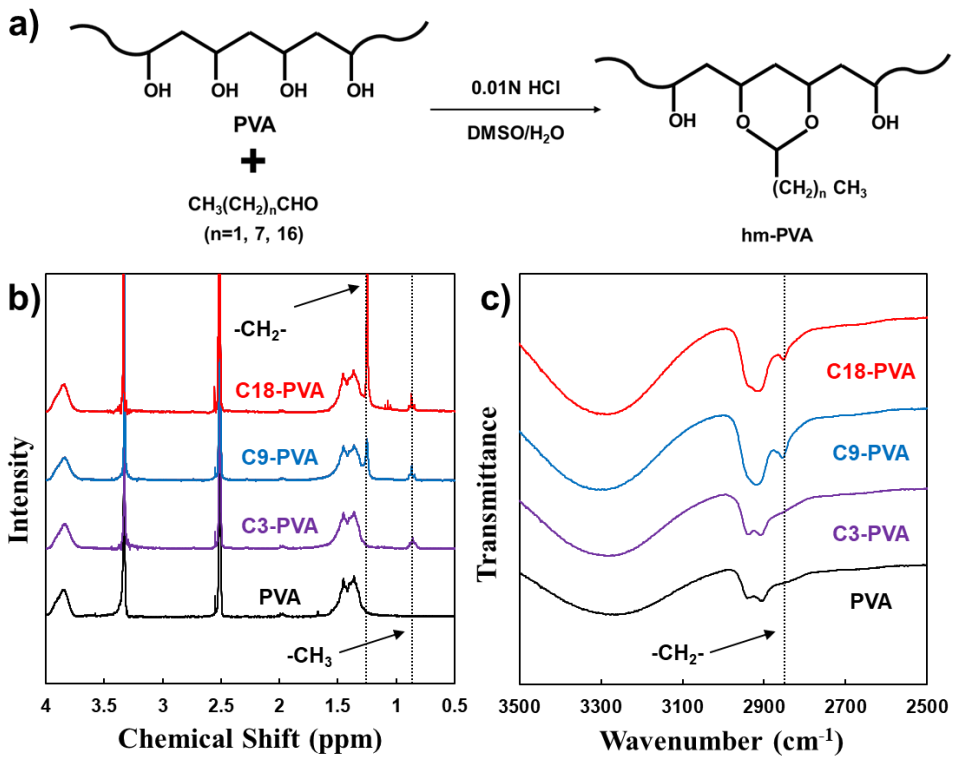

Figure 5-1. Synthesis and characterization of hm-PVAs. a) Synthesis of hm-PVAs. b) ^{1}H-NMR and c) FT-IR spectra of hm-PVAs.

5.4.2. Shear viscosity of α-CD/hm-PVA mixtures

Synthesized hm-PVAs with long alkyl chains (C9, C18) could not be dissolved in water, owing to their strong hydrophobic interaction. Therefore, to dissolve hm-PVAs in water, α-CD was mixed to form an α-CD/hm-PVA complex. It is well known that α-CD can disrupt the hydrophobic association through formation of a special threading rotaxane structure [20, 26]. Based on this feature of α-CD, α-CD/hm-PVA mixtures were prepared as shown in Figure 5-2a.

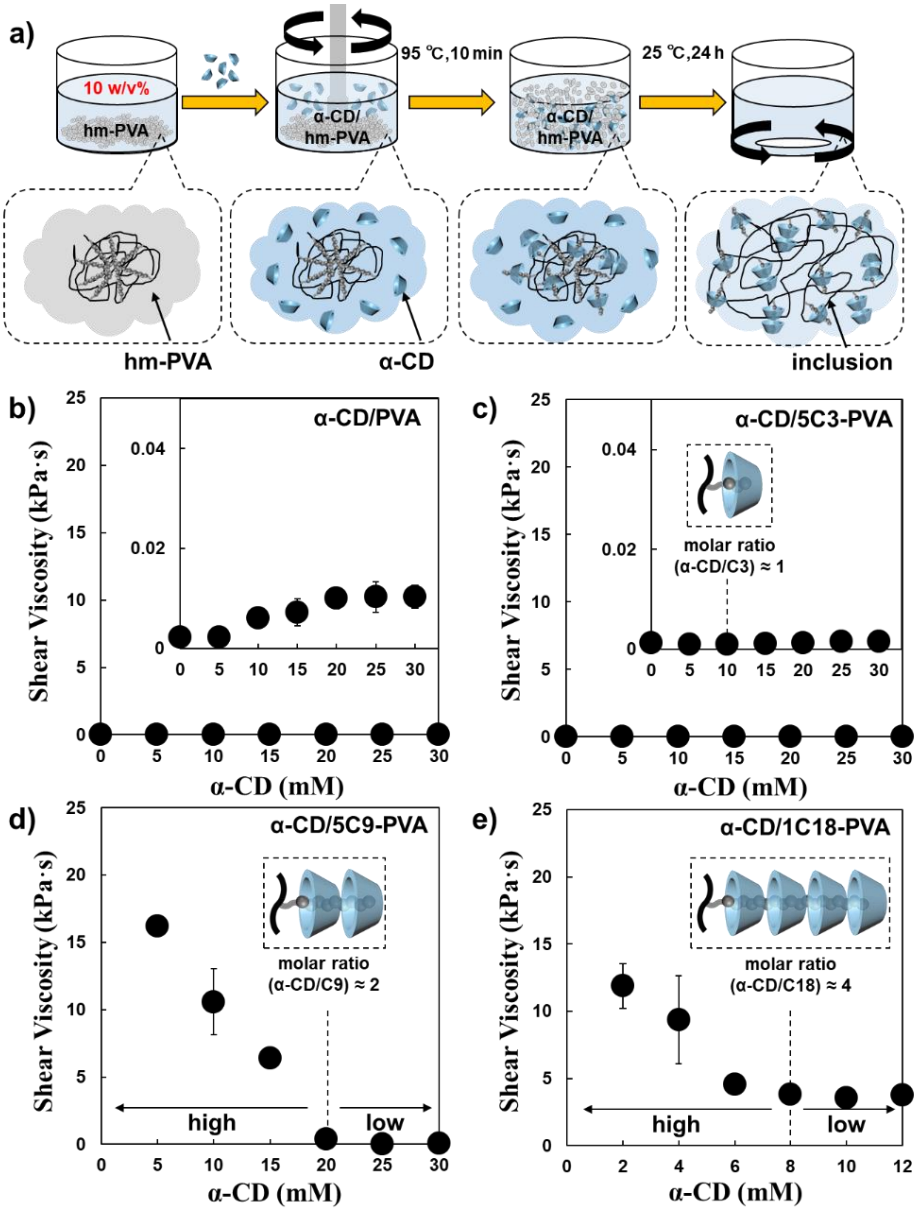

Figure 5-2. Shear viscosity of α-CD/PVA or α-CD/hm-PVA mixtures with different mixing ratios. a) Preparation procedure of the α-CD/hm-PVA mixtures. b-e) Shear viscosity of the α-CD/PVA mixture and α-CD/hm-PVA mixtures as a function of the α-CD concentration (polymer concentration was set at 10 w/v%). Shear rate = 0.1 S^{-1}. (n = 5)

As expected, hm-PVA could be dissolved in water by addition of α-CD. Further, to confirm the dependency of α-CD addition on viscosity of hm-PVAs, shear viscosity was measured using rheometer. In Figure 5-2b, the shear viscosity of the α-CD/PVA mixture was found to be very low (~0.01 kPa·s), due to the lack of enough alkyl chain. However, as the concentration of α-CD increased, the viscosity of α-CD/PVA mixture increased slightly from 0.0023 ± 0.0003 kPa·s (0 mM α-CD) to 0.0104 ± 0.0023 kPa·s (30 mM α-CD), probably due to the hydrogen bond between α-CD and PVA at higher concentrations. Interestingly, the shear viscosity of the α-CD/5C3-PVA mixture remained stable around 0.001 kPa·s at different concentrations of α-CD (Figure 5-2c), probably due to inhibition of the hydrogen bonding between hydroxyl groups of 5C3-PVA by the short alkyl chain (C3). In contrast, the shear viscosity of α-CD/5C9-PVA and α-CD/1C18-PVA mixtures showed a dramatic decrease with α-CD addition (Figure 5-2d and 5-2e). As shown in Figure 5-2d, the shear viscosity of the α-CD/5C9-PVA mixture changed from high viscosity (6.414 ± 0.023 kPa·s, 15 mM

α-CD) to low viscosity (0.029 ± 0.005 kPa·s, 15 mM α-CD) around 20 mM α-CD (molar ratio of α-CD/C9 groups is close to 2). A similar phenomenon was observed in the α-CD/1C18-PVA mixture; however, the decrease in shear viscosity of the α-CD/5C9-PVA mixture was much higher compared to the α-CD/1C18-PVA mixture. Further, shear viscosity of the α-CD/1C18-PVA mixture changed from high viscosity (4.542 ± 0.263 kPa·s, 6 mM α-CD) to low viscosity (3.548 ± 0.151 kPa·s, 10 mM α-CD) around 8 mM α-CD (molar ratio of α-CD/C9 groups is close to 4).

From these results, we hypothesized that α-CD/hm-PVA inclusion complexes were formed around critical inclusion concentrations (molar ratio of α-CD/C3 is 1:1, molar ratio of α-CD/C9 is 2:1, molar ratio of α-CD/C18 is 4:1). When only a small amount of α-CD was added, α-CD could not fully interact with the hydrophobic groups due to the relatively strong hydrophobic association of the polymer (hm-PVA). It is well known that short alkyl chain lengths (C5) can be included in the hydrophobic pocket of α-CD [27]. Thus, two α-CDs are needed for intermediate-length alkyl chains (C9), while four α-CDs are needed for longer alkyl chains (C18). Once the α-CDs started to form an inclusion complex with hydrophobic groups distributed along the polymer chains, the unfolding of the polymer main chains would promote cooperative complexation of α-CD. Therefore, our results show good correlation with previous results.

5.4.3. 2D ^{1}H-NMR study of α-CD/hm-PVA inclusion complexes

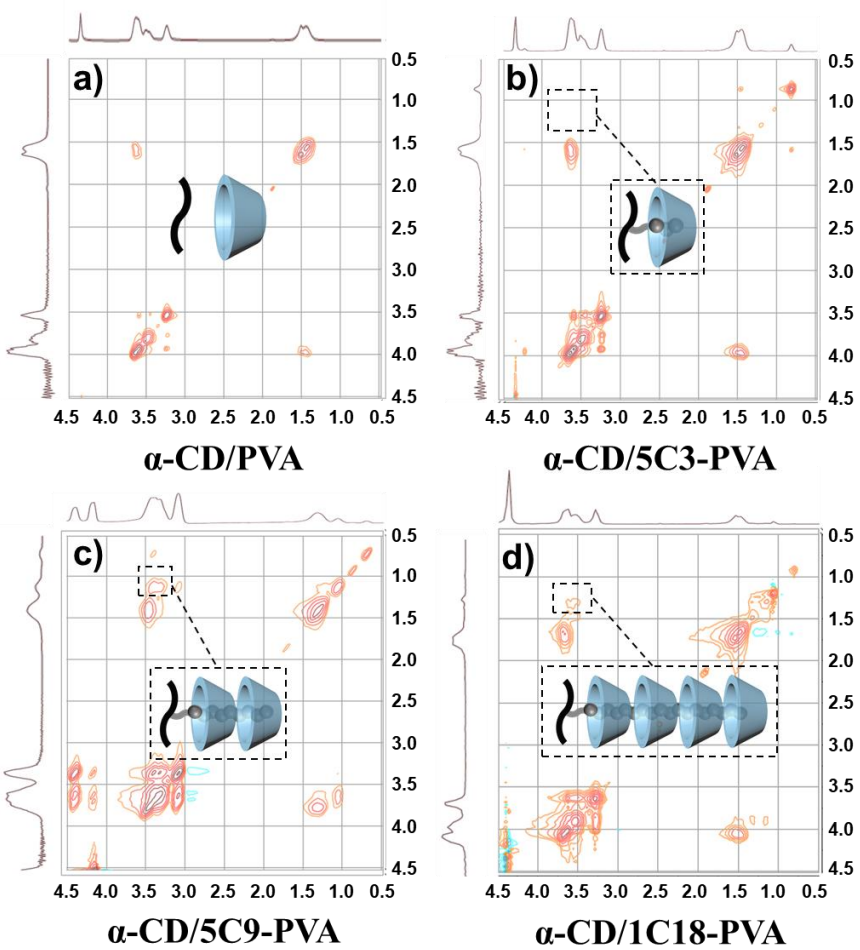

Figure 5-3. 2D NOESY spectra of a) 1 w/v% PVA with 1 mM α-CD, b) 1 w/v% 5C3-PVA with 1 mM α-CD (molar ratio of α-CD/C3 is close to 1 : 1), c) 1 w/v% 5C9-PVA with 2 mM α-CD (molar ratio of α-CD/C9 is close to 2 : 1), d) 1 w/v% 1C18-PVA with 0.8 mM α-CD (molar ratio of α-CD/C18 is close to 4 : 1) in D_2O (298 K).

To demonstrate formation of a threaded inclusion complex between the hydrophobic groups of hm-PVA and α-CD, 2D NOESY spectra of the α-CD/hm-PVA mixture in D_2O at 298 K were analyzed by NMR (Figure 5-3a-d). Correlation peaks of the α-CD/PVA mixture were clear, indicating that a threaded inclusion complex was not formed between α-CD and the PVA molecule (Figure 5-3a). A similar spectrum was observed in the α-CD/5C3-PVA mixture, suggesting unstable inclusion between α-CD and C3-PVA. In comparison, α-CD/hm-PVA with longer alkyl chain (C9, C18) mixtures displayed clear NOE correlations between the protons of α-CD (3.75 ppm) and the hydrophobic group in hm-PVA (1.25 ppm), indicating formation of a threaded inclusion complex between α-CD and the hm-PVA molecule.

5.4.4. Structural recovery evaluation

Structural recovery of different compositions of α-CD/hm-PVA inclusion complexes was evaluated using a rheometer.

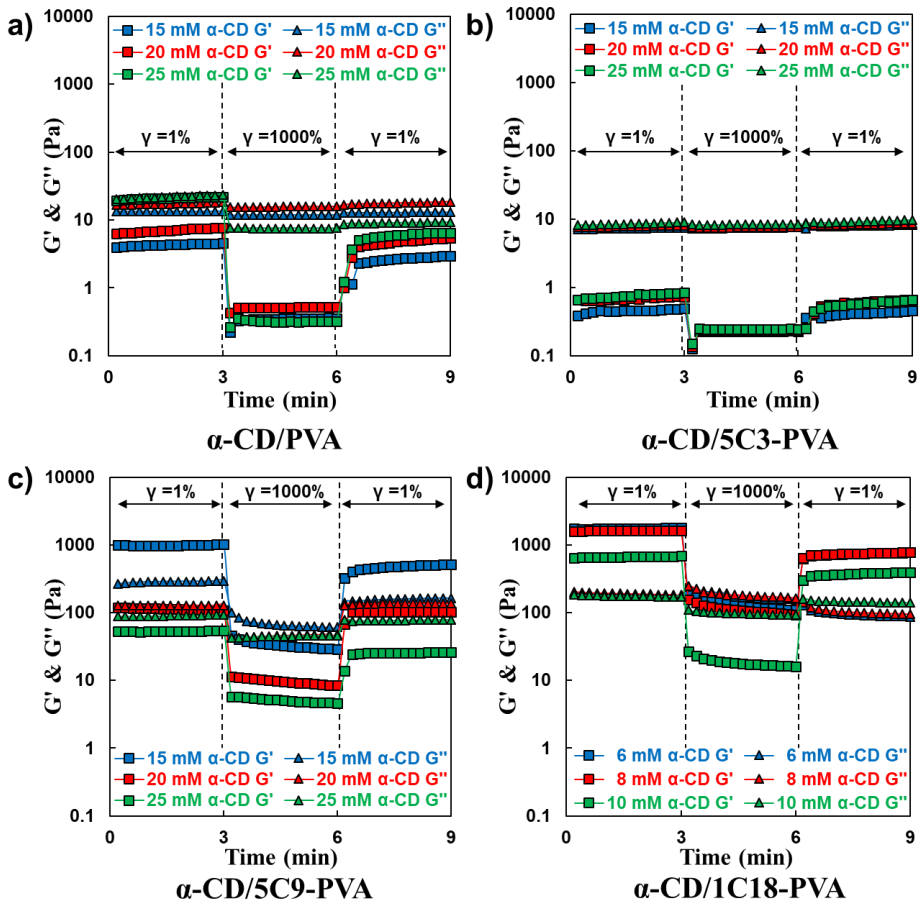

Figure 5-4. Storage modulus G' and loss modulus G'' as a function of strain. a) PVA with 15, 20, and 25 mM α-CD; b) 5C3-PVA with 15, 20, and 25 mM α-CD; c) 5C9-PVA with 15, 20, and 25 mM α-CD; d) 1C18-PVA with 6, 8, and 10 mM α-CD. A shear strain amplitude of 1–1000% and an angular frequency of 10 rad s^{-1} were applied. The temperature was set at 25 °C.

Figure 5-4a shows the change in the modulus of PVA (10 w/v%) with 15, 20, and 25 mM α-CD in aqueous solutions as a function of strain. At small (γ = 1%) and large (γ = 1000%) strain amplitude, the loss modulus G'' was significantly greater than the storage modulus G', which indicated the free-flowing sol state. Further, this same phenomenon was observed with 5C3-PVA (10 w/v%). As shown in Figure 5-5a and 5-5b,

PVA with 15 mM α-CD and 5C3-PVA with 15 mM α-CD demonstrated typical Newtonian fluid [28], probably due to weak interactions with α-CD by both PVA and C3-PVA .

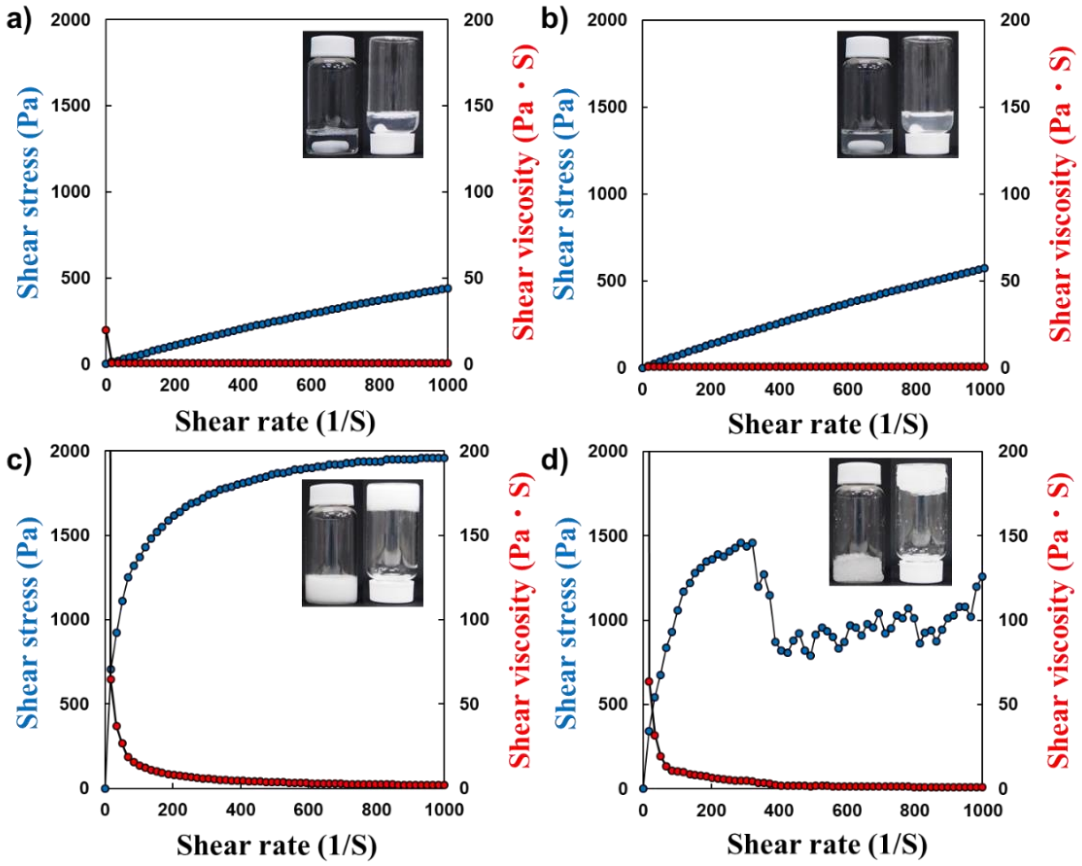

Figure 5-5. Thixotropic evaluation of α-CD/hm-PVA inclusion complexes. a) PVA with 15 mM α-CD, b) 5C3-PVA with 15 mM α-CD, c) 5C9-PVA with 15 mM α-CD, d) 1C18-PVA with 6 mM α-CD.

Interestingly, the α-CD/5C9-PVA inclusion complex showed a unique structural recovery property (Figure 5-4c). At stage I (γ = 1%), the storage modulus G' of 5C9-PVA (10 w/v%) with 15 mM α-CD in aqueous solution was higher than the loss modulus G'', indicating the gel state of this inclusion complex. However, the storage modulus G' showed a dramatic decrease at stage II (γ = 1000%), becoming lower than the loss modulus G'', indicating the sol state of the inclusion complex. While a small oscillation amplitude (similar to stage I) was applied, the storage modulus G' and loss modulus G'' recovered to the initial state, implying that the mixture returned to gel state. As shown in Figure 5-5c, this curve shows typical pseudoplastic property [28]. Therefore, 5C9-PVA with 15 mM α-CD had thixotropic property (non-Newtonian fluid). The mechanism of structural recovery may be due to regeneration of physical crosslinking such as hydrophobic interactions and hydrogen bonds, as illustrated in Figure 5-6. When the α-CD/5C9-PVA inclusion complex was applied for the small oscillation amplitude (γ = 1%) in stage I, the hydrophobic interaction and hydrogen bond were stable. However, under the large strain amplitude (γ = 1000%), the physical crosslinking collapsed. Interestingly, the same small oscillation amplitude (as in stage I) was applied again, and the physical crosslinking recovered immediately. As the α-CD concentration increased, the α-CD/5C9-PVA inclusion complex lost the gel-sol switchable property due to the decrease in the hydrophobic interaction. Compared to the α-CD/5C9-PVA mixture, the α-CD/1C18-PVA mixture showed much stronger recovery ability because of the longer alkyl chain (Figure 5-4d). However, 1C18-PVA with 6 mM α-CD did not show thixotropic property (Figure 5-5d).

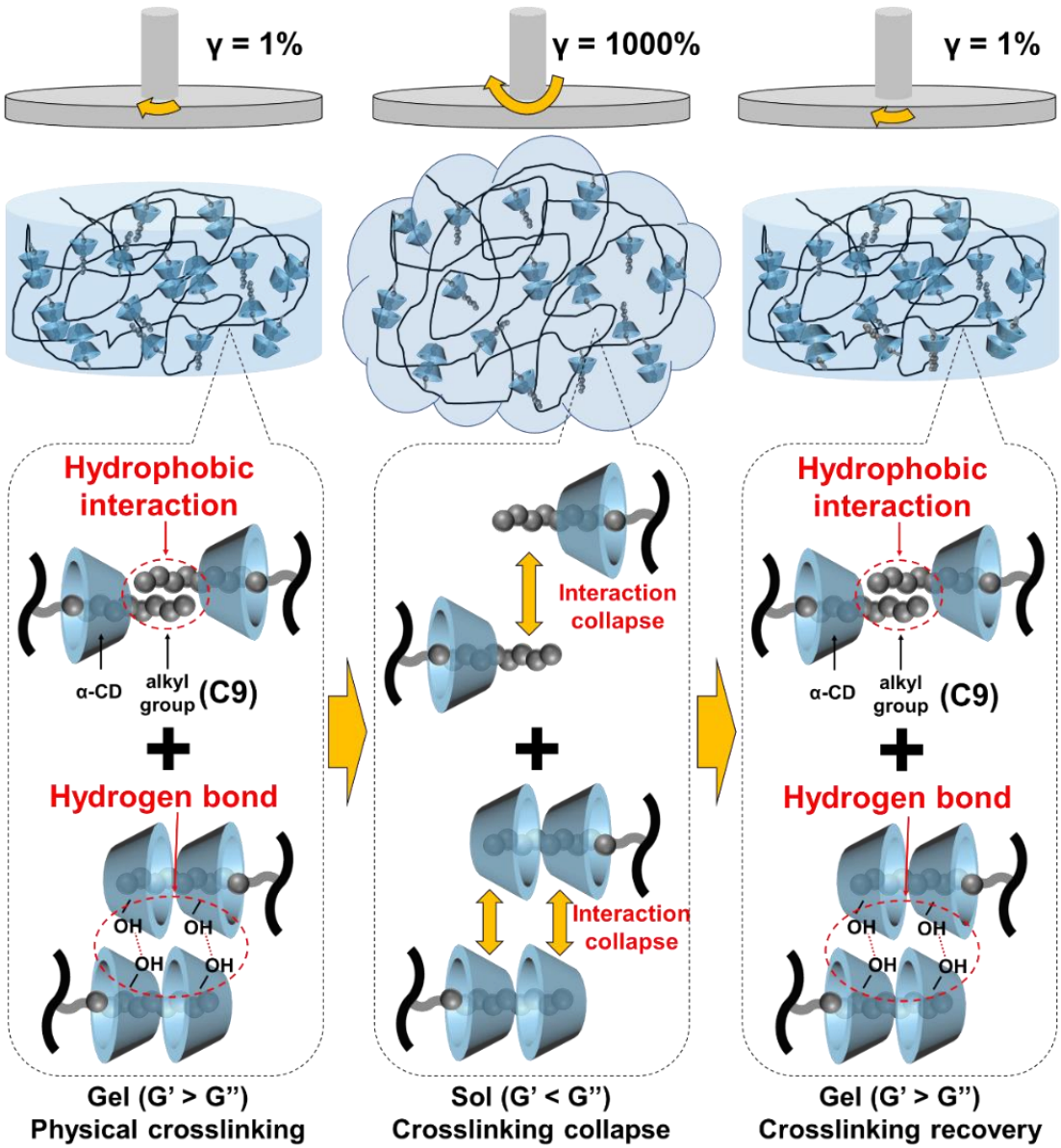

Figure 5-6. The mechanism of structural recovery of the α-CD/5C9-PVA inclusion complex.

5.4.5. Evaluation of Injectability

For catheter treatment of the cerebral artery, α-CD/hm-PVA inclusion complexes should be injectable using small diameter-sized catheters. We, therefore, evaluated injectability according to the previously reported method [24, 25] (Figure 5-7a). Injection was stopped when injection force became over 250 N. As shown in Figure 5-7b, injectability of 10 w/v% PVA with 15 mM α-CD, 10 w/v% 5C3-PVA with 15 mM α-CD, and 10 w/v% 5C9-PVA with 15 mM α-CD was over 90% when a 20 G or 25 G needle was used. However, 10 w/v% 1C18-PVA with 6 mM α-CD showed strong resistance with the 25 G needle due to a strong hydrophobic interaction. The injection force of α-CD/hm-PVA inclusion complexes during the injection process is shown in Figure 5-7c. Predictably, the injection force increased with increasing alkyl chain length and decreasing inner diameter of the needle. As such, over 250 N was needed to inject α-CD (6 mM)/1C18-PVA with a 25 G needle.

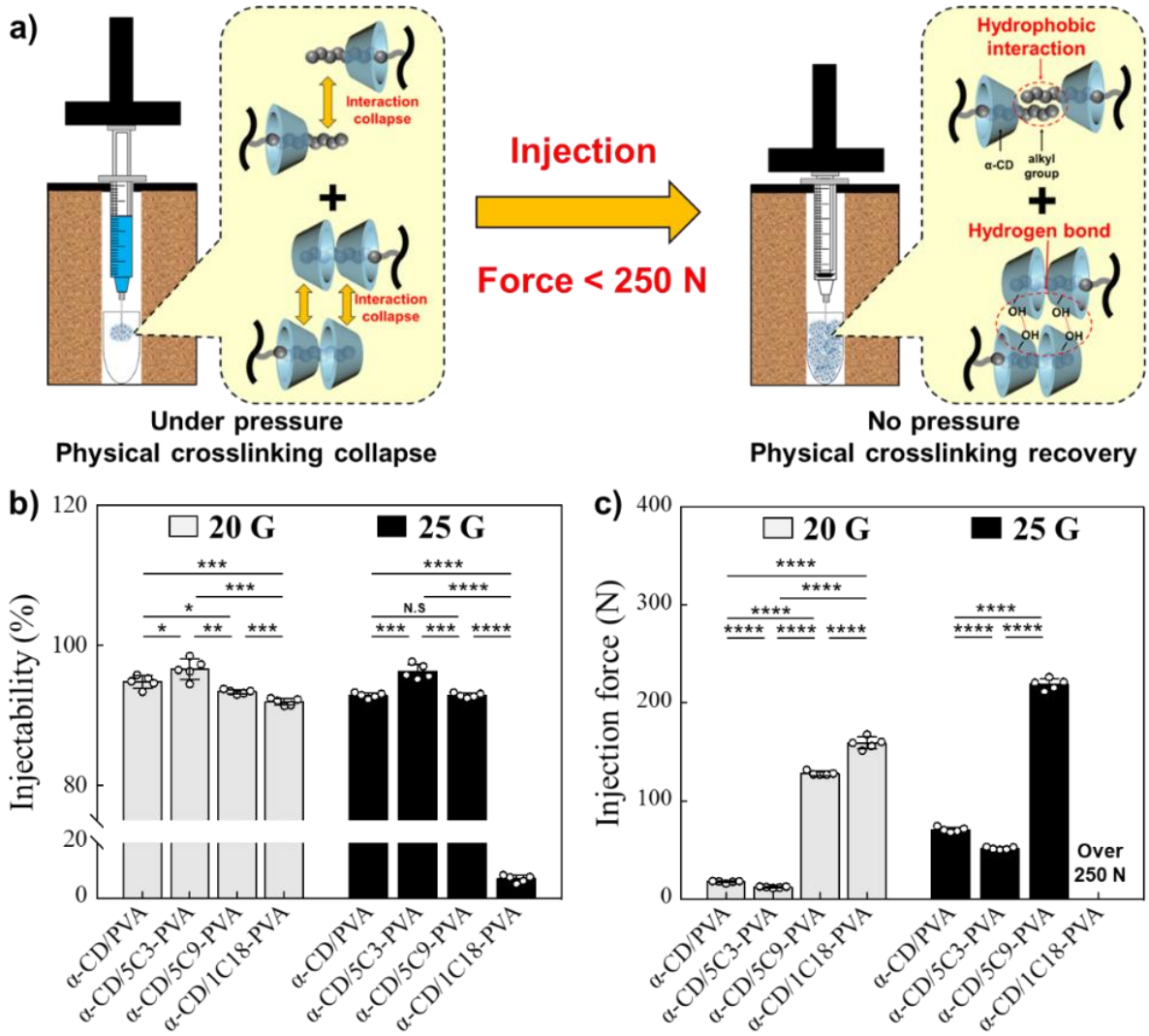

Figure 5-7. Injectability test of α-CD/hm-PVA inclusion complexes using syringe. a) Injectability test system, b) injectability, and c) injection force of α-CD/hm-PVA inclusion complex. (*P < 0.05, **P < 0.01, ***P < 0.001, ****P < 0.0001, n = 5)

5.4.6. Embolization of cerebral aneurysm model with α-CD/hm-PVA inclusion complexes

In addition to injectability, stability of α-CD/hm-PVA inclusion complexes after embolization of cerebral aneurysm in a water environment is required to promote stable structure formation. Therefore, a cerebral aneurysm model (Figure 5-8a) was prepared to evaluate the stability of α-CD/hm-PVA inclusion complexes with different alkyl chain lengths after injection. After injection of α-CD/hm-PVA inclusion complexes into the cerebral aneurysm model, the model was subsequently incubated in PBS solution at 37 °C for 24 h. As shown in Figure 5-8b, the cerebral aneurysm model could be completely filled with all samples just after injection. However, the α-CD/PVA mixture and α-CD/5C3-PVA inclusion complex were dissolved in PBS after a few minutes, indicating that the α-CD/5C3-PVA inclusion complex only had a weak hydrogen bond between hydroxyl groups in α-CD and 5C3-PVA, resulting in swelling and diffusion due to its short alkyl chain length. Conversely, embolization with α-CD/5C9-PVA and α-CD/1C18-PVA inclusion complex was completely stable in PBS, even after incubation for 24 h. Further, the injected shapes of these α-CD/hm-PVA inclusion complexes were maintained well after 24 h.

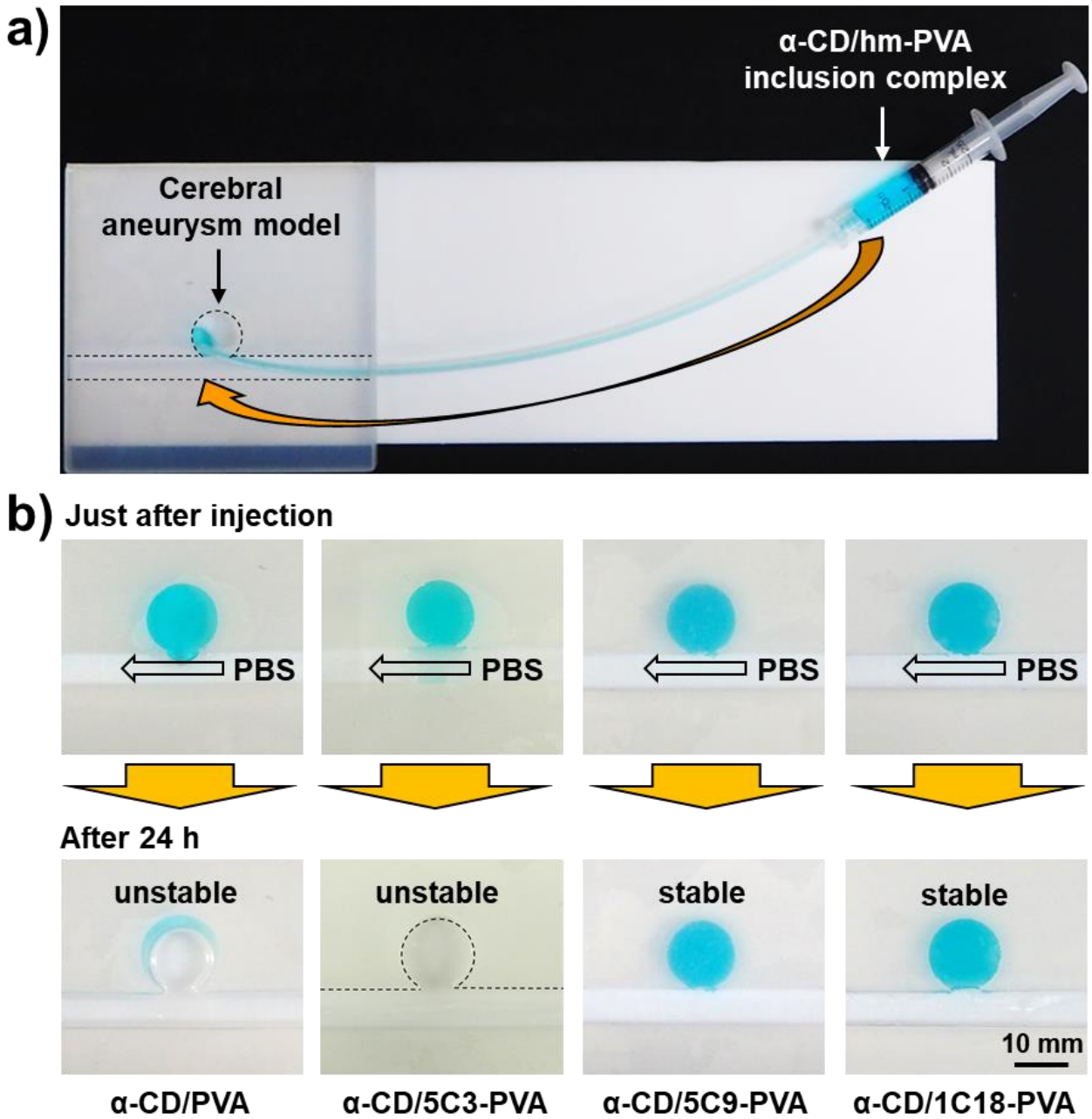

Figure 5-8. Embolization of cerebral aneurysm model using α-CD/hm-PVA. a) Injection of α-CD/hm-PVA inclusion complex into a cerebral aneurysm model. b) The stability of α-CD/hm-PVA inclusion complexes with different alkyl chain lengths in PBS after incubation at 37 ℃ for 24 h.

These phenomena were due to adequate hydrophobic interaction and the hydrogen bond between α-CD and hm-PVA. Additionally, it was found that storage modulus G' of the α-CD/5C9-PVA inclusion complex (2,020 ± 169 Pa) was much higher than loss modulus G'' of the α-CD/5C9-PVA inclusion complex (408 ± 84 Pa) from 15 ℃ to 45 ℃ (Figure 5-9). This indicates that the α-CD/5C9-PVA inclusion complex was a stable gel at different temperatures, suggesting that the α-CD/5C9-PVA inclusion complex could be injected into the cerebral aneurysm site and fill the space.

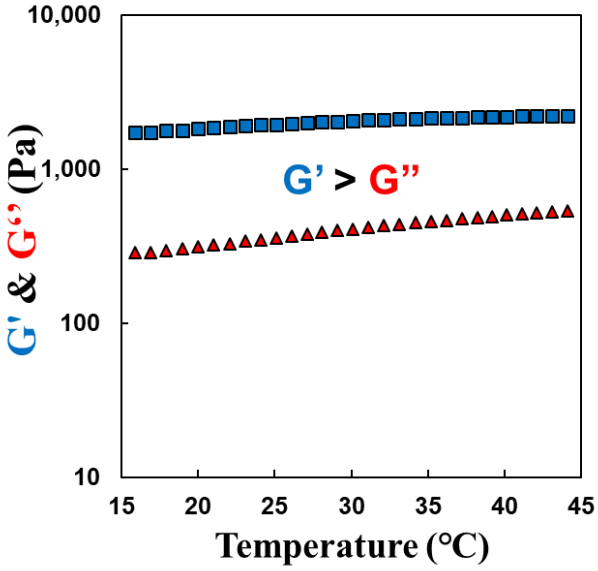

Figure 5-9. Stability test of α-CD/5C9-PVA inclusion complexes with 15 mM α-CD at different temperatures.

5.5. Conclusions

Injectable inclusion complexes for cerebral aneurysm treatment were developed using α-CD and hm-PVA with various alkyl chain lengths (3–18). With addition of α-CD, the water-insoluble hm-PVA could be dissolved in aqueous solution. Further, the viscosity of the α-CD/hm-PVA solution decreased slightly as the α-CD concentration increased. Additionally, 2D-NMR NOESY spectra indicated that a threaded inclusion complex was established between α-CD and the hm-PVA molecule. Among the prepared inclusion complexes, α-CD/5C9-PVA (5C9-PVA with 15 mM α-CD) showed thixotropic property, and its injectability was over 90%, even using a 25G needle. Moreover, the α-CD/5C9-PVA inclusion complex was stable in PBS after incubation at 37℃ for 24 h. Therefore, the α-CD/5C9-PVA inclusion complex is a promising material that could be applied for cerebral aneurysm treatment.

References

[1] I. van der Schaaf, A. Algra, M. Wermer, A. Molyneux, M. Clarke, J. van Gijn, G. Rinkel, Endovascular coiling versus neurosurgical clipping for patients with aneurysmal subarachnoid haemorrhage, The Cochrane database of systematic reviews, (2005) CD003085-CD003085.
[2] L. Zhao, L. Zhang, X. Zhang, Z. Li, L. Tian, Y.-X.J. Wang, An Analysis of 1256 Cases of Sporadic Ruptured Cerebral Aneurysm in a Single Chinese Institution, Plos One, 9 (2014).
[3] M. Korja, J. Kaprio, Controversies in epidemiology of intracranial aneurysms and SAH, Nature Reviews Neurology, 12 (2016) 50-55.
[4] A.K. Petridis, M.A. Kamp, J.F. Cornelius, T. Beez, K. Beseoglu, B. Turowski, H.J. Steiger, Aneurysmal Subarachnoid Hemorrhage, Dtsch Arztebl Int, 114 (2017) 226-236.
[5] G.J.E. Rinkel, M. Djibuti, A. Algra, J. van Gijn, Prevalence and risk of rupture of intracranial aneurysms - A systematic review, Stroke, 29 (1998) 251-256.
[6] C.W. Huh, J.I. Lee, C.H. Choi, T.H. Lee, J.Y. Choi, J.K. Ko, Endosaccular Treatment of Very Large and Giant Intracranial Aneurysms with Parent Artery Preservation : Single Center Experience with Long Term Follow-up, Journal of Korean Neurosurgical Society, 61 (2018) 450-457.
[7] N. Ajiboye, N. Chalouhi, R.M. Starke, M. Zanaty, R. Bell, Unruptured Cerebral Aneurysms: Evaluation and Management, TheScientificWorldJournal, 2015 (2015) 954954-954954.
[8] N.A. Martin, The combination of endovascular and surgical techniques for the treatment of intracranial aneurysms, Neurosurgery Clinics of North America, 9 (1998) 897-916.
[9] L.B. Ross, A. Weill, M. Piotin, J. Moret, Endovascular treatment of distally located giant aneurysms, Neurosurgery, 47 (2000) 1147-1152.
[10] G. Guglielmi, History of the genesis of detachable coils A review, Journal of Neurosurgery, 111 (2009) 1-8.
[11] G. Canton, D.I. Levy, J.C. Lasheras, Changes in the intraaneurysmal pressure due to HydroCoil embolization, American Journal of Neuroradiology, 26 (2005) 904-907.
[12] H.S. Kang, M.H. Han, B.J. Kwon, O.K. Kwon, S.H. Kim, S.H. Choi, K.H. Chang, Short-term outcome of intracranial aneurysms treated with polyglycolic acid/lactide copolymer-coated coils compared to historical controls treated with bare platinum coils: A single-center experience, American Journal of Neuroradiology, 26 (2005) 1921-1928.
[13] A.J. Molyneux, S. Cekirge, I. Saatci, G. Gal, Cerebral Aneurysm Multicenter European Onyx (CAMEO) trial: Results of a prospective observational study in 20 European centers, American Journal of Neuroradiology, 25 (2004) 39-51.
[14] M. Kurdi, S. Baeesa, M. Bin-Mahfoodh, K. Kurdi, Onyx Embolization of Ruptured Intracranial Aneurysm Associated with Behcet's Disease, Case reports in vascular medicine, 2013 (2013) 797045-797045.
[15] J.I. Hamada, Y. Kai, T. Mizuno, M. Morioka, K. Kazekawa, H. Iwata, Y. Ushio, A nonadhesive liquid embolic agent of ethylene vinyl alcohol copolymer and ethanol mixture for cerebral arteriovenous malformations - Clinical experience, Interventional Neuroradiology, 10 (2004) 135-142.
[16] X. Chen, T. Taguchi, Hydrophobically modified poly(vinyl alcohol)s as antithrombogenic coating materials, Materials Science & Engineering C-Materials for Biological Applications, 102 (2019) 289-298.
[17] X. Chen, T. Taguchi, Injectable, Non-Diffusible, and Pre-Filled Bone Paste Composed of α-Tricalcium Phosphate and Hydrophobically Modified Poly(Vinyl Alcohol), Advanced Engineering Materials, 21 (2019) 1900660.
[18] H.S. Mansur, C.M. Sadahira, A.N. Souza, A.A.P. Mansur, FTIR spectroscopy characterization of poly (vinyl alcohol) hydrogel with different hydrolysis degree and chemically crosslinked with glutaraldehyde,

Mater. Sci. Eng. C-Biomimetic Supramol. Syst., 28 (2008) 539-548.
[19] K. Tomihata, Y. Ikada, Crosslinking of hyaluronic acid with glutaraldehyde, J. Polym. Sci. Pol. Chem., 35 (1997) 3553-3559.
[20] X. Hao, M. Xu, J. Hu, Q. Yan, Photoswitchable thermogelling systems based on a host-guest approach, Journal of Materials Chemistry C, 5 (2017) 10549-10554.
[21] Q. Li, D.G. Barret, P.B. Messersmith, N. Holten-Andersen, Controlling Hydrogel Mechanics via Bio-Inspired Polymer-Nanoparticle Bond Dynamics, Acs Nano, 10 (2016) 1317-1324.
[22] C. Yuece, N. Willenbacher, Challenges in Rheological Characterization of Highly Concentrated Suspensions - A Case Study for Screen-printing Silver Pastes, Jove-Journal of Visualized Experiments, (2017).
[23] E.B. Montufar, T. Traykova, E. Schacht, L. Ambrosio, M. Santin, J.A. Planell, M.-P. Ginebra, Self-hardening calcium deficient hydroxyapatite/gelatine foams for bone regeneration, Journal of Materials Science-Materials in Medicine, 21 (2010) 863-869.
[24] M.H. Chen, L.L. Wang, J.J. Chung, Y.-H. Kim, P. Atluri, J.A. Burdick, Methods To Assess Shear-Thinning Hydrogels for Application As Injectable Biomaterials, Acs Biomaterials Science & Engineering, 3 (2017) 3146-3160.
[25] A. Sivashanmugam, P. Charoenlarp, S. Deepthi, A. Rajendran, S.V. Nair, S. Iseki, R. Jayakumar, Injectable Shear-Thinning CaSO4/FGF-18-Incorporated Chitin PLGA Hydrogel Enhances Bone Regeneration in Mice Cranial Bone Defect Model, Acs Applied Materials & Interfaces, 9 (2017) 42639-42652.
[26] I. Tomatsu, A. Hashidzume, A. Harada, Photoresponsive hydrogel system using molecular recognition of alpha-cyclodextrin, Macromolecules, 38 (2005) 5223-5227.
[27] P. Jara, L. Barrientos, B. Herrera, I. Sobrados, Inclusion compounds of alpha-cyclodextrin with alkylthiols, Journal of the Chilean Chemical Society, 53 (2008) 1474-1476.
[28] R.P. Chhabra, Non-Newtonian Fluids: An Introduction, 2010.

Chapter 6

Adhesive submucosal injection material with multi-functions for endoscopic submucosal dissection

6.1. Abstract

Submucosal cushion and wound sealing are both important for endoscopic submucosal dissection (ESD). Although many submucosal injection materials (SIMs) for uplift of lesion have been developed, there is still lack of material with multi-functions such as stable submucosal cushion formation, emergency perforation closure, blood coagulation and wound sealing ability. In this study, a novel adhesive submucosal injection material (AdSIM) for ESD was prepared by α-cyclodextrin (α-CD) and hydrophobically modified poly(vinyl alcohol) (hm-PVA). Focusing on the water insolubility of hm-PVA, in which alkyl group (nonanal, C9) is introduced into PVA, and the hydrophobic groups inclusion ability of α-cyclodextrin (α-CD), an inclusion complex (α-CD/C9-PVA) was fabricated in aqueous solution. Inclusion complex of 2.5 mol% nonanal-modified PVA (2.5C9-PVA) with 5 mM α-CD showed a good gel-sol switchable property under different strain amplitudes (1% and 1000%). Additionally, the α-CD/2.5C9-PVA inclusion complex showed good injectability, even upon using a 25 G needle. The α-CD/2.5C9-PVA inclusion complex had good performance at submucosal cushion formation, emergency perforation closure, blood coagulation and wound sealing. These results demonstrate that the α-CD/2.5C9-PVA inclusion complex could be an ideal material for ESD.

6.2. Introduction

Endoscopic resection of various gastrointestinal (GI) lesions has changed dramatically since the emergence of endoscopic submucosal dissection (ESD) in the 1990s [1] which is developed from endoscopic mucosal resection (EMR) [2]. This kind of therapeutic modality is less invasive and relies on flexible, tube-like imaging tools called endoscopes to remove neoplasms formed at GI mucosa and submucosa. Compared with EMR, ESD can realize the complete resection of lesions and show favorable treatment outcomes [3]. Currently, ESD technique is widely used in Japan as the first-line treatment for early-stage GI cancer with low risk of lymph node metastasis [4].

Since early GI tumor does not clearly protrude on the surface of mucosa, serious situations such as inadequate resection, perforation, or bleeding may occur during surgical operation [5]. To minimize these damages, submucosal injection material (SIM) has been applied to separate the mucosa and muscularis layers which then enables safe circumferential mucosal incision and submucosal dissection by electrosurgical knife [6]. As the essential part of ESD, an optimal SIM should be able to generate a thick and durable submucosal cushion to lift cancerous lesion up after administration [7, 8]. The normal saline is the most commonly used SIM as it is cheap and easy to use [9]. However, the cushion created by normal saline is sustained for a short period due to the rapid resorption by surrounding tissue [1]. As a result, repeated injections are needed which may compromise the efficiency of ESD. To overcome the limitation of normal saline, several SIMs have been investigated including polysaccharides (such as glucose) and charged molecules that are more viscous and less easily resorbed than normal saline [6-8, 10]. Of all, only sodium hyaluronate solution and sodium alginate solution are approved as material for submucosal injection in Japan [1]. However, there are concerns that sodium hyaluronate might stimulate tumor cell proliferation at wound sites [11]. On the other hand, since sodium alginate solution was launched in 2019, the sufficient clinical results have not been reported yet. Although these SIMs could reduce the risk of perforation or bleeding during ESD surgery, the functions of emergency perforation closure and hemostasis were not considered.

After submucosal dissection, the remnant tissues will be exposed to various stimuli including stomach acid and food, resulting in severe inflammatory responses [12]. As a result of the contraction of granulation tissues, differentiation of fibroblasts into contractile myofibroblasts, collagen deposition and postoperative scar contracture (SC) develops [13]. In many cases, SC can lead to cicatricial stricture, prolonging hospitalization and lowering quality of life [14, 15]. Then, wound dressing materials (polymeric meshes [16], hydrogels [17], nano particles [12] and decellularized constructs [18]) for the GI tract were designed to protect the submucosa from endoluminal factors and infection after ESD. These wound dressing materials have the ability to support a series of regenerative processes, including tissue formation, angiogenesis, and re-epithelialization.

Therefore, submucosal cushion and wound sealing are both important for ESD. Although many SIMs for uplift of lesion have been developed, to our knowledge, there is still lack of material with multi-functions such as submucosal cushion formation, emergency perforation closure, blood coagulation and wound sealing ability.

Herein, we report a novel adhesive injection material (AdSIM) consisting of hydrophobically modified polyvinyl alcohol (hm-PVA) and α-cyclodextrin (α-CD) for submucosal cushion formation, emergency perforation closure, blood coagulation during ESD and wound sealing after ESD (Scheme 6-1). Focusing on the water insolubility of hm-PVA, in which alkyl group (nonanal, C9) is introduced into PVA, and the hydrophobic groups inclusion ability of α-cyclodextrin (α-CD) [19-21], an inclusion complex (α-CD/C9-PVA) was fabricated in aqueous solution (as potential submucosal injection and wound sealing material). After the injection of α-CD/C9-PVA inclusion complex, the submucosal cushion formation, tissue adhesion, burst strength of perforation site, blood coagulation and wound sealing effect were evaluated.

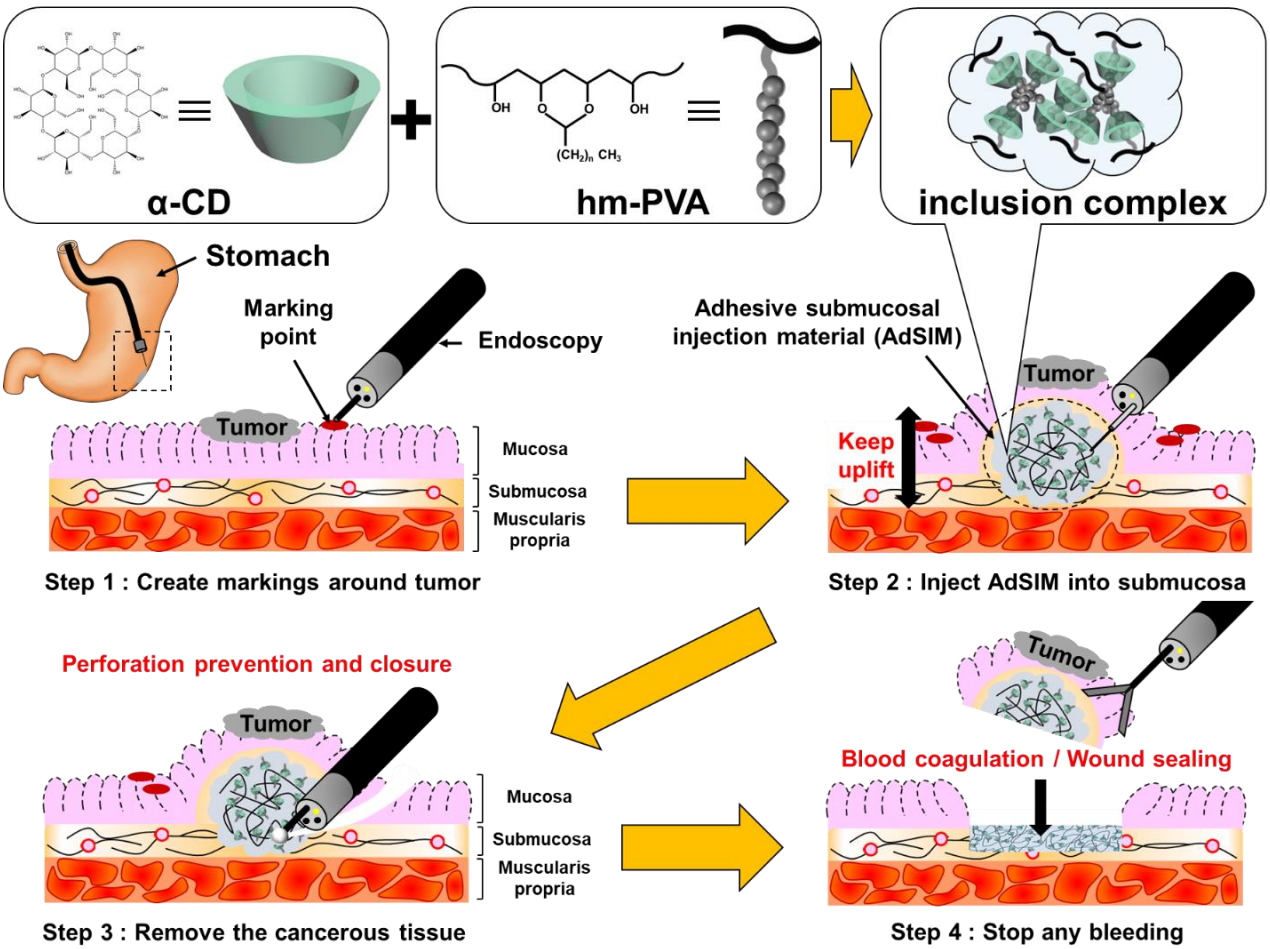

Scheme 6-1. Schematics indicating with submucosal cushion formation and wound sealing ability of AdSIM (α-CD/hm-PVA inclusion complex) for ESD. The α-CD/hm-PVA inclusion complex is easy to inject into submucosa. Due to the recovery of physical crosslinks (hydrophobic interaction and hydrogen bond), the α-CD/hm-PVA inclusion complex can uplift the mucosa for a long time. The submucosal cushion could prevent complications of perforation and bleeding. What's more, under water condition, α-CD/hm-PVA inclusion complex will form stable hydrogel on the wound surface due to α-CD release. The hm-PVA film could protect the postoperative wound from various stimuli including stomach acid and food resulted in severe inflammatory responses.

6.3. Materials and methods

6.3.1. Materials

Ethanol (EtOH, 99.5%), dimethyl sulfoxide (DMSO), 6N hydrochloric acid (HCl), 10% formalin neutral buffer solution, α-cyclodextrin (α-CD), sodium azide and 99.9% dimethyl sulfoxide-d_6 (DMSO-d_6) containing 0.05 w/v% tetramethylsilane (TMS) were purchased from Wako Pure Chemical Industries, Ltd. (Osaka, Japan). Otsuka normal saline 2-port was purchased from Otsuka Pharmaceutical Co., Ltd. (Tokyo, Japan). PVA (Mw = 88,000, saponification degree was over 98.5%) was purchased from Nacalai Tesque, Inc. (Kyoto, Japan). Nonanal (C9) was purchased from Tokyo Chemical Industry Co., Ltd (Tokyo, Japan). Deuterium oxide (D_2O) containing 0.05 wt % 3-(trimethylsilyl) propionic-2,2,3,3-d_4 acid was purchased from Sigma Chemical Co. (St. Louis, MO, USA). Porcine stomach and porcine whole blood were purchased from Tokyo Shibaura Organ Co., Ltd (Tokyo, Japan). MucoUp® (0.8 wt% aqueous sodium hyaluronate, SH) was

purchased from Boston Scientific Co., Ltd. (Massachusetts, USA). Riftal K® (1.2 wt% aqueous sodium alginate, SA) was purchased from Kaigen Pharma Co., Ltd. (Osaka, Japan). Beriplast P Combi-Set Tissue adhesion was purchased from CSL Behring Co., Ltd (Tokyo, Japan). Super glue LPJ-005 was purchased from Henkel Co. (Tokyo, Japan).

6.3.2. Synthesis of hm-PVAs

The hm-PVAs were prepared through the nucleophilic substitution reaction between an aldehyde and the hydroxyl groups of PVA by following previously reported procedure [22, 23]. Firstly, PVA (10 g) was dissolved in 48 mL of H_2O at 80 ℃ for 60 min. Then 150 mL of DMSO and 2 mL of 1N HCl were added to form a 200 mL solution of 5 w/v% PVA and 1 v/v% 1N HCl. Different amounts of aldehyde groups (nonanal, C9) were added into the solution, and the resulting mixtures were stirred at 50 ℃ for 1 h. A reflux condenser was used in all processes. After the reaction, the obtained hm-PVA (H_2O/DMSO = 25/75 (v/v)) solution was added to 600 mL (around 3 times) of cold EtOH under stirring for 1 h. Afterwards, the precipitated hm-PVA was filtered and further washed with 200 mL of EtOH at least three times to remove the unreacted aldehyde and DMSO. Finally, the solvent was evaporated under vacuum to obtain purified hm-PVAs as white crystals. All the crystals were crushed finely using a crusher for further experiments (Wonder crusher WC-3, Osaka Chemical, Osaka, Japan).

6.3.3. Characterization of hm-PVAs

The chemical structures of the hm-PVAs were analyzed by nuclear magnetic resonance (^{1}H-NMR) spectroscopy (AL300, JEOL, Tokyo, Japan) using a 0.5 w/v% hm-PVA/DMSO-d_6 solution at 25 ℃. The number of scans was 8 times for each sample. Fourier transform-infrared spectroscopy (FT-IR, 8400S, Shimadzu, Kyoto, Japan) analysis was carried out to confirm the presence of acetal groups in the hm-PVAs. The scan range was from 700 cm^{-1} to 4000 cm^{-1} and the number of scans was 64 times for each sample. Hydrophobic group modification ratios of the hm-PVAs were determined by ^{1}H-NMR spectroscopy. The modification ratios were calculated by following equation:

$$\text{Modification ratio (mol\%)} = [\{\text{Integral area } (CH_3 \text{ proton})/3\}6.3.4 \,/\, \text{Integral area } (\alpha\text{CH proton})]\times 100$$

where integral area (αCH proton) is the area of peak at 3.87 ppm corresponded to the αCH proton in the backbone of PVA and hm-PVAs, integral area (CH_3 proton) is the area of peak at 0.85 ppm assigned to the CH_3 proton in the hydrophobic groups of hm-PVAs.

6.3.4. Preparation of α-CD/hm-PVA inclusion complexes

The α-CD/hm-PVA inclusion complexes were prepared as described below. At first, hm-PVA powder (200 mg) was added into a mayonnaise bottle with 2 mL of H_2O to form a 10 w/v% hm-PVA suspension. Then, different amounts of α-CDs were added into this suspension, followed by heating in autoclave (LSX-500, TOMY, Tokyo, Japan) at 95 ℃ for 10 min. Finally, α-CD/hm-PVA solutions were stirred (200 rpm) at 25 ℃ for overnight to form α-CD/hm-PVA inclusion complexes with different concentration of α-CD (0-20 mM).

6.3.5. Shear viscosity

The shear viscosity of α-CD/hm-PVA inclusion complexes was evaluated by rheometer (MCR301, Anton paar, Graz, Austria) according to the method previously reported [21]. α-CD/hm-PVA inclusion complexes (hm-PVA concentration was 10 w/v%) containing 0-20 mM α-CD were prepared as mentioned above. The shear viscosity was measured by using jig PP25 (dimeter = 25 mm) with shear rate of 0.1 S^{-1} at 298 K. Each sample was measured 5 times.

6.3.6. Structural recovery evaluation

Three-stage structural recovery tests were conducted by rheometer (MCR301, Anton paar, Graz, Austria) equipped with a plate of PP 25 according to the previously reported method [24, 25]. The required volume of α-CD/hm-PVA inclusion complex was 0.5 mL. The three-stage oscillation tests with different oscillation amplitudes at constant frequency (ω = 10 rad/s) were carried out. Specifically, Stage I: Small oscillation amplitude was applied for a period of 180 s to obtain the shear moduli of the initial state (γ = 1%). Stage II: The large strain amplitude (γ = 1000%) was applied for a period of 180 s. Stage III: The same small oscillation amplitude with stage I was applied for 180 s to follow the recovery within a short time.

6.3.7. Evaluation of injectability

The injectability of prepared α-CD/hm-PVA inclusion complexes was evaluated respectively with a testing machine (EZ-LX, Shimadzu Co., Kyoto, Japan) [26]. The inclusion complex was filled in a 2.5 mL syringe with 20 G or 25 G needle (Terumo Co., Tokyo, Japan), which was then set into a mold with a hole. Under pressure, the α-CD/hm-PVA inclusion complex was extruded, and this process was stopped when the extrusion force reached 250 N [27, 28]. Five specimens were tested for each group. Injectability was calculated by the following equation:

$$\text{Injectability (\%)} = 100 \times (Wt-Wr) / Wt$$

where Wt and Wr are the weight of the total paste and the remaining paste in syringe, respectively.

6.3.8. Mucosa elevation effect

The mucosa elevation effect of α-CD/hm-PVA inclusion complexes was evaluated according to the previously reported method [29]. Firstly, the porcine stomach was cleaned and cut with a dumbbell cutter into a 35 mm diameter circle. Then, 0.5 mL of the α-CD/hm-PVA inclusion complex in syringe was injected into the submucosa of the stomach with a 25 G needle. At the same time, normal saline, Mucoup® (0.8 wt% aqueous sodium hyaluronate, SH), Riftal K® (1.2 wt% aqueous sodium alginate, SA) and α-CD/PVA solution were also evaluated for comparison. After injection, these samples were kept at 25 °C for 30 min and then frozen in a freezer (−20 °C). Finally, frozen stomach samples were cut with a scalpel from the raised site to determine the raised height. The test was performed six times for each sample.

6.3.9. Evaluation of tissue adhesion

The tissue adhesion property of the α-CD/hm-PVA inclusion complex was evaluated according to ASTM F2258-05. The adhesion strength and adhesion energy were measured using a Texture Analyzer (TA-XT2i, Stable Microsystems, Godalming, UK). Briefly, the porcine stomach of which the mucosal membrane had been peeled was cut into a square (25 mm × 25 mm). These tissues were bound to the probe (top) and the surface of the heater which was kept at 37 °C (bottom) by a cyanoacrylate adhesive (Loctite, Super glue LPJ-005). To remove excess water from the stomach tissue, the surface was gently wiped using a mesh. Next, the α-CD/hm-PVA inclusion complex (0.2 mL) was applied to the tissue at the bottom, and top probe approached under a stress of 2 N for 3 min. Thereafter, the probe was pulled up at a tracking speed of 10 mm/min, and the bonding strength of the α-CD/hm-PVA inclusion complex was measured. The adhesion energy was calculated from the stress-distance curve using Image J software. Normal saline, SH, SA and α-CD/PVA solution were evaluated as comparison, and each sample was performed five times.

6.3.10. Burst strength measurement

Burst strength of a porcine stomach was performed according to ASTM F2392-04. A fresh porcine stomach of which the mucosa layer had been peeled was employed as the adherent. Inclusion complex with fixed diameter (15 mm) and thickness (1 mm) was applied to cover the hole (3 mm in diameter) which was made in the center of disk-shaped porcine stomach. The burst strength was then measured by running saline from the lower portion of the tissue at a flow rate of 2 mL/min at 37 °C. After the cover was fractured, the maximum burst strength was defined as the individual burst strength. For comparison, normal saline, SH, SA, α-CD/PVA solution and fibrin sealant were also evaluated.

To elucidate the adhesion mechanism, a cross section of the test samples after the burst strength measurements was observed. The test sample was fixed in a 10% formalin neutral buffer solution, stained with hematoxylin and eosin (H&E), and analyzed using inverted fluorescence phase contrast microscope (BZ-X700, Keyence Co., Tokyo, Japan).

6.3.11. Blood coagulation evaluation

The blood coagulation evaluation was performed according to the study previously reported [30, 31]. 1 mL of porcine whole blood containing sodium citrate and 1mL of α-CD/hm-PVA inclusion complex were mixed, followed by stirring with vortex for 2 seconds. The rheological properties of blood mixtures were determined using a rheometer (MCR301, Anton Paar GmbH, Granz, Austria). The storage modulus and loss modulus were obtained by frequency dependent measurements (angular frequency, 1–100 rad/s; strain, 5%), and the shear modulus was determined from the result of storage modulus at a frequency of 10 rad/s.

6.3.12. Underwater stability test

After ESD procedure, α-CD/hm-PVA inclusion complexes were remained on the surface of wounds. To evaluate the adhesiveness and stability of α-CD/hm-PVA inclusion complexes in wet environments like in the esophagus, underwater stability test was performed as follows [32]. Firstly, the porcine stomach of which the mucosal membrane was peeled was cut into a square (25 mm × 25 mm), and 0.5 mL of the α-CD/hm-PVA inclusion complex was uniformly applied to the surface. Next, the coated tissue sample was immersed in 50 mL of normal saline (containing 0.2 mg/mL of sodium azide). After incubation for 1, 3 and 7 days at 37 °C, the samples were fixed with 10% formalin phosphate buffer. The hydrogel remaining on the tissue surface was confirmed by H&E staining. For comparison, normal saline, SH, SA and α-CD/PVA solution were also

evaluated. The images of H&E staining were scanned using a digital slide scanner (NanoZoomer S210, Hamamatsu Photonics Co., Japan). The area of hydrogel layer was quantified using Image J software.

6.3.13. Statistical analysis

Statistical analysis was carried out using Tukey-Kramer test with KyPlot software. Statistically significant differences were accepted when $p < 0.05$. Data were presented as means ± standard deviations (SD).

6.4. Results and discussion

6.4.1. Synthesis and characterization of hm-PVAs

The hm-PVAs were prepared via the reaction between the hydroxyl groups of PVA and an aldehyde (Figure 6-1) [33, 34]. Under acidic conditions, aldehydes react with hydroxyl groups via nucleophilic substitution reaction to form stable hexagonal ring structure in a short time. Figure 6-1a shows ^{1}H-NMR spectra of C9-PVAs with different modification ratio. The typical chemical shifts at 0.85 ppm and 1.26 ppm were assigned to CH_3 proton and αCH_2 proton in hydrophobic moiety of hm-PVAs respectively, which indicated the successful introduction of aldehyde groups to PVA backbone. Additionally, the hm-PVAs was analyzed by FT-IR spectra (Figure 6-1b). The peak observed at 2,930 cm^{-1} was attributed to C-H stretching vibration of αCH_2 in the acetal groups of hm-PVAs. Taken together, these results demonstrated that hm-PVAs were successfully synthesized. The modification ratio of hydrophobic groups (shown in Table 6-1) was calculated from ^{1}H-NMR results.

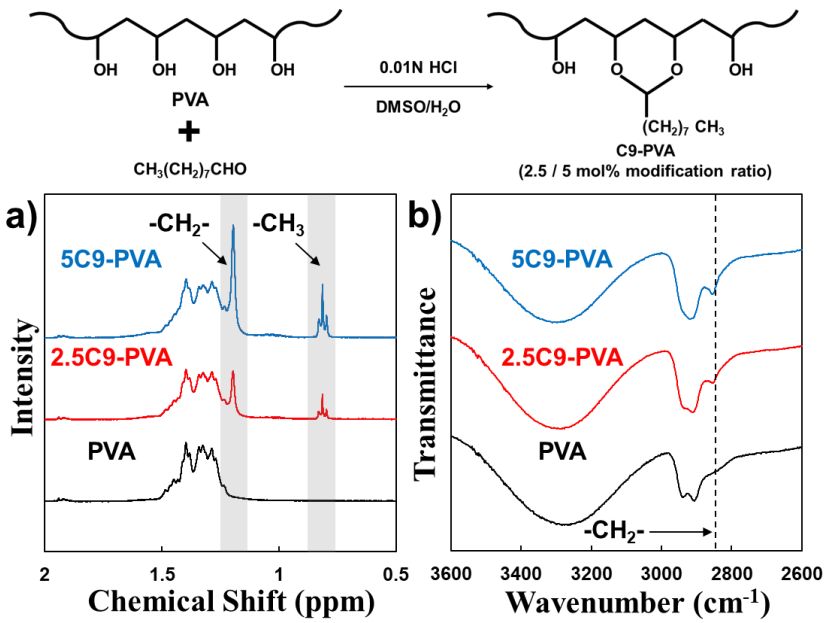

Figure 6-1. Synthesis and characterization of hm-PVAs. a) ^{1}H-NMR and b) FT-IR spectra of the hm-PVAs

Table 6-1. Modification ratios of the hm-PVAs.

Abbreviation	Hydrophobic group reagent	Hydrophobic group reagent added (mol%)	Hydrophobic group modification (mol%)
2.5C9-PVA	Nonanal	5	2.5
5C9-PVA	Nonanal	10	5

6.4.2. Shear viscosity of α-CD/hm-PVA inclusion complexes

The synthesized C9-PVAs with different modification ratio could not be dissolved in water owing to their strong hydrophobic interaction. It is well known that α-CD can destruct the hydrophobic association through the formation of a special threading rotaxane structure. Based on the feature of α-CD, α-CD/hm-PVA inclusion complex was prepared as depicted in Figure 6-2a. As expected, with the addition of α-CD, the hm-PVA could dissolve in water. Meanwhile, when mixing different amount of α-CD with PVA or hm-PVA, the shear viscosity varied a lot. In the case of α-CD/PVA mixture (Figure 6-2b), regardless of low or high concentration of α-CD, the shear viscosity was constantly low (~0.01 kPa·s) because of the high hydrophilicity of the two components. Unlike the α-CD/PVA mixture, the shear viscosity of α-CD/2.5C9-PVA and α-CD/5C9-PVA inclusion complexes showed a dramatic decrease with the concentration of α-CD increasing as shown in Figure 6-2c and 6-2d. In detail, the shear viscosity of α-CD/2.5C9-PVA inclusion complex changed from high viscosity (5.924 ± 0.991 kPa·s, α-CD/C9 = 0.5) to low viscosity (0.012 ± 0.001 kPa·s, α-CD/C9 = 1.5) around 5 mM α-CD. The similar phenomenon was observed in α-CD/5C9-PVA inclusion complex as the shear viscosity changed from (8.778 ± 0.912 kPa·s, α-CD/C9 = 1) to low viscosity (0.291 ± 0.030 kPa·s, α-CD/C9 = 2) around 15 mM α-CD. The probable reason for such alterations in shear viscosity was described as follows. When only a small amount of α-CD was added, α-CD could not fully interact with the hydrophobic groups due to the relatively stronger hydrophobic association of the polymer (hm-PVA). It has been reported that short alkyl chain length (C5) can be included in the hydrophobic pocket of one α-CD. Thus, theoretically two α-CDs are needed to completely include long alkyl chain length (C9). Once the α-CDs started to form an inclusion complex with hydrophobic groups distributed along the polymer chains, the unfolding of the polymer main chains would promote the cooperative complexation with α-CD.

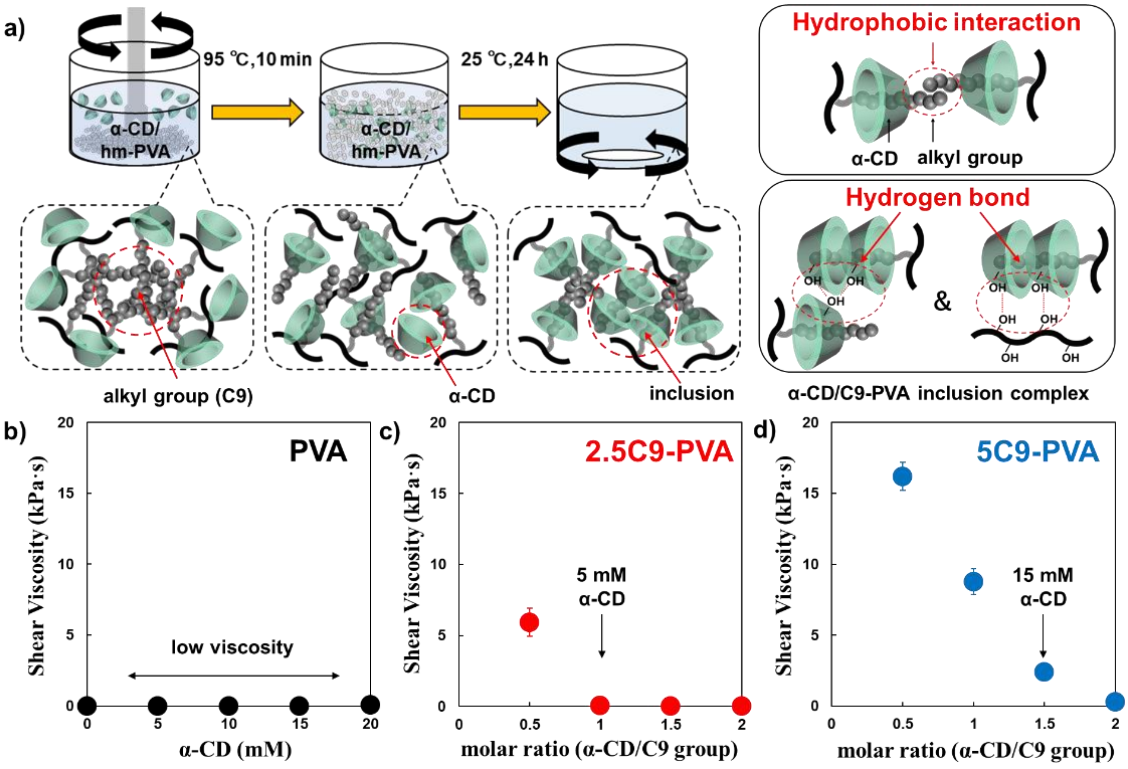

Figure 6-2. a) The preparation procedure of α-CD/hm-PVA inclusion complex. b-d) Shear viscosity of α-CD/PVA mixture and α-CD/hm-PVA inclusion complexes as a function of the α-CD concentration (polymer concentration was set at 10 w/v%) at 25 °C. Shear rate = 0.1 S^{-1}. (n = 5)

6.4.3. Structural recovery evaluation

The structural recovery of α-CD/hm-PVA inclusion complexes was evaluated using rheometer. Figure 6-3a shows the change in the modulus of PVA (10 w/v%) with 5 and 15 mM of α-CD in aqueous solutions as a function of strain. At small (γ = 1%) and large (γ = 1000%) strain amplitude, the loss modulus G'' was obviously greater than the storage modulus G', which indicated the free-flowing sol state. Interestingly, α-CD/2.5C9-PVA inclusion complex showed unique structural recovery property in Figure 6-3b. At stage I (γ = 1%), the storage modulus G' of 2.5C9-PVA (10 w/v%) with 5 mM α-CD in aqueous solution was higher than the loss modulus G'', representing the gel state of this inclusion complex. However, the storage modulus G' showed a dramatic decrease at stage II (γ = 1000%), and then became lower than the loss modulus G'', indicating the sol state of the inclusion complex. While the same small oscillation amplitude with stage I was applied, the storage modulus G' and loss modulus G'' recovered to initial state, which implied that the mixture returned to gel state. The mechanism of the structural recovery may be ascribed to the regeneration of physical crosslinks such as hydrophobic interactions and hydrogen bonds as illustrated in Figure 6-2a. When the α-CD/2.5C9-PVA inclusion complex was applied for small oscillation amplitude (γ = 1%) in stage I, the hydrophobic interaction and hydrogen bond were stable. However, under the large strain amplitude (γ = 1000%), the physical crosslinks collapsed. The collapsed status was not irreversible and once the same small oscillation amplitude like in stage I was applied again, the physical crosslinks recovered immediately. Compared to the α-CD/2.5C9-PVA inclusion complex, α-CD/5C9-PVA inclusion complex shows much stronger recovery ability because of possessing more alkyl chains (Figure 6-3c).

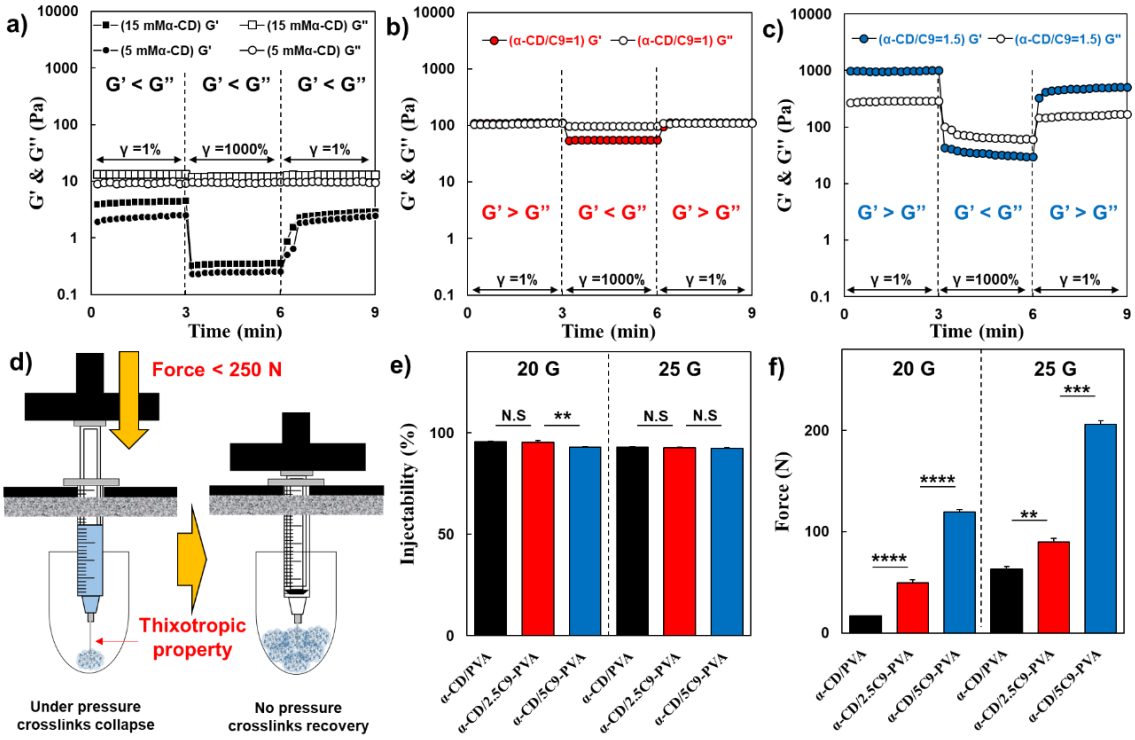

Figure 6-3. The structure recovery property and injectability of α-CD/hm-PVA inclusion complexes. Storage modulus G' and loss modulus G'' as a function of strain. A shear strain amplitude of 1-1000% and an angular frequency of 10 rad s^{-1} were applied. The temperature was set at 25 °C. a) PVA with 5 and 15 mM α-CD, b) 2.5C9-PVA with 5 mM α-CD, c) 5C9-PVA with 15 mM α-CD. d) Injectability test of α-CD/hm-PVA inclusion complexes using syringe. e) Injectability and f) injection force of α-CD/hm-PVA inclusion complex. (**P < 0.01, ***P < 0.001, ****P < 0.0001, n = 5)

6.4.4. Evaluation of Injectability

We evaluated the injectability according to the method previously reported (Figure 6-3d). We stopped injection when injection force reached 250 N [27, 28]. As shown in Figure 6-3e, it was clear that injectability of 10 w/v% PVA with 5 mM α-CD, 10 w/v% 2.5C9-PVA with 5 mM α-CD and 10 w/v% 5C9-PVA with 15 mM α-CD was over 90% when 20 G or 25 G needle was used. However, 10 w/v% 5C9-PVA with 15 mM α-CD showed strong resistance due to the strong hydrophobic interaction. The injection force of α-CD/hm-PVA inclusion complexes during injection process are shown in Figure 6-3f. Predictably, the injection force increased with the increasing alkyl chain length and decreasing inner diameter of needle. From these results, we convinced that α-CD/hm-PVA inclusion complex could be used as an ideal submucosal injection material.

Table 6-2. Submucosal injection material used in this study.

Abbreviation	Full name	Component	Concentration
Saline	normal saline	NaCl	0.9 w/v%
SH	sodium hyaluronate	sodium hyaluronate	0.8 wt%
SA	sodium alginate	sodium alginate	1.2 wt%
α-CD/PVA	α-CD/PVA mixture	α-CD PVA	5 mM 10 w/v%
α-CD/2.5C9-PVA	α-CD/2.5C9-PVA inclusion complex	α-CD 2.5C9-PVA	5 mM 10 w/v%
α-CD/5C9-PVA	α-CD/5C9-PVA inclusion complex	α-CD 5C9-PVA	15 mM 10 w/v%

6.4.5. Mucosa elevation effect of α-CD/hm-PVA inclusion complexes

The mucosa elevation effect of α-CD/hm-PVA inclusion complexes was evaluated according to the previously reported method [29] as shown in Figure 6-4a. Figure 6-4b shows the cross section of stomachs injected with different SIMs (Table 6-2). It was clear that normal saline, SH and SA did not have enough uplift effect. The cushions created by these three SIMs were sustained for a short period due to the rapid resorption by surrounding tissue. Interestingly, SIMs with high polymer concentration (α-CD/2.5C9-PVA inclusion complex and α-CD/5C9-PVA inclusion complex) showed better uplift effect. Under pressure, the α-CD/hm-PVA inclusion complexes could be injected as sol state by physical crosslinks collapse, and then returned to gel state after injection by physical crosslinks recovery. As a result, the cushions generated by α-CD/hm-PVA inclusion complexes could keep for a long time. Raised height by different SIMs was determined from the corresponding cross section observation of stomachs and the quantitative data are shown in Figure 6-4c. The raised height of normal saline was 2.87 ± 0.26 mm, which was much lower than the other samples. The two commercial SIMs had similar value, 4.05 ± 0.39 mm for SH and 4.08 ± 0.45 mm for SA. Due to the higher polymer concentration, injection of α-CD/PVA mixture resulted in better raised height (4.90 ± 0.46 mm) than normal saline and commercial SIMs (SH and SA). As expected, α-CD/hm-PVA inclusion complexes (injectable gel) displayed the best effect on mucosa elevation than previous three groups, and there was no significant difference between α-CD/2.5C9-PVA inclusion complex (5.90 ± 0.38 mm) and α-CD/5C9-PVA

inclusion complex (5.98 ± 0.56 mm). Considering injectability and mucosa elevation effect, α-CD/2.5C9-PVA inclusion complex could be promising candidate of SIMs for ESD surgery.

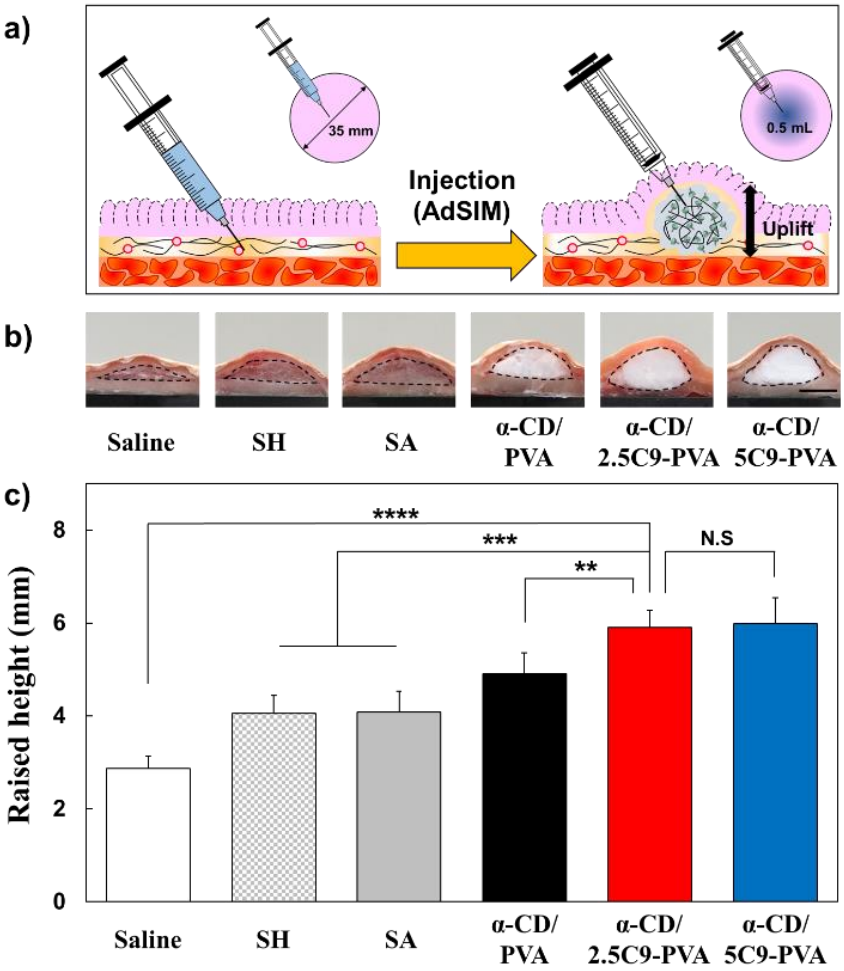

Figure 6-4. Evaluation of submucosal cushion after injection of α-CD/hm-PVA inclusion complexes. a) Schematic illustration of the procedure used for submucosal cushion measurement. b) Cross section observation of stomachs injected with different SIMs (scale bar = 5 mm). c) Quantitative data of raised height. (**P < 0.01, ***P < 0.001, ****P < 0.0001, n = 6)

6.4.6. Evaluation of tissue adhesion

The adhesion properties of α-CD/hm-PVA inclusion complexes was evaluated using bonding strength according to ASTM F2258-05 as illustrated in Figure 6-5a. Figure 6-5b shows cross section observation during adhesion test. It was found that only α-CD/2.5C9-PVA inclusion complex adhered to both side of the tissue (porcine stomach without mucosa). Figure 6-5c shows force-distance curve of bonding strength measurement. The bonding strength and bonding energy of the SIMs on the surface of porcine stomach without mucosa was calculated from the height and area of force-distance curve (Figure 6-5d and 6-5e). It was clear that the bonding strength of α-CD/2.5C9-PVA inclusion complex (2.38 ± 0.42 kPa) was much higher than that of the other SIMs (0.92 ± 0.1 kPa ~ 1.54 ± 0.17 kPa) as shown in Figure 6-5d. What's more, the bonding energy of α-CD/2.5C9-PVA inclusion complex (4.13 ± 1.05 J/m^2) was almost 10 times higher than that of normal saline (0.43 ± 0.06 J/m^2) as calculated in Figure 6-5e. The 5C9-PVA has more alkyl chain than 2.5C9-PVA, however, the bonding energy of α-CD/5C9-PVA inclusion complex was 1.37 ± 0.14 J/m^2 which was one third of the value of α-CD/2.5C9-PVA inclusion complex. The α-CD/2.5C9-PVA inclusion complex

was easy to cover and penetration into the gap on tissue surface, and the introduced alkyl groups (C9) were easily anchored to cell membranes and exerted high interfacial adhesion [35]. On the other hand, weak adhesion occurred between tissue surface and α-CD/PVA mixture as unmodified PVA had no alkyl side chain. Although α-CD/5C9-PVA inclusion complex can also exert an anchor effect of alkyl groups, it could not obtain high adhesion strength/energy due to the high stability (strong structure recovery property) which limited the penetration into the gap on the skin surface.

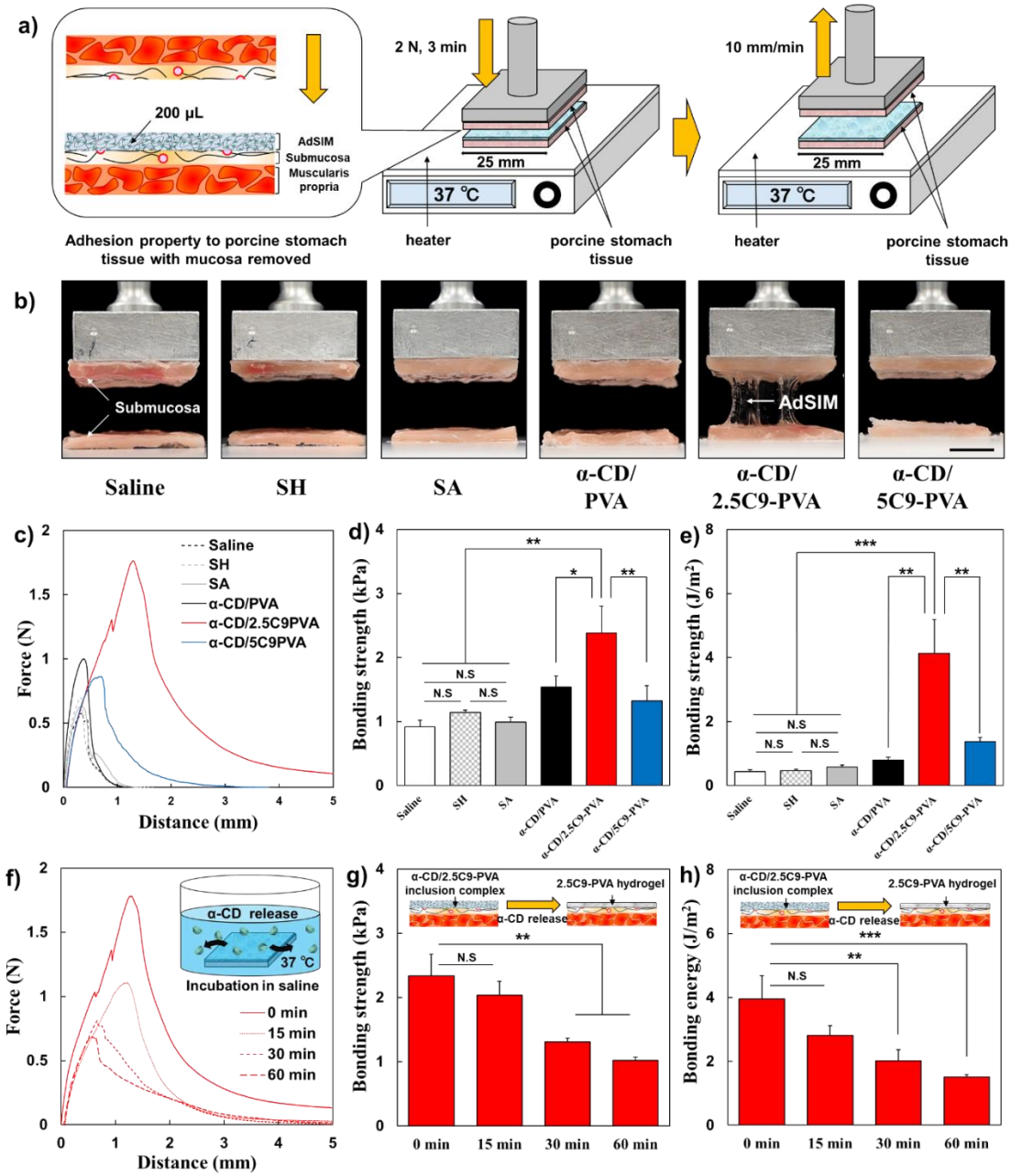

Figure 6-5. Adhesive strength evaluation test. a) Schematic illustration of the apparatus used for bonding energy measurement. b) Cross section observation during adhesion test (scale bar = 10 mm). c) Force-distance curve of bonding strength measurement of different SIMs. d) Bonding strength and e) bonding energy of SIMs to porcine stomach without mucosa. (*P < 0.05, **P < 0.01, ***P < 0.001, n = 5) f) Force-distance curve of bonding strength measurement of α-CD/2.5C9-PVA inclusion complex after incubation in saline at 37 °C. g) Bonding strength and h) bonding energy of α-CD/2.5C9-PVA inclusion complex after incubation in saline to porcine stomach without mucosa. (**P < 0.01, ***P < 0.001, n = 3)

It was found that α-CD in α-CD/2.5C9-PVA inclusion complex was easy to undergo burst release in water environment (such as saline) at 37 °C, leading to aggregation of hydrophobic groups (C9). Finally, stable 2.5C9-PVA hydrogel was formed on the tissue shown in Figure 6-5f-h. Figure 6-5f shows force-distance curve of bonding strength measurement for α-CD/2.5C9-PVA inclusion complex after incubation in saline. Interestingly, the bonding strength and bonding energy of α-CD/2.5C9-PVA inclusion complex were decreased with an increasing of incubation time in saline (Figure 6-5g and Figure 6-5h). After incubation for 60 min, the bonding strength of α-CD/2.5C9-PVA inclusion complex decreased to 1.02 ± 0.07 kPa which was only half of the initial value at 0 min. The same trend was observed in bonding energy of α-CD/2.5C9-PVA inclusion complex incubated in saline. We hypothesized that most of α-CDs remained after 15 min of incubation, since there was no significant difference between adhesion strength of α-CD/2.5C9-PVA inclusion complex without incubation and with 15 min of incubation. However, almost all of the α-CDs released after incubation for 60 min. With the diffusion of α-CDs, hydrophobic groups aggregated in the molecule, and the amount of hydrophobic groups that could be anchored to the tissue surface decreased, resulting in a decrease in adhesive strength. Based on these results, it was suggested that α-CD/2.5C9-PVA inclusion complex had ability for prevention of postoperative adhesion. In addition, the unique α-CDs release and hydrophobic groups aggregation property could deal with the conditions such as perforation and bleeding during ESD surgery.

6.4.7. Measurement of the burst strength of a porcine stomach

The burst strength was performed according to ASTM F2392-04. Figure 6-6a is the standard testing method including measurement procedure and sample preparation. Figure 6-6b shows the burst strength of porcine stomach without mucosa covered by SIMs without incubation in saline. Among all the SIMs, α-CD/2.5C9-PVA inclusion complex exhibited the highest burst strength (0.60 ± 0.18 kPa) as it was well adhered to porcine submucosa. Normal saline, SH, SA and α-CD/PVA mixture were solution, therefore these SIMs had low burst strength (0.08 ± 0.05 kPa ~ 0.13 ± 0.05 kPa). The burst strength of α-CD/5C9-PVA inclusion complex was 0.23 ± 0.10 kPa which was one third of the value of α-CD/2.5C9-PVA inclusion complex, due to the weak adhesion to porcine submucosa. This result was well correlated with adhesion measurement in Figure 6-5e.

Furthermore, the burst strength was also evaluated after incubation of α-CD/2.5C9-PVA inclusion complex in saline. After 12 h incubation, α-CD/2.5C9-PVA inclusion complex changed to stable 2.5C9-PVA film as the α-CD released over time. In Figure 6-6c, the burst strength of 2.5C9-PVA hydrogel (1.80 ± 0.37 kPa) was 3-fold higher than that of α-CD/2.5C9-PVA inclusion complex without incubation. The increase in burst strength is believed to be due to the increase in bulk strength of the material. Besides, compared with the commercial fibrin sealant (1.20 ± 0.29 kPa), the burst strength of 2.5C9-PVA hydrogel was 1.5-fold higher. After burst strength measurement, cross sections of tissue were analyzed to investigate the adhesion mechanism. Figure 6-6d shows the histology of SIMs and fibrin sealant after burst strength measurement. It was obvious that normal saline and α-CD/PVA mixture didn't remain in hole and on upper surface of tissue. On the other hand, α-CD/2.5C9-PVA inclusion complex without incubation partially remained bound to stomach tissue even after burst strength measurement. However, adhesion failure was observed (as shown in hole and upper surface) due to weak interaction between α-CD/2.5C9-PVA inclusion complex and tissue at early stage. Interestingly, the α-CD/2.5C9-PVA inclusion complex after 12 h incubation in saline was completely left in both hole and upper surface after burst strength measurement. With the diffusion of α-CD, more alkyl groups (C9) became free and these hydrophobic groups could anchor to tissue surface to increase interfacial bond or aggregate together to form stable hydrogel with high bulk strength. With regard to fibrin sealant, the adhesion failure was also observed, indicating weak interaction between fibrin sealant and tissue

[35]. From these results, it was indicated that α-CD/2.5C9-PVA inclusion complex had the potential to overcome perforation during ESD surgery.

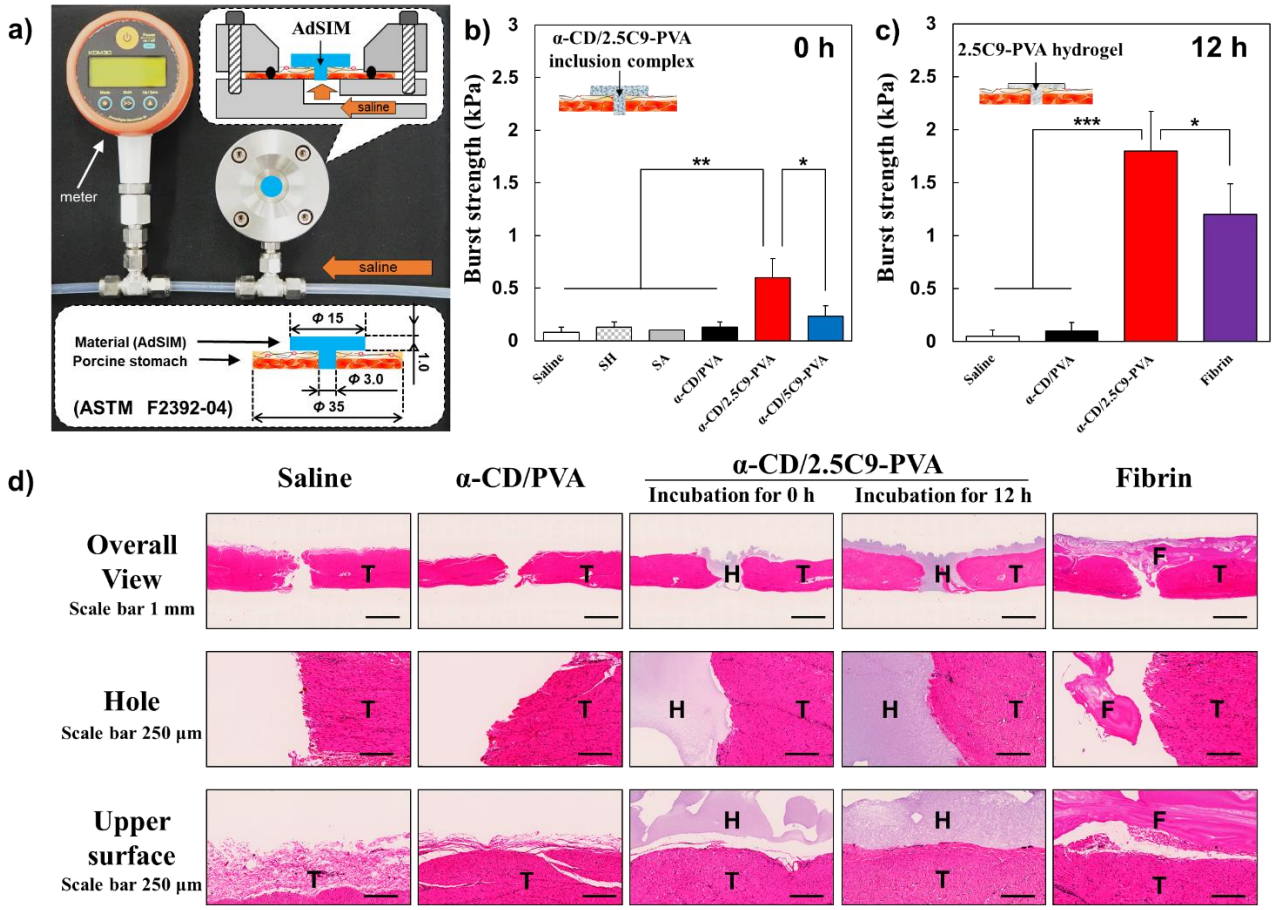

Figure 6-6. Burst strength evaluation test. a) Schematic illustration of the apparatus used for burst strength measurement. b) Burst strength of different SIMs to porcine stomach without mucosa. c) Burst strength of α-CD/2.5C9-PVA inclusion complex to porcine stomach without mucosa after incubation in saline for 12 h compared with fibrin sealant. (*P < 0.05, **P < 0.01, ***P < 0.001, n = 4) d) Histology of SIMs and fibrin sealant after burst strength measurement. The tissue (T), hydrogel (H) and fibrin sealant (F) are indicated in the picture.

6.4.8. Blood coagulation evaluation

The blood coagulation evaluation was performed according to the study previous reported [30, 31]. After mixing 1 mL of α-CD/2.5C9-PVA inclusion complex with 1 mL of porcine whole blood containing sodium citrate, blood coagulation was occurred (Figure 6-7a). In contrast, the mixing of 1 mL of α-CD/PVA mixture and 1 mL of same porcine whole blood didn't induce blood coagulation. Then, the rheological properties of blood mixtures, storage modulus and loss modulus were obtained by frequency dependent measurements at 1–100 rad/s angular frequency and 5% strain. It was found that blood mixture containing α-CD/2.5C9-PVA inclusion complex showed gel state (G' > G'') at 1–100 rad/s angular frequency, while α-CD/PVA mixture + blood sample showed sol state (G' < G''). Figure 6-7b shows the storage modulus and loss modulus of blood only, α-CD/PVA mixture + blood and α-CD/2.5C9-PVA inclusion complex + blood at the condition of 10 rad/s angular frequency and 5% strain. It was revealed that blood only and α-CD/PVA mixture + blood were stable sol state, while α-CD/2.5C9-PVA inclusion complex + blood was stable gel state during the test. The shear modulus was determined from the result of storage modulus at a frequency of 10 rad/s

shown in Figure 6-7c. α-CD/2.5C9-PVA inclusion complex + blood exhibited the much higher shear modulus (86 ± 3.73 Pa) than that of blood only (0.2 ± 0.05 Pa) and α-CD/PVA mixture + blood (0.8 ± 0.12 Pa). The probable reason for this phenomenon is illustrated in Figure 6-7d. When α-CD/2.5C9-PVA inclusion complex mixing with porcine whole blood, α-CD starts to release and the exposed free alkyl groups (C9) in 2.5C9-PVA can anchor to blood cells to form new physical crosslinks. Taken all the phenomena together, α-CD/2.5C9-PVA inclusion complex had the ability to stop bleeding during ESD surgery.

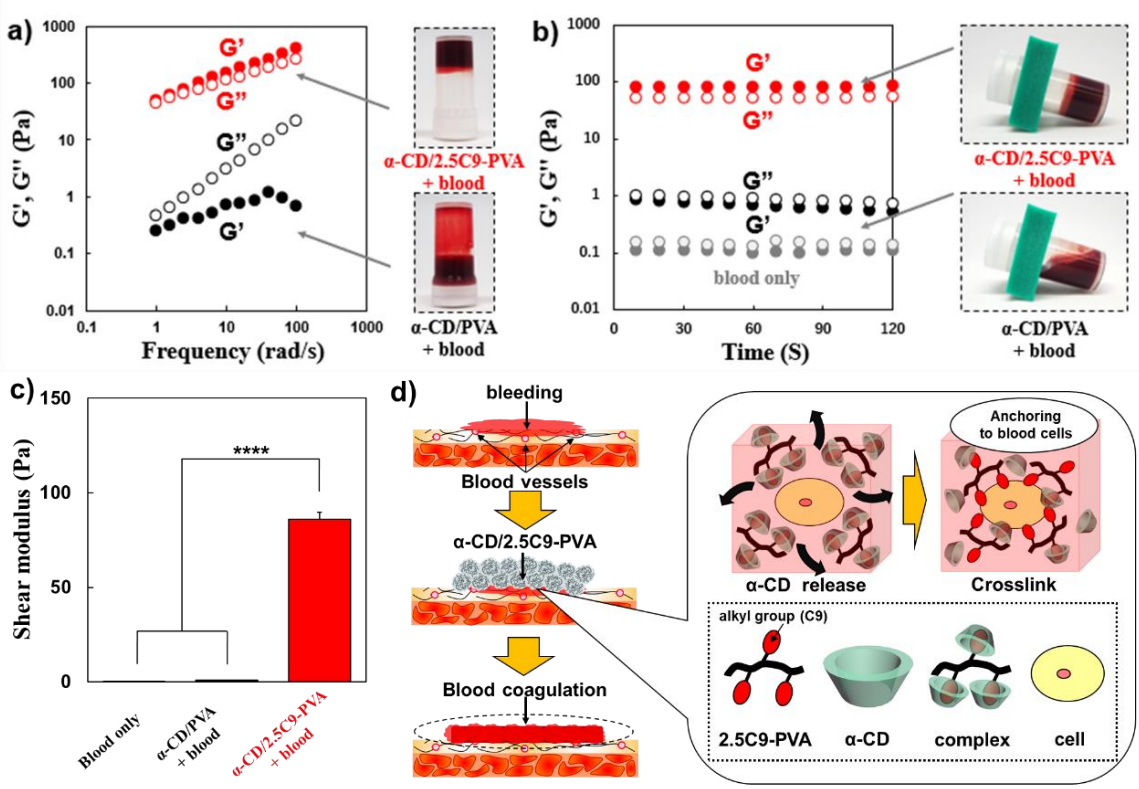

Figure 6-7. Blood coagulation evaluation test. a) The rheological properties of blood mixtures (porcine whole blood : α-CD/2.5C9-PVA inclusion complex = 1:1) obtained by frequency dependent measurements at 37 °C (angular frequency, 1–100 rad/s; strain, 5%). b) Storage modulus and loss modulus at a frequency of 10 rad/s (37 °C). c) Shear modulus determined from the result of storage modulus at a frequency of 10 rad/s. (****P < 0.0001, n = 5) d) The blood coagulation mechanism of α-CD/2.5C9-PVA inclusion complex at bleeding site.

6.4.9. Water stability test

The water stability of α-CD/2.5C9-PVA inclusion complex was performed as the study previous reported [32]. Figure 6-8a shows the process of the water stability test of α-CD/2.5C9-PVA inclusion complex. After immersion of porcine stomach coated by α-CD/2.5C9-PVA inclusion complex in saline, due to α-CD release and hydrophobic groups aggregation, 2.5C9-PVA hydrogel was formed on the tissue. This hydrogel covered tissue was further incubated for one week. Figure 6-8b shows the histology of porcine stomach coated by α-CD/2.5C9-PVA inclusion complex after incubation in normal saline for 1 day to 7 days. It was clear to see that 2.5C9-PVA hydrogel area decreased with increasing incubation time. From the quantitative results as shown in Figure 6-8c, after 24 h incubation, 2.5C9-PVA hydrogel area was 4.28 ± 0.39 mm^2, and the area decreased to 3.38 ± 0.27 mm^2 after 3 days and 2.18 ± 0.33 mm^2 after 7 days, respectively. Therefore, over one week, the formed 2.5C9-PVA hydrogel still adhered on the surface of submucosa. For other SIMs the histology of treated porcine stomach was also compared after incubation in normal saline for 7 days. In Figure 6-8d,

only the tissue (porcine stomach without mucosa) coated with α-CD/2.5C9-PVA inclusion complex showed obvious remnants on the surface. Due to the low concentration of polymer, SH and SA were diffused into solution. Although the polymer concentration of α-CD/PVA mixture was high, the mixture could not remain on the surface due to the high hydrophilic property of α-CD and PVA. α-CD/5C9-PVA inclusion complex was stable, but its tissue adhesion ability was low due to high hydrophobic interaction. During the incubation, 5C9-PVA hydrogel was peeled off from the surface of tissue. In contrast, α-CD/2.5C9-PVA inclusion complex could adhere well to submucosa by anchoring effect. Figure 6-8e shows the area of swelling submucosa covered by different SIMs after incubation in normal saline for 7 days. Severe submucosa swelling was observed on the tissue surface coated with normal saline, SH, SA and α-CD/PVA mixture, and the area of swelling submucosa (1.70 ± 0.17 mm^2 ~ 2.21 ± 0.13 mm^2) was 3~4-fold higher than that of α-CD/2.5C9-PVA inclusion complex (0.52 ± 0.1 mm^2). As the high stability was observed in the hydrogel formed by α-CD/2.5C9-PVA inclusion complex in saline, it can cover and protect the wound site from irritants after ESD surgery.

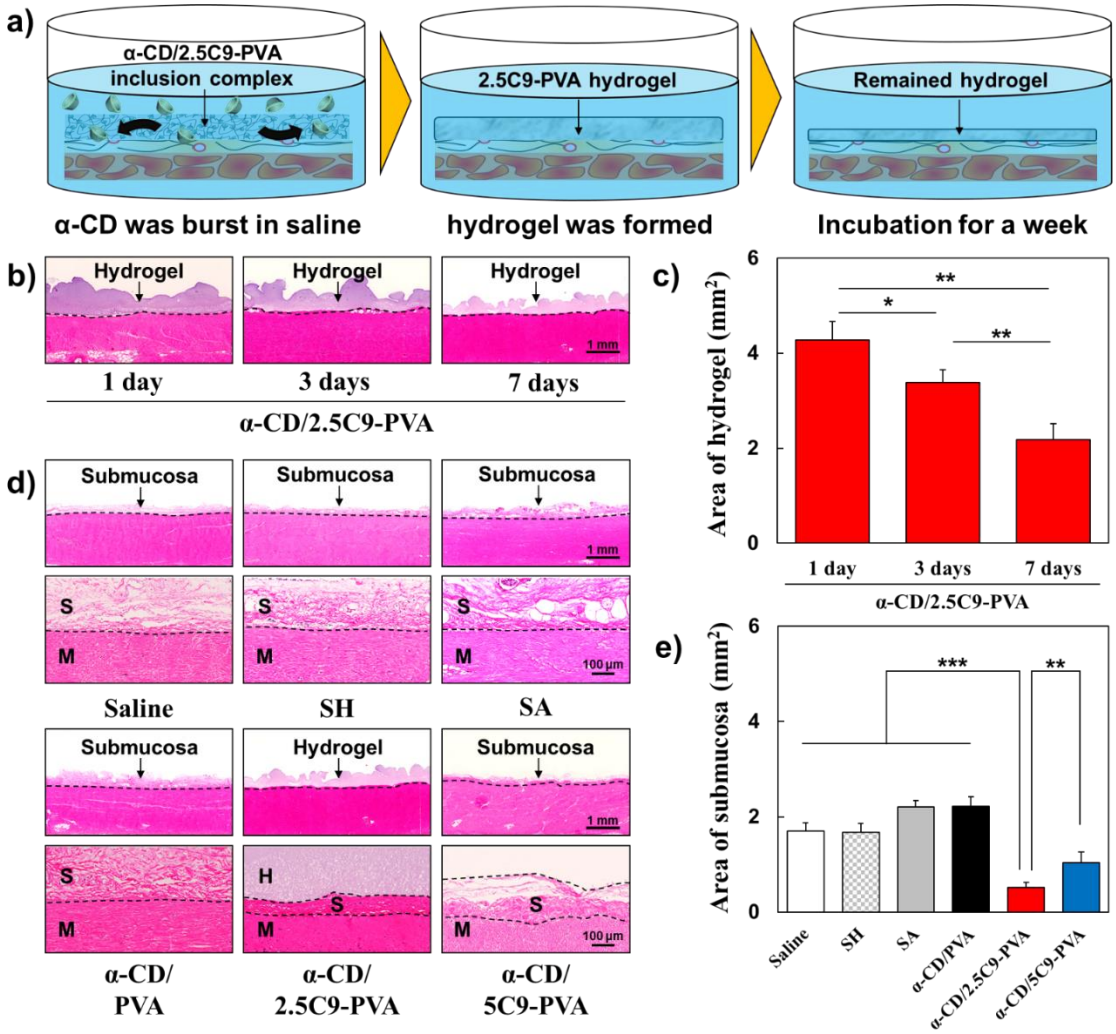

Figure 6-8. The water stability test. a) The process of the water stability test of α-CD/2.5C9-PVA inclusion complex. b) Histology of α-CD/2.5C9-PVA inclusion complex after incubation in normal saline 37 °C for different time (1, 3 and 7 days). c) Percentage of 2.5C9-PVA film area determined from H&E staining. (*P < 0.05, **P < 0.01, n = 4) d) Histology of SIMs after incubation in normal saline for 7 days. (S = submucosa; M = muscularis propria; H = hydrogel) e) Thickness of swelling submucosa covered by different SIMs after incubation in normal saline for 7 days. (**P < 0.01, ***P < 0.001, n = 12)

6.5. Conclusions

In this study, AdSIM for ESD was developed using α-cyclodextrin (α-CD) and hydrophobically modified poly(vinyl alcohol) (hm-PVA). Focusing on the water insolubility of hm-PVA and the hydrophobic groups inclusion ability of α-cyclodextrin (α-CD), an inclusion complex (α-CD/hm-PVA) was fabricated in aqueous solution. The shear viscosity of the α-CD/hm-PVA solution decreased slightly as the α-CD concentration increased. Interestingly, α-CD/2.5C9-PVA inclusion complex showed good gel-sol switchable property under different strain amplitudes (1% and 1000%). Additionally, this inclusion complex showed good injectability using a 25 G needle. The α-CD/2.5C9-PVA inclusion complex could form good submucosal cushion after injection into submucosa due to good structure recovery property. What's more, this material had the potential to deal with complications such as perforation and bleeding. Finally, stable 2.5C9-PVA hydrogel could be formed on the wound after incubation as the α-CD release, which means that α-CD/2.5C9-PVA inclusion complex had the potential to wound sealing after submucosal dissection. These results demonstrate that the α-CD/2.5C9-PVA inclusion complex could be an ideal material for ESD.

References

[1] T. Kuwai, Y. Tamaru, R. Kusunoki, S. Ishaq, Submucosal Injection Solutions for ESD: Separating the Winners from the Losers, Digestive Diseases and Sciences, 64 (2019) 2699-2700.
[2] N. Kakushima, M. Fujishiro, Endoscopic submucosal dissection for gastrointestinal neoplasms, World Journal of Gastroenterology, 14 (2008) 2962-2967.
[3] G. Terheggen, E.M. Horn, M. Vieth, H. Gabbert, M. Enderle, A. Neugebauer, B. Schumacher, H. Neuhaus, A randomised trial of endoscopic submucosal dissection versus endoscopic mucosal resection for early Barrett's neoplasia, Gut, 66 (2017) 783-793.
[4] S. Takayama, T. Wakasugi, H. Funahashi, H. Takeyama, Strategies for gastric cancer in the modern era, World Journal of Gastrointestinal Oncology, 2 (2010) 335-341.
[5] B.P. Saunders, Z.P. Tsiamoulos, Endoscopic mucosal resection and endoscopic submucosal dissection of large colonic polyps, Nature Reviews Gastroenterology & Hepatology, 13 (2016) 486-496.
[6] S.H. Eun, J.Y. Cho, I.S. Jung, B.M. Ko, S.J. Hong, C.B. Ryu, J.O. Kim, S.Y. Jin, J.S. Lee, M.S. Lee, C.S. Shim, B.S. Kim, Effectiveness of Sodium Alginate as a Submucosal Injection Material for Endoscopic Mucosal Resection in Animal, Gut and Liver, 1 (2007) 27-32.
[7] H. Yamamoto, N. Yahagi, T. Oyama, T. Gotoda, T. Doi, S. Hirasaki, T. Shimoda, K. Sugano, H. Tajiri, T. Takekoshi, D. Saito, Usefulness and safety of 0.4% sodium hyaluronate solution as a submucosal fluid "cushion" in endoscopic resection for gastric neoplasms: a prospective multicenter trial, Gastrointestinal Endoscopy, 67 (2008) 830-839.
[8] S. Hirasaki, T. Kozu, H. Yamamoto, Y. Sano, N. Yahagi, T. Oyama, T. Shimoda, K. Sugano, H. Tajiri, T. Takekoshi, D. Saito, Usefulness and safety of 0.4% sodium hyaluronate solution as a submucosal fluid "cushion" for endoscopic resection of colorectal mucosal neoplasms: A prospective multi-center open-label trial, Bmc Gastroenterology, 9 (2009).
[9] R. Castro, D. Libanio, I. Pita, M. Dinis-Ribeiro, Solutions for submucosal injection: What to choose and how to do it, World Journal of Gastroenterology, 25 (2019) 777-788.
[10] N. Uemura, I. Oda, Y. Saito, H. Ono, J. Fujisaki, N. Matsuhashi, K. Ohata, N. Yahagi, T. Yada, M. Satoh, H. Tajiri, M. Inomata, S. Kitano, Efficacy and safety of 0.6% sodium alginate solution in endoscopic submucosal dissection for esophageal and gastric neoplastic lesion: A randomized controlled study, Digestive Endoscopy, 31 (2019) 396-404.
[11] Y. Matsui, M. Inomata, K. Izumi, K. Sonoda, N. Shiraishi, S. Kitano, Hyaluronic acid stimulates tumor-cell proliferation at wound sites, Gastrointestinal Endoscopy, 60 (2004) 539-543.
[12] A. Nishiguchi, F. Sasaki, H. Maeda, M. Kabayama, A. Ido, T. Taguchi, Multifunctional Hydrophobized Microparticles for Accelerated Wound Healing after Endoscopic Submucosal Dissection, Small, 15 (2019).
[13] J.J. Tomasek, G. Gabbiani, B. Hinz, C. Chaponnier, R.A. Brown, Myofibroblasts and mechano-regulation of connective tissue remodelling, Nat. Rev. Mol. Cell Biol., 3 (2002) 349-363.
[14] S. Ono, M. Fujishiro, K. Niimi, O. Goto, S. Kodashima, N. Yamamichi, M. Omata, Long-term outcomes of endoscopic submucosal dissection for superficial esophageal squamous cell neoplasms, Gastrointestinal Endoscopy, 70 (2009) 860-866.
[15] K. Funakawa, H. Uto, F. Sasaki, Y. Nasu, S. Mawatari, S. Arima, J. Nakazawa, H. Taguchi, S. Hashimoto, S. Kanmura, H. Setoyama, M. Numata, H. Tsubouchi, A. Ido, Effect of Endoscopic Submucosal Dissection for Superficial Esophageal Neoplasms and Risk Factors for Postoperative Stricture, Medicine (Baltimore), 94 (2015) 7.
[16] C.I. Kwon, G. Kim, K.H. Ko, Y. Jung, I.K. Chung, S. Jeong, D.H. Lee, S.P. Hong, K.B. Hahm, Bio-sheet graft therapy for artificial gastric ulcer after endoscopic submucosal dissection: an animal feasibility study,

Gastrointestinal Endoscopy, 81 (2015) 989-996.
[17] D. Kumar, V.L. Workman, M. O'Brien, J. McLaren, L. White, K. Ragunath, F. Rose, A. Saiani, J.E. Gough, Peptide Hydrogels-A Tissue Engineering Strategy for the Prevention of Oesophageal Strictures, Advanced Functional Materials, 27 (2017) 12.
[18] A. Nieponice, K. McGrath, I. Qureshi, E.J. Beckman, J.D. Luketich, T.W. Gilbert, S.F. Badylak, An extracellular matrix scaffold for esophageal stricture prevention after circumferential EMR, Gastrointestinal Endoscopy, 69 (2009) 289-296.
[19] I. Tomatsu, A. Hashidzume, A. Harada, Photoresponsive hydrogel system using molecular recognition of alpha-cyclodextrin, Macromolecules, 38 (2005) 5223-5227.
[20] P. Jara, L. Barrientos, B. Herrera, I. Sobrados, Inclusion compounds of alpha-cyclodextrin with alkylthiols, Journal of the Chilean Chemical Society, 53 (2008) 1474-1476.
[21] X. Hao, M. Xu, J. Hu, Q. Yan, Photoswitchable thermogelling systems based on a host-guest approach, Journal of Materials Chemistry C, 5 (2017) 10549-10554.
[22] H.S. Mansur, C.M. Sadahira, A.N. Souza, A.A.P. Mansur, FTIR spectroscopy characterization of poly (vinyl alcohol) hydrogel with different hydrolysis degree and chemically crosslinked with glutaraldehyde, Mater. Sci. Eng. C-Biomimetic Supramol. Syst., 28 (2008) 539-548.
[23] K. Tomihata, Y. Ikada, Crosslinking of hyaluronic acid with glutaraldehyde, J. Polym. Sci. Pol. Chem., 35 (1997) 3553-3559.
[24] Q. Li, D.G. Barret, P.B. Messersmith, N. Holten-Andersen, Controlling Hydrogel Mechanics via Bio-Inspired Polymer-Nanoparticle Bond Dynamics, Acs Nano, 10 (2016) 1317-1324.
[25] C. Yuece, N. Willenbacher, Challenges in Rheological Characterization of Highly Concentrated Suspensions - A Case Study for Screen-printing Silver Pastes, Jove-Journal of Visualized Experiments, (2017).
[26] E.B. Montufar, T. Traykova, E. Schacht, L. Ambrosio, M. Santin, J.A. Planell, M.-P. Ginebra, Self-hardening calcium deficient hydroxyapatite/gelatine foams for bone regeneration, Journal of Materials Science-Materials in Medicine, 21 (2010) 863-869.
[27] M.H. Chen, L.L. Wang, J.J. Chung, Y.-H. Kim, P. Atluri, J.A. Burdick, Methods To Assess Shear-Thinning Hydrogels for Application As Injectable Biomaterials, Acs Biomaterials Science & Engineering, 3 (2017) 3146-3160.
[28] A. Sivashanmugam, P. Charoenlarp, S. Deepthi, A. Rajendran, S.V. Nair, S. Iseki, R. Jayakumar, Injectable Shear-Thinning CaSO4/FGF-18-Incorporated Chitin PLGA Hydrogel Enhances Bone Regeneration in Mice Cranial Bone Defect Model, Acs Applied Materials & Interfaces, 9 (2017) 42639-42652.
[29] E. Wedi, P. Koehler, J. Hochberger, J. Maiss, S. Milenovic, M. Gromski, N. Ho, C. Gabor, U. Baulain, V. Ellenrieder, C. Jung, Endoscopic submucosal dissection with a novel high viscosity injection solution (LiftUp) in an ex vivo model: a prospective randomized study, Endoscopy international open, 7 (2019) E641-E646.
[30] M.B. Dowling, R. Kumar, M.A. Keibler, J.R. Hess, G.V. Bochicchio, S.R. Raghavan, A self-assembling hydrophobically modified chitosan capable of reversible hemostatic action, Biomaterials, 32 (2011) 3351-3357.
[31] R. Mizuta, T. Taguchi, Hemostatic properties of in situ gels composed of hydrophobically modified biopolymers, Journal of Biomaterials Applications, 33 (2018) 315-323.
[32] A. Nishiguchi, Y. Kurihara, T. Taguchi, Underwater-adhesive microparticle dressing composed of hydrophobically-modified Alaska pollock gelatin for gastrointestinal tract wound healing, Acta Biomater, 99 (2019) 387-396.
[33] X. Chen, T. Taguchi, Hydrophobically modified poly(vinyl alcohol)s as antithrombogenic coating materials, Materials Science & Engineering C-Materials for Biological Applications, 102 (2019) 289-298.
[34] X. Chen, T. Taguchi, Injectable, Non-Diffusible, and Pre-Filled Bone Paste Composed of α-Tricalcium Phosphate and Hydrophobically Modified Poly(Vinyl Alcohol), Advanced Engineering Materials, 21 (2019)

1900660.
[35] R. Mizuta, T. Ito, T. Taguchi, Effect of alkyl chain length on the interfacial strength of surgical sealants composed of hydrophobically-modified Alaska-pollock-derived gelatins and poly(ethylene)glycol-based four-armed crosslinker, Colloids Surf B Biointerfaces, 146 (2016) 212-220.

Chapter 7

Concluding remarks

Concluding remarks

Chapter 1 showed the history of PVA and the bio-application of PVA in many fields.

Chapter 2 described the effect of alkyl chain length on the interfacial strength of hydrophobically modified poly(vinyl alcohol) (hm-PVA) films to soft tissue. Hm-PVAs with various alkyl chain lengths were prepared and evaluated their surface/ mechanical properties, cytocompatibility, and adhesive strength to porcine skin. Hm-PVAs exhibited 10 °C higher glass transition temperature than that of poly(vinyl alcohol) (PVA). The water contact angle (WCA) of hm-PVA films increased with an increasing of alkyl chain length or an increasing of hydrophobic group modification ratio. The tensile strength of hm-PVA films decreased with an increasing of alkyl chain length or hydrophobic group modification ratio. Hm-PVA with short chain length (4 mol% propanal-modified PVA, 4C3-PVA) showed low cytotoxicity compared with hm-PVAs with long alkyl chain lengths (4 mol% hexanal and nonanal-modified PVA, 4C6- and 4C9-PVA). Among the hm-PVA films, the 4C3-PVA film showed highest adhesion strength to porcine skin. Therefore, 4C3-PVA film is useful as a promising adhesive film for fixing wearable medical devices.

Chapter 3 described the effect of alkyl chain length on the antithrombogenic property of hm-PVA. Hm-PVAs with various alkyl chain lengths (3–12) were synthesized and were coated on poly (propylene) (PP) films. The blood compatibilities of the hm-PVAs-coated films were evaluated. The C6-PVA-coated PP film showed suppressed platelet adhesion as compared to the other hm-PVA-coated PP films, especially the 15C6-PVA-coated PP film. The fibrinogen adsorption was also inhibited on this film. The hydration water structure of the films was analyzed using differential scanning calorimetry (DSC). 15C6-PVA showed the highest intermediate water (IW), and hence exhibited good blood compatibility. The fibrinogen γ chain activity of the 15C6-PVA-coated PP film was lower than that of the PP film, indicating that hm-PVAs can inhibit fibrinogen γ chain activation. These results showed that by simple hydrophobic modification, PVA could be used as a blood contacting material.

Chapter 4 described the effect of alkyl chain length on the mechanical property and cell adhesion of bone paste composed of α-tricalcium phosphate (α-TCP) and hm-PVAs. The bone pastes developed were injectable and non-diffusible. The resulting bone pastes showed high injectability when the solid-liquid ratio was low. The non-diffusion property of α-TCP/hm-PVAs bone pastes in water and fresh porcine blood was observed compared with α-TCP alone, α-TCP/original PVA (Org-PVA), and commercial calcium phosphate paste. Compressive strength of α-TCP/nonanal modified PVA (C9-PVA) bone pastes reached to max value after 3 days in water. Young's modulus of α-TCP/C9-PVA bone pastes was lower than that of commercial calcium phosphate paste and poly(methyl methacrylate)-based bone cement. Furthermore, the surface of α-TCP/C9-PVA bone pastes showed excellent cell adhesion of cultured osteoblastic cells. These results demonstrated that α-TCP/C9-PVA bone paste is a promising bone filler for percutaneous vertebroplasty (PVP) surgery.

Chapter 5 described the effect of alkyl chain length on mechanical property and volume embolization ratio of cerebral aneurysm embolization material composed of α-cyclodextrin (α-CD) and hm-PVAs. As expect, the water-insoluble hm-PVA could be dissolved in aqueous solution with addition of α-CD. Additionally, 2D-NMR NOESY spectra indicated that a threaded inclusion complex was established between α-CD and the hm-PVA molecule. Among the prepared inclusion complexes, α-CD/5C9-PVA (5C9-PVA with 15 mM α-CD) showed thixotropic property, and its injectability was over 90%, even using a 25G needle. Moreover, the α-CD/5C9-PVA inclusion complex was stable in PBS after incubation at 37 °C for 24 h. Therefore, the α-CD/5C9-PVA inclusion complex is a promising material that could be applied for cerebral aneurysm treatment.

Chapter 6 described the effect of hydrophobic group modification ratio on multi-functions of adhesive submucosal injection material (AdSIM) composed of α-cyclodextrin (α-CD) and hm-PVAs. Focusing

on the water insolubility of hm-PVA and the hydrophobic groups inclusion ability of α-cyclodextrin (α-CD), an inclusion complex (α-CD/hm-PVA) was fabricated in aqueous solution. Interestingly, α-CD/2.5C9-PVA inclusion complex showed good gel-sol switchable property and good injectability using a 25 G needle. The α-CD/2.5C9-PVA inclusion complex could form good submucosal cushion after injection into submucosa due to good structure recovery property. What's more, this material had the potential to deal with complications such as perforation and bleeding. Finally, stable 2.5C9-PVA hydrogel could be formed on the wound after incubation as the α-CD release, which means that α-CD/2.5C9-PVA inclusion complex had the potential to wound sealing after submucosal dissection. These results demonstrate that the α-CD/2.5C9-PVA inclusion complex could be an ideal material for ESD.

PVA has been widely used in various areas including the biotechnological and biomedical field due to its excellent chemical and physical properties, easy processing technique and high cytocompatibility. Applications of PVA in the biomedical field include contact lenses, wound dressing, coatings for sutures and catheters. In recent years, research and product development of functionalized PVA have been promoted. As a result, PVA is attracting attention from many fields. In this study, hm-PVAs with various alkyl chain lengths (3–18) were synthesized and their multifunctionality was evaluated. From these research results, it was clear that the partial hydrophobic modification of PVA can be applied to various applications. It is considered that this cheap and potentially functional hm-PVA can be expected as a novel biomaterial material.

List of publication

First-authored paper

1. **Chen, X.**; Mizuta, R.; Fukata, N.; Taguchi, T., Design of bio-inspired adhesive surface composed of hexanoyl group-modified gelatin and silicon nanowire. *Colloids and Surfaces B: Biointerfaces* **2019**, 178, 111-119.
2. **Chen, X.**; Taguchi, T., Hydrophobically modified poly(vinyl alcohol)s as antithrombogenic coating materials. *Materials Science & Engineering C* **2019**, 102, 289-298.
3. **Chen, X.**; Taguchi, T., Injectable, non-diffusible and pre-filled bone paste composed of α-Tricalcium phosphate and hydrophobically modified poly(vinyl alcohol). *Advanced engineering materials* **2019**, 21, 1900660
4. **Chen, X.**; Taguchi, T., Enhanced skin adhesive property of hydrophobically-modified poly(vinyl alcohol) films. *ACS Omega* **2019**, DOI: 10.1021/acsomega.9b03305
5. **Chen, X.**; Taguchi, T., An injectable inclusion complex composed of α-cyclodextrin and hydrophobically modified poly(vinyl alcohol) as a cerebral aneurysm embolization material. *Polymer Journal* **2020** *accepted*
6. **Chen, X.**; Nishiguchi, A.; Taguchi, T., Adhesive submucosal injection material with multi-function for endoscopic submucosal dissection. Submitted to *ACS applied materials & interfaces*

List of presentation and awards

Poster presentation

1. Chen, X.; Mizuta, R.; Fukata, N.; Taguchi, T. “Design of Bio-inspired Adhesive Surface Using Hexanoyl Group-modified Gelatin and Silicon Nanowire” Tsukuba Global Science Week (TGSW) 2016, September 17-19, Ibaraki, Japan

2. 陳曦、水田亮、深田直樹、田口哲志　「構造的・機能的接着を可能にするバイオインスパイアード表面の設計」、日本バイオマテリアル学会シンポジウム 2016、2016 年 11 月 21-22 日、福岡

3. 陳曦、水田亮、深田直樹、田口哲志　「ヘキサノイル化ゼラチンとシリコンナノワイヤーを用いたバイオインスパイアード接着表面の調製と機能評価」、つくば医工連携フォーラム 2017、2017 年 1 月 20 日、茨城

4. 陳曦、水田亮、深田直樹、田口哲志　「ナノ構造とアルキル基との複合化によるバイオインスパイアード接着表面の設計」、SAT テクノロジー・ショーケース 2017、2017 年 1 月 31 日、茨城

5. 陳曦、水田亮、深田直樹、田口哲志　「構造的・機能的接着性を有する バイオインスパイアード接着表面の設計」、日本接着学会年次大会、2017 年 6 月 15-16 日、大阪

6. 陳曦、水田亮、深田直樹、田口哲志　「構造的・機能的接着を可能にするバイオインスパイアード表面の作製」、第 55 回日本人工臓器学会大会、2017 年 9 月 1-3 日、東京

7. Chen, X.; Mizuta, R.; Fukata, N.; Taguchi, T. “Evaluation of bio-inspired surface for the structural and functional adhesion” Tsukuba Global Science Week-Interdisciplinary Work Shop on Science and Patents (TGSW-IWP) 2017, September 25-27, Ibaraki, Japan

8. 陳曦、田口哲志　「疎水化ポリビニルアルコールコーティングによる血栓形成抑制効果」、第 67 回高分子学会年次大会、2018 年 5 月 23-25 日、名古屋

9. 陳曦、田口哲志　「アセタール化 PVA 表面の血栓形成抑制効果」、第 56 回日本人工臓器学会大会、2018 年 11 月 1-3 日、東京

10. 陳曦、田口哲志　「アセタール化 PVA コーティング表面の抗血栓形成性評価」、第 40 回日本バイオマテリアル学会、2018 年 11 月 12-13 日、神戸

11. 陳曦、田口哲志　「アセタール化 PVA コーティング表面の血栓形成抑制効果の解析」、つくば医工連携フォーラム 2019、2019 年 1 月 25 日、茨城

12. 陳曦、田口哲志　「血液中で硬化するプレフィールド型骨ペーストの開発」、第 57 回日本人工臓器学会大会、2019 年 11 月 12-15 日、大阪

Oral presentation

13. Chen, X.; Taguchi, T. “Injectable, Non-diffusible and Pre-filled Type Bone Pastes” TERMIS-AP + ABMC7 Congress, October 13-17, Brisbane, Australia

Award

Chen, X.; Mizuta, R.; Fukata, N.; Taguchi, T. “Evaluation of bio-inspired surface for the structural and functional adhesion” Tsukuba Global Science Week-Interdisciplinary Work Shop on Science and Patents (TGSW-IWP 2017), September 25-27, Tsukuba, Ibaraki, Japan “Best Presentation Award”

陳曦、田口哲志　「水環境で硬化するプレフィールドタイプ骨ペーストの開発」、第 41 回日本バイオマテリアル学会大会、2019 年 11 月 24-26 日、つくば　ハイライト発表選出

陳曦、田口哲志　「水環境で硬化するプレフィールドタイプ骨ペーストの開発」、第 41 回日本バイオマテリアル学会大会、2019 年 11 月 24-26 日、つくば　優秀研究ポスター賞

陳曦、田口哲志　「早期消化管がん部位の膨隆と創部被覆を可能にする内視鏡局注材の開発」、つくば医工連携フォーラム 2020、 2020 年 1 月 22 日、つくば　研究奨励賞

Acknowledgements

I would like to express my deepest appreciation to my supervisor Prof. Tetsushi Taguchi for his valuable guidance and appropriate advices, and generous support. Prof. Tetsushi Taguchi also gave me a lot of opportunities to present our works and teach me the presentation skills I have gained a lot of knowledge and skills in his laboratory. Icould broaden my perspective thanks to him.

I would like to express my gratitude to the thesis committee members. I could not complete my thesis without their specialty and intelligence.

I would like to extend special thanks to Prof. Naoki Fukata, Dr. Akihiro Nishiguchi and Dr. Kennichi Omori for their helpful advices and supports.

My study could not succeed without a lot of help. Mrs. Tomoka Kojima, Mrs. Takumi Iwano and Mrs. Meiko Ishikawa kindly supported me with hospitality. I really appreciate their kind help from Mrs. M. Katano, Mrs. S. Watanabe, Mrs. Y. Kurihara, Mrs. C. Mizumo and Mrs. Y. Nakagawa of the Polymeric Biomaterials Group at the National Institute for Materials Science (NIMS). I am also grateful to students at university of Tsukuba, Dr. R. Mizuta, Mr Y. Mizuno, and they spared time to give me hands.

Finally, I must thank my family for their unconditional support throughout my life.

Xi Chen
February 2020